ANALYSIS OF FUNCTIONALLY GRADED SANDWICH BEAMS UNDER HYGRO – THERMO – MECHANICAL LOADS

By

NGUYEN BA DUY

DISSERTATION

Submitted to Ho Chi Minh City University of Technology and Education
in partial fullfillment of the requirements
for the degree of

Doctor of Philosophy
2019

MAJOR : ENGINEERING MECHANICS

Ho Chi Minh City, September 2019

ANALYSIS OF FUNCTIONALLY GRADED SANDWICH BEAMS UNDER HYGRO – THERMO – MECHANICAL LOADS

By

NGUYEN BA DUY

DISSERTATION

Submitted to Ho Chi Minh City University of Technology and Education
in partial fullfillment of the requirements
for the degree of

Doctor of Philosophy
2019

MAJOR : ENGINEERING MECHANICS

Ho Chi Minh City, September 2019

THE PhD THESIS HAS BEEN COMPLETED AT:
HO CHI MINH CITY UNIVERSITY OF TECHNOLOGY AND EDUCATION

PhD thesis is protected in front of

EXAMINATION COMMITTEE FOR PROTECTION OF DOCTORAL THESIS

HO CHI MINH CITY UNIVERSITY OF TECHNOLOGY AND EDUCATION,

Date .... month .... year .....

ORIGINALITY STATEMENT

I hereby declare that this submission is my own work and to the best of my knowledge it contains no materials previously published or written by another person, or substantial proportions of material which have been accepted for the award of any other degree or diploma at Ho Chi Minh City University of Technology and Education (HCMUTE) or any other educational institution, except where due acknowledgement is made in the thesis. Any contribution made to the research by others, with whom I have worked at HCMUTE or elsewhere, is explicitly acknowledged in the thesis. I also declare that the intellectual content of this thesis is the product of my own work, except to the extent that assistance from others in the project's design and conception in style, presentation and linguistic expression is acknowledged.

Date……...

Signed……

ACKNOWLEDGEMENTS

My thanks go to many people who provided great support and had an important role in this research. I would like to express my gratitude to my supervisor, Assoc. Prof. Nguyen Trung Kien, and co-supervisors Prof. Vo Phuong Thuc of the Northumbria University for their continuous support and valuable guidance throughout this research.

I had also the opportunity to work with people in GACES of HCMUTE. Therefore, my acknowledgments are extended to Prof. Nguyen Hoai Son and Nguyen Ngoc Duong for his technical guidance and training. Dr. Nguyen Van Hau is thanked for his comment and discussion on functionally graded materials (FGM). My thanks also go to Le Quoc Cuong who helped and provided me a useful matlab. Thank you to everyone else who help me with this research.

Last but not least, I wish to profoundly thank my parents, my wife, my son and my sister for their unconditional love and unlimited support. Without their encouragement, I would not have been able to overcome many difficulties and challenges during this research.

Contents

LISTS OF TABLES

LISTS OF FIGURES

LISTS OF SYMBOLS

FGMs	Functionally graded materials
FG	Functionally graded
CBT	Classical beam theory
FSDT	The first order shear deformation theory
FSBT	The first order shear deformation beam theory
HSDTs	The higher order shear deformation theories
HSBT	The higher order shear deformation beam theory
TSDT	The third shear deformation theories
TSBT	The third shear deformation beam theories
GACES	Group of Advanced Computations in Engineering Sciences
CNTs	Carbon nanotubes
T_t	Temperature on the top
T_b	Temperature on the bottom
C_t	Moisture on the top
C_b	Moisture on the bottom
TD	Temperature dependent
TID	Temperature Independent
FEM	The Finite Element Method
MCST	Modified couple stress beam theory
MLSPs	Material length scale parameters
DQM	Differential Quadrature Method
Eq.	Equations
∇	Laplacian operator
μ	Parameter of scale length for FG nano beams
ς	The material length scale parameters **(**MLSPs) for FG micro beams
E	Young's modulus
E_t	Young's modulus on the top
E_b	Young's modulus on the bottom
ρ	The Mass density
ν	The Poisson's ratio
RM	Ritz method
BCs	Boundary conditions
S – S	Simply – Supported
C – C	Clamped – Clamped
H – H	Hinged – Hinged
C – H	Clamped – Hinged
C – S	Clamped – Simply Supported

C – F	Clamped – Free
UTR	Uniform temperature rise
UMR	Uniform moisture rise
LTR	Linear temperature rise
LMR	Linear moisture rise
NLTR	Nonlinear temperature rise
NLMR	Nonlinear moisture rise
MEMS	Micro electro mechanical systems
U.K	United Kingdom

Abstracts

Functionally Graded Materials is a composite class in which the volume fractions of constituted components are changed gradually leading to the smooth variation of material properties in specific directions. This material class has been applied widely in various fields of engineering such as aerospace, marine, automotive, civil and medical industries thanks to the striking features of high ability in thermal resistance and mechanical ductility. The widespread applications of this material class results in the development of different theories and numerical methods to analyse properly the static, vibration and buckling behaviours. In this thesis proposes a novel general higher-order shear deformation beam theory for analysis of isotropic and functionally graded sandwich beams under hygro-thermal-mechanical loads. A general theoretical formulation is derived from the fundamental of two-dimensional elasticity theory and then novel higher-order shear deformation beam theories are obtained. Analysis of functionally graded beam with effects of moisture and temperature rises is studied. The temperature and moisture are supposed to be varied uniformly, linearly and non-linearly. In addition, the effects of scale-size of functionally graded beams is proposed. The governing equations of motion are obtained using the variational principle. Analytical and numerical methods, including new Ritz methods and finite element methods were applied to achieve the static, free vibration and buckling behaviours of functionally graded beam. The present results were validated by comparing to the literature and the conclusions about the proposed models are deduced. The effects of the material parameters and homogenization schemes, the aspect and the slenderness ratios, boundary conditions and the sandwich schemes on the bending deflection, stress, natural frequency and buckling loads were investigated. This thesis can be a theoretical guidance in developing the applications of functionally graded beam and functionally graded sandwich beams in some engineering industries.

Chapter 1
General Introduction

This chapter is to present a general introduction of composite structures, research context of objective the thesis.

The highlight of this chapter is followed:

- Applications of composite materials in the engineering fields
- A literature review of composite beam theories.
- A literature review of analytical and numerical methods
- A literature review of behaviors of hygro-thermal-mechanical loads
- Objective and novelty of the thesis.
- Thesis outline

1.1 Introduction and Objectives

The most well-known advantages of high stiffness-to-weight and strength-to-weight ratios, composite materials have been commonly used in many engineering fields such as aerospace (Figure 1.1), mechanical engineering, construction, etc. Composite structures can be categorized into two main types: Laminated composite structures and functionally graded ones. Laminated composite structures are ones made of laminae bonded together at the interfaces of layer in which their fibre orientations can be changed to meet structural performances. The disadvantage of these structures is material discontinuity at the interfaces of layer, that can lead to the stress concentration and delamination effects. To overcome this adverse, the functionally graded structures have been developed in which the properties of constituent materials vary continuously in a required direction and there thus is no interfacial effect.

Potential applications of the composite materials in the engineering fields led to the development of composite structure theory. The composite beams are one of the most important structural components of the engineering structures which attracted many researches with different theories, numerical and analytical approaches, only some representative references are herein cited.

For composite beam models, a literature review on the composite beam theories can be seen in the previous works of Ghugal and Shimpi [1], Sayyad and Ghugal [2]. Many beam theories have been developed in which it can be divided into three main categories: classical theory, first-order shear deformation theory, higher-order shear deformation theory. The classical theory neglects transverse shear strain effects and therefore it is only suitable for thin structures. In order to overcome this problem, the first-order shear deformation theory accounts for the transverse shear strain effect, however it requires a shear correction factor to correct inadequate distributions of the transverse shear stresses through its thickness [3, 4]. The higher-order shear deformation theory predicts more accurate than the other theories due to their appropriate distribution of transverse shear

stresses. However, the accuracy of this theory depends on the choice of higher-order shape functions [5, 6]. In addition, several other authors proposed higher-order shear deformation models and techniques to reduce number of field variables. This approach led to refined higher-order shear deformation theories which are a priori efficient and simple [7-9]. It can be seen that the development of simple and efficient composite beam models is a significant topic interested by many researchers.

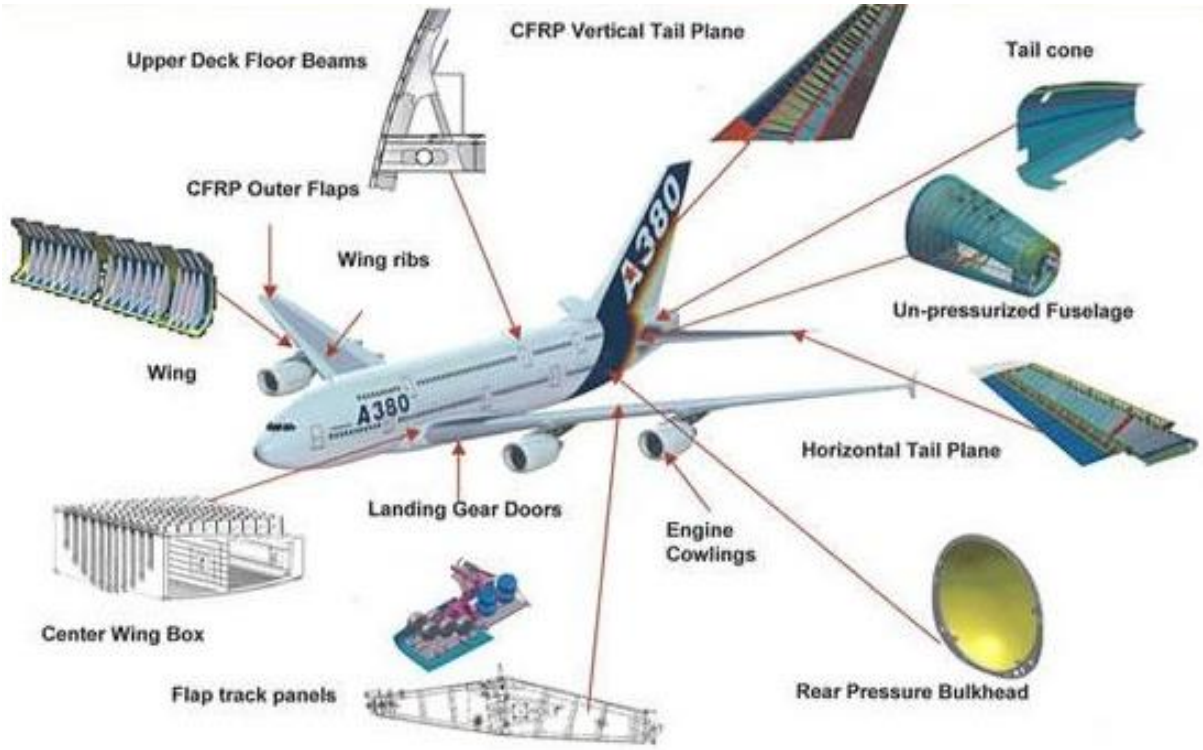

Figure 1.1 Application of composite materials in engineering

https://tantracomposite.com/

Moreover, when the behaviors of beam are considered at a small scale, the experimental studies showed that the size effect is significant to be accounted, that led to the development of Eringen's nonlocal elasticity theory [10] to account for scale effect in elasticity, was used to study lattice dispersion of elastic waves, wave propagation in composites, dislocation mechanics, fracture mechanics and surface tension fluids. After

this, Peddieson et al. [11] first applied the nonlocal continuum theory to the nanotechnology in which the static deformations of beam structures were obtained by using a simplified nonlocal beam model based on the nonlocal elasticity theory of Eringen [10] and the modified couple stress theory (MCST), which was developed by Yang et al. [12] by modifying the classical couples stress theory [13-16], is advantageous since it requires only one additional material length scale parameter together with two from the classical continua. This feature was presented by the theoretical framework in [12] which proved that the antisymmetric part of curvature does not appear explicitly in the strain energy. Based on this approach, several studies have been investigated and applied for analysis of composite micro beams and nano beams [17-19]. Due to the difficulty in introducing the constitutive equations of micro beams into the energy functional, it is observed from the literature on micro beams that the effect of boundary conditions on the behaviors of micro beams are still limited.

For computational methods, many computational methods have been developed in order to predict accurately responses of composite structures with analytical and numerical approaches. For analytical approaches, Navier procedure can be seen as the simplest one in which the displacement variables are approximated under trigonometric shape functions that satisfy the boundary conditions (BCs). Although this method is only suitable for simply supported BCs, it has widespread used by many authors by its simplicity [20, 21]. Alternatively, the Ritz method is the most general one which accounts for various BCs. However, the accuracy of this approach requires an accurate choice of the approximate shape functions. The shape functions can be satisfied the BCs, conversely a penalty method can be used to incorporate the BCs. Several previous works developed the Ritz-type solution method with trigonometric, exponential and polynomial shape functions for analysis of composite beams [22-24]. Other analytical approaches have been investigated for analysis of composite beams and plates such as differential quadrature method (DQM) by Bellman and Casti [25] that applied

successfully for solving nonlinear differential equations system and for behavior analysis of composite beams [26, 27]. Moreover, due to the limitation of analytical method in practical applications, especially for complex geometries, numerical methods have been developed with various degrees of success in which the finite element method (FEM) is the most popular one which attracted a number of researches for behavior analysis of composite beams [7, 28, 29]. In practice, the FEM has difficulties to conveniently construct conformable plate elements of high-order as required for thin beam and plates, and to overcome the stiffness excess phenomena characterizing the shear-locking problem. Other numerical approaches can be considered for analysis of composite beams such as meshless method [30, 31], isogeometric finite element method [32, 33]. This literature survey indicates that a simple and efficient computational method for behavior analysis of composite beams is also an interesting topic.

In Vietnam, the behavior analysis of composite structures has attracted a number of researches, only some representative research groups are cited. Research group of Nguyen et al. [34-36] at the Hutech University. Nguyen et al. [37-39] at the Ton Duc Thang University. These groups of computational mechanic's focus on the development of advanced numerical methods such as the FEM, S-FEM, meshless method, isogeometry method and optimization theory of structures. Nguyen et al. [40-43] developed analytical methods for analysis of composite plates and shells with various geometric shapes and loading conditions. Tran et al. [44, 45] carried out some experimental studies on composite structures. Hoang et al. [46, 47] studied responses of functionally graded plates and shells under thermo-mechanical loads. Nguyen et al. [48, 49] investigated behaviors of functionally graded beams by the FEM under some different geometric and loading conditions. Group of GACES at HCMC University of Technology and Education developed analytical and numerical methods for analysis of composite beams, plates and shells, beam and plate models under hygro-thermo-mechanical loads [50-52].

A literature review on the behaviors of composite beams showed that the following points are necessary to be developed "ANALYSIS OF FUNCTIONALLY GRADED SANDWICH BEAMS UNDER HYGRO – THERMO – MECHANICAL LOADS".

- Develop novel general higher-order shear deformation model for analysis of functionally graded isotropic and sandwich beams
- Develop a functionally graded micro beam and nano beam model with various boundary conditions
- Develop a novel hybrid shape function for studying FG beams with different boundary conditions
- Develop finite element solution for analysis of functionally graded beams with different boundary conditions

1.2 Objective and novelty of the thesis

The object of this thesis is to propose some beam models for static, buckling and vibration analysis of functionally graded isotropic and sandwich beams embedded in hygro-thermo-mechanical environments.

The outline of this objective is followed:

- Novel general higher-order shear deformation beam theories are developed for analysis of functionally graded isotropic and sandwich beams. It is derived from the fundamental of elasticity theory.
- Develop a functionally graded microbeam and nanobeam model with various boundary conditions
- Develop a novel hybrid shape function for studying FG beams with different boundary conditions
- Develop finite element solution for analysis of functionally graded beams with different boundary conditions

1.3 Thesis outline

This thesis contains 7 chapters to describe the whole procedure of development and investigation, which is structured as follows:

- **Chapter 1:** The objective of this chapter is to introduce a brief literature review on computational theories and methods of composite beams, from which several novel findings are found and proposed.
- **Chapter 2:** It presents more details of the composite materials, its microstructure and method of estimating the effective elastic properties. A literature review also focuses on the topics that are relevant to this research such as beam theories, analytical and numerical approaches for bending, buckling and vibration analysis of beams in hygro-thermo-mechanical environment.
- **Chapter 3:** This chapter proposes a novel general higher-order shear deformation beam theory for analysis of functionally graded beams. A general theoretical formulation of higher-order shear deformation beam theory is derived from the fundamental of two-dimensional elasticity theory and then novel different higher-order shear deformation beam theories are obtained. Moreover, two other beam models are also proposed. A HSBT model with a new inverse hyperbolic-sine higher-order shear function and a novel three-variable quasi-3D shear deformation beam theory for analysis of functionally graded beams are proposed. Numerical results are carried out to verify the accuracy of the proposed theories and to investigated effects of material distribution, thickness ratio of layer, span-to-thickness ratio and boundary conditions on deflection and stresses, critical buckling loads and natural frequencies.
- **Chapter 4:** This chapter investigates effects of moisture and temperature rises on vibration and buckling responses of functionally graded beams. The present work is based on a higher-order shear deformation theory which accounts for a hyperbolic distribution of both in-plane and out-of-plane displacements. The temperature and moisture are supposed to be varied uniformly, linearly and non-linearly.

- **Chapter 5:** This chapter proposes the effects of scale-size on the buckling and vibration behaviors of functionally graded beams in thermal environments. A general theoretical formulation is derived from the fundamental of two-dimensional elasticity theory. The effects of boundary conditions on behaviors of functionally graded beam are considered.
- **Chapter 6:** A finite element model for vibration and buckling of functionally graded beams based on a refined shear deformation theory is presented. Governing equations of motion and boundary conditions are derived from the Hamilton's principle. Effects of the power-law index, the span-to-height ratio and the various boundary conditions on the natural frequencies, critical buckling loads of functionally graded beams are discussed.
- **Chapter 7:** This chapter presents a summary of the investigation and the important conclusions of this research are presented. The further work related to this research is suggested for future development and investigation.

1.4 List of publications

- **Articles in ISI-covered journal**

1. Trung-Kien Nguyen, **Ba-Duy Nguyen.** *A new higher-order shear deformation theory for static, buckling and free vibration analysis of functionally graded sandwich beams*. Journal of Sandwich Structures and Materials, pages 613-631, November 2015.
2. Nguyen T-K, Vo T.P, **Nguyen B-D**, Lee J. *An analytical solution for buckling and vibration analysis of functionally graded sandwich beams using a quasi-3D shear deformation theory*. Composite Structures, Vol. 156, pages 238-252, November 2016.
3. Trung-Kien Nguyen, **Ba-Duy Nguyen**, Vo T.P, Huu-Tai Thai. *Hygro-thermal effects on vibration and thermal buckling behaviours of functionally graded beams*. Composite Structures, Vol. 176, pages 1050-1060, September 2017.

- **Articles in national scientific journal**

1. **Nguyen Ba Duy,** Nguyen Trung Kien. *Free vibration analysis of functionally graded sandwich beams based on a higher-order shear deformation theory.* Journal of Science and Technology 52 (2C), pages 240-249, 2014.

- **National Conference**

1. **Nguyen Ba Duy**, Nguyen Trung Kien. *Analysis of free vibration of sandwich beams with functionally graded faces and homogeneous core*. Proceedings of the 11th National Conference on Solid Mechanics, Ho Chi Minh City, Viet Nam, pp. 392 – 400, 2013.
2. **Nguyen Ba Duy,** Nguyen Trung Kien. *Vibration and buckling analysis of sandwich beams with functionally graded faces and homogeneous core.* Proceedings of the National Conference on Mechanical Engineering, Da Nang City, Viet Nam, pp. 178-188, 2015.
3. **Nguyen Ba Duy,** Nguyen Trung Kien. *Thermo-mechanical behavior of functionally graded sandwich beams using a higher-order shear deformation theory.* Proceedings of the 12th National Conference on Solid Mechanics, Da Nang City, Viet Nam, pp. 825-832, 2015.
4. **Nguyen Ba Duy**, Nguyen Trung Kien, Mai Duc Dai. *Vibration analysis of functionally graded nano beams with various boundary conditions*. Proceedings of the 10th National Conference on Mechanical Engineering, Ha Noi City, Viet Nam, pp. 459-467, 2018.

Chapter 2

Literature review on behaviors of functionally graded beams in hygro-thermo-mechanical environments

---

This chapter is to present a literature review on computational theories and methods for bending, buckling, and vibration analysis of FG sandwich beams under mechanical, thermal and moisture loads.

The highlight of this chapter is followed:

- A brief introduction about composite material and functionally graded materials as well as their applications.
- Various techniques used to determine the effective elastic properties of functionally graded materials.
- Functionally graded beams in thermal and moisture environments.
- Different beam theories for analysis of isotropic and functionally graded sandwich beams and novel shear function for higher-order shear deformation beam theory.
- Analytical and numerical approaches on the behavior analysis of isotropic and FG sandwich beams.
- Concluding remarks on literature review and novel findings of future works.

2.1 Composite and functionally graded materials

Composite materials: Composite materials are engineering materials which consist of two or more material phases whose hygro-thermo-mechanical performance and properties are designed to be superior to those of the constituents. One of the phases being usually discontinuous, stiffer, and stronger, is namely reinforcement whereas the softer and weaker phase being continuous is namely matrix. The matrix material surrounds and supports the reinforcement materials by maintaining their relative positions. The reinforcements impart their special mechanical and physical properties to improve the matrix properties. Moreover, an additional material can practically be added to reinforcement-matrix composite in order to enhance chemical interactions or other processing effects.

a) b)

Figure 2.1 Particulate and fiber composite materials
https://www.researchgate.net/figure/Different-types-of-composite-materials_fig2_313880039

Composite materials are classified into two main categories depending on the type, geometry, orientation and arrangement of the reinforcement phase: Particulate composites and fiber composites (Figure 2.1). Particulate composites compose of particles of various sizes and shapes randomly dispersed within the matrix, which can be therefore regarded as quasi homogeneous on a scale larger than the particle size. Fiber composites are composed of fibers as the reinforcing phase whose form is either discontinuous (short fibers or whiskers) or continuous (long fibers). Fibers arrangement

and their orientation can be customized for required performances. Recently, the new generation of composite materials was made by the carbon nanotubes (CNTs) composites added into the polymer matrix to fabricate polymer matrix nanocomposites and it will be the potential application of fiber composite materials. In practice, the CNTs are tiny tubes with diameters of a few nanometers and lengths of several microns made of carbon atoms. The CNTs have been used in various fields of applications in last decade due to their high physical, chemical and mechanical properties. The development of composite materials with different processing methods led to the birth of multilayered structures which compose of thin layers of different materials bonded together (Figure 2.2a). However practically, the main disadvantages of such an assembly is to create a material discontinuity through the interfaces of layers along which stress concentrations may be high, more specifically when high temperatures are involved. It can result in damages, cracks and failures of the structure. One way to overcome this adverse is to use functionally graded materials within which material properties vary continuously. The concept of functionally graded material (FGM) was proposed in 1984 by the material scientists in the Sendai area of Japan [53].

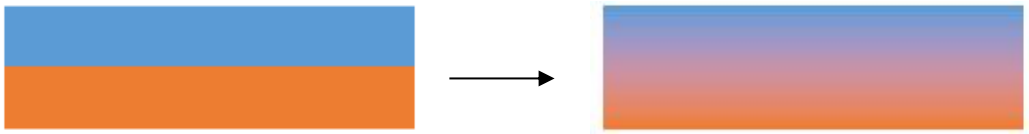

(a) Laminated composite (b) FGM

Figure 2.2 Laminated composite and functionally graded materials

Functionally graded materials: FGMs are advanced composite materials whose properties vary smoothly and continuously in a required direction (Figure 2.2b). This new material overcomes material discontinuity found in laminated composite materials and therefore presents a large potential application. The earliest FGMs were introduced by Japanese scientists as ultra-high temperature resistant materials for aerospace applications and then spread in electrical devices, energy transformation, biomedical engineering, optics, etc.([54, 55]). FGMs are actually applied to many engineering fields

such as cutting tools, machine parts, and engine components, incompatible functions such as heat, moisture, wear, and corrosion resistance plus toughness, etc. (Figure 2.3).

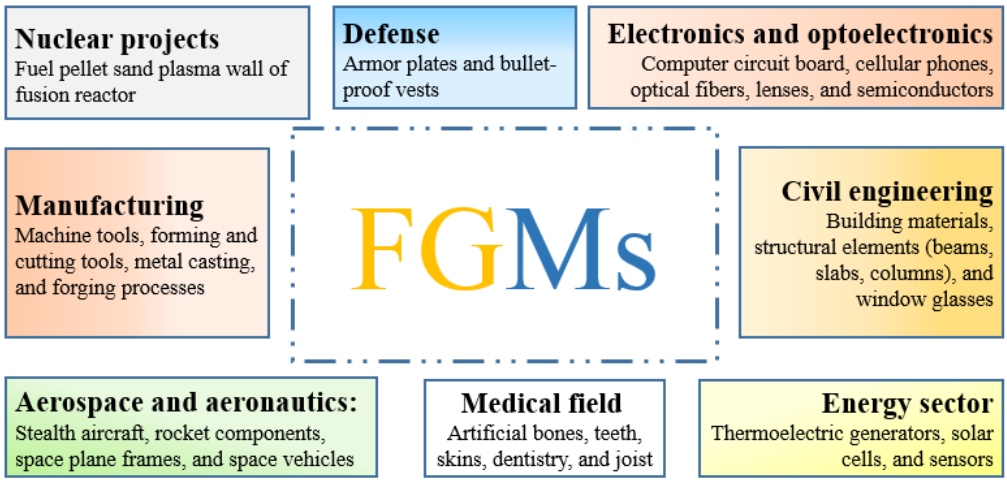

Figure 2.3 Potentially applicable fields for FGMs [55].

The earliest purpose of FGM development is to produce extreme temperature resistant materials so that ceramics are used as refractories and mix with other materials. In practice, the ceramics cannot be themselves used to make engineering structures subjected to high amounts of mechanical loads. It is due to its poor property in toughness. In the other cases, the metals and polymers are good at toughness and therefore used to mix with ceramics in order to combine the advantages of each material.

An example of FGMs used for a re-entry vehicle is shown in Figure 2.4. The FGMs can be used to produce the shuttle structures. The heat source is created by the air friction of high velocity movement. If the structures of the vehicle are made from FGMs, the hot air flow is blocked by the outside surface of ceramics and transfers slightly into the lower surface. Consequently, the temperature at the lower surface is much reduced, which therefore prevents or minimizes structural damage due to thermal stresses and thermal shock.

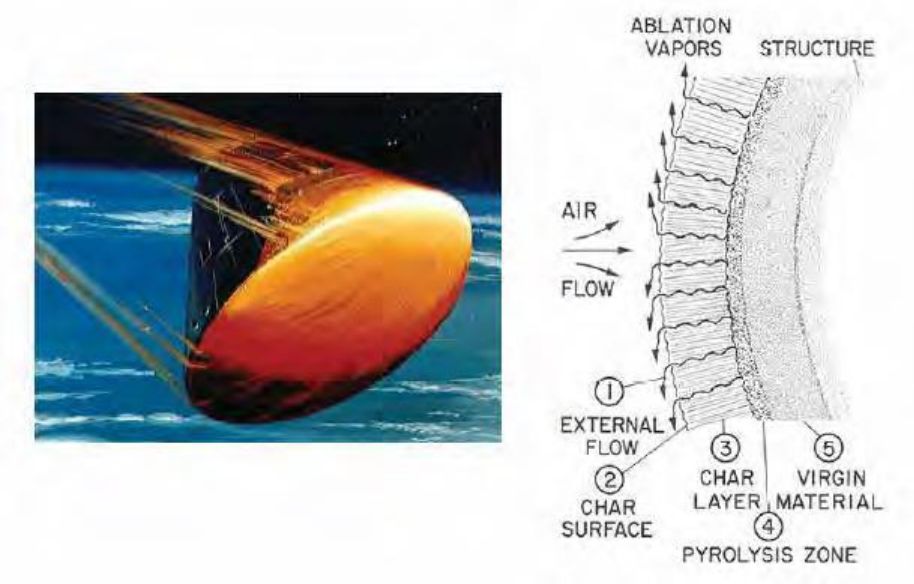

Figure 2.4 An example of FGM application for aerospace engineering [56].

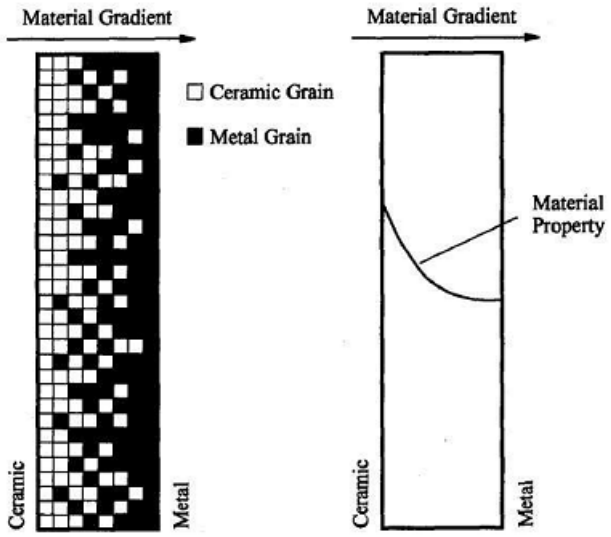

Figure 2.5 A discrete and continuous model of FG material [57].

2.2 Homogenized elastic properties of functionally graded beams

A FGM is formed by varying the microstructure from one material to another material with a specific gradient. Although the FGM is heterogeneous at microscopic scale, it varies continuously at macroscopic one (Figure 2.5). In order to estimate effective elastic

properties of the FGM, analytical homogenization approaches can be used to simplify computations of heterogeneous complex microstructures (a brief literature review on homogenization of heterogeneous composite materials can be seen in [58]. The purpose of this section is thus to review some simple approximations which are commonly used to estimate the homogenized elastic properties of the FGMs, especially for the FG beams.

(a) **Type A:** A single layer functionally graded beam

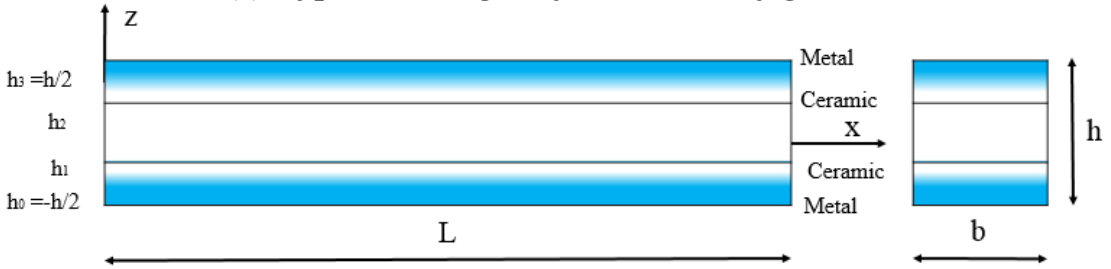

(b) **Type B:** FG sandwich beam with FG face sheets and isotropic core.

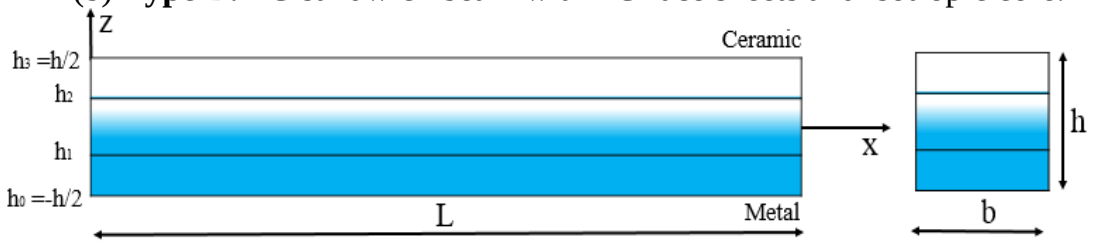

(c) **Type C:** FG sandwich beam with isotropic face sheets and FG core.

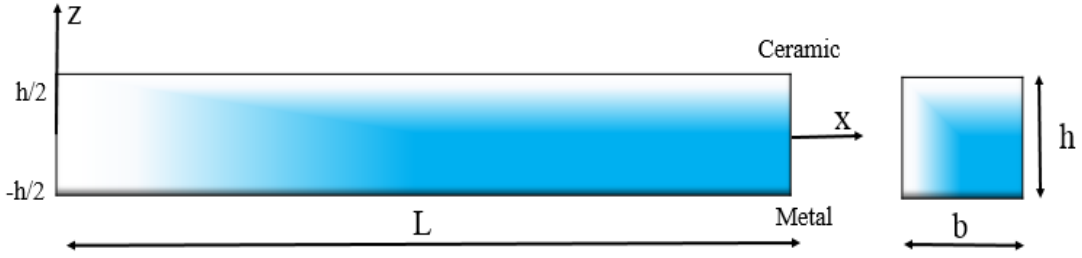

(d) **Type D:** FG sandwich beam with 2D FG .

Figure 2.6 Geometry and coordinate systems of FG sandwich beams.

The variation of material properties of the FGM can be expressed in term of the volume fraction of constituent materials under following forms: the power-law function, the exponential-law function and the sigmoid function [54]. In order to detail these material distributions, FG beams with length L and section $b \times h$ are considered. It is composed of ceramic and metal materials whose properties vary continuously through the beam thickness. Four types of FG beams are investigated: FG beam (Type A), FG sandwich beam with FG faces and homogeneous core (Type B), FG sandwich beam with FG core and homogeneous beam (Type C), and bi-directional FG beam (Type D) (Figure 2.6).

2.2.1 Power function

The rule of mixtures is the simplest technique widely used by many researchers for material gradation. In this rule, the effective property of FGM can be approximated based on an assumption that a composite property is the volume weighted average of the properties of the constituents. The power-law for the material gradation was first introduced by Wakashima et al. [59]. Furthermore, this law is widely used by many researchers for the modeling and analysis of FG sandwich beams. The law follows linear rule of mixture and properties are varying across the dimensions of FG beam.

The power-law for FG beam graded across the thickness [60]:

$$P(z) = (P_c - P_m)V(z) + P_m \tag{2.1}$$

where P_c and P_{m} are Young's modulus (E), Poisson's ratio (ν), mass density (ρ), coefficient of thermal expansion (α), coefficient of moisture expansion (β), thermal conductivity coefficient (k) of ceramic and metal materials, respectively.

- **Type A:** The volume fraction function $V(z)$ for single layer FG beam

$$V(z) = \left(\frac{2z+h}{2h}\right)^p \text{ với } z \in \left[-\frac{h}{2}, \frac{h}{2}\right] \tag{2.2}$$

where p is the power-law index

- **Type B:** The volume fraction function $V(z)$ for sandwich beam with FG face sheets

$$\begin{cases} V_c^{(1)}(z) = \left(\dfrac{z - h_0}{h_1 - h_0} \right)^p ; \quad z \in [h_0, h_1] \\ V_c^{(2)}(z) = 1; \quad z \in [h_1, h_2] \\ V_c^{(3)}(z) = \left(\dfrac{z - h_3}{h_2 - h_3} \right)^p ; \quad z \in [h_2, h_3] \end{cases} \tag{2.3}$$

➢ **Type C:** The volume fraction function $V(z)$ for sandwich beam with FG core

$$\begin{cases} V_c^{(1)}(z) = 0; \quad z \in [h_0, h_1] \\ V_c^{(2)}(z) = \left(\dfrac{z - h_1}{h_2 - h_1} \right)^p ; \quad z \in [h_1, h_2] \\ V_c^{(3)}(z) = 1; \quad z \in [h_2, h_3] \end{cases} \tag{2.4}$$

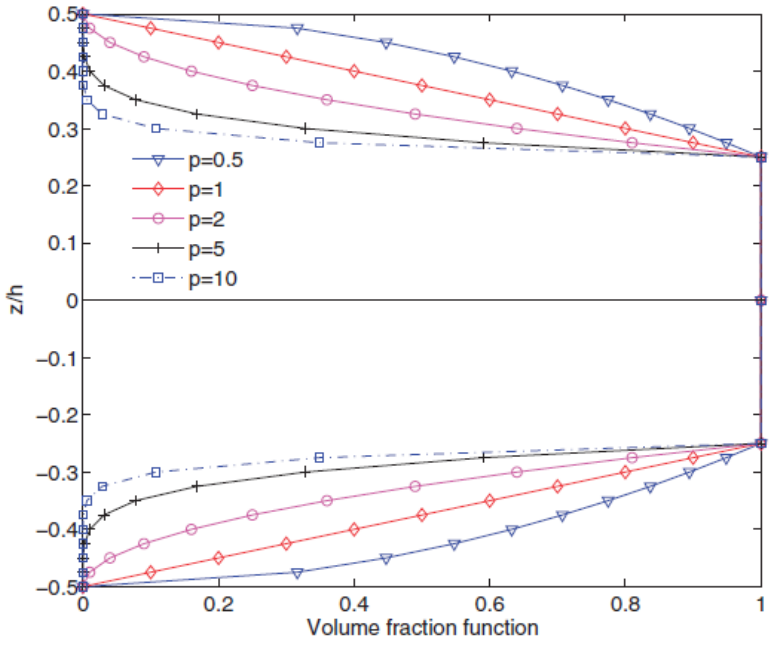

Figure 2.7 The volume fraction function $V(z)$ for the power-law (Type B).

2.2.2 Exponential function

The exponential law is more common in fracture studies of FGM beams and plates (E-FGM). It is given by Delate and Erdogan [61]. The distribution of properties of single

layer FG beams or plates across the thickness according to the exponential law is as follows:

$$P(z) = Ae^{B(z+h/2)} \tag{2.5}$$

where $A = P_m; B = \frac{1}{h}\ln\left(\frac{P_c}{P_m}\right)$ (2.6)

This form of distribution is also mentioned in the research of Mantari et al [62] (Figure 2.8).

$$P(z) = P_m e^{p\left(\frac{z}{h}+\frac{1}{2}\right)} \tag{2.7}$$

$$P_c = P_m e^p \tag{2.8}$$

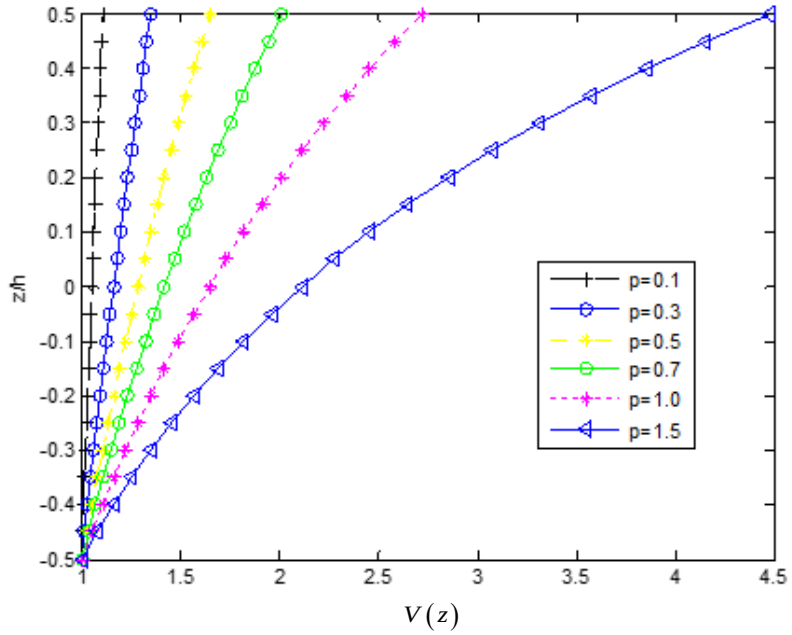

Figure 2.8 The volume fraction function $V(z)$ for the exponential-law

The exponential material distribution for bi-directional FG beams or plates across the thickness is given by:

$$P(x,z) = P_m e^{p_x\eta(x)+p_z\xi(z)} \tag{2.9}$$

with

$$\eta(x)=\frac{x}{L}+\frac{1}{2},\ \xi(z)=\frac{z}{h}+\frac{1}{2} \tag{2.10}$$

where p_x and p_z are the gradient indexes which determine the material properties through the thickness (h) and length of the beam (L), respectively. When the p_x and p_z are set to zero then the beam becomes homogeneous.

2.2.3 Sigmoid function

To reduce the abrupt variation of FG materials near the upper and lower surfaces of the beam, the material distribution using two power-law functions can be used [63], namely sigmoid function whose material volume fraction is given by the following form:

$$\begin{cases} P(z)=1-\frac{1}{2}\left(\frac{h-2z}{h}\right)^{p} & \text{for } 0\le z\le \frac{h}{2} \\ P(z)=\frac{1}{2}\left(\frac{h-2z}{h}\right)^{p} & \text{for } -\frac{h}{2}\le z\le 0 \end{cases} \tag{2.11}$$

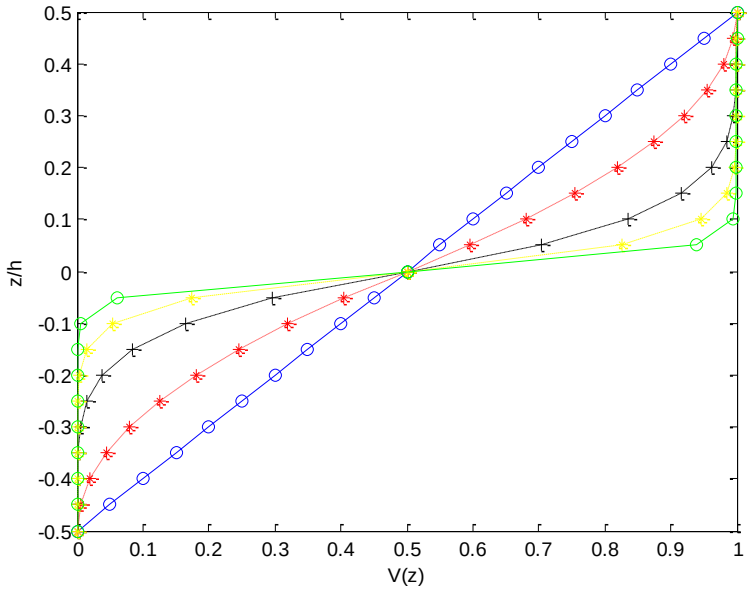

Figure 2.9 The volume fraction function $V(z)$ for the Sigmoid -law

2.3 Hygral and thermal variations in FG beams

It is known that the rises of temperature and moisture influence to behaviors of the FG beams. In order to investigate these effects, many earlier works have been realized as

mentioned in Section 2.1 in which it can be distinguished into three following different case: uniform moisture and temperature rise, linear moisture and temperature rise, nonlinear moisture and temperature rise.

2.3.1 Uniform moisture and temperature rise

In this case, the temperature and moisture are supposed to vary uniformly in the beam and increased from a reference T_0 and C_0, thus their current values of temperature and moisture are respectively followed [64].

$$\begin{aligned} T &= T_0 + \Delta T \\ C &= C_0 + \Delta C \end{aligned} \tag{2.12}$$

where T_0 and C_0 are reference temperature and moisture, respectively, which are supposed to be at the bottom surface of the beam.

2.3.2 Linear moisture and temperature rise

In this case, The temperature and moisture are linearly increased as follows [65].

$$\begin{aligned} T(z) &= (T_t - T_b)\left(\frac{2z+h}{2h}\right) + T_b \\ C(z) &= (C_t - C_b)\left(\frac{2z+h}{2h}\right) + C_b \end{aligned} \tag{2.13}$$

where T_t and T_b are temperatures as well as C_t and C_b are moisture content at the top and bottom surfaces of the beam.

2.3.3 Nonlinear moisture and temperature rise

The temperature and moisture in this case are varied nonlinearly according to a sinusoidal law [66] as follows.

$$\begin{aligned} T(z) &= (T_t - T_b)\left[1 - \cos\frac{\pi}{2}\left(\frac{2z+h}{2h}\right)\right] + T_b \\ C(z) &= (C_t - C_b)\left[1 - \cos\frac{\pi}{2}\left(\frac{2z+h}{2h}\right)\right] + C_b \end{aligned} \tag{2.14}$$

In addition, the temperature distribution obtained from Fourier equation of steady-state one-dimensional heat conduction is also considered:

$$T(z) = T_b + \frac{T_t - T_b}{\int_{-h/2}^{h/2} \frac{1}{k(z)} dz} \int_{-h/2}^{z} \frac{1}{k(z)} dz \tag{2.15}$$

2.4 Theories for behavior analysis of FG beams

The kinematics of FG beams can be represented by using the classical beam theory (CBT), the first shear deformation theory (FSDT), and higher-order shear deformation beam theories (HSDTs). It is known that the CBT neglects the effect of the transverse shear deformation, therefore it is only suitable for thin beams. The FSDT considers the effect of transverse shear deformation, it therefore predicts responses of the beam more accurate than the CBT, however practically it requires a shear correction factor to correct inadequate distribution of the transverse shear stress. To overcome this adverse, HSBT with a higher-order variation of axial displacement or both axial and transverse displacements requires no shear correction coefficient and predicts more accurate than the FSBT. Moreover, the recent researches indicate that when the behaviors of beams are considered at a small scale, the experimental studies showed that the size effect is significant to be accounted, that led to the development of Eringen's nonlocal elasticity theory, strain gradient theory, modified couple stress with different degrees of success. The following sections briefly summarize the theories for behavior analysis of FG beams.

2.4.1 Classical beam theory (CBT)

The CBT is developed by Euler–Bernoulli [67]. It is also referred to as Euler–Bernoulli beam theory. The CBT is the simplest beam theory and assumes that the plane sections which are perpendicular to the neutral layer before bending remain plane and perpendicular to the neutral layer after bending. Both transverse shear and transverse normal strains are neglected by using these assumptions.

The displacement field of the CBT can be written as:

$$u(x,z,t) = u_0(x,t) + z\frac{\partial w_0}{\partial t}$$
$$w(x,z,t) = w_0(x,t) \tag{2.16}$$

where u_0 and w_0 are the displacement of any point of the beam in x and z-directions, t is the time, respectively.

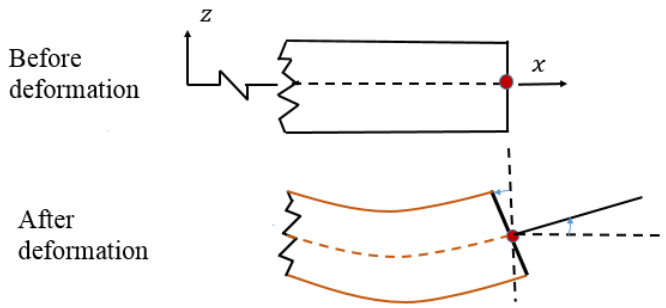

Figure 2.10 Kinematics of the Euler–Bernoulli beam

2.4.2 First-order shear deformation theory (FSDT)

The FSDT, commonly known as Timoshenko beam theory, predicts constant transverse shear stress through the thickness of beam. The FSDT assumes that the plane sections which are perpendicular to the neutral layer before bending remain plane but not necessarily perpendicular to the neutral layer after bending. The FSDT requires the shear correction factor to properly account for the effect of transverse shear deformation.

The displacement fields of Timoshenko's beam theory can be written as

$$u(x,z,t) = u_0(x,t) + z\theta(x,t)$$
$$w(x,z,t) = w_0(x,t) \tag{2.17}$$

where the comma indicates partial differentiation with respect to the coordinate subscript that follows; u_0 and θ are the axial displacement and rotation, and w_0 is the transverse displacement, respectively.

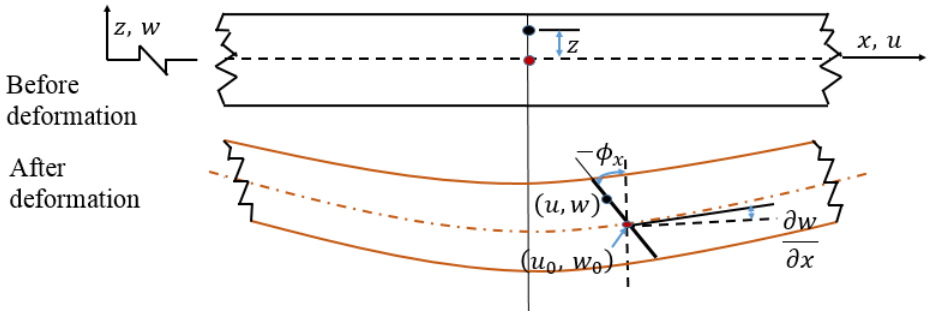

Figure 2.11 Kinematics of the Timoshenko beam

2.4.3 Higher-order shear deformation beam theories

The mentioned limitations of the CBT and FSDT led the development of HSDTs. The HSDTs use polynomial or non-polynomial shape functions to account the effect of higher-order transverse shear deformation and to get the quasi-realistic variation of transverse shear stress across the thickness of the beam. In practice, many theories have been developed with different higher-order shape functions in which the kinematics are based on higher-order variations of axial displacement. A common used HSBT is expressed as followed:

$$\begin{aligned} u(x,z,t) &= u_0(x,t) - zw_{0,x}(x,t) + f\left(z\right)\theta(x,t) \\ w(x,z,t) &= w_0(x,t) \end{aligned} \tag{2.18}$$

where *f(z)* is the shear function which is assigned with respect to realistic distribution of transverse shear stress through the thickness of the beam. It can be seen that the accuracy of present theory depends strictly on a choice of a *f*-function. Many previous works of choosing this function have been carried out with different approaches [2, 28, 68]. Moreover, when the transverse displacement is decomposed into bending part $w_b(x,t)$ and shear one $w_s(x,t)$, a refined HSBT is obtained:

$$\begin{aligned} u(x,z,t) &= u_0(x,t) - zw_{b,x}(x,t) + \left(f\left(z\right) - z\right)w_{s,x}(x,t) \\ w(x,z,t) &= w_b(x,t) + w_s(x,t) \end{aligned} \tag{2.19}$$

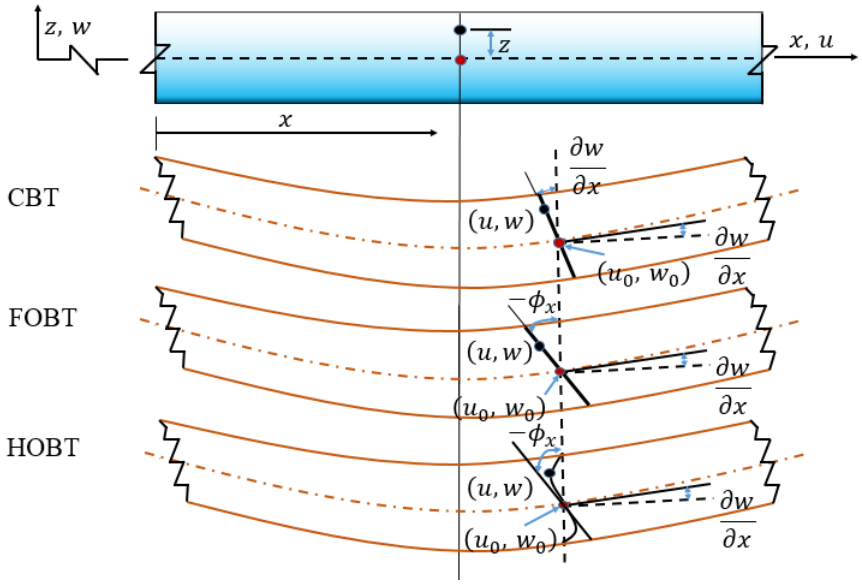

Figure 2.12 Kinematics of the CBT, FOBT, HOBT

2.4.4 Quasi-3D beam theory

In order to calculate effects of transverse normal stress and to predict more accurate behaviors of FG beams. A spread form of the HSBT is developed in which the transverse displacement is expressed in term of higher-order shear shape function so that the effect of transverse normal strain is captured. Based on this kinematic, a unified displacement field of higher order beam theory (quasi 3D beam theory) is established as follows:

$$\begin{aligned} u(x,z,t) &= u_0(x,t) - zw_{0,x} + f\left(z\right)\theta(x,t) \\ w(x,z,t) &= w_0(x,t) + g\left(z\right)w_z\left(x,t\right) \end{aligned} \tag{2.20}$$

where the comma indicates partial differentiation with respect to the coordinate subscript that follows; u_0 and θ are the axial displacement and rotation, and w_0 and w_z are the transverse displacement, respectively.

2.4.5 Review of the shear functions

A. Shear stresses in the rectangular beams

It is well known that the transverse shear stress of a rectangle section homogeneous beam is expressed by the following expression:

$$\sigma_{xz}(x,z)=\frac{QS_y}{bI_y} \tag{2.21}$$

where Q is the transverse shear force; $I_y=\frac{bh^3}{12}$ is moment of inertia of the section; b is the width of the cross section; S_y is section modulus of an area which is calculted as follows:

$$S_y=\int_{z_1}^{c} zdA=\frac{b}{2}\left(\frac{h^2}{4}-z_1^2\right) \tag{2.22}$$

Substituting Eq. (2.22) into Eq. (2.21) leads to the expression of the transverse shear stress at any given point z as follows:

$$\sigma_{xz}(x,z)=\frac{6Q}{bh^3}\left(\frac{h^2}{4}-z_1^2\right) \tag{2.23}$$

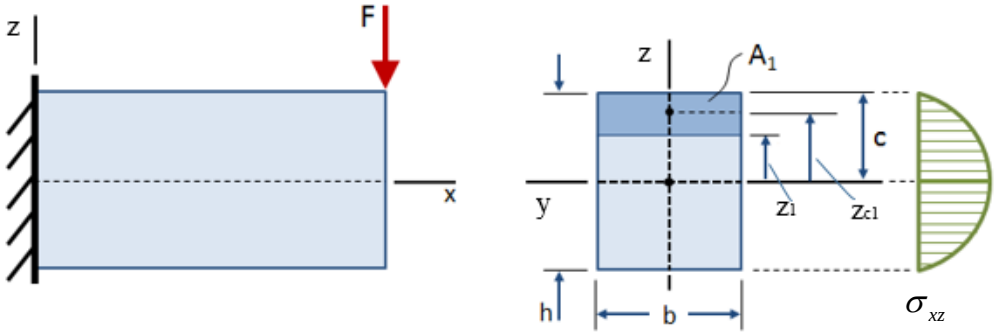

Figure 2.13 The shear stress varies over the height of the cross section

The variation of transverse shear stress through the beam depth is displaced in Figure 2.13 in which it can be seen from this figure and Eq. (2.23) that it satisfies the traction-free boundary conditions at the top and bottom surfaces of the beam and that the shear stress varies in terms of a second-order polynomial of z. Furthermore, if the displacement fields of the beams given in Eqs. (18) – (20) are considered, the shear functions of the homogeneous beams should be a third-order polynomial.

B. Review of the shear functions

Different theories can be obtained by chossing their respective shape function $f(x)$. This topic has attracted many researches with the choice of different polynomial and non-polynomial shear functions. Table 2.1 summarises some representative the shear functions.

Table 2.1 The Shear function *f(z)*

Model	*f(z)*
Polynomial function:	
Reddy[69], Murthy[70], Levinson [42]	$f(z)=z\left(1-\frac{4z^2}{3h^2}\right)$
Kaczkowski [71], Reissner [72], Panc [73]	$f(z)=z\left(\frac{5}{4}-\frac{5z^2}{3h^2}\right)$
Ambartsumian [22]	$f(z)=\frac{h^2}{8}z-\frac{z^3}{6}$
Trigonometric function:	
Nguyen et al. [74]	$f(z)=\cot^{-1}\left(\frac{h}{z}\right)-\frac{16z^3}{15h^3}$
Nguyen et al. [22]	$f(z)=h\tan^{-1}\left(\frac{rz}{h}\right)-\frac{16rz^3}{3h^2(r^2+4)};r=1$
Touratier[75], Levy[72], Stein[76]	$f(z)=\frac{h}{\pi}\sin\left(\frac{\pi z}{h}\right)$
Exponential function:	
Karama et al.[77]	$f(z)=ze^{-2(z/h)^2}$
Hyperbolic function:	
Soldatos[69]	$f(z)=h\sinh\left(\frac{z}{h}\right)-z\cosh\left(\frac{1}{2}\right)$
Akavci[73]	$f(z)=\frac{3\pi}{2}h\tanh\left(\frac{z}{h}\right)-\frac{3\pi}{2}z\,\mathrm{sech}^2\left(\frac{1}{2}\right)$

C. New of the shear functions

The idea of setting the shear function:

- Continuous function
- The deformed face is a curved face.

- Satisfy the free condition of the shear stress at the upper and lower boundary of the beam.
- A 3rd – order polynomial to account for homogeneity of the beam while another function used for gradient properties of the FGM.

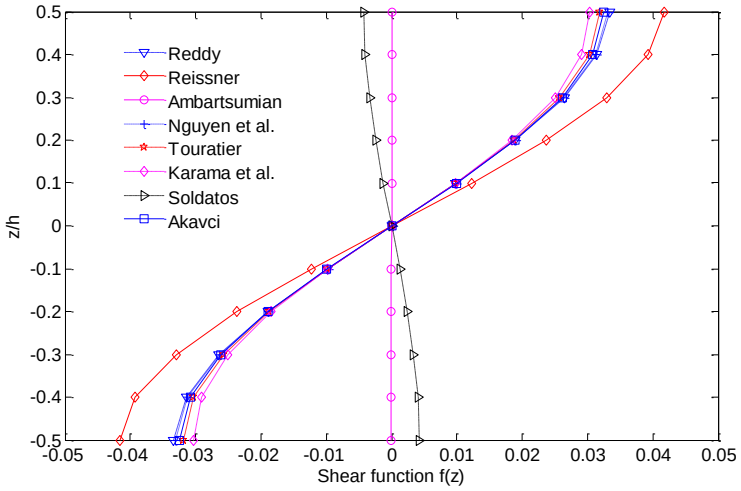

(a)

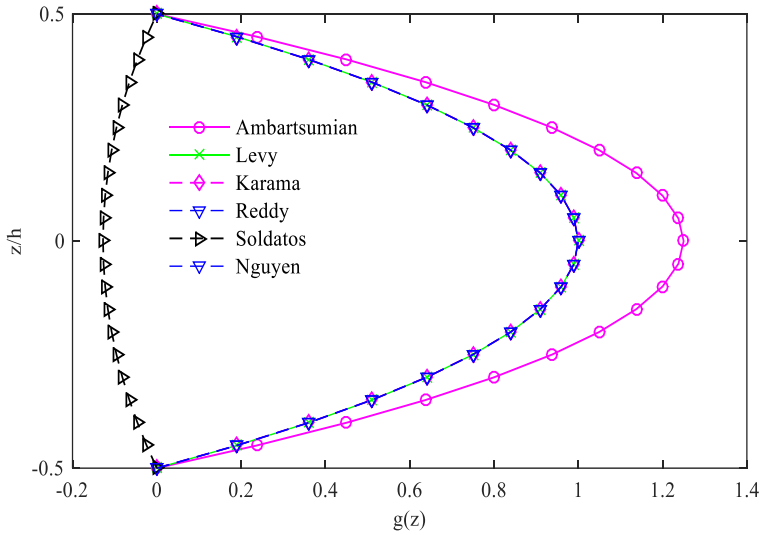

(b)

Figure 2.14 Variation of the shear functions and its derivative through the beam thickness

Therefore, the form function is selected in the following form:

$$f(z) = f_1(z) + f_2(z) = f_1(z) + \xi z^3 \tag{2.24}$$

where the coefficient ξ are constants. In Eq. (2.24), $f_2(z) = \xi z^3$ is a 3rd – order polynomial to account for homogeneity of the beam, and $f_1(z)$ is a function used for gradient properties of the FGM.

A novel higher-order shear function is proposed as follows:

$$f(z) = \sinh^{-1}\left(\frac{rz}{h}\right) - \frac{8rz^3}{3h^3\sqrt{r^2+4}} \tag{2.25}$$

and its derivative is expressed by:

$$g(z) = \frac{r}{\sqrt{r^2z^2+h^2}} - \frac{8rz^2}{h^3\sqrt{r^2+4}} \tag{2.26}$$

where a parameter *r* is introduced, namely correction parameter which enables to correct the solutions of FG beams.

2.4.6 Nonlocal elasticity and modified couple stress beam theories

Nonlocal elasticity beam theory: The experimental studies recently showed that when the behaviors of beams are considered at a small scale, the size effect is significant to be accounted. Several theories have been developed in which it can be united into Eringen's nonlocal elasticity theory, strain gradient theory, modified couple stress with different degrees of success. Based on the Eringen's nonlocal elasticity theory [78], nonlocal constitutive equations are expressed by:

$$\left(1-\mu\nabla^2\right)\sigma_{ij} = t_{ij} \tag{2.27}$$

where ∇ denotes Laplacian operator; $\mu = (e_0 a)^2$ is parameter of scale length that considers the influences of small size on the response of nanostructures with e_0 is a constant appropriate to each material, *a* is an internal characteristics length (e.g.,

latticeparameter, granular distance) and t_{ij} are global stresses. The constitutive equations of FG nano beams are hence written under the following expressions:

$$\begin{aligned}\sigma_x - \mu\sigma_{x,xx} &= \bar{Q}_{11}(z)\varepsilon_x \\ \sigma_{xz} - \mu\sigma_{xz,xx} &= \bar{Q}_{55}(z)\gamma_{xz}\end{aligned} \tag{2.28}$$

where $\bar{Q}_{11}(z) = \dfrac{E(z)}{1-\nu^2}$, $\bar{Q}_{55}(z) = \dfrac{E(z)\nu}{2(1+\nu)}$

Modified couple stress beam theory: According to the modified couple stress theory proposed by Yang et al. [12], the strain energy density is a function of both strain tensor (conjugated with stress tensor) and curvature tensor (conjugated with couple stress tensor). Then, the strain energy in a deformed isotropic linear elastic body occupying a volume V can be written as

$$U_M = \frac{1}{2}\int_V (\boldsymbol{\sigma}\boldsymbol{\varepsilon} + \mathbf{m}\boldsymbol{\chi})\, dV \tag{2.29}$$

where $\boldsymbol{\sigma}$ is the stress tensor, $\boldsymbol{\varepsilon}$ is the strain tensor, **m** is the deviatoric part of the couple stress tensor, and $\boldsymbol{\chi}$ is the symmetric curvature tensor. These tensors are defined by

$$\boldsymbol{\sigma} = \lambda tr(\varepsilon)\mathbf{I} + 2\mu\varepsilon \tag{2.30}$$

$$\mathbf{m} = 2l^2\mu\chi \tag{2.31}$$

$$\boldsymbol{\varepsilon} = \frac{1}{2}\left[\nabla\mathbf{u} + (\nabla\mathbf{u})^T\right] \tag{2.32}$$

$$\boldsymbol{\chi} = \frac{1}{2}\left[\nabla\theta + (\nabla\theta)^T\right] \tag{2.33}$$

where u is the displacement vector, λ and μ are Láme's constants, l is the material length scale parameter which reflects the effect of couple stress, and θ is the rotation vector that can be expressed as

$$\theta = \frac{1}{2}\mathrm{curl}\,\mathbf{u} \tag{2.34}$$

Based on the kinematics of the beams, the rotation around the coordinate axes *x*, *y* and *z* is added into its kinematics as follows:

$$\begin{aligned}\theta_x(x,z,t) &= \frac{1}{2}\left(u_{,y} + v_{,z}\right) = 0 \\ \theta_y(x,z,t) &= \frac{1}{2}\left(u_{,z} + w_{,x}\right) \\ \theta_z(x,z,t) &= \frac{1}{2}\left(v_{,x} - u_{,y}\right) = 0\end{aligned} \tag{2.35}$$

Substitution of Eq. (2.35) into (2.33) yields the following expression for the non-zero components of the symmetric curvature tensor

$$\chi_{xy} = \frac{\partial \theta_y}{\partial x}, \quad \chi_{zy} = \frac{\partial \theta_y}{\partial z}, \; \chi_{xx} = \chi_{yy} = \chi_{zz} = \chi_{xz} = 0 \tag{2.36}$$

2.5 Analytical and numerical methods for analysis of FG beam

Various analytical and numerical approaches have been used for the analysis of FG beams, only some representative are presented in this section. It is known that the analytical methods generally lead to the solutions with high accuracy, however its application is limited to the problems with simple geometries, boundary, and loading conditions. Therefore, for complex problems, the numerical methods are commonly used. Until now, different analytical and numerical methods are employed by researchers for analyzing FG beams such as Navier solution, Levy solution, Ritz method, differential quadrature method, Lagrange multiplier method, Chebyshev collocation method, finite element method, shooting method, meshless method etc. In this section, a literature on the use of analytical and numerical methods for the analysis of FG beams is reviewed.

2.5.1 Navier method

Navier procedure is known as the simplest one to analyse behaviours of FG beams, however this solution is only applied to the simply-supported beams. Based on this approach, the displacement variables are approximated under trigonometric functions

that satisfy the simply supported boundary conditions. For example, the displacement in Eq. (2.17) as follows,

$$u(x,t) = \sum_{j=1}^{N} u_j \cos\alpha_j x e^{i\omega t} \tag{2.37a}$$

$$w(x,t) = \sum_{j=1}^{N} w_j \sin\alpha_j x e^{i\omega t} \tag{2.37b}$$

$$\theta(x,t) = \sum_{j=1}^{N} \theta_j \cos\alpha_j x e^{i\omega t} \tag{2.37c}$$

where $\alpha_j = \frac{j\pi}{L}$, ω is the natural frequency, i^2 = -1 the imaginary unit. The transverse mechanical load q is also approximated under sinus form:

$$q(x) = \sum_{j=1}^{N} q_j \sin\alpha_j x \tag{2.38}$$

where

$$q_j = \frac{2}{L}\int_0^L q \sin\alpha_j x dx \tag{2.39}$$

where q_j is amplitude of the load. For a uniform load with density q_0, $q_j = \frac{4q_0}{j\pi}$ with j=1, 3, 5, . . .

2.5.2 Differential Quadrature Method (DQM)

The Differential Quadrature Method (DQM) was developed by Bellman and Casti [25] but it has been popularized in recent years by Jang et al. [79], Striz et al. [80], Bert et al. [76], Laura and Gutierrez [81]. This approach has been used for analysis of FG beams and plates. Liew et al.[82], Han and Liew [83] also used a similar approach to analyze irregular quadrilateral thick plates. Lam [84] introduced a mapping technique to apply the DQM for conduction, torsion, and heat flow problems with arbitrary geometries. Pradhan and Murmu [85] presented thermo-mechanical vibration analysis of FG beams. The basic idea in the DQM is to approximate the derivative of a function as a weighted linear combination of the function values at all the discrete grid points in the whole

domain of the spatial coordinate. Let consider a polynomial *P(x)*, the derivatives of order *m* of *P(x)* as a linear combination of the values $P(x_j)$ as follows:

$$P^{(m)}\left(x_i\right)=\sum_{j=1}^{N} c_{ij} P\left(x_j\right) \tag{2.40}$$

where the discrete grid points x_i and the weighting coefficients x_j can be determined by different methods [86]. The coefficients c_{ij} are determined by letting Eq. (2.40) be exact to a test function which can be chosen under polynomial, generalized polynomial Legendre. Once the weighting coefficient c_{ij} is obtained, the high order differential equations could be easily obtained by repeating the same method. Thus, any partial differential equations can be reduced to a system of linear algebraic equations. This method has been successfully applied for static, buckling and free vibration analysis of FG beams [87-90]. In practice, the disadvantages of the DQM result in the uncertainties or controversy with selecting the test functions and the grid points.

2.5.3 Ritz method

In order to avoid the limitations of Navier approach, various studies have been focused on the development of Ritz method for analysis of FG beams. Some representative previous works can be cited herein. Simsek [24] carried out static analysis of a FG simply supported beam subjected to a uniformly distributed load by using the Ritz method within the framework of Timoshenko and the higher order shear deformation beam theories. In this study, various material distributions on the displacements and the stresses of the FG beam are examined. Recently, Simsek [91] applied Euler–Bernoulli and Timoshenko beam models for the first time to investigate the buckling of beams composed of 2D-FGM. The dimensionless critical buckling load is obtained for 2D-FG beams. Pradhan and Chakraverty [23, 92, 93] presented the free vibration analysis of FG beams subjected to different sets of boundary conditions using Ritz method and Euler–Bernoulli's beam theory, Timoshenko's beam theory and HSDTs. Fazzolari [94] investigated the free vibration characteristics of metallic and FG short and slender beams with arbitrary boundary conditions. It is carried out based on advanced and refined quasi-

3D beam models by using the method of power series expansion of displacement components and the Ritz method. Chen et al. [95] presented the elastic buckling and static bending of FG porous beams with various boundary conditions and two different porosity distributions using Timoshenko's beam theory. The Ritz method is employed to obtain the critical buckling load, transverse bending deflection, and normal bending stress. The effects of porosity coefficient and slenderness ratio on the critical buckling load, maximum deflection, and associated stress distribution are discussed. Chen et al. [96] also presented the free and forced vibration characteristics of FG porous beams with non-uniform porosity distribution using Timoshenko's beam theory. Zhang [97, 98] developed a new model of the FG beams based on physical neutral surface and HSDT for the nonlinear bending and buckling analysis using the Ritz method. Wattanasakulpong et al. [99] presented free vibration of FG beams under ambient temperature based on improved third order shear deformation theory using the Ritz method. Ghiasian et al. [100] studied dynamic buckling and imperfection sensitivity of the FG Timoshenko's beam subjected to sudden uniform temperature rise by using the Ritz method.

Based on the Ritz method, the displacement variables are approximated as follows:

$$u(x,t) = \sum_{j=1}^{N} \psi_j(x) u_j(t) \tag{2.41a}$$

$$w(x,t) = \sum_{j=1}^{N} \varphi_j(x) w_j(t) \tag{2.41b}$$

$$\theta(x,t) = \sum_{j=1}^{N} \psi_j(x) \theta_j(t) \tag{2.41c}$$

Where u_j, w_j, θ_j are variables to be determined; $\psi_j(x)$ and $\varphi_j(x)$ are shape functions. It is noted that the accuracy of solution depends on choice of these functions. These shape functions can be satisfying kinetic boundary conditions, conversely a penalty function method can be used to recover the boundary conditions.

Properties of approximation functions

In order to ensure that the characteristic equations resulting from the Ritz procedure have a solution, and the approximate solution converges to the exact solution of the problem as the number of parameters N is increased, the choice of the shape function should be satisfied the following requirements [101]:

1. φ, ψ should satisfy the specified essential boundary conditions associated with the variational formulation
2. φ, ψ should satisfy the following three conditions:
   (a) Be continuous as required in the variational statement (i.e., φ, ψ should be such that it has a nonzero contribution to the virtual work statement);
   (b) Satisfy the homogeneous form of the specified essential boundary conditions;

the set φ_j, ψ_j are linearly independent and complete.

The completeness property is defined mathematically as follows. Given a function *u* and a real number $\varepsilon > 0$, the sequence φ_j, ψ_j is said to be complete if there exists an integer N (which depends on ε) and scalars $u_1, u_2, \ldots, u_N$ such that:

$$\left\| u - \sum_{j}^{N} c_j \varphi_j \right\| < \varepsilon \qquad (2.42)$$

where $\|.\|$ denotes a norm in the vector space of functions *u*. The linear independence of a set of functions φ_j refers to the property that there exists no trivial relation among them; i.e., the relation

$$\alpha_1 \varphi_1 + \alpha_2 \varphi_2 + \ldots + \alpha_N \varphi_N = 0 \qquad (2.43)$$

holds only for all $\alpha_j = 0$. Thus no function is expressible as a linear combination of others in the set.

The Ritz method can be applied, in principle, to any physical problem that can be cast in a *weak form* - a form that is equivalent to the governing equations and natural boundary

conditions of the problem. In particular, the Ritz method can be applied to all structural problems since a virtual work principle exists.

2.5.4 Finite element method

The Finite Element Method (FEM) is a well-established numerical method that can be used for a variety of engineering applications. It is a robust method that uses a systematic approach to solve complex systems by breaking the problem down into simpler forms. Polynomial shape functions are typically used, and then an element mass and stiffness matrices are produced. For modal analysis, the problem reduces into a linear eigenvalue problem, which when solved yields the natural frequencies, static, bending and mode shapes of the system. The strength of FEM lies in its versatility, complex/irregular geometries and bodies of different materials can be analyzed with relative ease. Various loading types and boundary conditions can be introduced into a model. By its advantage, many authors used the FEM for behavior analysis of FG beams, only some representative previous works are citing herein. Alshorbagy et al. [102] investigated free vibration characteristics of FG beams by using a finite element method and Euler–Bernoulli beam theory. The material constituents of beams assumed to be varying through the thickness and longitudinal directions according to a simple power law. The effects of various boundary conditions, power-law index and slenderness ratio are investigated in this study. Vo et al. [7] developed a finite element model based on a refined shear deformation theory which accounts for shear deformation effect and coupling coming from the material anisotropy to study the static and vibration analysis of FG beams with various boundary conditions. Chakraborty et al. [103] developed a new beam element to study the thermo elastic behavior of FG cantilever beam based on the FSDT. Both exponential and power law variations of material property distribution are used to examine different stress variations. It has been found that presence of FG layer in structures results in a significant difference in its response from its parent material beams due to the presence of coupled stiffness and inertial parameters. El-Ashmawy et al. [104]

carried out static and dynamic analysis of axially or transversally FG beams using the FSDT-based finite element method. Nazargah [105] investigated performance of NURBS-based is geometric approach for the coupled thermo-mechanical analysis of bidirectional FG beams using high-order global–local theory. Anandrao et al. [106, 107] studied large amplitude free vibration and thermal post-buckling of FG beams using finite element formulation based on Timoshenko's beam theory.

The beam is represented as a (disjoint) collection of finite elements $\Omega = \bigcup_{\Omega_e \in \Omega} \Omega_e$ in (Figure. 2.15).

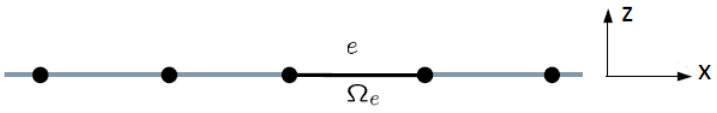

Figure 2.15 Discrete beams into finite elements.

On each element displacements and the test function are interpolated using shape functions and the corresponding nodal values.

$$u(x,t) = \sum_{j=1}^{n} \psi_j(x) u_j$$
$$w(x,t) = \sum_{j=1}^{n} \varphi_j(x) w_j \qquad (2.44)$$
$$\theta(x,t) = \sum_{j=1}^{n} \psi_j(x) \theta_j$$

where *n* is number of nodes per element, u_j, w_j, θ_j are nodal values of displacements; $\psi_j(x)$ and $\varphi_j(x)$ are the shape function of node *j*. To obtain the characteristic FE equations, the preceding approximative variables are introduced into the energy functional. It is noted that the integrals in the weak form depend on the derivatives of u, w and θ. Therefore, a continuity characteristic on the approximate function is required. A function *f*: $\Omega \to \Re$ is of class $C^k = C^k(\Omega)$ if its derivatives of order i^{th}-order, where $0 \le i \le k$ are continuous functions.

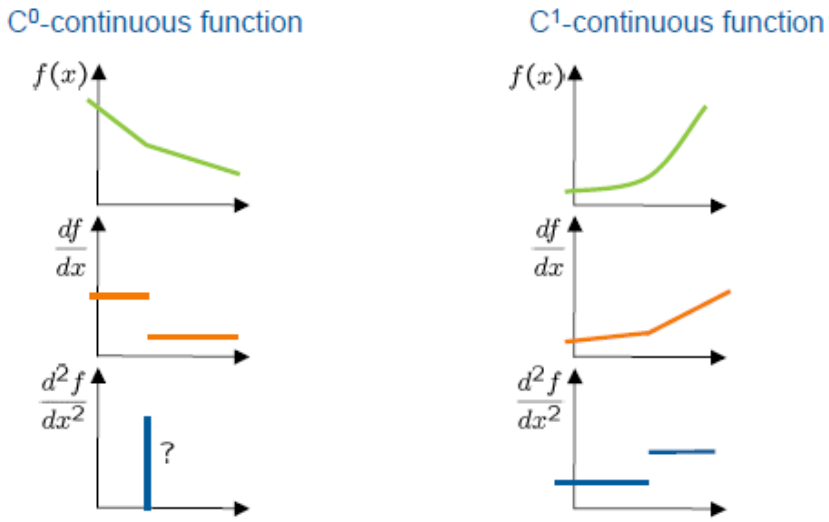

Figure 2.16 Continuous function C^0 and C^1.

For example, it is known that the weak form of energy functional of HSBT is expressed in terms of the first derivative of axial displacement *u* and rotation angle θ, and second derivative of transverse displacement *w*. Therefore, the interpolation function of *u* and θ can use linear interpolation functions which satisfy continuous condition C^0 while the Hermite interpolation function can be used for approximating the transverse displacement to satisfy continuous condition C^1. In addition, these interpolation functions need to satisfy the delta knonecker condition.

Linear shape function:

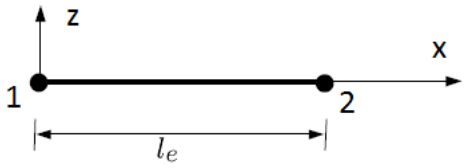

Figure 2.17 Linear shape functions for an element of length l_e

The linear shape function is the most polynomial for the two-nodes beam element in Figure 2.17 is drawn from the two displacement conditions at the two nodes, written in the following form:

$$\psi_1(x) = 1 - \frac{x}{l_e}, \psi_2(x) = \frac{x}{l_e} \tag{2.45}$$

Hermite shape function:

Hermite shape function for beams is a 3rd – order polynomial which is approximated through the value of linear displacement in the *z* direction and its derivative at the nodes. It is given as follows:

$$\varphi_1(x)=1-3\left(\frac{x}{l_e}\right)^2+2\left(\frac{x}{l_e}\right)^3;\quad \varphi_2(x)=x-\frac{2x^2}{l_e}+\frac{x^3}{l_e^2}$$
$$\varphi_3(x)=3\left(\frac{x}{l_e}\right)^2-2\left(\frac{x}{l_e}\right)^3;\quad \varphi_4(x)=-\frac{x^2}{l_e}+\frac{x^3}{l_e^2} \tag{2.46}$$

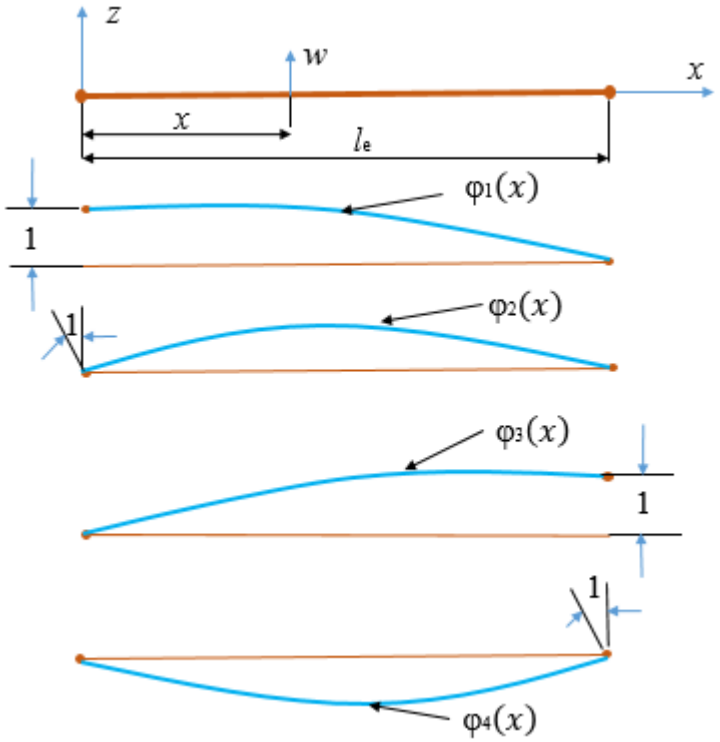

Figure 2.18 Hermite shape functions for one-dimensional finite element

2.5.5 Other methods

As mentioned in the previous section, the study on behaviors of FG beams has attracted a number of researches with different approaches. Beside Navier method, Ritz method, DQM, FEM, other methods have been used for analysis of FG beams can be listed as follows. Trinh et al. [108] presented Levy's solution for investigating vibration and

buckling behaviors of FG beams subjected to thermo-mechanical loads using Reddy's third-order shear deformation theory. Shvartsman and Majak [109] presented the method of initial parameters for the buckling analysis of FG beams resting on elastic foundation using Euler–Bernoulli's beam theory. Huynh et al. [110] analysed free vibration of bidirectional FG Timoshenko's beams using isogeometric finite element method with 1D-NURBS basis functions. Meshless methods which are the most promising ones for analysis of complex engineering problems, have been used for static and dynamic analysis of FG beams. Giunta et al. [111] presented a unified formulation of 1D beam models for the static analysis of FG beams using a meshless method based on multiquadric radial basis functions. Yang et al. [112] presented forced vibration of 2D FG beams using meshfree boundary-domain integral equation method. Qian and Ching [113] used a meshless Local Petrov–Galerkin method to study the free and forced vibration of FG cantilever beam. In this work, an orthogonal transformation technique is used to directly enforce nodal variables in the essential boundary areas, and the test function is chosen to equal the weight function of the moving least squares approximation.

2.6 Conclusions

This chapter focused on a review of literature on beam theories and solution methods for the bending, buckling, and vibration analysis of FG beams. Following conclusions can be drawn based on the literature reviewed.

- The development of higher-order shear deformation beam theories has been recently studied, however a number of researches on the development of a general HSBT is still limited. Moreover, in the whole literature, more attention is given to the analysis of the FG beams without effects of transverse normal deformations. As far as the authors are aware, these effects of transverse normal deformations are still limited available in the literature.

- The Ritz method shows an efficient and simple one in predicting behaviors of composite structures, however practically the accuracy of this approach depends on a suitable choice of the shape function. A development of the shape function of the Ritz method is also a research topic to carry out.
- Despite of many works available on the bending, buckling and vibration analysis of single layer FG beams under mechanical loads, the studies on the bending, buckling and vibration analysis of FG sandwich beams in hygro-thermo-mechanical environments are rare in the literature.
- The effect of boundary conditions on behaviors of FG microbeams is also a problem which is still not studied yet.
- A novel shear function for the higher-order shear deformation beam theory has been proposed in which it composed of a third-order polynomial and inverse hyperpolic sinus function, and that a correction parameter has also introduced to correct the solution field of FG beams.

Chapter 3

Novel higher-order shear deformation theories for analysis of isotropic and functionally graded sandwich beams

---

This chapter proposes a novel general higher-order shear deformation beam theory for analysis of isotropic and functionally graded sandwich beams. A general theoretical formulation is derived from the fundamental of two-dimensional elasticity theory and then novel higher-order shear deformation beam theories are obtained.

The highlight of this chapter is follows:

- A new unified theoretical formulation of higher-order shear deformation beam theory is established.
- A new inverse hyperbolic-sine higher-order shear deformation beam theory for analysis of functionally graded beams is proposed.
- A novel three-variable quasi-3D shear deformation theory for analysis of functionally graded beams.
- Numerical results derived the Navier and Ritz methods are compared to those from previous works in order to verify the accuracy of the proposed theories and to investigate effects of material distribution through the beam thickness, thickness ratio of layers, span-to-thickness ratio and boundary conditions on the deflection, stresses, critical buckling load and natural frequencies.

3.1 Introduction

Functionally graded (FG) materials are composite materials formed of two or more constituent phases with a continuously variable composition. Sandwich structures are widely employed in aerospace and many other industries. These structures become even more attractive due to the introduction of FG materials for the faces and the core. Typically, there are three typical FG beams: isotropic FG beams, sandwich beams with homogeneous core and FG faces, and sandwich beams with FG core and homogeneous faces. With an increase of the application of FG sandwich structures in the engineering field, understanding behaviors of FG sandwich beams becomes an important task.

For FG beams, their behaviors can be generally predicted using either three-dimensional (3D) elasticity theory or equivalent single-layer beam theories such as classical beam theory (CBT), first-order shear deformation beam theory (FSBT), third-order shear deformation beam theory (TSBT) and higher-order shear deformation beam theory (HSBT). Based on the 3D elasticity theory, Sankar [114] derived the exact solutions for bending analysis of FG beams subjected to transverse loads. Zhong and Yu [115] also used 3D elasticity theory to predict the bending responses of cantilever FG beams under concentrated and uniformly distributed loads. The bending responses of FG beams were investigated by Benatta et al. [75], Ben-Oumrane et al. [116] and Thai and Vo [117] using various equivalent single-layer beam theories. Kapuria et al. [118] presented a finite element model for static and free vibration responses of layered FG beams using third-order zigzag theory and validated against experiments for two different FGM systems under various boundary conditions. Using a unified formulation, Giunta et al. [119] presented several beam theories for the static analysis of FG beams. Chakraborty et al. [103] developed a new beam finite element based on the FSBT to study static, free vibration and wave propagation problems in bi-material beams fused with FGM layer. Li [120] presented a new unified approach for analyzing the static and dynamic behaviors of FG beams with the rotary inertia and shear deformation included. Li and

Batra [121] derived analytical relations between the critical buckling load of a FG Timoshenko's beam and that of the corresponding homogeneous Euler-Bernoulli beam subjected to axial compressive load. Kadoli et al. [122] adopted the TSBT to develop a beam finite element to study the static behavior of FG beams under uniformly distributed loads. Li et al. [123] derived analytical solutions for static and dynamic analysis of FG beams using TSBT. Based on the FSBT, Nguyen et al. [4] recently proposed the static and free vibration analysis of axially loaded FG beams in which an improved transverse shear stiffness has been introduced. It should be noted that the CBT is applicable to slender beams only. For moderately deep beams, it underestimates deflection and overestimates buckling load and natural frequencies due to ignoring the shear deformation effect. The FSBT accounts for the shear deformation effect, but requires a shear correction factor. Alternatively, the HSBT considers the shear deformation effect without requiring any shear correction factors. However, the efficiency of the HSBT depends on the appropriate choice of displacement field which is an interesting subject that attracted many research (see [7, 20, 28, 99, 116, 118, 122-128] for more details).

Although there are many works on the FG beams, the studies on behaviors of FG sandwich beams are still limited. Bhangale and Ganesan [129] studied vibration and buckling behaviors of an FG sandwich beam having constrained viscoelastic layer in thermal environment by using finite element formulation. Amirani et al. [130] used the element-free Galerkin method for free vibration analysis of sandwich beam with FG core. Bui et al. [31] investigated transient responses and natural frequencies of sandwich beams with inhomogeneous FG core using a truly mesh-free radial point interpolation method. Vo et al. [131] studied free vibration and buckling behaviors of FG sandwich beams by a finite element model using the TSBT. Nguyen et al. [5] proposed vibration and buckling analysis of FG sandwich beams with various boundary conditions using Ritz methods. In order to take into account shear and normal deformations, the quasi-3D theories are developed based on a higher-order variation of both axial and transverse

displacements. Based on 1D Carrera's Unified Formulation [132], he and his co-workers [119, 133, 134] investigated various structural problems. As far as the knowledge of the authors goes, there is still limited work on static, vibration and buckling of FG sandwich beams using a quasi-3D theory. Vo et al. [135, 136] developed finite element models to investigate FG sandwich beams using a quasi-3D polynomial theory. Mantari and Yarascab [137, 138], and Osofero et al.[139] derived Navier solution for bending, vibration and buckling of FG sandwich beams using non-polynomial quasi-3D theories, respectively.

This chapter aims to present novel unified higher-order shear deformation theories for bending, buckling and free vibration analysis of FG sandwich beams in which a new general theoretical formulation based on the framework of elasticity theory, a new inverse hyperbolic-sine shape function for a higher-order shear deformation theory and a new three-variable quasi-3D beam theory are proposed. Variational functional of Hamilton's and Lagrange's are used to derive characteristic equations of motion, and then the Navier and Ritz solution methods are applied to solve the problems. Three types of FG sandwich beams namely FG beams (Type A), FG faces and homogeneous ceramic core (Type B) and FG core and homogeneous faces (Type C) are considered. Numerical results are compared with those from previous studies and to investigate effects of the material distribution, span-to-depth ratio, skin-core-skin thickness ratios and boundary conditions on the static, buckling and free vibration behaviors of FG sandwich beams.

3.2 Novel unified theoretical formulation of higher–order shear deformation beam theories

Consider a beam in Figure 2.1 with length L and cross-section $b \times h$. In order to derive a general kinetic displacement field of the beam, a plane stress problem in (x, z) - coordinate system is supposed.

The relations of strain – stress for two-dimensional problem are given by:

$$\varepsilon_x = \frac{1}{E}\left(\sigma_x - \nu\sigma_z\right) \tag{3.1a}$$

$$\varepsilon_z = \frac{1}{E}\left(\sigma_z - \nu\sigma_x\right) \tag{3.1b}$$

$$\gamma_{xz} = \frac{1}{G}\sigma_{xz} \tag{3.1c}$$

where E, ν are Young's modulus and Poisson's ratio; $G = \frac{E}{2\left(1+\nu\right)}$ is shear modulus.

The linear relations of strains and displacements are expressed by:

$$\varepsilon_x = u_{,x}, \varepsilon_z = w_{,z}, \gamma_{xz} = u_{,z} + w_{,x} \tag{3.2}$$

where u, w are axial and transverse displacements, respectively; the comma indicates partial differentiation with respect to the coordinate subscript that follows. Substituting Eq. 3.2 into Eqs. 3.1 leads to:

$$u_{,x} = \frac{1}{E}\left(\sigma_x - \nu\sigma_z\right) \tag{3.3a}$$

$$w_{,z} = \frac{1}{E}\left(\sigma_z - \nu\sigma_x\right) \tag{3.3b}$$

$$u_{,z} + w_{,x} = \frac{1}{G}\sigma_{xz} \tag{3.3c}$$

By supposing that $\sigma_{xz}\left(x,z\right) = g_1\left(z\right)Q_x\left(x\right)$ where $Q_x\left(x\right)$ is transverse shear force, $g_1\left(z\right)$ is a shape function that satisfies the traction-free boundary conditions at the top and bottom surface of the beam. Integration Eq. 3.3b leads to:

$$w\left(x,z\right) = w_0\left(x\right) + \int_0^z \frac{1}{E}\left(\sigma_z - \nu\sigma_x\right)dz \tag{3.4}$$

and then substituting Eq. (3.4) into Eq.(3.3c) leads to:

$$u_{,z} + w_{,x} = -w_{0,x}\left(x\right) - \int_0^z \frac{1}{E}\left(\sigma_{z,x} - \nu\sigma_{x,x}\right)dz + \frac{g_1\left(z\right)}{G}Q_x\left(z\right) \tag{3.5}$$

If the effect of the integral term is neglected, the integration of Eq. (3.5) leads to:

$$u(x,z) = u_0(x) - w_{0,x} z + f_1(z) Q_x(x) \tag{3.6}$$

with $f_1(z) = \frac{g_1(z)}{G}$. Moreover, the equilibrium equations of the beams without volume forces are expressed by:

$$\sigma_{x,x} + \sigma_{xz,z} = 0\,, \quad \sigma_{xz,x} + \sigma_{z,z} = 0 \tag{3.7}$$

from which by omitting the integral coefficients, the axial and normal transverse stresses are determined from the transverse shear stress as follows:

$$\sigma_x(x,z) = -g_1'(z) R_x(x) \tag{3.8a}$$

$$\sigma_z(x,z) = -g_2(z) Q_{x,x} \tag{3.8b}$$

where,

$$R_x(x) = \int_0^x Q_x dx \tag{3.9a}$$

$$g_2(z) = \int_0^z g_1(z) dx \tag{3.9b}$$

Substituting Eqs. (3.8) into Eq. (3.4) leads to:

$$w(x,z) = w_0(x) - f_2(z) Q_{x,x} + f_3(z) R_x \tag{3.10}$$

where

$$f_2(z) = \int_0^z \frac{g_2(z)}{E} dz \tag{3.11a}$$

$$f_3(z) = \int_0^z \frac{\nu g_1'(z)}{E} dz \tag{3.11b}$$

A general formulation of the displacement field of the beam is finally obtained by Eqs. (3.6) and (3.10) as follows:

$$u(x,z) = u_0(x) - w_{0,x} z + f_1(z) Q_x(x) \tag{3.12a}$$

$$w(x,z) = w_0(x) - f_2(z) Q_{x,x} + f_3(z) R_x \tag{3.12b}$$

from which different HSBTs can be derived. It is noted that the expression given in Eq. (3.12) is a general displacement of the beam based on the elasticity theory in which both axial and transverse displacements are approximated in the beam thickness direction. If the effect of normal transverse strain is neglected, i.e. $w(x,z)=w_0(x)$, Eqs. (3.12) becomes:

$$u(x,z)=u_0(x)-w_{0,x}z+f_1(z)Q_x(x) \tag{3.13a}$$

$$w(x,z)=w_0(x) \tag{3.13b}$$

Example 1: The material properties are supposed to be constant in the beam, the transverse shear force is assumed to be expressed as follows ([140]):

$$Q_x(x)=\frac{5Gh}{6}\left(\theta_x+w_{0,x}\right) \tag{3.14}$$

Where θ_x is rotation at the mid-axis of the beam. Eqs. (3.13) lead to a novel general formulation of the HSBT as follows:

$$u(x,z)=u_0(x)+\left(\frac{5hg_2}{6}-z\right)w_{0,x}+\frac{5hg_2}{6}\theta_x(x) \tag{3.15a}$$

$$w(x,z)=w_0(x) \tag{3.15b}$$

where it holds three variables u_0, w_0, θ_x and a higher-order shape function $g_2(z)$ defined in Eq. (3.9b). It is noted that the accuracy of the theory strictly depends on a choice of the shape function. For example, taking the shape function given by Reissner [140]: $g_1(z)=\frac{3}{2h}\left(1-\frac{4z^2}{h^2}\right)$, $g_2(z)=\frac{3}{2h}\left(z-\frac{4z^3}{3h^2}\right)$ into Eq. (3.15a) leads to:

$$u(x,z)=u_0(x)+\left(\frac{z}{4}-\frac{5z^3}{3h^2}\right)w_{0,x}+\left(\frac{5z}{4}-\frac{5z^3}{3h^2}\right)\theta_x(x) \tag{3.16a}$$

$$w(x,z)=w_0(x) \tag{3.16b}$$

which is a HSBT proposed Reissner [140] and Shi [141] for analysis of plates. The earlier numerical results based on Eqs. (3.16) for the plates showed its accuracy and efficiency in predicting static and dynamic behaviors of the plates.

Example 2: Another approach is supposed that the transverse shear force is expressed under the form:

$$Q_x(x) = G\theta_x \tag{3.17}$$

that leads to another HSBT which is commonly used by many researches:

$$u(x,z) = u_0(x) - w_{0,x}z + g_2(z)\theta_x(x) \tag{3.18a}$$

$$w(x,z) = w_0(x) \tag{3.18b}$$

Example 3: For functionally graded beams, the previous work of Nguyen et al. [3, 4] revealed that the transverse shear force is expressed by:

$$Q_x(x) = H\left(\theta_x + w_{0,x}\right) \tag{3.19}$$

where the improved shear stiffness is given by:

$$H = \left[\int_{-h/2}^{h/2} \frac{\left(\bar{b}A_z + \bar{d}B_z\right)^2}{G} dz\right]^{-1} \text{ with } A_z = \int_{-h/2}^{z} Q_{11}(\xi)d\xi, B_z = \int_{-h/2}^{z} Q_{11}(\xi)d\xi \tag{3.20}$$

and $\bar{b}$, $\bar{d}$ are components of the compliance matrix (see [4] for more details). Substituting Eq. (3.19) into Eq. (3.13a) leads to another novel HSBT as follows:

$$u(x,z) = u_0(x) + \left[Hf_1(z) - z\right]w_{0,x} + Hf_1(z)\theta_x(x) \tag{3.21a}$$

$$w(x,z) = w_0(x) \tag{3.21b}$$

Example 4: In order to consider the effect of transverse normal strain, the general form of the transverse displacement in Eq. (3.12b) should be considered in which for simplicity purpose, the effect of normal stress can be neglected, that leads to:

$$u(x,z) = u_0(x) - w_{0,x}z + f_1(z)Q_x(x) \tag{3.22a}$$

$$w(x,z) = w_0(x) + f_3(z)R_x \tag{3.22b}$$

which is a general form of quasi-3D beam theory. For the shear force given in Eq. (3.17) and the material properties are supposed to a priori constant, a common quasi-3D beam theory is recovered:

$$u(x,z) = u_0(x) - w_{0,x} z + g_2(z)\theta_x(x) \tag{3.23a}$$

$$w(x,z) = w_0(x) + \frac{\nu}{2(1+\nu)} g_1(z) w_z(x) \tag{3.23b}$$

where $w_z(x) = \int_0^x \left(\theta_x + w_{0,x}\right) dx$. If the term $\frac{\nu}{2(1+\nu)}$ is neglected, the displacement field in Eqs. (3.23) is commonly used by many researches.

$$u(x,z) = u_0(x) - w_{0,x} z + g_2(z)\theta_x(x) \tag{3.24a}$$

$$w(x,z) = w_0(x) + g_1(z) w_z(x) \tag{3.24b}$$

Similarly, if the transverse shear force is taken as Eq. (3.14), a new quasi-3D beam theory is obtained as follows:

$$u(x,z) = u_0(x) + \left(\frac{5hg_2}{6} - z\right) w_{0,x} + \frac{5hg_2}{6}\theta_x(x) \tag{3.25a}$$

$$w(x,z) = w_0(x) + \frac{5\nu h}{12(1+\nu)} g_1(z) w_z(x) \tag{3.25b}$$

Moreover, if the expression of the transverse shear force in Eq. (3.19) is considered for functionally graded beams, another novel quasi-3D beam theory is obtained as follows:

$$u(x,z) = u_0(x) + \left[Hf_1(z) - z\right] w_{0,x} + Hf_1(z)\theta_x(x) \tag{3.26a}$$

$$w(x,z) = w_0(x) + Hf_3(z) w_z(x) \tag{3.26b}$$

Some novel beam models based on the higher-order shear deformation theory with higher-order variations of axial displacement or both axial and transverse displacements are summarized in Table 3.1.

Table 3.1 Unified higher-order shear deformation theories

Name	Kinematics
HSBT1	$u(x,z)=u_0(x)-w_{0,x}z+g_2(z)\theta_x(x)$
	$w(x,z)=w_0(x)$
HSBT2	$u(x,z)=u_0(x)+\left(\frac{5hg_2}{6}-z\right)w_{0,x}+\frac{5hg_2}{6}\theta_x(x)$
	$w(x,z)=w_0(x)$
HSBT3	$u(x,z)=u_0(x)+\left[Hf_1(z)-z\right]w_{0,x}+Hf_1(z)\theta_x(x)$
	$w(x,z)=w_0(x)$
Quasi-3D0	$u(x,z)=u_0(x)-w_{0,x}z+g_2(z)\theta_x(x)$
	$w(x,z)=w_0(x)+g_1(z)w_z(x)$
Quasi-3D1	$u(x,z)=u_0(x)-w_{0,x}z+g_2(z)\theta_x(x)$
	$w(x,z)=w_0(x)+\frac{\nu}{2(1+\nu)}g_1(z)w_z(x)$
Quasi-3D2	$u(x,z)=u_0(x)+\left(\frac{5hg_2}{6}-z\right)w_{0,x}+\frac{5hg_2}{6}\theta_x(x)$
	$w(x,z)=w_0(x)+\frac{5\nu h}{12(1+\nu)}g_1(z)w_z(x)$
Quasi-3D3	$u(x,z)=u_0(x)+\left[Hf_1(z)-z\right]w_{0,x}+Hf_1(z)\theta_x(x)$
	$w(x,z)=w_0(x)+Hf_3(z)w_z(x)$

Table 3.2 Unified refined higher-order shear deformation theories

Name	Kinematics
RHSBT1	$u(x,z)=u_0(x)-w^b_{0,x}z-g_2(z)w^s_{0,x}(x)$
	$w(x,z)=w^b_0(x)+w^s_0(x)$
RHSBT2	$u(x,z)=u_0(x)+\left(\frac{5hg_2}{6}-z\right)w^b_{0,x}-\frac{5hg_2}{6}w^s_{0,x}(x)$
	$w(x,z)=w^b_0(x)+w^s_0(x)$
RHSBT3	$u(x,z)=u_0(x)+\left[Hf_1(z)-z\right]w^b_{0,x}-Hf_1(z)w^s_{0,x}(x)$
	$w(x,z)=w^b_0(x)+w^s_0(x)$
Rquasi-3D0	$u(x,z)=u_0(x)-w^b_{0,x}z-g_2(z)w^s_{0,x}(x)$
	$w(x,z)=w^b_0(x)+w^s_0(x)+g_1(z)w_z(x)$
Rquasi-3D1	$u(x,z)=u_0(x)-w^b_{0,x}z-g_2(z)w^s_{0,x}(x)$
	$w(x,z)=w^b_0(x)+w^s_0(x)+\frac{\nu}{2(1+\nu)}g_1(z)w_z(x)$
Rquasi-3D2	$u(x,z)=u_0(x)+\left(\frac{5hg_2}{6}-z\right)w^b_{0,x}-\frac{5hg_2}{6}w^s_{0,x}(x)$
	$w(x,z)=w^b_0(x)+w^s_0(x)+\frac{5\nu h}{12(1+\nu)}g_1(z)w_z(x)$
Rquasi-3D3	$u(x,z)=u_0(x)+\left[Hf_1(z)-z\right]w^b_{0,x}-Hf_1(z)w^s_{0,x}(x)$
	$w(x,z)=w^b_0(x)+w^s_0(x)+Hf_3(z)w_z(x)$

Furthermore, the transverse displacement can be decomposed into a bending part and shear one: $w_0(x) = w_0^b(x) + w_0^s(x)$ and by setting $\theta_x = -w_{0,x}^s$, the displacement field given in Examples 1-4 can be rewritten to formulate refined HSBTs as Table 3.2.

3.3 Analysis of static, buckling and vibration of FG beams based on the HSBTs

In order to formulate varied functional of the FG beams based on the HSBTs proposed in Table 3.1, only the displacement field of **HSBT2** is chosen for details.

3.3.1 Kinematics, strains and stresses

The displacement field of the **HSBT2** is given by:

$$u(x,z) = u_0(x) + \bar{g}_1(z) w_{0,x} + \bar{g}_2(z)\theta_x(x) \tag{3.27a}$$

$$w(x,z) = w_0(x) \tag{3.27b}$$

where $\bar{g}_1(z) = \frac{5hg_2}{6} - z$, $\bar{g}_2(z) = \frac{5hg_2}{6}$. The non-zeros strains associated to displacements in Eqs. (3.27) are expressed by:

$$\varepsilon_x(x,z) = u_{0,x}(x) + \bar{g}_1(z) w_{0,xx} + \bar{g}_2(z)\theta_{x,x}(x) \tag{3.28a}$$

$$\gamma_{xz}(x,z) = \frac{5hg_1}{6}\left(\theta_x + w_{0,x}\right) \tag{3.28a}$$

where $g_1(z) = g_2^{'}(z)$ which is chosen under form: $g_1\left(z = \pm\frac{h}{2}\right) = 0$. The constitutive equations are therefore obtained as follows:

$$\sigma_x(x,z) = E\varepsilon_x(x,z) = E\left[u_{0,x}(x) + \bar{g}_1(z) w_{0,xx} + \bar{g}_2(z)\theta_{x,x}(x)\right] \tag{3.29a}$$

$$\sigma_{xz}(x,z) = G\gamma_{xz}(x,z) = \frac{5Ghg_1}{6}\left(\theta_x + w_{0,x}\right) \tag{3.29b}$$

It is noted from Eq. 3.29b that the transverse shear stress satisfies the traction-free boundary conditions on top and bottom surfaces of the beam.

3.3.2 Variation formulation

In order to derive the equations of motion of the beam, Hamilton's principle is used:

$$\int_0^T \delta\left(U+V-K\right)dT=0 \tag{3.30}$$

where *U, V, K* are strain energy, work done by external force and kinetic energy of the beams. The variation of the strain energy is given by:

$$\begin{aligned}\delta U &= \int_V \left(\sigma_x \delta\varepsilon_x + \sigma_{xz}\delta\gamma_{xz}\right)dV \\ &= \int_0^L \left[N_x \delta u_{0,x} + M_x^b \delta w_{0,xx} + M_x^s \delta\theta_{x,x} + Q_x\left(\delta\theta_x + \delta w_{0,x}\right)\right]dx\end{aligned} \tag{3.31}$$

where the stress resultants N_x, M_x^b, M_x^b are defined by:

$$\left(N_x, M_x^b, M_x^s\right) = \int_{-h/2}^{h/2} \sigma_x\left(1, \bar{g}_1, \bar{g}_2\right)bdz \tag{3.32a}$$

$$Q_x = \int_{-h/2}^{h/2} \frac{5hg_1(z)}{6}\sigma_{xz}bdz \tag{3.32b}$$

which can be written under the explicit form as follows:

$$N_x = Au_{0,x} + Bw_{0,xx} + B^s\theta_{x,x} \tag{3.33a}$$

$$M_x^b = Bu_{0,x} + Dw_{0,xx} + D^s\theta_{x,x} \tag{3.33b}$$

$$M_x^s = B^s u_{0,x} + D^s w_{0,xx} + H^s\theta_{x,x} \tag{3.33c}$$

$$Q_x = A^s\left(\theta_x + w_{0,x}\right) \tag{3.33d}$$

where $A, B, D, B^s, D^s, H^s, A^s$ are the stiffness's of the beams defined by:

$$\left(A, B, B^s, D, D^s, H^s\right) = \int_{-h/2}^{h/2} E(z)\left(1, \bar{g}_1, \bar{g}_2, \bar{g}_1^2, \bar{g}_1\bar{g}_2, \bar{g}_2^2\right)bdz \tag{3.34a}$$

$$A^s = \int_{-h/2}^{h/2} G\left(\frac{5hg_1}{6}\right)^2 bdz \tag{3.34b}$$

The variation of work done by transverse load *q* and axial force N_x^0 is calculated by:

$$\delta V = -\int_0^L q\delta w_0 dx - \int_0^L N_x^0 w_{0,xx}\delta w_0 dx \tag{3.35}$$

The variation of kinetic energy is expressed by:

$$\begin{aligned}
\delta K &= \int_V \rho\left(\dot{u}\delta\dot{u} + \dot{w}\delta\dot{w}\right)dV \\
&= \int_V \rho\left[\left(\dot{u}_0 + \bar{g}_1\dot{w}_{0,x} + \bar{g}_2\dot{\theta}_x\right)\left(\delta\dot{u}_0 + \bar{g}_1\delta\dot{w}_{0,x} + \bar{g}_2\delta\dot{\theta}_x\right) + \dot{w}_0\delta\dot{w}_0\right]dV \\
&= \int_0^L \Big(I_0\dot{u}_0\delta\dot{u}_0 + I_1\dot{u}_0\delta\dot{w}_{0,x} + I_2\dot{u}_0\delta\dot{\theta}_x + I_1\dot{w}_{0,x}\delta\dot{u}_0 + J_1\dot{w}_{0,x}\delta\dot{w}_{0,x} \\
&\quad + K_1\dot{w}_{0,x}\delta\dot{\theta}_x + I_2\dot{\theta}_x\delta\dot{u}_0 + K_1\dot{\theta}_x\delta\dot{w}_{0,x} + J_2\dot{\theta}_x\delta\dot{\theta}_x + I_0\dot{w}_0\delta\dot{w}_0\Big)dx
\end{aligned} \tag{3.36}$$

where the terms of inertia $I_0, I_1, I_2, J_1, J_2, K_1$ are defined by:

$$\left(I_0, I_1, I_2, J_1, K_1, J_2\right) = \int_{-h/2}^{h/2} \rho\left(1, \bar{g}_1, \bar{g}_2, \bar{g}_1^2, \bar{g}_1\bar{g}_2, \bar{g}_2^2\right)bdz \tag{3.37}$$

Substituting Eqs. (3.31), (3.35) and (3.36) into Eq. (3.30), and then integrating by part the subsequence leads to the following equilibrium equations:

$$\delta u_0 : N_{x,x} = I_0\ddot{u}_0 + I_1\ddot{w}_{0,x} + I_2\ddot{\theta}_x \tag{3.38a}$$

$$\delta w_0 : M^b_{x,xx} - Q_{x,x} - q - N_x^0 w_{0,xx} = I_0\ddot{w}_0 + I_1\ddot{u}_{0,x} + J_1\ddot{w}_{0,xx} + K_1\ddot{\theta}_{x,x} \tag{3.38b}$$

$$\delta\theta_x : M^s_{x,x} - Q_x = I_2\ddot{u}_0 + K_1\ddot{w}_{0,x} + J_2\ddot{\theta}_x \tag{3.38c}$$

Substituting Eqs. (3.33) into Eqs. (3.38) leads to:

$$Au_{0,xx} + Bw_{0,xxx} + B^s\theta_{x,xx} = I_0\ddot{u}_0 + I_1\ddot{w}_{0,x} + I_2\ddot{\theta}_x \tag{3.39a}$$

$$\begin{aligned}
&Bu_{0,xxx} + Dw_{0,xxxx} + D^s\theta_{x,xxx} - A^s\left(\theta_{x,x} + w_{0,xx}\right) - q - N_x^0 w_{0,xx} \\
&= I_0\ddot{w}_0 + I_1\ddot{u}_{0,x} + J_1\ddot{w}_{0,xx} + K_1\ddot{\theta}_{x,x}
\end{aligned} \tag{3.39b}$$

$$B^s u_{0,xx} + D^s w_{0,xxx} + H^s\theta_{x,xx} - A^s\left(\theta_x + w_{0,x}\right) = I_2\ddot{u}_0 + K_1\ddot{w}_{0,x} + J_2\ddot{\theta}_x \tag{3.39c}$$

Eqs. (3.39) are equations of motion of the beam from which the bending, buckling and vibration responses of the beam can be obtained.

3.3.3 Navier solution

The Navier solution procedure is used to determine analytical solutions for simply-supported functionally graded beams. The solution is assumed to be of the form:

$$u_0(x,t) = \sum_{m=1}^{\infty} u_m \cos \lambda x e^{i\omega t} \tag{3.40a}$$

$$w_0(x,t) = \sum_{m=1}^{\infty} w_m \sin \lambda x e^{i\omega t} \tag{3.40b}$$

$$\theta_x(x,t) = \sum_{m=1}^{\infty} \theta_m \cos \lambda x e^{i\omega t} \tag{3.40c}$$

where ω is the natural frequency, $i^2 = -1$ the imaginary unit, $\lambda = m\pi / L$.The transverse load $q(x)$ is also expressed as:

$$q(x) = \sum_{m=1}^{\infty} q_m \sin \lambda x \tag{3.41}$$

where $q_m = 4q_0 / m\pi$ ($m = 1,3,5,\ldots$, etc.) for uniformly distributed load with density q_0. Assuming that the beam is subjected to an in-plane compressive load $N_{xx}^0 = -N^0$. Substituting Eqs. (3.40) and (3.41) into Eqs. (3.39), the following characteristic problem is obtained:

$$\left(\begin{bmatrix} k_{11} & k_{12} & k_{13} \\ k_{12} & k_{22} & k_{23} \\ k_{13} & k_{23} & k_{33} \end{bmatrix} - \omega^2 \begin{bmatrix} m_{11} & m_{12} & m_{13} \\ m_{12} & m_{22} & m_{23} \\ m_{13} & m_{23} & m_{33} \end{bmatrix} \right) \begin{Bmatrix} u_m \\ w_m \\ \theta_m \end{Bmatrix} = \begin{Bmatrix} 0 \\ q_m \\ 0 \end{Bmatrix} \tag{3.42}$$

where,

$$\begin{aligned} &k_{11} = A\lambda^2, k_{12} = B\lambda^3, k_{13} = B^s\lambda^2, \\ &k_{22} = D\lambda^4 + A^s\lambda^2 - N_0\lambda^2, k_{23} = D^s\lambda^3 + A^s\lambda, \\ &k_{33} = H^s\lambda^2 + A^s; \\ &m_{11} = I_0, m_{12} = I_1\lambda, m_{13} = I_2, m_{22} = I_0 + J_1\lambda^2, \\ &m_{23} = K_1\lambda, m_{33} = J_2 \end{aligned} \tag{3.43}$$

3.4 Analysis of static, buckling and vibration of FG beams based on the Quasi-3D

In order to formulate varied functional of the FG beams based on the quasi-3Ds proposed in Table 3.1, only the displacement field of **Quasi-3D2** is chosen for details.

3.4.1 Kinematics, strains and stresses

The displacement field of **Quasi-3D2** is given by:

$$u(x,z) = u_0(x) + \bar{g}_1(z) w_{0,x} + \bar{g}_2(z) \theta_x(x) \tag{3.44a}$$

$$w(x,z) = w_0(x) + \frac{5\nu h}{12(1+\nu)} g_1(z) w_z(x) \tag{3.44b}$$

The non-zeros strains associated to displacements in Eqs. (3.44) are expressed by:

$$\varepsilon_x(x,z) = u_{0,x}(x) + \bar{g}_1(z) w_{0,xx} + \bar{g}_2(z) \theta_{x,x}(x) \tag{3.45a}$$

$$\varepsilon_z(x,z) = \frac{5\nu h}{12(1+\nu)} g_1'(z) w_z(x) \tag{3.45b}$$

$$\gamma_{xz}(x,z) = \frac{5hg_1}{6}\left[\theta_x + w_{0,x} + G w_{z,x}\right] \tag{3.45c}$$

The constitutive equations are therefore obtained as follows:

$$\begin{Bmatrix} \sigma_x \\ \sigma_z \\ \sigma_{xz} \end{Bmatrix} = \frac{E}{1-\nu^2} \begin{bmatrix} 1 & \nu & 0 \\ \nu & 1 & 0 \\ 0 & 0 & \frac{1-\nu}{2} \end{bmatrix} \begin{Bmatrix} \varepsilon_x \\ \varepsilon_z \\ \gamma_{xz} \end{Bmatrix} = \begin{bmatrix} Q_{11} & Q_{13} & 0 \\ Q_{13} & Q_{11} & 0 \\ 0 & 0 & Q_{55} \end{bmatrix} \begin{Bmatrix} \varepsilon_x \\ \varepsilon_z \\ \gamma_{xz} \end{Bmatrix} \tag{3.46}$$

Eqs. (3.45c) and (3.46) show that the transverse shear stress satisfies the traction-free boundary conditions on top and bottom surfaces of the beam.

3.4.2 Variation formulation

In order to derive the equations of motion of the beam, Hamilton's principle is used:

$$\int_0^T \delta(U + V - K)\, dT = 0 \tag{3.47}$$

where U, V, K are strain energy, work done by external force and kinetic energy of the beams. The variation of the strain energy is given by:

$$\begin{aligned}\delta U &= \int_V \left(\sigma_x \delta\varepsilon_x + \sigma_z \delta\varepsilon_z + \sigma_{xz}\delta\gamma_{xz}\right) dV \\ &= \int_0^L \left[N_x \delta u_{0,x} + M_x^b \delta w_{0,xx} + M_x^s \delta\theta_{x,x} + R_z \delta w_z + Q_x \left(\delta\theta_x + \delta w_{0,x} + \delta w_{z,x}\right)\right] dx\end{aligned} \tag{3.48}$$

where the stress resultants N_x, M_x^b, M_x^s, R_z and Q_x are defined by:

$$\left(N_x, M_x^b, M_x^s\right) = \int_{-h/2}^{h/2} \sigma_x \left(1, \bar{g}_1, \bar{g}_2\right) b dz \tag{3.49a}$$

$$R_z = \int_{-h/2}^{h/2} \frac{5\nu h}{12(1+\nu)} g_1^{'}(z)\sigma_z b dz \tag{3.49b}$$

$$Q_x = \int_{-h/2}^{h/2} \frac{5h g_1(z)}{6} \sigma_{xz} b dz \tag{3.49c}$$

which can be written under the explicit form as follows:

$$N_x = A u_{0,x} + B w_{0,xx} + B^s \theta_{x,x} + X w_z \tag{3.50a}$$

$$M_x^b = B u_{0,x} + D w_{0,xx} + D^s \theta_{x,x} + Y w_z \tag{3.50b}$$

$$M_x^s = B^s u_{0,x} + D^s w_{0,xx} + H^s \theta_{x,x} + X^s w_z \tag{3.50c}$$

$$R_z = X u_{0,x} + Y w_{0,xx} + X^s \theta_{x,x} + Y^s w_z \tag{3.50d}$$

$$Q_x = A^s \left(w_{0,x} + \theta_x + w_{z,x}\right) \tag{3.50e}$$

where $A, B, D, B^s, D^s, H^s, A^s$ are the stiffness's of the beams defined by:

$$\left(A, B, B^s, D, D^s, H^s, Y^s\right) = \int_{-h/2}^{h/2} Q_{11}(z)\left(1, \bar{g}_1, \bar{g}_2, \bar{g}_1^2, \bar{g}_1\bar{g}_2, \bar{g}_2^2, \bar{g}_{2,zz}^2\right) b dz \tag{3.51a}$$

$$\left(X, Y, X^s\right) = \int_{-h/2}^{h/2} Q_{13}(z)\left(1, \bar{g}_1, \bar{g}_2\right)\bar{g}_{2,zz} b dz \tag{3.51a}$$

$$A^s = \int_{-h/2}^{h/2} G\left(\frac{5hg_1}{6}\right)^2 b dz \tag{3.51b}$$

The variation of work done by transverse axial force N_x^0 is calculated by:

$$\delta V = -\int_0^L q\delta w_0 dx - \int_0^L N_x^0 w_{0,xx}\delta w_0 dx \tag{3.52}$$

The variation of kinetic energy is expressed by:

$$\begin{aligned}
&\delta K = \int_V \rho\left(\dot{u}\delta\dot{u} + \dot{w}\delta\dot{w}\right)dV \\
&= \int_V \rho\Big[\left(\dot{u}_0 + \bar{g}_1\dot{w}_{0,x} + \bar{g}_2\dot{\theta}_x\right)\left(\delta\dot{u}_0 + \bar{g}_1\delta\dot{w}_{0,x} + \bar{g}_2\delta\dot{\theta}_x\right) \\
&+\left(\dot{w}_0 + \frac{5hG}{6}g_1\dot{w}_z\right)\delta\left(\dot{w}_0 + \frac{5hG}{6}g_1\dot{w}_z\right)\Big]dV \\
&= \int_0^L \Big(I_0\dot{u}_0\delta\dot{u}_0 + I_1\dot{u}_0\delta\dot{w}_{0,x} + I_2\dot{u}_0\delta\dot{\theta}_x + I_1\dot{w}_{0,x}\delta\dot{u}_0 + J_1\dot{w}_{0,x}\delta\dot{w}_{0,x} \\
&+K_1\dot{w}_{0,x}\delta\dot{\theta}_x + I_2\dot{\theta}_x\delta\dot{u}_0 + K_1\dot{\theta}_x\delta\dot{w}_{0,x} + J_2\dot{\theta}_x\delta\dot{\theta}_x + I_0\dot{w}_0\delta\dot{w}_0 \\
&+L_1\dot{w}_0\delta\dot{w}_z + L_1\dot{w}_z\delta\dot{w}_0 + L_2\dot{w}_z\delta\dot{w}_z\Big)dx
\end{aligned} \tag{3.53}$$

where the terms of inertia $I_0, I_1, I_2, J_1, J_2, K_1, L_1$ and L_2 are defined by:

$$\left(I_0, I_1, I_2, J_1, K_1, J_2\right) = \int_{-h/2}^{h/2} \rho\left(1, \bar{g}_1, \bar{g}_2, \bar{g}_1^2, \bar{g}_1\bar{g}_2, \bar{g}_2^2\right)b dz \tag{3.54a}$$

$$\left(L_1, L_2\right) = \int_{-h/2}^{h/2} \rho\left(\frac{5h}{6}Gg_1, \left(\frac{5h}{6}Gg_1\right)^2\right)b dz \tag{3.54b}$$

Substituting Eqs. (3.48), (3.52) and (3.53) into Eq. (3.47), and then integrating by part the subsequence leads to the following equilibrium equations:

$$\delta u_0 : N_{x,x} = I_0\ddot{u}_0 + I_1\ddot{w}_{0,x} + I_2\ddot{\theta}_x \tag{3.55a}$$

$$\delta w_0 : M^b_{x,xx} - Q_{x,x} - q - N_x^0 w_{0,xx} = I_1\ddot{u}_{0,x} + J_1\ddot{w}_{0,xx} + I_0\ddot{w}_0 + K_1\ddot{\theta}_{x,x} + L_1\dot{w}_z \tag{3.55b}$$

$$\delta\theta_x : M^s_{x,x} - Q_x = I_2\ddot{u}_0 + K_1\ddot{w}_{0,x} + J_2\ddot{\theta}_x \tag{3.55c}$$

$$\delta w_z : R_z - Q_x = L_1 \dot{w}_0 + L_2 \ddot{w}_z \tag{3.55d}$$

Substituting Eqs. (3.50) into Eqs. (3.55) leads to:

$$Au_{0,xx} + Bw_{0,xxx} + B^s \theta_{x,xx} + Xw_{z,x} = I_0 \ddot{u}_0 + I_1 \ddot{w}_{0,x} + I_2 \ddot{\theta}_x \tag{3.56a}$$

$$\begin{aligned} Bu_{0,xxx} + Dw_{0,xxxx} + D^s \theta_{x,xxx} + Yw_{z,xx} - A^s \left(w_{0,xx} + \theta_{x,x} + w_{z,xx} \right) - q - N_x^0 w_{0,xx} \\ = I_1 \ddot{u}_{0,x} + J_1 \ddot{w}_{0,xx} + I_0 \ddot{w}_0 + K_1 \ddot{\theta}_{x,x} + L_1 \ddot{w}_z \end{aligned} \tag{3.56b}$$

$$\begin{aligned} B^s u_{0,xx} + D^s w_{0,xxx} + H^s \theta_{x,xx} + X^s w_{z,x} - A^s \left(w_{0,x} + \theta_x + w_{z,x} \right) \\ = I_2 \ddot{u}_0 + K_1 \ddot{w}_{0,x} + J_2 \ddot{\theta}_x \end{aligned} \tag{3.56c}$$

$$Xu_{0,x} + Yw_{0,xx} + X^s \theta_{x,x} + Y^s w_z - A^s \left(w_{0,x} + \theta_x + w_{z,x} \right) = L_1 \dot{w}_0 + L_2 \ddot{w}_z \tag{3.56d}$$

Eqs. (3.56) are equations of motion of the beam from which the bending, buckling and vibration responses of the beam can be obtained.

3.4.3 Navier solution

The Navier solution procedure is used to determine analytical solutions for simply-supported functionally graded beams. The solution is assumed to be of the form:

$$u_0 \left(x,t \right) = \sum_{m=1}^{\infty} u_m \cos \lambda x e^{i\omega t} \tag{3.57a}$$

$$w_0 \left(x,t \right) = \sum_{m=1}^{\infty} w_m \sin \lambda x e^{i\omega t} \tag{3.57b}$$

$$\theta_x \left(x,t \right) = \sum_{m=1}^{\infty} \theta_m \cos \lambda x e^{i\omega t} \tag{3.57c}$$

$$w_z \left(x,t \right) = \sum_{m=1}^{\infty} w_{zm} \sin \lambda x e^{i\omega t} \tag{3.57d}$$

where ω is the natural frequency, $i^2 = -1$ the imaginary unit, $\lambda = m\pi / L$ .The transverse load *q*(x) is also expressed as:

$$q\left(x \right) = \sum_{m=1}^{\infty} q_m \sin \lambda x \tag{3.58}$$

where $q_m = 4q_0 / m\pi$ ($m = 1,3,5,\ldots$, etc.) for uniformly distributed load with density q_0. Assuming that the beam is subjected to an in-plane compressive load $N_{xx}^0 = -N^0$. Substituting Eqs. (3.57) and (3.58) into Eqs. (3.56), the following characteristic problem is obtained:

$$\left(\begin{bmatrix} k_{11} & k_{12} & k_{13} & k_{14} \\ k_{12} & k_{22} & k_{23} & k_{24} \\ k_{13} & k_{23} & k_{33} & k_{34} \\ k_{14} & k_{24} & k_{34} & k_{44} \end{bmatrix} - \omega^2 \begin{bmatrix} m_{11} & m_{12} & m_{13} & m_{14} \\ m_{12} & m_{22} & m_{23} & m_{24} \\ m_{13} & m_{23} & m_{33} & m_{34} \\ m_{14} & m_{24} & m_{34} & m_{44} \end{bmatrix} \right) \begin{Bmatrix} u_m \\ w_m \\ \theta_m \\ w_{zm} \end{Bmatrix} = \begin{Bmatrix} 0 \\ q_m \\ 0 \\ 0 \end{Bmatrix} \tag{3.59}$$

where,

$$\begin{aligned}
&k_{11} = A\lambda^2,\ k_{12} = B\lambda^3, k_{13} = B^s\lambda^2, k_{14} = X\lambda, \\
&k_{21} = k_{12}, k_{22} = D\lambda^4 - A^s\lambda^2 - N_0\lambda^2 - q, \\
&k_{23} = D^s\lambda^3 - A^s\lambda, k_{24} = Y\lambda^2 - A^s\lambda^2 \\
&k_{31} = k_{13}, k_{32} = k_{23}, k_{33} = H^s\lambda^2 - A^s; k_{34} = X^s\lambda - A^s; \\
&k_{41} = k_{14}, k_{42} = k_{24}; k_{43} = k_{34}; k_{44} = Y^s - A^s\lambda; \\
&m_{11} = I_0,\ m_{12} = I_1\lambda,\ m_{13} = I_2,\ m_{14} = 0; \\
&m_{21} = m_{12},\ m_{22} = I_0 + J_1\lambda^2, m_{23} = K_1\lambda, m_{24} = L_1; \\
&m_{31} = m_{13},\ m_{32} = m_{23}, m_{33} = J_2, m_{34} = 0; \\
&m_{41} = 0,\ m_{42} = m_{24}, m_{43} = m_{34}, m_{44} = L_2;
\end{aligned} \tag{3.60}$$

3.5 A novel three-variable quasi-3D shear deformation theory

3.5.1 Displacement, strain, and stresses

The displacement field of the present theory is given by Rquasi-3D0:

$$\begin{aligned}
u(x,z,t) &= u_0(x) - zw_{b,x} + f(z)w_{s,x} \\
w(x,z,t) &= w_b(x) + w_s(x) + g(z)w_z(x)
\end{aligned} \tag{3.61}$$

where $g = 1 + f_{,z}; u_0, w_b, w_s, w_z$ are four variables at the middle-plane of the beam; the comma subscript is used to indicate differentiation of variable that follows.

The non-zeroes strains derived from the displacements in Eq. (3.61) are given by:

$$\varepsilon_x = u_{0,x} - zw_{b,xx} + fw_{s,xx}$$
$$\varepsilon_z = g_{,z} w_z \tag{3.62}$$
$$\gamma_{xz} = g\left(w_{s,x} + w_{z,x}\right)$$

The strains and stresses are related by the following elastic constitutive equation:

$$\begin{Bmatrix} \sigma_x \\ \sigma_z \\ \sigma_{xz} \end{Bmatrix} = \begin{bmatrix} \bar{Q}_{11} & \bar{Q}_{13} & 0 \\ \bar{Q}_{13} & \bar{Q}_{11} & 0 \\ 0 & 0 & \bar{Q}_{55} \end{bmatrix} \begin{Bmatrix} \varepsilon_x \\ \varepsilon_z \\ \gamma_{xz} \end{Bmatrix} \tag{3.63}$$

where $\bar{Q}_{11} = \dfrac{E(z)}{1-\nu^2}$, $\bar{Q}_{13} = \dfrac{E(z)\nu}{1-\nu^2}$, $\bar{Q}_{55} = \dfrac{E(z)\nu}{2(1+\nu)}$

Moreover, the equilibrium equations without body forces of static two-dimensional elasticity theory are given by:

$$\sigma_{x,x} + \sigma_{xz,z} = 0$$
$$\sigma_{xz,x} + \sigma_{z,z} = 0 \tag{3.64}$$

The equilibrium equations can be rewritten in terms of stress resultants by integrating Eq. (3.64) over the cross-section with boundary conditions $\sigma_{xz} = 0$ at $z = \pm h/2$ and $\sigma_{zz} = -q(x)$ at $z = h/2$. The resulting equilibrium equations are given by:

$$N_{x,x} = 0$$
$$M_{x,x} - Q_x = 0 \tag{3.65}$$
$$Q_{x,x} - q = 0$$

where the stress resultants are defined as:

$$N_x = \int_{-h/2}^{h/2} \sigma_x b dz = Au_{0,x} - Bw_{b,xx} + B^s w_{s,xx} + E^s w_z$$
$$M_x = \int_{-h/2}^{h/2} z\sigma_x b dz = Bu_{0,x} - Dw_{b,xx} + D^s w_{s,xx} + F^s w_z \tag{3.66}$$
$$Q_x = \int_{-h/2}^{h/2} \sigma_{xz} b dz = A^s\left(w_{s,x} + w_{z,x}\right)$$

where

$$\left(A,B,D,B^s,D^s\right)=\int_{-h/2}^{h/2}\left(1,z,z^2,f,zf\right)\bar{Q}_{11}bdz$$

$$\left(E^s,F^s\right)=\int_{-h/2}^{h/2}\left(1,z\right)\bar{Q}_{13}g_{,z}bdz$$

$$A^s=\int_{-h/2}^{h/2}\bar{Q}_{55}gbdz$$

Substituting Eq. (3.66) into Eq. (3.65) and setting $\beta=B/A$ yield:

$$Bu_{0,xx}-\beta Bw_{b,xxx}+\beta B^s w_{s,xxx}+\beta E^s w_{z,x}=0 \tag{3.67a}$$

$$Bu_{0,xx}-Dw_{b,xxx}+D^s w_{s,xxx}+F^s w_{z,x}-A^s\left(w_{s,x}+w_{z,x}\right)=0 \tag{3.67b}$$

$$A^s\left(w_{s,xx}+w_{z,xx}\right)-q=0 \tag{3.67c}$$

Subtracting Eq. (3.67a) to Eq. (3.67b) and then integrating the result over the beam thickness lead to:

$$w_z=\eta_1 w_{b,xx}+\eta_2 w_{s,xx}-\eta_3 w_s \tag{3.68}$$

where it is noted that the integration constant has been omitted for simplicity and coefficients η_1,η_2,η_3 are defined as:

$$\eta_1=\frac{\beta B-D}{A^s+\beta E^s-F^s},\ \eta_2=\frac{D^s-\beta B^s}{A^s+\beta E^s-F^s},\ \eta_3=\frac{A^s}{A^s+\beta E^s-F^s} \tag{3.69}$$

Substituting Eq. (3.68) into Eq. (3.61) leads to a novel three-variables Quasi-3D theory:

$$\begin{aligned}u\left(x,z,t\right)&=u_0\left(x\right)-zw_{b,x}+f\left(z\right)w_{s,x}\\ w\left(x,z,t\right)&=w_b\left(x\right)+\left(1-\eta_3 g\right)w_s\left(x\right)+g\left(z\right)\left(\eta_1 w_{b,xx}+\eta_2 w_{s,xx}\right)\end{aligned} \tag{3.70}$$

It is observed from Eq. (3.70) that there are only three unknowns in the quasi-3D beam theory. The strains are therefore, determined as follows:

$$\begin{aligned}\varepsilon_x&=u_{0,x}-zw_{b,xx}+fw_{s,xx}\\ \varepsilon_z&=-\eta_3 g_{,z}w_s+g_{,z}\left(\eta_1 w_{b,xx}+\eta_2 w_{s,xx}\right)\\ \gamma_{xz}&=g\left[\left(1-\eta_3\right)w_{s,x}+\eta_1 w_{b,xxx}+\eta_2 w_{s,xxx}\right]\end{aligned} \tag{3.71}$$

3.5.2 Variation formulation

The strain energy *U* of system is expressed by:

$$
\begin{aligned}
U &= \frac{1}{2}\int_V \left(\sigma_x \varepsilon_x + \sigma_z \varepsilon_z + \sigma_{xz}\gamma_{xz}\right) dV \\
&= \frac{1}{2}\int_0^L \Big[\left\{ \bar{Q}_{11}\left(u_{,x} - z w_{b,xx} - f w_{s,xx}\right)^2 + \bar{Q}_{11} g'^2 \left(-\eta_3 w_s + \eta_1 w_{b,xx} + \eta_2 w_{s,xx}\right)^2 \right. \\
&+ 2\bar{Q}_{13} g' \left(u_{,x} - z w_{b,xx} - f w_{s,xx}\right)\left(-\eta_3 w_s + \eta_1 w_{b,xx} + \eta_2 w_{s,xx}\right) \\
&\left. + \bar{Q}_{55} g^2 \left[\left(1-\eta_3\right) w_{s,x} + \eta_1 w_{b,xxx} + \eta_2 w_{s,xxx}\right]^2 \right\} dV
\end{aligned}
\tag{3.72}
$$

The work done V by axial compressive load is expressed by:

$$
V = -\frac{1}{2}\int_0^L N^0 \left(w_{b,x} + w_{s,x}\right)^2 dx \tag{3.73}
$$

The kinetic energy K is expressed by:

$$
\begin{aligned}
K &= \frac{1}{2}\int_V \rho\left(\dot{u}^2 + \dot{w}^2\right) dV \\
&= \frac{1}{2}\int_V \rho \left\{ \left(\dot{u}_0 - z\dot{w}_{b,x} - f\dot{w}_{s,x}\right)^2 + \left[\dot{w}_b + \left(1-\eta_3 g\right)\dot{w}_s + g\left(\eta_1 \dot{w}_{b,xx} + \eta_2 \dot{w}_{s,xx}\right)\right] \right\} dV
\end{aligned}
\tag{3.74}
$$

Lagrangian functional is used to derive the governing equations of motion:

$$
\Pi = U + V - K \tag{3.75}
$$

3.6 Solution method

3.6.1 Ritz method for solution 1

For quasi-3D2 beam theory given in Eq. (3.56), in order to derive the equations of motion, the solution field u_0, w, θ_x, and w_z are approximated as the following forms:

$$
\begin{aligned}
u\left(x,t\right) &= \sum_{j=1}^{m} u_j \psi_j\left(x\right) e^{i\omega t} \\
w\left(x,t\right) &= \sum_{j=1}^{m} w_j \varphi_j\left(x\right) e^{i\omega t} \\
\theta\left(x,t\right) &= \sum_{j=1}^{m} \theta_j \psi_j\left(x\right) e^{i\omega t} \\
w_z\left(x,t\right) &= \sum_{j=1}^{m} w_{zj} \varphi_j\left(x\right) e^{i\omega t}
\end{aligned}
\tag{3.76}
$$

where ω is the natural frequency of free vibration of the beam, $\sqrt{i} = -1$ the imaginary unit, $(u_j, w_j, \theta_j \text{ and } w_{zj})$ denotes the values to be determined, $\psi_j(x)$ and $\varphi_j(x)$ are the shape functions. To derive analytical solutions, the shape functions $\psi_j(x)$ and $\varphi_j(x)$ are chosen for various boundary conditions (S – S: Simply Supported, C-C: Clamped – Clamped, and C – F: Clamped – Free beams) as follows:

$$\psi(x) = x^{j-1}, \varphi(x) = x^{j-1} \tag{3.77}$$

In order to impose the various boundary conditions, the method of Lagrange multipliers can be used so that the Lagrangian functional of the problem is rewritten as follows:

$$\Pi^* = \Pi + \beta_i \hat{u}_i(\bar{x}) \tag{3.78}$$

where β_i are the Lagrange multipliers which are the support reactions of the problem, $\hat{u}_i(\bar{x})$ denote the values of prescribed displacement at location $\bar{x} = 0, L$.

By substituting Eq. (3.77) into the equations of motion, and using Lagrange's equations:

$$\frac{\partial \Pi^*}{\partial q_j} - \frac{d}{dt}\frac{\partial \Pi^*}{\partial \dot{q}_j} = 0 \tag{3.79}$$

with q_j representing the values of $(u_j, w_j, \theta_j, w_{zj}, \beta_j)$ that leads to:

$$\left(\begin{bmatrix} \mathbf{K}^{11} & \mathbf{K}^{12} & \mathbf{K}^{13} & \mathbf{K}^{14} & \mathbf{K}^{15} \\ {}^T\mathbf{K}^{12} & \mathbf{K}^{22} & \mathbf{K}^{23} & \mathbf{K}^{24} & \mathbf{K}^{25} \\ {}^T\mathbf{K}^{13} & {}^T\mathbf{K}^{23} & \mathbf{K}^{33} & \mathbf{K}^{34} & \mathbf{K}^{35} \\ {}^T\mathbf{K}^{14} & {}^T\mathbf{K}^{24} & {}^T\mathbf{K}^{34} & \mathbf{K}^{44} & \mathbf{K}^{45} \\ {}^T\mathbf{K}^{15} & {}^T\mathbf{K}^{25} & {}^T\mathbf{K}^{35} & {}^T\mathbf{K}^{45} & \mathbf{0} \end{bmatrix} - \omega^2 \begin{bmatrix} \mathbf{M}^{11} & \mathbf{M}^{12} & \mathbf{M}^{13} & \mathbf{0} & \mathbf{0} \\ {}^T\mathbf{M}^{12} & \mathbf{M}^{22} & \mathbf{M}^{23} & \mathbf{M}^{24} & \mathbf{0} \\ {}^T\mathbf{M}^{13} & {}^T\mathbf{M}^{23} & \mathbf{M}^{33} & \mathbf{0} & \mathbf{0} \\ \mathbf{0} & {}^T\mathbf{M}^{24} & \mathbf{0} & \mathbf{M}^{44} & \mathbf{0} \\ \mathbf{0} & \mathbf{0} & \mathbf{0} & \mathbf{0} & \mathbf{0} \end{bmatrix} \right) \begin{Bmatrix} u \\ w \\ \theta_x \\ w_z \\ \beta \end{Bmatrix} = \begin{Bmatrix} \mathbf{0} \\ \mathbf{0} \\ \mathbf{0} \\ \mathbf{0} \\ \mathbf{0} \end{Bmatrix} \tag{3.80}$$

where the components of the stiffness matrix **K** and the mass matrix **M** are given as follows:

$$
\begin{aligned}
&K_{ij}^{11} = A\int_0^L \psi_{i,x}\psi_{j,x}dx, K_{ij}^{12} = -B\int_0^L \psi_{i,x}\varphi_{j,xx}dx, K_{ij}^{13} = B^s\int_0^L \psi_{i,x}\psi_{j,x}dx,\\
&K_{ij}^{14} = X\int_0^L \psi_{i,x}\varphi_j dx, K_{ij}^{22} = D\int_0^L \varphi_{i,xx}\varphi_{j,xx}dx - N^0\int_0^L \varphi_{i,x}\varphi_{j,x}dx\\
&K_{ij}^{23} = -D^s\int_0^L \varphi_{i,xx}\psi_{j,x}dx, K_{ij}^{24} = -Y\int_0^L \varphi_{i,xx}\varphi_j dx,\\
&K_{ij}^{33} = H^s\int_0^L \psi_{i,x}\psi_{j,x}dx + A_{55}^s\int_0^L \psi_i\psi_j dx\\
&K_{ij}^{34} = Y^s\int_0^L \psi_{i,x}\varphi_j dx + A_{55}^s\int_0^L \psi_i\varphi_{j,x}dx\\
&K_{ij}^{44} = Z\int_0^L \varphi_i\varphi_j dx + A_{55}^s\int_0^L \varphi_{i,x}\varphi_{j,x}dx;\\
&M_{ij}^{11} = I_0\int_0^L \psi_i\psi_j dx, M_{ij}^{12} = -I_1\int_0^L \psi_i\varphi_{j,x}dx, M_{ij}^{13} = J_1\int_0^L \psi_i\psi_j dx,\\
&M_{ij}^{22} = I_0\int_0^L \varphi_i\varphi_j dx + I_2\int_0^L \varphi_{i,x}\varphi_{j,x}dx, M_{ij}^{23} = -J_2\int_0^L \varphi_{i,x}\psi_j dx\\
&M_{ij}^{24} = L_1\int_0^L \varphi_i\varphi_j dx, M_{ij}^{33} = K_2\int_0^L \psi_i\psi_j dx, M_{ij}^{44} = L_2\int_0^L \varphi_i\varphi_j dx
\end{aligned}
\tag{3.81}
$$

and the components of $\mathbf{K}^{15}, \mathbf{K}^{25}, \mathbf{K}^{35}, \text{and}\, \mathbf{K}^{45}$ depend on number of boundary conditions and associated prescribed displacements in the **Table 3.3.**

Table 3.3 Kinematic BCs of the beams.

BCs	Position	Value
S-S	$x=0$	$w=0$
	$x=L$	$w=0$
C-F	$x=0$	$u=0, w=0, w_{,x}=0, \theta=0, w_z=0$
	$x=L$	
C-C	$x=0$	$u=0, w=0, w_{,x}=0, \theta=0, w_z=0$
	$x=L$	$u=0, w=0, w_{,x}=0, \theta=0, w_z=0$

3.6.2 Ritz for solution 2

For three-variable quasi-3D beam theory given in Eq. (3.75), based on Ritz method, the displacement field is approximated in the following forms:

$$\begin{aligned} u(x,t) &= \sum_{j=1}^{m} \psi_j(x) u_j e^{i\omega t} \\ w_b(x,t) &= \sum_{j=1}^{m} \varphi_j(x) w_{bj} e^{i\omega t} \\ w_s(x,t) &= \sum_{j=1}^{m} \varphi_j(x) w_{sj} e^{i\omega t} \end{aligned} \tag{3.82}$$

where ω is the frequency, $i^2 = -1$ the imaginary unit; u_j, w_{bj} and w_{sj} are unknown and need to be determined; $\psi_j(x)$ and $\varphi_j(x)$ are the shape functions in Eqs. (3.77). In order to impose the various boundary conditions, the method of Lagrange multipliers can be used so that the Lagrangian functional of the problem is Eqs. (3.80).

By substituting Eq. (3.82) into the equations of motion, and using Lagrange's equations given in Eq. (3.79), that leads to:

$$\begin{bmatrix} \mathbf{K}^{11} & \mathbf{K}^{12} & \mathbf{K}^{13} & \mathbf{K}^{14} \\ {}^T\mathbf{K}^{12} & \mathbf{K}^{22} & \mathbf{K}^{23} & \mathbf{K}^{24} \\ {}^T\mathbf{K}^{13} & \mathbf{K}^{23} & \mathbf{K}^{33} & \mathbf{K}^{34} \\ {}^T\mathbf{K}^{14} & {}^T\mathbf{K}^{24} & {}^T\mathbf{K}^{24} & 0 \end{bmatrix} - \omega^2 \begin{bmatrix} \mathbf{M}^{11} & \mathbf{M}^{12} & \mathbf{M}^{13} & 0 \\ {}^T\mathbf{M}^{12} & \mathbf{M}^{22} & \mathbf{M}^{23} & 0 \\ {}^T\mathbf{M}^{13} & \mathbf{M}^{23} & \mathbf{M}^{33} & 0 \\ 0 & 0 & 0 & 0 \end{bmatrix} \begin{Bmatrix} u \\ w_b \\ w_s \\ \beta \end{Bmatrix} = \begin{Bmatrix} 0 \\ 0 \\ 0 \\ 0 \end{Bmatrix} \tag{3.83}$$

where

$$K_{\mathrm{ij}}^{11} = A\int_0^L \psi_{i,\mathrm{x}}\psi_{\mathrm{j,x}}dx, K_{\mathrm{ij}}^{12} = \left(\eta_1 E^s - B\right)\int_0^L \psi_{i,\mathrm{x}}\varphi_{j,xx}^{b}dx,$$

$$K_{\mathrm{ij}}^{13} = \left(\eta_2 E^s - B^s\right)\int_0^L \psi_{i,\mathrm{xx}}\varphi_{\mathrm{j,xx}}dx - \eta_3 E^s\int_0^L \psi_{i,\mathrm{x}}\varphi_{\mathrm{j}}dx,$$

$$K_{\mathrm{ij}}^{22} = \left(D - \eta_1 F^s + \eta_1^2 G^s\right)\int_0^L \varphi_{i,\mathrm{xx}}\varphi_{\mathrm{j,xx}}dx + \eta_1^2 Z^s\int_0^L \varphi_{i,\mathrm{xxx}}\varphi_{\mathrm{j,xxx}}dx - N^0\int_0^L \varphi_{i,\mathrm{x}}\varphi_{\mathrm{j,x}}dx$$

$$K_{\mathrm{ij}}^{23}=\left(D^{s}+\eta_1\eta_2G^{s}-\eta_2F^{s}-\eta_1Y^{s}\right)\int_0^L\varphi_{i,\mathrm{xx}}\varphi_{\mathrm{j,xx}}dx+\left(\eta_3F^{s}-\eta_1\eta_3G^{s}\right)\int_0^L\varphi_{i,\mathrm{xx}}\varphi_{\mathrm{j}}dx$$

$$+\eta_1\eta_2Z^{s}\int_0^L\varphi_{i,\mathrm{xxx}}\varphi_{\mathrm{j,xxx}}dx+\eta_1\left(1-\eta_3\right)Z^{s}\int_0^L\varphi_{i,\mathrm{xxx}}\varphi_{\mathrm{j,x}}dx-N^{0}\int_0^L\varphi_{i,\mathrm{x}}\varphi_{\mathrm{j,x}}dx,$$

$$K_{\mathrm{ij}}^{33}=\left(H^{s}+\eta_2^{2}G^{s}-\eta_2Y^{s}\right)\int_0^L\varphi_{i,\mathrm{xx}}\varphi_{\mathrm{j,xx}}dx+\left(\eta_3Y^{s}-\eta_2\eta_3G^{s}\right)\int_0^L\varphi_{i,\mathrm{xx}}\varphi_{\mathrm{j}}dx \qquad (3.84)$$

$$+\eta_3^{2}G^{s}\int_0^L\varphi_i\varphi_{\mathrm{j}}dx+\eta_2^{2}Z^{s}\int_0^L\varphi_{i,\mathrm{xxx}}\varphi_{\mathrm{j,xxx}}dx+\left(1-\eta_3\right)^{2}Z^{s}\int_0^L\varphi_{i,\mathrm{x}}\varphi_{\mathrm{j,x}}dx$$

$$+\left(1-\eta_3\right)\eta_2Z^{s}\int_0^L\varphi_{i,\mathrm{xxx}}\varphi_{\mathrm{j,x}}dx-N^{0}\int_0^L\varphi_{i,\mathrm{x}}\varphi_{\mathrm{j,x}}dx$$

$$M_{\mathrm{ij}}^{11}=I_0\int_0^L\psi_i\psi_{\mathrm{j}}dx,M_{\mathrm{ij}}^{12}=-I_1\int_0^L\psi_i\varphi_{\mathrm{j,x}}dx,M_{\mathrm{ij}}^{13}=-J_1\int_0^L\psi_i\varphi_{\mathrm{j,x}}dx,$$

$$M_{\mathrm{ij}}^{22}=I_0\int_0^L\varphi_i\varphi_{\mathrm{j}}dx+I_2\int_0^L\varphi_{i,\mathrm{x}}\varphi_{\mathrm{j,x}}dx+\eta_1^{2}L_2\int_0^L\varphi_{i,\mathrm{xx}}\varphi_{\mathrm{j,xx}}dx+\eta_1L_1\int_0^L\varphi_i\varphi_{\mathrm{j,xx}}dx,$$

$$M_{\mathrm{ij}}^{23}=J_2\int_0^L\varphi_{i,\mathrm{x}}\varphi_{\mathrm{j,x}}dx+\eta_1\eta_2L_2\int_0^L\varphi_{i,\mathrm{xx}}\varphi_{\mathrm{j,xx}}dx+\eta_2L_1\int_0^L\varphi_i\varphi_{\mathrm{j,xx}}dx+\left(I_0-\eta_3L_1\right)\int_0^L\varphi_i\varphi_{\mathrm{j}}dx+\eta_1\left(L_1-\eta_3L_2\right)\int_0^L\varphi_{i,\mathrm{xx}}\varphi_{\mathrm{j}}dx$$

$$M_{\mathrm{ij}}^{33}=K_2\int_0^L\varphi_{i,\mathrm{x}}\varphi_{\mathrm{j,x}}dx+\eta_2^{2}L_2\int_0^L\varphi_{i,\mathrm{xx}}\varphi_{\mathrm{j,xx}}dx+\left(I_0-\eta_3L_1+\eta_3^{2}L_2\right)\int_0^L\varphi_i\varphi_{\mathrm{j}}dx+\eta_2\left(L_1-\eta_3L_2\right)\int_0^L\varphi_{i,\mathrm{xx}}\varphi_{\mathrm{j}}dx$$

with

$$\left(H^{s},G^{s}\right)=\int_{-h/2}^{h/2}\left(f^{2},g'^{2}\right)\bar{Q}_{11}bdz$$

$$Y^{s}=\int_{-h/2}^{h/2}\bar{Q}_{13}fg'\left(z\right)bdz$$

$$Z^{s}=\int_{-h/2}^{h/2}\bar{Q}_{55}g^{2}bdz$$

$$\left(I_0,I_1,I_2,J_1,J_2,K_2,L_1,L_2\right)=\int_{-h/2}^{h/2}\rho\left(z\right)\left(1,z,z^{2},f,zf,f^{2},g,g^{2}\right)bdz$$

The buckling and natural frequencies of the FG beams will be determined by solving Eq. (3.83).

3.7 Numerical results and discussion

Several numerical examples are analyzed in this section to verify the accuracy of present study and investigate the deflections, stresses, natural frequencies and critical buckling loads of FG sandwich beams. Unless mentioned otherwise, three types of FG beams (Types A, B and C) are constituted by a mixture of isotropic ceramic (Al_2O_3) and metal (Al).

The material properties of Aluminum (Al) are $E = 70GPa, \nu = 0.3, \rho = 2707kg/m^3$ and those of Alumina (Al_2O_3) are $E = 380GPa, \nu = 0.3, \rho = 3960kg/m^3$.

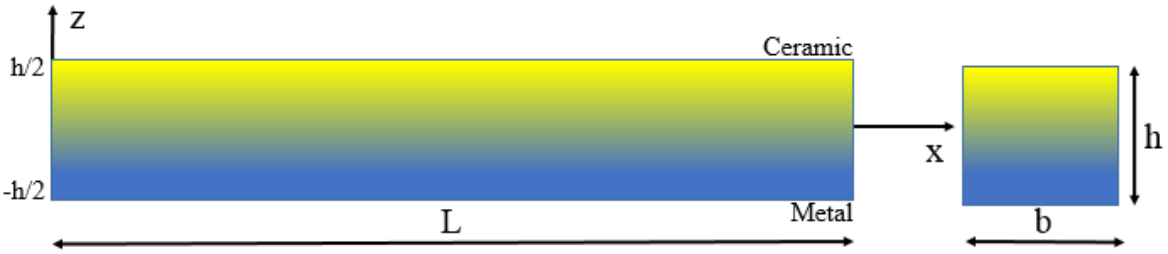

(a) **Type A:** FG beams

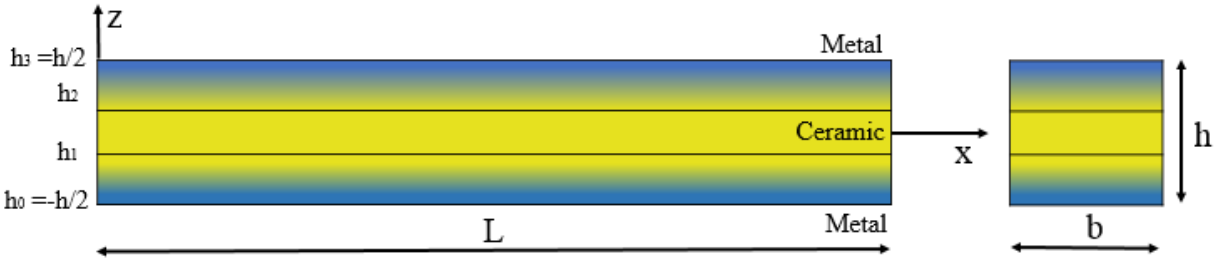

(b) **Type B:** Sandwich beams with FG-faces, Ceramic-core

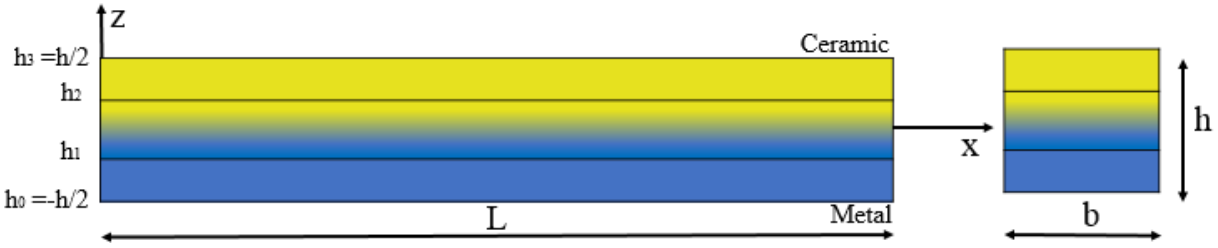

(c) **Type C:** Sandwich beams with FG-core, homogeneous-faces

Figure 3.1 Geometry of FG sandwich beams.

Unless mentioned otherwise, three types of FG beams (Types A, B and C) are constituted by a mixture of isotropic ceramic (Al_2O_3) and metal (Al).

- Hard core: Homogeneous core with $\mathrm{Al_2O_3}\left(E_b,\nu_b,\rho_b\right)$ and FG faces with top and bottom surfaces made of $\mathrm{Al}\left(E_t,\nu_t,\rho_t\right)$.
- Soft core: Homogeneous core with $\mathrm{Al}\left(E_b,\nu_b,\rho_b\right)$ and FG faces with top and bottom surfaces made of $\mathrm{Al_2O_3}\left(E_t,\nu_t,\rho_t\right)$.

The material property distribution of FG sandwich beams through the beam height is given by the power-law form:

$$P(z)=(P_c-P_m)V_c\,(z)+P_m \tag{3.85}$$

where P_c and P_m are Young's moduli (E), Poisson's ratio (ν), mass density (ρ) of ceramic and metal materials, respectively. $V_c(z)$ is the volume fraction of ceramic materials given in Eqs (2.2) - (2.4).

Moreover, for convenience, the following non-dimensional parameters are used

$$\begin{aligned}&\bar{w}=\frac{wh^3}{12}\frac{384E_m}{5q_0L^4},\bar{\sigma}_{xx}\left(z\right)=\sigma_{xx}\left(\frac{L}{2},z\right)\frac{h}{q_0L},\bar{\sigma}_{xz}\left(z\right)=\sigma_{xz}\left(0,z\right)\frac{h}{q_0L}\\&\bar{N}_{cr}=N_{cr}\frac{12L^2}{E_mh^3},\varpi=\frac{\omega L^2}{h}\sqrt{\frac{\rho_m}{E_m}}\end{aligned} \tag{3.86}$$

where E_m,ρ_m are Young's modulus and Poisson's ratio of metal, respectively.

Example 1: Vibration and buckling responses of RHSBT1, HSBT2 and quasi-3D2 FG beams (Type A, S-S)

For verification purpose, Tables 3.5 and 3.6 present the comparisons of the non-dimensional fundamental frequencies and critical buckling loads of $\mathrm{Al/Al_2O_3}$ FG beams with S-S BCs (Type A), various values of the power-law index *p* and two span-to-height ratio *L/h* = 5, 20 are considered. It is noted that the present numerical results are calculated by the following beam models: Those of HSBT2 and Quasi-3D2 with

$g_1(z)=\frac{3}{2h}\left(1-\frac{4z^2}{h^2}\right)$, $g_2(z)=\frac{3}{2h}\left(z-\frac{4z^3}{3h^2}\right)$ while that of RHSBT1, Rquasi-3D1 with novel shear function $f(z)=\sinh^{-1}\left(\frac{rz}{h}\right)-\frac{8rz^3}{3h^3\sqrt{r^2+4}}$ with r=1. The obtained results are compared to those from the HSBT [5] and the third-order shear deformation beam theory (TSBT) [117].

It is seen that the solutions obtained from the proposed theory are in well agreements with those obtained from previous results for both deep and thin beams. In addition, the fundamental frequencies and critical buckling loads of the FG beams calculated from quasi-3D2 are smaller than the HSBTs. It shows that the transverse normal effect in quasi-3D makes the beam softer.

On the other hand, in Tables 3.4-3.5, the results of Rquasi-3D0^{3V} show that the effects on FG beams are reasonable but it is not as expected. So the thesis will not continue to develop for Rquasi-3D0^{3V}.

Table 3.4 Non-dimensional fundamental frequency ($\bar{\omega}$) of FG beams with S-S boundary conditions (Type A).

L/h	Theory	*p*					
		0	0.5	1	2	5	10
5	HSBT1 [5]	5.1528	4.4102	3.9904	3.6264	3.4011	3.2816
	TSBT [117]	5.1527	4.4107	3.9904	3.6264	3.4012	3.2816
	HSBT2	5.1527	4.4088	3.9904	3.6264	3.4012	3.2817
	RHSBT1	5.3924	4.5900	4.1462	3.7777	3.5933	3.4907
	Quasi-3D2	4.4870	3.7518	3.4345	3.2383	3.1657	3.0680
	Rquasi-3D0^{3V}	3.7261	3.1642	2.9726	2.9064	2.9318	2.7975
20	HSBT[5]	5.4603	4.6506	4.2051	3.8361	3.6485	3.5390
	TSBT [117]	5.4603	4.6511	4.2051	3.8361	3.6485	3.5390
	HSBT2	5.4603	4.6492	4.2050	3.8361	3.6485	3.5391
	RHSBT1	5.4659	4.6547	4.2087	3.8397	3.6533	3.5442
	Quasi-3D2	3.5424	2.9693	2.7368	2.5891	2.4650	2.3598
	Rquasi-3D0^{3V}	3.7385	3.1794	2.9894	2.9217	2.9399	2.8021

3V: A three-variable quasi-3D

Table 3.5 Non-dimensional critical buckling load ($\bar{N}_{cr}$) of FG beams with S-S boundary conditions (Type A).

L/h	Theory	*p*					
		0	0.5	1	2	5	10
5	HSBT1 [5]	48.8402	32.0011	24.6893	19.1581	15.7373	14.1456
	TSBT [117]	48.8401	32.0094	24.6911	19.1605	15.7400	14.1468
	HSBT2	48.8400	31.9816	24.6891	19.1583	15.7386	14.1466
	RHSBT1	53.5265	34.6904	26.6838	20.8259	17.6121	16.0426
	Quasi-3D2	36.2031	22.5337	17.8194	14.9778	13.4697	12.2279
	Rquasi-3D0^{3V}	24.3760	15.6845	13.0268	11.6938	11.1452	9.8261
20	HSBT1 [5]	53.2546	34.5401	26.5696	20.7249	17.4914	15.9176
	HSBT2	53.2545	34.5188	26.5694	20.7249	17.4917	15.9181
	RHSBT1	53.3841	34.6132	26.6240	20.7710	17.5447	15.9727
	Quasi-3D2	48.4228	31.1342	24.1390	19.1794	16.5068	15.0284
	Rquasi-3D0^{3V}	24.8806	16.0882	13.3807	11.9786	11.3164	9.9445

3V: The three-variable quasi-3D

Example 2: Bending, buckling and vibration responses of RHSBT1 FG beams (Type B, S-S)

For verification purpose, Tables 3.6–3.9 present the comparisons of the non-dimensional fundamental frequencies and critical buckling loads of Al/Al_2O_3 sandwich beams with homogeneous hardcore and soft core.

For verification purpose further and investigate effects of the thickness ratio of layer and span-to-thickness ratio on the bending, buckling and vibration behaviors of FG sandwich beams, Tables 3.6–3.9 present the comparisons of the non-dimensional fundamental frequencies and critical buckling loads of Al/Al_2O_3 sandwich beams with homogeneous hardcore and soft core. The results are estimated for six schemes of thickness ratio of layers, various values of the power-law index p and the two span-to-height ratio (*L/h*= 5 and 20), and compared to those obtained by Vo et al. [131] based on the TSBT. It is seen from these tables that there are no significant differences between the present solutions and those of [131] for both buckling and vibration behaviors.

Moreover, the effects of the power-law index and thickness ratio of layers on the fundamental frequency and critical buckling load are also displayed in Figures 3.2 and 3.3. These figures show that the fundamental frequency and critical buckling load

decrease with an increase of the power-law index for FG sandwich beams with homogeneous hardcore, and inversely they increase with *p* for homogeneous soft core.

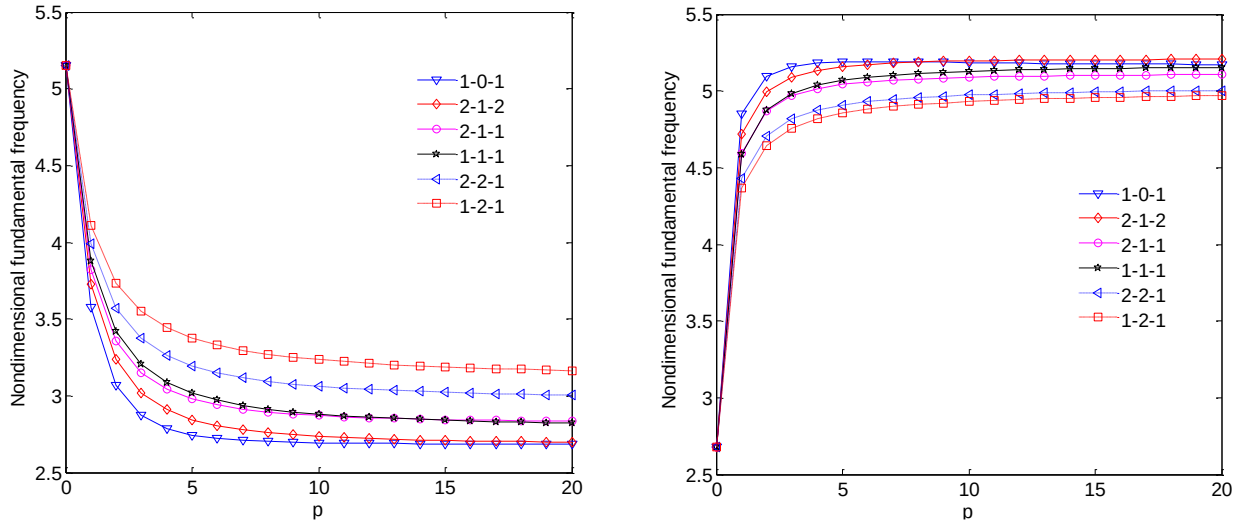

(a) Homogeneous hard core (b) Homogeneous soft core

Figure 3.2 Effect of the power-law index *p* on the non-dimensional fundamental frequency ($\bar{\omega}$) of FG sandwich beams (Type B, *L*/*h*=5).

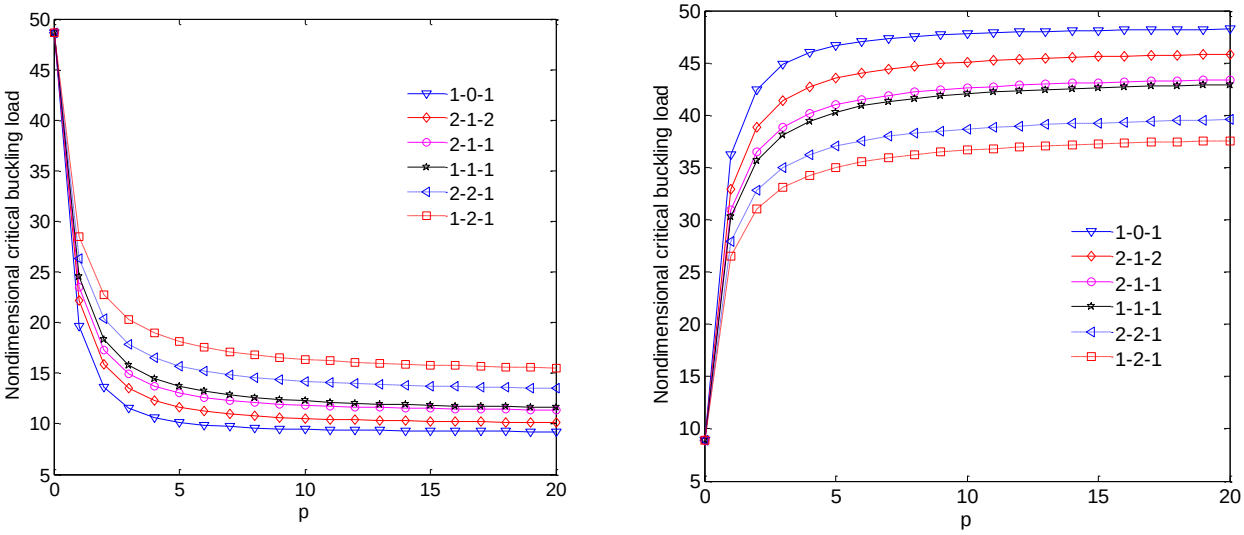

(a) Homogeneous hard core (b) Homogeneous soft core

Figure 3.3 Effect of the power-law index *p* on the non-dimensional critical buckling load ($\bar{N}_{cr}$) of FG sandwich beams (Type B, *L*/*h*=5).

That can be explained by the fact that the higher value of *p* corresponds to higher portion of metal phase, and thus makes the beams become softer. It can be observed from these figures that the lowest and highest values of the fundamental frequency and critical buckling load correspond to the (1-0-1) and (1-2-1) sandwich beams with homogeneous hardcore, and inversely for homogeneous soft core.

Table 3.6 Non-dimensional fundamental frequency $(\bar{\omega})$ of Al/Al_2O_3 sandwich beams (Type B, Homogeneous hardcore).

L/h	*p*	Theory	1-0-1	2-1-2	2-1-1	1-1-1	2-2-1	1-2-1
5	0	RHSBT1	5.1528	5.1528	5.1528	5.1528	5.1528	5.1528
		Vo et al [131]	5.1528	5.1528	5.1528	5.1528	5.1528	5.1528
	0.5	RHSBT1	4.1254	4.2340	4.2943	4.3294	4.4045	4.4791
		Vo et al [131]	4.1268	4.2351	4.2945	4.3303	4.4051	4.4798
	1	RHSBT1	3.5735	3.7298	3.8206	3.8756	3.9911	4.1105
		Vo et al [131]	3.5735	3.7298	3.8187	3.8755	3.9896	4.1105
	5	RHSBT1	2.7448	2.8440	2.9789	3.0181	3.1965	3.3771
		Vo et al [131]	2.7446	2.8439	2.9746	3.0181	3.1928	3.3771
	10	RHSBT1	2.6934	2.7356	2.8715	2.8809	3.0629	3.2357
		Vo et al [131]	2.6932	2.7355	2.8669	2.8808	3.0588	3.2356
20	0	RHSBT1	5.4603	5.4603	5.4603	5.4603	5.4603	5.4603
		Vo et al [131]	5.4603	5.4603	5.4603	5.4603	5.4603	5.4603
	0.5	RHSBT1	4.3132	4.4278	4.4960	4.5315	4.6158	4.6972
		Vo et al [131]	4.3148	4.4290	4.4970	4.5324	4.6170	4.6979
	1	RHSBT1	3.7147	3.8768	3.9775	4.0328	4.1603	4.2889
		Vo et al [131]	3.7147	3.8768	3.9774	4.0328	4.1602	4.2889
	5	RHSBT1	2.8440	2.9311	3.0776	3.1111	3.3030	3.4921
		Vo et al [131]	2.8439	2.9310	3.0773	3.1111	3.3028	3.4921
	10	RHSBT1	2.8042	2.8188	2.9665	2.9662	3.1616	3.3406
		Vo et al [131]	2.8041	2.8188	2.9662	2.9662	3.1613	3.3406

Table 3.7 Non-dimensional fundamental frequency $(\bar{\omega})$ of Al/Al_2O_3 sandwich beams (Type B, Homogeneous soft core).

L/h	*p*	Theory	1-0-1	2-1-2	2-1-1	1-1-1	2-2-1	1-2-1
5	0	RHSBT1	2.6773	2.6773	2.6773	2.6773	2.6773	2.6773
		Vo et al [131]	2.6773	2.6773	2.6773	2.6773	2.6773	2.6773
	0.5	RHSBT1	4.4437	4.3052	4.1998	4.1844	4.0549	3.9926
		Vo et al [131]	4.4427	4.3046	4.1960	4.1839	4.0504	3.9921
	1	RHSBT1	4.8519	4.7168	4.5947	4.5848	4.4305	4.3656
		Vo et al [131]	4.8525	4.7178	4.5916	4.5858	4.4270	4.3663
	5	RHSBT1	5.1876	5.1592	5.0422	5.0687	4.9070	4.8547
		Vo et al [131]	5.1880	5.1603	5.0399	5.0703	4.9038	4.8564
	10	RHSBT1	5.1846	5.1957	5.0885	5.1286	4.9730	4.9307
		Vo et al [131]	5.1848	5.1966	5.0866	5.1301	4.9700	4.9326
20	0	RHSBT1	2.8371	2.8371	2.8371	2.8371	2.8371	2.8371
		Vo et al [131]	2.8371	2.8371	2.8371	2.8371	2.8371	2.8371
	0.5	RHSBT1	4.8594	4.7473	4.6065	4.6305	4.4630	4.4168
		Vo et al [131]	4.8579	4.7460	4.6050	4.6294	4.4611	4.4160
	1	RHSBT1	5.2990	5.2216	5.0544	5.1159	4.9124	4.8937
		Vo et al [131]	5.2990	5.2217	5.0541	5.1160	4.9121	4.8938
	5	RHSBT1	5.5645	5.6381	5.4836	5.6241	5.4169	5.4841
		Vo et al [131]	5.5645	5.6382	5.4834	5.6242	5.4166	5.4843
	10	RHSBT1	5.5302	5.6451	5.5074	5.6620	5.4670	5.5573
		Vo et al [131]	5.5302	5.6452	5.5073	5.6621	5.4667	5.5575

Table 3.8 Non-dimensional critical buckling load $\left(\bar{N}_{cr}\right)$ of Al/Al_2O_3 sandwich beams (Type B, Homogeneous hardcore).

L/h	*p*	Theory	1-0-1	2-1-2	2-1-1	1-1-1	2-2-1	1-2-1
5	0	RHSBT1	48.5960	48.5960	48.5960	48.5960	48.5960	48.5960
		Vo et al [131]	48.5960	48.5960	48.5960	48.5960	48.5960	48.5960
	0.5	RHSBT1	27.8374	30.0141	31.0576	31.8649	33.2339	34.7551
		Vo et al [131]	27.8574	30.0301	31.0728	31.8784	33.2536	34.7653
	1	RHSBT1	19.6531	22.2113	23.5246	24.5598	26.3609	28.4444
		Vo et al [131]	19.6525	22.2108	23.5246	24.5596	26.3611	28.4447
	5	RHSBT1	10.1473	11.6685	13.0272	13.7218	15.7307	18.0914
		Vo et al [131]	10.1460	11.6676	13.0270	13.7212	15.7307	18.0914
	10	RHSBT1	9.4526	10.5356	11.8372	12.2611	14.1995	16.3787
		Vo et al [131]	9.4515	10.5348	11.8370	12.2605	14.1995	16.3783
20	0	RHSBT1	53.2364	53.2364	53.2364	53.2364	53.2364	53.2364
		Vo et al [131]	53.2364	53.2364	53.2364	53.2364	53.2364	53.2364
	0.5	RHSBT1	29.6965	32.0367	33.2217	34.0722	35.6202	37.3054
		Vo et al [131]	29.7175	32.2629	33.2376	34.0862	35.6405	37.3159
	1	RHSBT1	20.7213	23.4212	24.8793	25.9588	27.9537	30.2307
		Vo et al [131]	20.7212	23.4211	24.8796	25.9588	27.9540	30.2307
	5	RHSBT1	10.6175	12.0885	13.5519	14.2285	16.3829	18.8874
		Vo et al [131]	10.6171	12.0883	13.5523	14.2284	16.3834	18.8874
	10	RHSBT1	9.9849	10.9074	12.3080	12.6819	14.7520	17.0445
		Vo et al [131]	9.9847	10.9075	12.3084	12.6819	14.7525	17.0443

Table 3.9 Non-dimensional critical buckling load $\left(\bar{N}_{cr}\right)$ of Al/Al_2O_3 sandwich beams (Type B, Homogeneous soft core).

L/h	*p*	Theory	1-0-1	2-1-2	2-1-1	1-1-1	2-2-1	1-2-1
5	0	RHSBT1	8.9519	8.9519	8.9519	8.9519	8.9519	8.9519
		Vo et al [131]	8.9519	8.9519	8.9519	8.9519	8.9519	8.9519
	0.5	RHSBT1	28.4414	25.9582	24.5519	24.0603	22.4005	21.3879
		Vo et al [131]	28.4280	25.9503	24.5423	24.0540	22.3861	21.3821
	1	RHSBT1	36.2005	32.8830	30.9224	30.2305	27.8779	26.4709
		Vo et al [131]	36.2103	32.8974	30.9311	30.2449	27.8873	26.4801
	5	RHSBT1	46.6437	43.5149	40.9711	40.2969	37.0187	35.0091
		Vo et al [131]	46.6504	43.5338	40.9813	40.3235	37.0356	35.0357
	10	RHSBT1	47.7789	45.0980	42.5918	42.0433	38.6854	36.6575
		Vo et al [131]	47.7825	45.1141	42.6000	42.0693	38.7018	36.6874
20	0	RHSBT1	9.8067	9.8067	9.8067	9.8067	9.8067	9.8067
		Vo et al [131]	9.8067	9.8067	9.8067	9.8067	9.8067	9.8067
	0.5	RHSBT1	33.2392	30.8707	28.8664	28.8300	26.5315	25.6157
		Vo et al [131]	33.2187	30.8546	28.8514	28.8167	26.5120	25.6086
	1	RHSBT1	42.1802	39.4111	36.5663	36.8431	33.5141	32.5794
		Vo et al [131]	42.1810	39.4124	36.5675	36.8445	33.5153	32.5803
	5	RHSBT1	52.3646	50.7591	47.3042	48.5138	44.0822	43.7611
		Vo et al [131]	52.3655	50.7608	47.3056	48.5163	44.0843	43.7637
	10	RHSBT1	53.0327	51.9791	48.6919	50.0879	45.6712	45.6009
		Vo et al [131]	53.0331	51.9804	48.6930	50.0902	45.6732	45.6040

Furthermore, in order to estimate the effects of the power-law index, thickness ratio of layers on the static responses of Al/Al_2O_3 sandwich beams with homogeneous hardcore and soft core, Tables 3.10–3.12 introduce the non-dimensional mid-span displacement, axial and transverse shear stresses of Al/Al_2O_3 sandwich beams subjected to uniformly distributed load. The results are also plotted in Figures 3.4–3.6 with an increase of the power-law index, the deflection increases for homogeneous hardcore and decreases for homogeneous soft core. Figure 3.5a and Table 3.11 show that the variation of axial stresses of FG sandwich beams with homogeneous hardcore is linear for p=0 and nonlinear in the face sheets for p>0. The maximum values of compressive and tensile stresses are located at the interfaces of faces and core for p>0. Figure 3.5b shows that the maximum axial stress tends to decrease with an increase of the power-law index.

Figure 3.6 presents the variations of non-dimensional transverse shear stress through the depth of (1-2-1) FG sandwich beams for various values of the power law index. Obviously, for homogeneous hardcore, the maximum stresses are located at the mid-plane of the beam while for homogeneous soft core, they reside in the faces of FG sandwich beams.

Table 3.10 Non-dimensional mid-span transverse displacement $\left(\bar{w}\right)$ of Al/Al_2O_3 sandwich beams (Type B, Homogeneous hardcore and soft core).

Core	*L/h*	*p*	1-0-1	2-1-2	2-1-1	1-1-1	2-2-1	1-2-1
Hard core	5	0	0.2026	0.2026	0.2026	0.2026	0.2026	0.2026
		0.5	0.3539	0.3282	0.3172	0.3092	0.2964	0.2834
		1	0.5014	0.4437	0.4189	0.4012	0.3738	0.3464
		5	0.9714	0.8450	0.7568	0.7185	0.6267	0.5449
		10	1.0425	0.9359	0.8329	0.8042	0.6943	0.6019
	20	0	0.1854	0.1854	0.1854	0.1854	0.1854	0.1854
		0.5	0.3323	0.3080	0.2970	0.2896	0.2770	0.2645
		1	0.4763	0.4214	0.3967	0.3802	0.3530	0.3264
		5	0.9295	0.8164	0.7282	0.6936	0.6024	0.5225
		10	0.9884	0.9048	0.8018	0.7782	0.6690	0.5790
Soft core	5	0	1.0997	1.0997	1.0997	1.0997	1.0997	1.0997
		0.5	0.3456	0.3785	0.4003	0.4083	0.4386	0.4593
		1	0.2715	0.2987	0.3178	0.3248	0.3523	0.3708
		5	0.2109	0.2259	0.2400	0.2437	0.2654	0.2803
		10	0.2060	0.2180	0.2309	0.2337	0.2540	0.2677
	20	0	1.0062	1.0062	1.0062	1.0062	1.0062	1.0062
		0.5	0.2968	0.3196	0.3418	0.3422	0.3719	0.3852
		1	0.2339	0.2503	0.2698	0.2678	0.2944	0.3028
		5	0.1884	0.1944	0.2086	0.2034	0.2238	0.2254
		10	0.1861	0.1898	0.2026	0.1970	0.2163	0.2160

Table 3.11 Non-dimensional axial stress $\left(\bar{\sigma}_{xx}\left(h/2\right)\right)$ of Al/Al_2O_3 sandwich beams (Type B, Homogeneous hardcore and soft core).

Core	*L/h*	*p*	1-0-1	2-1-2	2-1-1	1-1-1	2-2-1	1-2-1
Hard core	5	0	3.8022	3.8022	3.8022	3.8022	3.8022	3.8022
		0.5	1.2547	1.1632	1.0699	1.0939	1.0036	0.9995
		1	1.7967	1.5898	1.3885	1.4349	1.2475	1.2330
		5	3.5001	3.0730	2.4070	2.6124	2.0195	1.9706
		10	3.7235	3.4044	2.6296	2.9294	2.2200	2.1827
	20	0	15.013	15.013	15.013	15.013	15.013	15.013
		0.5	4.9665	4.6036	4.2305	4.3281	3.9673	3.9520
		1	7.1229	6.3018	5.4960	5.6850	4.9364	4.8801
		5	13.9065	12.2220	9.5507	10.3835	8.0109	7.8194
		10	14.7788	13.5456	10.4356	11.6513	8.8104	8.6665
Soft core	5	0	3.8022	3.8022	3.8022	3.8022	3.8022	3.8022
		0.5	6.1022	6.5726	7.6712	7.0355	8.3738	7.9087
		1	4.8124	5.1557	6.0989	5.5150	6.7123	6.2280
		5	3.8727	4.0058	4.6474	4.1974	5.0955	4.6539
		10	3.8209	3.9096	4.4773	4.0649	4.8950	4.4686
	20	0	15.013	15.013	15.013	15.013	15.013	15.013
		0.5	23.9372	25.7407	30.1970	27.5464	32.9517	31.0018
		1	18.8683	20.1527	23.9954	21.5297	26.3863	24.3265
		5	15.2386	15.6797	18.3034	16.3681	20.0297	18.0929
		10	15.0579	15.3246	17.6441	15.8662	19.2507	17.3701

Table 3.12 Non-dimensional transverse shear stress $\left(\bar{\sigma}_{xz}\left(0\right)\right)$ of Al/Al_2O_3 sandwich beams (Type B, Homogeneous hardcore and soft core).

Core	*L/h*	*p*	1-0-1	2-1-2	2-1-1	1-1-1	2-2-1	1-2-1
Hard core	5	0	0.7350	0.7350	0.7350	0.7350	0.7350	0.7350
		0.5	0.8959	0.8371	0.8354	0.8087	0.8032	0.7830
		1	1.0349	0.9139	0.9106	0.8602	0.8496	0.8141
		5	1.7725	1.1854	1.1755	1.0133	0.9873	0.8940
		10	2.3128	1.3065	1.2888	1.0670	1.0347	0.9165
	20	0	0.7470	0.7470	0.7470	0.7470	0.7470	0.7470
		0.5	0.9070	0.8476	0.8460	0.8189	0.8134	0.7931
		1	1.0466	0.9241	0.9209	0.8699	0.8594	0.8235
		5	1.7927	1.1976	1.1877	1.0237	0.9972	0.9030
		10	2.3411	1.3196	1.3023	1.0779	1.0450	0.9258
Soft core	5	0	0.7350	0.7350	0.7350	0.7350	0.7350	0.7350
		0.5	0.3923	0.4762	0.4756	0.5370	0.5454	0.6079
		1	0.3006	0.3888	0.3885	0.4614	0.4725	0.5570
		5	0.1769	0.2484	0.2507	0.3204	0.3345	0.4422
		10	0.1564	0.2216	0.2250	0.2899	0.3045	0.4121
	20	0	0.7470	0.7470	0.7470	0.7470	0.7470	0.7470
		0.5	0.4009	0.4870	0.4859	0.5492	0.5577	0.6214
		1	0.3069	0.3976	0.3968	0.4720	0.4830	0.5697
		5	0.1802	0.2536	0.2556	0.3276	0.3416	0.4524
		10	0.1591	0.2261	0.2292	0.2963	0.3108	0.4216

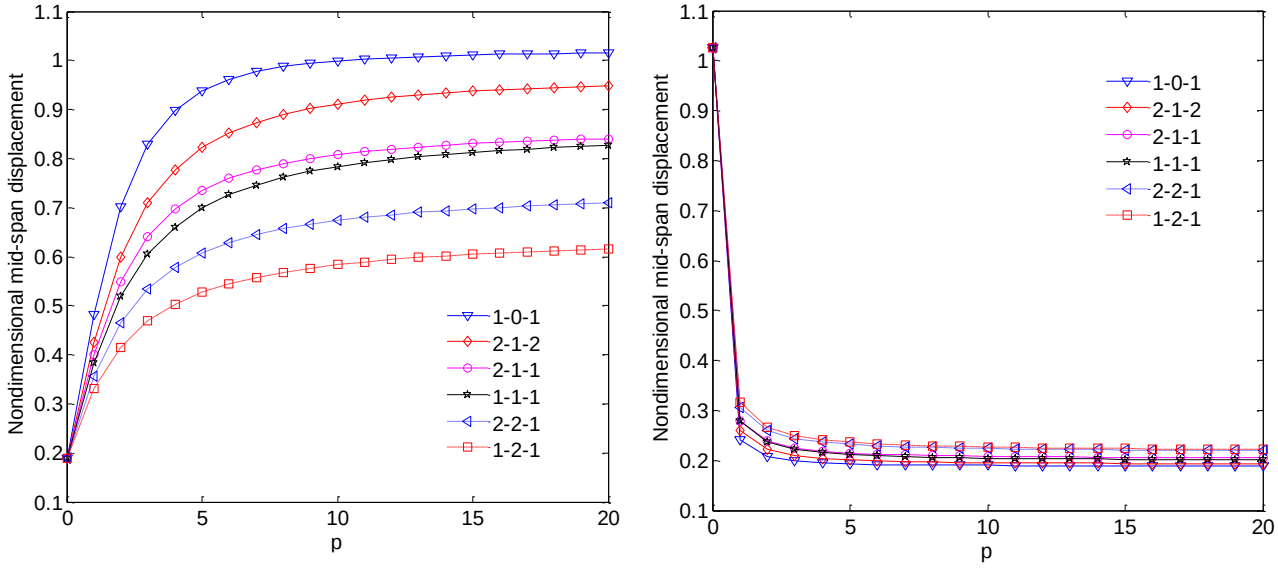

(a) Hard core (b) Soft core

Figure 3.4 Effect of the power-law index *p* on the non-dimensional mid-span transverse displacement $(\bar{w})$ of FG sandwich beams (Type B, *L*/*h*=10).

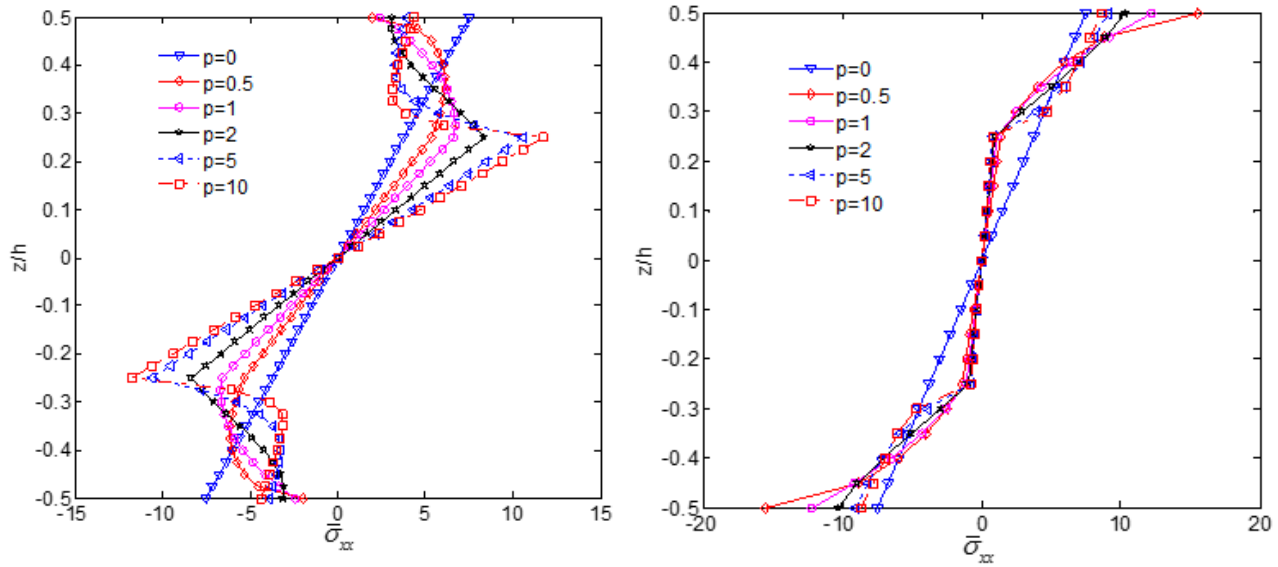

(a) Hard core (b) Soft core

Figure 3.5 Distribution of non-dimensional axial stress $(\bar{\sigma}_{xx})$through the height of (1-2-1) FG sandwich beams (Type B, *L*/*h*=10).

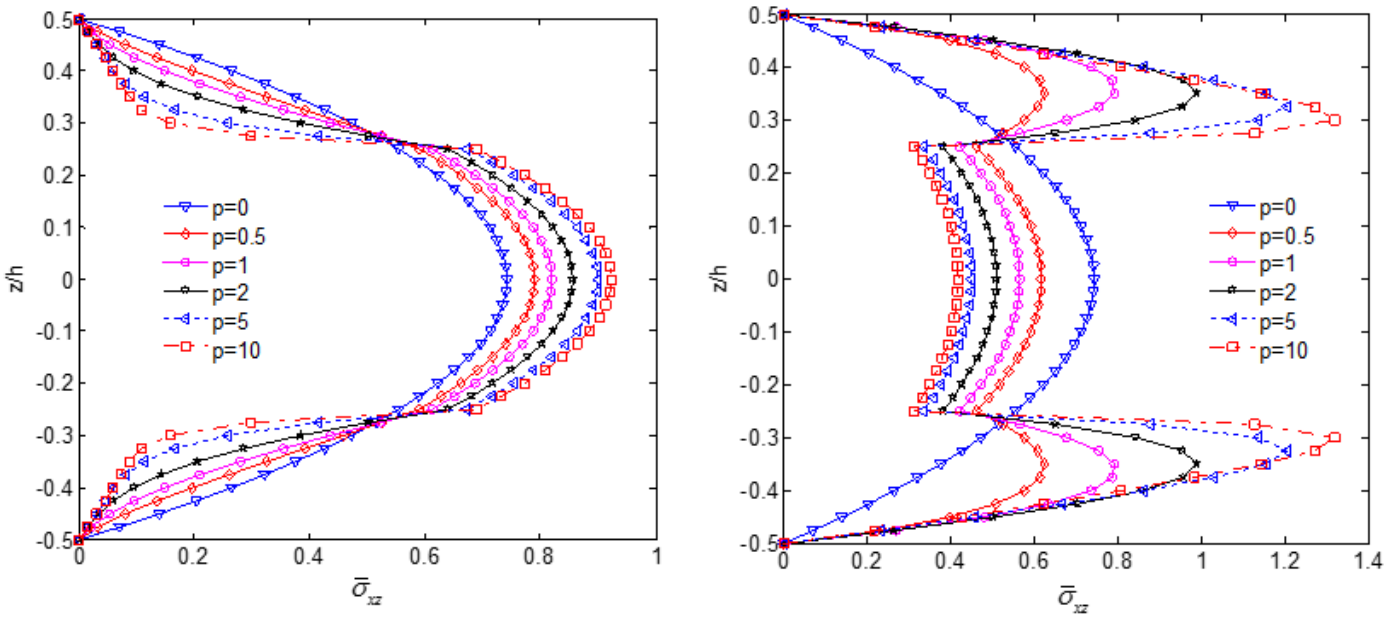

(a) Hard core (b) Soft core

Figure 3.6 Distribution of non-dimensional transverse shear stress $\left(\bar{\sigma}_{xz}\right)$ through the height of (1-2-1) FG sandwich beams (Type B, *L*/*h*=10).

Example 3: Buckling and vibration responses of Quasi-3D0 FG beams (Type B, C)

In order to evaluate the effect of transverse shear strain on behaviors of FG sandwich beams, a quasi-3D0 beam with the shear function $f\left(z\right)$ given in Nguyen et al. [5] is used $f\left(z\right)=\cot^{-1}\left(\frac{h}{z}\right)-\frac{16z^3}{15h^3}$. Tables 3.4 and 3.5 present the comparisons of the non-dimensional fundamental frequencies and critical buckling loads of Al/Al_2O_3 FG beams with S-S BCs (Type A), various values of the power-law index *p* and two span-to-height ratio *L*/*h* = 5, 20 are considered. It is noted that the present numerical results are calculated by using the Ritz method with polynomial shape functions and for the different beam models: HSBT2, quasi-3D2.

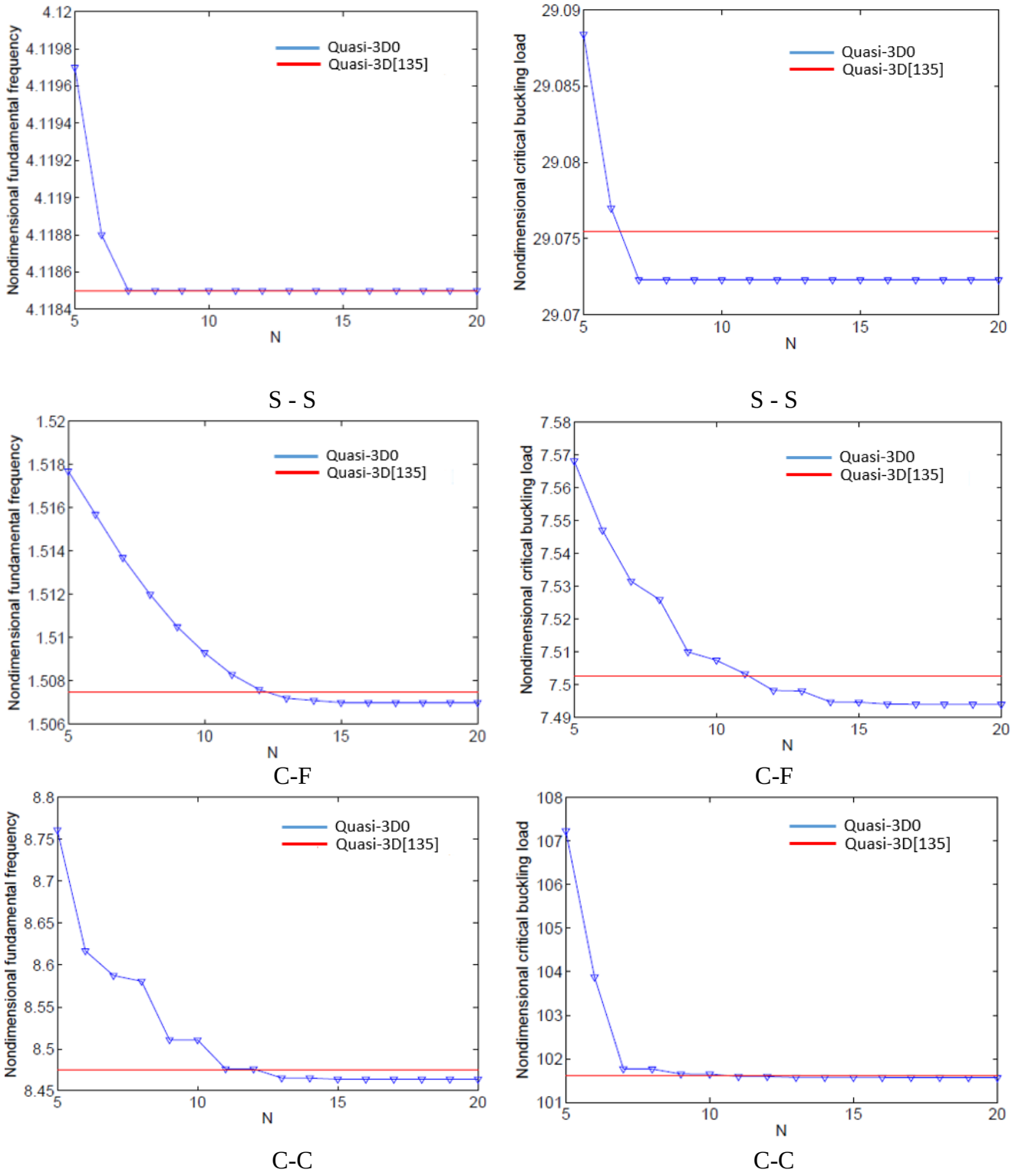

Figure 3.7 Convergence of the non-dimensional fundamental frequency ($\bar{\omega}$) and critical buckling load ($\bar{N}_{cr}$) of FG sandwich beams (Type B, p = 1, L/h = 5).

Firstly, the convergence of the present polynomial series solution is studied. Quasi-3D0 FG sandwich beams (Type B, 1-2-1) with the span-to-height ratio (L/h=5) and the power-law index (p=1) are considered. This is carried out for the fundamental frequency and critical buckling loads with three boundary conditions. The present results are compared with those based on a polynomial quasi-3D theory [135] in Figure 3.7. It can be seen that the solution of S-S boundary condition converges more quickly than C-F and C-C ones, and that the number of terms N=14 is sufficient to obtain an accurate solution. This number will be therefore used throughout the numerical examples.

Table 3.13 Non-dimensional fundamental frequency ($\bar{\omega}$) of FG sandwich beams (Type B, S-S, L/h=5).

p	Theory	1-0-1	2-1-2	2-1-1	1-1-1	2-2-1	1-2-1	1-8-1
0	Quasi-3D0	5.1620	5.1620	5.1620	5.1620	5.1620	5.1620	5.1620
	HSBT [5]	5.1528	5.1528	5.1528	5.1528	5.1528	5.1528	-
	TSBT [131]	5.1528	5.1528	5.1528	5.1528	5.1528	5.1528	5.1528
	Quasi-3D [135]	5.1618	5.1618	5.1618	5.1618	5.1618	5.1618	5.1618
0.5	Quasi-3D0	4.1329	4.2417	4.3037	4.3373	4.4143	4.4874	4.8504
	HSBT [5]	4.1254	4.2340	4.2943	4.3294	4.4045	4.4791	-
	TSBT [131]	4.1268	4.2351	4.2945	4.3303	4.4051	4.4798	4.8422
	Quasi-3D [135]	4.1344	4.2429	4.3041	4.3383	4.4146	4.4881	4.8511
1	Quasi-3D0	3.5804	3.7369	3.8318	3.8830	4.0018	4.1185	4.6883
	HSBT [5]	3.5736	3.7298	3.8206	3.8756	3.9911	4.1105	-
	TSBT [131]	3.5735	3.7298	3.8187	3.8755	3.9896	4.1105	4.6795
	Quasi-3D [135]	3.5803	3.7369	3.8301	3.8830	4.0005	4.1185	4.6884
2	Quasi-3D0	3.0739	3.2428	3.3685	3.4258	3.5848	3.7410	4.5229
	HSBT [5]	3.0682	3.2366	3.3546	3.4190	3.5719	3.7334	-
	TSBT [131]	3.0680	3.2365	3.3514	3.4190	3.5692	3.7334	4.5142
	Quasi-3D [135]	3.0737	3.2427	3.3656	3.4257	3.5825	3.7410	4.5231
5	Quasi-3D0	2.7497	2.8491	2.9955	3.0239	3.2122	3.3840	4.3587
	HSBT [5]	2.7450	2.8441	2.9790	3.0182	3.1966	3.3771	-
	TSBT [131]	2.7446	2.8439	2.9746	3.0181	3.1928	3.3771	4.3501
	Quasi-3D [135]	2.7493	2.8489	2.9912	3.0238	3.2087	3.3840	4.3589
10	Quasi-3D0	2.6982	2.7402	2.8886	2.8862	3.0797	3.2423	4.2862
	HSBT [5]	2.6936	2.7357	2.8716	2.8810	3.0630	3.2357	-
	TSBT [131]	2.6932	2.7355	2.8669	2.8808	3.0588	3.2356	4.2776
	Quasi-3D [135]	2.6978	2.7400	2.8839	2.8860	3.0757	3.2422	4.2864

In the next research, Tables 3.14-3.24 presents the comparison of the natural frequencies and critical buckling loads of FG sandwich beams of type B with three boundary conditions. They are calculated for various values of the power-law index, seven values of skin-core-skin thickness ratios and compared with the solutions obtained from HSBT [5], TSDT [131] and quasi-3D theory [135]. It is seen that the solutions obtained from the proposed theory are in excellent agreement with those obtained from [135]. Besides, various differences between the HSDTs and the present theory appeared for thick FG sandwich beams.

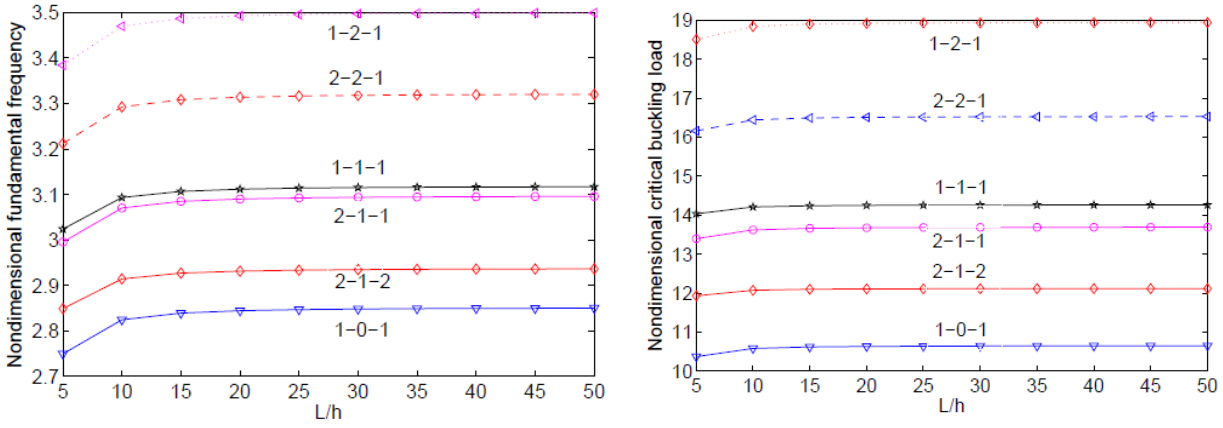

Figure 3.8 Effects of the span-to-depth ratio *L/h* on the non-dimensional fundamental frequency ($\bar{\omega}$) and critical buckling load ($\bar{N}_{cr}$) of FG sandwich beams (Type B, *p*= 5).

Furthermore, it can be seen from the tables that the results decrease with the increase of the power-law index. The lowest and highest values of natural frequency and critical buckling load correspond to the (1-0-1) and (1-8-1) sandwich beams. This is because these beams correspond to the lowest and highest volume fractions of the ceramic phase. The effect of the span-to-height ratio on the fundamental frequencies and critical buckling loads of S-S FG sandwich beams with p = 5 is plotted in Figure 3.8.

Table 3.14 Non-dimensional fundamental frequency ($\bar{\omega}$) of FG sandwich beams (Type B, S-S, *L*/*h*=20).

p	Theory	1-0-1	2-1-2	2-1-1	1-1-1	2-2-1	1-2-1	1-8-1
0	Quasi-3D0	5.4611	5.4611	5.4611	5.4611	5.4611	5.4611	5.4611
	HSBT [5]	5.4603	5.4603	5.4603	5.4603	5.4603	5.4603	-
	TSBT [131]	5.4603	5.4603	5.4603	5.4603	5.4603	5.4603	5.4603
	Quasi-3D [135]	5.4610	5.4610	5.4610	5.4610	5.4610	5.4610	5.4610
0.5	Quasi-3D0	4.3137	4.4284	4.4983	4.5321	4.6182	4.6979	5.1067
	HSBT [5]	4.3132	4.4278	4.4960	4.5315	4.6158	4.6972	-
	TSBT [131]	4.3148	4.4290	4.4970	4.5324	4.6170	4.6979	5.1067
	Quasi-3D [135]	4.3153	4.4296	4.4992	4.5330	4.6190	4.6985	5.1073
1	Quasi-3D0	3.7153	3.8774	3.9824	4.0334	4.1643	4.2896	4.9240
	HSBT [5]	3.7147	3.8768	3.9775	4.0328	4.1603	4.2889	-
	TSBT [131]	3.7147	3.8768	3.9774	4.0328	4.1602	4.2889	4.9233
	Quasi-3D [135]	3.7152	3.8773	3.9822	4.0333	4.1641	4.2895	4.9239
2	Quasi-3D0	3.1769	3.3471	3.4842	3.5395	3.7121	3.8775	4.7389
	HSBT [5]	3.1764	3.3465	3.4756	3.5389	3.7051	3.8769	-
	TSBT [131]	3.1764	3.3465	3.4754	3.5389	3.7049	3.8769	4.7382
	Quasi-3D [135]	3.1768	3.3469	3.4838	3.5394	3.7118	3.8774	4.7388
5	Quasi-3D0	2.8444	2.9315	3.0899	3.1116	3.3138	3.4927	4.5561
	HSBT [5]	2.8440	2.9311	3.0776	3.1111	3.3030	3.4921	-
	TSBT [131]	2.8439	2.9310	3.0773	3.1111	3.3028	3.4921	4.5554
	Quasi-3D [135]	2.8443	2.9314	3.0891	3.1115	3.3133	3.4926	4.5560
10	Quasi-3D0	2.8046	2.8192	2.9797	2.9666	3.1739	3.3412	4.4756
	HSBT [5]	2.8042	2.8188	2.9665	2.9662	3.1616	3.3406	-
	TSBT [131]	2.8041	2.8188	2.9662	2.9662	3.1613	3.3406	4.4749
	Quasi-3D [135]	2.8045	2.8191	2.9786	2.9665	3.1732	3.3411	4.4755

Table 3.15 Non-dimensional fundamental frequency ($\bar{\omega}$) of FG sandwich beams (Type B, C-F, *L/h*=5).

p	Theory	1-0-1	2-1-2	2-1-1	1-1-1	2-2-1	1-2-1	1-8-1
0	Quasi-3D0	1.9053	1.9053	1.9053	1.9053	1.9053	1.9053	1.9053
	HSBT [5]	1.8953	1.8953	1.8953	1.8953	1.8953	1.8953	-
	TSBT [131]	1.8952	1.8952	1.8952	1.8952	1.8952	1.8952	1.8952
	Quasi-3D [135]	1.9055	1.9055	1.9055	1.9055	1.9055	1.9055	1.9055
0.5	Quasi-3D0	1.5142	1.5543	1.5779	1.5901	1.6193	1.6467	1.7853
	HSBT [5]	1.5064	1.5463	1.5693	1.5819	1.6104	1.6383	-
	TSBT [131]	1.5069	1.5466	1.5696	1.5821	1.6108	1.6384	1.7764
	Quasi-3D [135]	1.5152	1.5551	1.5787	1.5908	1.6200	1.6474	1.7859
1	Quasi-3D0	1.3077	1.3648	1.4005	1.4189	1.4636	1.5071	1.7232
	HSBT [5]	1.3008	1.3576	1.3919	1.4115	1.4550	1.4993	-
	TSBT [131]	1.3007	1.3575	1.3918	1.4115	1.4549	1.4992	1.7145
	Quasi-3D [135]	1.3081	1.3652	1.4008	1.4193	1.4640	1.5075	1.7235
2	Quasi-3D0	1.1204	1.1810	1.2278	1.2483	1.3074	1.3653	1.6601
	HSBT [5]	1.1143	1.1747	1.2189	1.2416	1.2987	1.3582	-
	TSBT [131]	1.1143	1.1746	1.2188	1.2416	1.2986	1.3582	1.6518
	Quasi-3D [135]	1.1208	1.1815	1.2282	1.2488	1.3079	1.3658	1.6605
5	Quasi-3D0	1.0028	1.0361	1.0902	1.0997	1.1691	1.2323	1.5976
	HSBT [5]	0.9974	1.0304	1.0807	1.0936	1.1598	1.2258	-
	TSBT [131]	0.9973	1.0303	1.0806	1.0935	1.1597	1.2257	1.5897
	Quasi-3D [135]	1.0030	1.0365	1.0904	1.1002	1.1695	1.2329	1.5981
10	Quasi-3D0	0.9865	0.9965	1.0513	1.0491	1.1203	1.1798	1.5701
	HSBT [5]	0.9813	0.9910	1.0417	1.0432	1.1106	1.1734	-
	TSBT [131]	0.9812	0.9909	1.0416	1.0431	1.1106	1.1734	1.5624
	Quasi-3D [135]	0.9867	0.9969	1.0514	1.0495	1.1206	1.1804	1.5706

Table 3.16 Non-dimensional fundamental frequency ($\bar{\omega}$) of FG sandwich beams (Type B, C-F, *L*/*h*=20).

p	Theory	1-0-1	2-1-2	2-1-1	1-1-1	2-2-1	1-2-1	1-8-1
0	Quasi-3D0	1.9530	1.9530	1.9530	1.9530	1.9530	1.9530	1.9530
	HSBT [5]	1.9496	1.9496	1.9496	1.9496	1.9496	1.9496	-
	TSBT [131]	1.9496	1.9496	1.9496	1.9496	1.9496	1.9496	1.9496
	Quasi-3D [135]	1.9527	1.9527	1.9527	1.9527	1.9527	1.9527	1.9527
0.5	Quasi-3D0	1.5422	1.5832	1.6081	1.6203	1.6511	1.6796	1.8260
	HSBT [5]	1.5392	1.5801	1.6045	1.6171	1.6473	1.6764	-
	TSBT [131]	1.5397	1.5805	1.6048	1.6175	1.6477	1.6766	1.8229
	Quasi-3D [135]	1.5423	1.5831	1.6081	1.6201	1.6509	1.6794	1.8259
1	Quasi-3D0	1.3281	1.3860	1.4235	1.4418	1.4886	1.5335	1.7606
	HSBT [5]	1.3253	1.3831	1.4191	1.4388	1.4844	1.5304	-
	TSBT [131]	1.3253	1.3831	1.4191	1.4388	1.4844	1.5304	1.7573
	Quasi-3D [135]	1.3275	1.3855	1.4230	1.4413	1.4881	1.5329	1.7602
2	Quasi-3D0	1.1355	1.1964	1.2453	1.2651	1.3268	1.3860	1.6943
	HSBT [5]	1.1330	1.1937	1.2398	1.2623	1.3217	1.3831	-
	TSBT [131]	1.1330	1.1937	1.2398	1.2623	1.3217	1.3831	1.6911
	Quasi-3D [135]	1.1351	1.1958	1.2447	1.2646	1.3262	1.3855	1.6938
5	Quasi-3D0	1.0167	1.0478	1.1042	1.1122	1.1843	1.2484	1.6289
	HSBT [5]	1.0145	1.0454	1.0977	1.1096	1.1781	1.2456	-
	TSBT [131]	1.0145	1.0453	1.0977	1.1096	1.1781	1.2456	1.6257
	Quasi-3D [135]	1.0163	1.0473	1.1036	1.1116	1.1837	1.2478	1.6284
10	Quasi-3D0	1.0025	1.0077	1.0648	1.0604	1.1342	1.1943	1.6001
	HSBT [5]	1.0005	1.0053	1.0581	1.0578	1.1276	1.1915	-
	TSBT [131]	1.0005	1.0053	1.0581	1.0578	1.1276	1.1915	1.5969
	Quasi-3D [135]	1.0022	1.0072	1.0641	1.0598	1.1336	1.1937	1.5995

Table 3.17 Non-dimensional fundamental frequency ($\bar{\omega}$) of FG sandwich beams (Type B, C-C, *L*/*h*=5).

p	Theory	1-0-1	2-1-2	2-1-1	1-1-1	2-2-1	1-2-1	1-8-1
0	Quasi-3D0	10.1790	10.1790	10.1790	10.1790	10.1790	10.1790	10.1790
	HSBT [5]	10.0726	10.0726	10.0726	10.0726	10.0726	10.0726	-
	TSBT [131]	10.0678	10.0678	10.0678	10.0678	10.0678	10.0678	10.0678
	Quasi-3D [135]	10.1851	10.1851	10.1851	10.1851	10.1851	10.1851	10.1851
0.5	Quasi-3D0	8.4503	8.6657	8.7633	8.8381	8.9629	9.0924	9.6747
	HSBT [5]	8.3606	8.5736	8.6688	8.7442	8.8654	8.9969	-
	TSBT [131]	8.3600	8.5720	8.6673	8.7423	8.8648	8.9942	9.5731
	Quasi-3D [135]	8.4635	8.6780	8.7755	8.8498	8.9743	9.1036	9.6857
1	Quasi-3D0	7.4534	7.7769	7.9343	8.0504	8.2521	8.4653	9.4078
	HSBT [5]	7.3707	7.6910	7.8428	7.9623	8.1593	8.3747	-
	TSBT [131]	7.3661	7.6865	7.8390	7.9580	8.1554	8.3705	9.3076
	Quasi-3D [135]	7.4611	7.7854	7.9431	8.0595	8.2615	8.4752	9.4174
2	Quasi-3D0	6.4888	6.8660	7.0836	7.2237	7.5048	7.8008	9.1307
	HSBT [5]	6.4139	6.7867	6.9939	7.1412	7.4138	7.7149	-
	TSBT [131]	6.4095	6.7826	6.9908	7.1373	7.4105	7.7114	9.0343
	Quasi-3D [135]	6.4952	6.8740	7.0920	7.2328	7.5143	7.8114	9.1415
5	Quasi-3D0	5.7977	6.1060	6.3650	6.4701	6.8126	7.1550	8.8536
	HSBT [5]	5.7315	6.0335	6.2765	6.3925	6.7216	7.0723	-
	TSBT [131]	5.7264	6.0293	6.2737	6.3889	6.7188	7.0691	8.7605
	Quasi-3D [135]	5.8016	6.1124	6.3718	6.4780	6.8210	7.1652	8.8653
10	Quasi-3D0	5.6049	5.8793	6.1424	6.2028	6.5577	6.8934	8.7311
	HSBT [5]	5.5429	5.8104	6.0555	6.1278	6.4668	6.8119	-
	TSBT [131]	5.5375	5.8059	6.0527	6.1240	6.4641	6.8087	8.6391
	Quasi-3D [135]	5.6074	5.8848	6.1485	6.2099	6.5654	6.9030	8.7430

Table 3.18 Non-dimensional fundamental frequency ($\bar{\omega}$) of FG sandwich beams (Type B, C-C, *L*/*h*=20).

p	Theory	1-0-1	2-1-2	2-1-1	1-1-1	2-2-1	1-2-1	1-8-1
0	Quasi-3D0	12.2756	12.2756	12.2756	12.2756	12.2756	12.2756	12.2756
	HSBT [5]	12.2243	12.2243	12.2243	12.2243	12.2243	12.2243	-
	TSBT [131]	12.2228	12.2228	12.2228	12.2228	12.2228	12.2228	12.2228
	Quasi-3D [135]	12.2660	12.2660	12.2660	12.2660	12.2660	12.2660	12.2660
0.5	Quasi-3D0	9.7353	9.9933	10.1471	10.2246	10.4148	10.5924	11.4949
	HSBT [5]	9.6916	9.9484	10.0985	10.1788	10.3647	10.5455	-
	TSBT [131]	9.6942	9.9501	10.1001	10.1800	10.3668	10.5460	11.4459
	Quasi-3D [135]	9.7297	9.9865	10.1403	10.2172	10.4072	10.5842	11.4867
1	Quasi-3D0	8.3998	8.7663	8.9984	9.1158	9.4057	9.6866	11.0916
	HSBT [5]	8.3601	8.7248	8.9479	9.0729	9.3555	9.6419	-
	TSBT [131]	8.3594	8.7241	8.9474	9.0722	9.3550	9.6411	11.0421
	Quasi-3D [135]	8.3908	8.7569	8.9893	9.1061	9.3964	9.6768	11.0815
2	Quasi-3D0	7.1920	7.5799	7.8836	8.0128	8.3964	8.7690	10.6820
	HSBT [5]	7.1568	7.5422	7.8293	7.9732	8.3431	8.7268	-
	TSBT [131]	7.1563	7.5417	7.8293	7.9727	8.3430	8.7262	10.6336
	Quasi-3D [135]	7.1839	7.5711	7.8753	8.0035	8.3877	8.7593	10.6719
5	Quasi-3D0	6.4381	6.6461	6.9970	7.0536	7.5037	7.9092	10.2771
	HSBT [5]	6.4071	6.6121	6.9387	7.0174	7.4459	7.8696	-
	TSBT [131]	6.4064	6.6116	6.9389	7.0170	7.4461	7.8692	10.2298
	Quasi-3D [135]	6.4308	6.6379	6.9891	7.0451	7.4955	7.9000	10.2669
10	Quasi-3D0	6.3385	6.3920	6.7473	6.7277	7.1889	7.5700	10.0987
	HSBT [5]	6.3094	6.3595	6.6887	6.6928	7.1293	7.5315	-
	TSBT [131]	6.3086	6.3590	6.6889	6.6924	7.1296	7.5311	10.0519
	Quasi-3D [135]	6.3319	6.3841	6.7395	6.7194	7.1809	7.5609	10.0884

Table 3.19 Non-dimensional critical buckling load ($\bar{N}_{cr}$) of FG sandwich beams (Type B, S-S, *L/h*=5).

p	Theory	1-0-1	2-1-2	2-1-1	1-1-1	2-2-1	1-2-1	1-8-1
0	Quasi-3D0	49.5970	49.5970	49.5970	49.5970	49.5970	49.5970	49.5970
	HSBT [5]	48.5964	48.5964	48.5964	48.5964	48.5964	48.5964	-
	TSBT [131]	48.5959	48.5959	48.5959	48.5959	48.5959	48.5959	48.5959
	Quasi-3D [135]	49.5906	49.5906	49.5906	49.5906	49.5906	49.5906	49.5906
0.5	Quasi-3D0	28.4407	30.6650	31.7459	32.5547	33.9720	35.5032	42.8623
	HSBT [5]	27.8380	30.0146	31.0577	31.8650	33.2336	34.7546	-
	TSBT [131]	27.8574	30.0301	31.0728	31.8784	33.2536	34.7653	41.9897
	Quasi-3D [135]	28.4624	30.6825	31.7627	32.5699	33.9858	35.5156	42.8751
1	Quasi-3D0	20.0899	22.7061	24.0833	25.1060	26.9747	29.0723	39.6116
	HSBT [5]	19.6541	22.2121	23.5250	24.5602	26.3611	28.4440	-
	TSBT [131]	19.6525	22.2108	23.5246	24.5596	26.3611	28.4447	38.7838
	Quasi-3D [135]	20.7425	22.7065	24.0838	25.1075	26.9764	29.0755	39.6144
2	Quasi-3D0	13.8852	16.2761	17.7748	18.7756	20.8863	23.3002	36.4626
	HSBT [5]	13.5820	15.9167	17.3254	18.3596	20.3751	22.7859	-
	TSBT [131]	13.5801	15.9152	17.3249	18.3587	20.3750	22.7863	35.6914
	Quasi-3D [135]	13.8839	16.2761	17.7742	18.7772	20.8879	23.3042	36.4677
5	Quasi-3D0	10.3708	11.9320	13.3963	14.0352	16.1613	18.5058	33.4891
	HSBT [5]	10.1488	11.6697	13.0279	13.7226	15.7313	18.0915	-
	TSBT [131]	10.1460	11.6676	13.0270	13.7212	15.7307	18.0914	32.7725
	Quasi-3D [135]	10.3673	11.9301	13.3924	14.0353	16.1605	18.5092	33.4958
10	Quasi-3D0	9.6573	10.7715	12.1790	12.5402	14.6018	16.7550	32.2197
	HSBT [5]	9.4543	10.5370	11.8380	12.2621	14.2002	16.3789	-
	TSBT [131]	9.4515	10.5348	11.8370	12.2605	14.1995	16.3783	31.5265
	Quasi-3D [135]	9.6535	10.7689	12.1737	12.5393	14.5994	16.7574	32.2264

Table 3.20 Non-dimensional critical buckling load ($\bar{N}_{cr}$) of FG sandwich beams (Type B, S-S, L/h=20).

p	Theory	1-0-1	2-1-2	2-1-1	1-1-1	2-2-1	1-2-1	1-8-1
0	Quasi-3D0	53.3175	53.3175	53.3175	53.3175	53.3175	53.3175	53.3175
	HSBT [5]	53.2364	53.2364	53.2364	53.2364	53.2364	53.2364	-
	TSBT [131]	53.2364	53.2364	53.2364	53.2364	53.2364	53.2364	53.2364
	Quasi-3D [135]	53.3145	53.3145	53.3145	53.3145	53.3145	53.3145	53.3145
0.5	Quasi-3D0	29.7410	32.0853	33.2971	34.1242	35.7026	37.3626	45.6315
	HSBT [5]	29.6965	32.0368	33.2217	34.0722	35.6202	37.3054	-
	TSBT [131]	29.7175	32.2629	33.2376	34.0862	35.6405	37.3159	45.5742
	Quasi-3D [135]	29.7626	32.1022	33.3127	34.1380	35.7149	37.3617	45.6424
1	Quasi-3D0	20.7541	23.4584	24.9715	26.0001	28.0424	30.2785	41.9655
	HSBT [5]	20.7213	23.4212	24.8793	25.9588	27.9537	30.2306	-
	TSBT [131]	20.7212	23.4211	24.8796	25.9588	27.9540	30.2307	41.9004
	Quasi-3D [135]	20.7530	23.4572	24.9697	25.9989	28.0412	30.2774	41.9639
2	Quasi-3D0	14.2199	16.6317	18.2521	19.2309	21.5001	24.0284	38.4431
	HSBT [5]	14.1974	16.6051	18.1400	19.2000	21.3923	23.9899	-
	TSBT [131]	14.1973	16.6050	18.1404	19.3116	21.3927	23.9900	38.3831
	Quasi-3D [135]	14.2190	16.6307	18.2493	19.2299	21.4986	24.0276	38.4419
5	Quasi-3D0	10.6341	12.1078	13.6771	14.2515	16.5100	18.9180	35.1408
	HSBT [5]	10.6176	12.0886	13.5520	14.2285	16.3829	18.8874	-
	TSBT [131]	10.6171	12.0883	13.5523	14.2284	16.3834	18.8874	35.0856
	Quasi-3D [135]	10.6330	12.1068	13.6717	14.2505	16.5069	18.9172	35.1400
10	Quasi-3D0	10.0003	10.9246	12.4320	12.7023	14.8851	17.0723	33.7379
	HSBT [5]	9.9850	10.9075	12.3081	12.6820	14.7520	17.0445	-
	TSBT [131]	9.9847	10.9075	12.3084	12.6819	14.7525	17.0443	33.6843
	Quasi-3D [135]	9.9995	10.9239	12.4256	12.7014	14.8807	17.0712	33.7367

Table 3.21 Non-dimensional critical buckling load ($\bar{N}_{cr}$) of FG sandwich beams (Type B, C-F, *L/h*=5).

p	Theory	1-0-1	2-1-2	2-1-1	1-1-1	2-2-1	1-2-1	1-8-1
0	Quasi-3D0	13.1138	13.1138	13.1138	13.1138	13.1138	13.1138	13.1138
	HSBT [5]	13.0595	13.0595	13.0595	13.0595	13.0595	13.0595	-
	TSBT [131]	13.0594	13.0594	13.0594	13.0594	13.0594	13.0594	13.0594
	Quasi-3D [135]	13.1224	13.1224	13.1224	13.1224	13.1224	13.1224	13.1224
0.5	Quasi-3D0	7.3567	7.9357	8.2309	8.4366	8.8217	9.2289	11.2428
	HSBT [5]	7.3263	7.9026	8.1912	8.4016	8.7789	9.1913	-
	TSBT [131]	7.3314	7.9068	8.1951	8.4051	8.7839	9.1940	11.2021
	Quasi-3D [135]	7.3700	7.9482	8.2431	8.4486	8.8334	9.2404	11.2557
1	Quasi-3D0	5.1480	5.8182	6.1882	6.4447	6.9446	7.4948	10.3484
	HSBT [5]	5.1246	5.7922	6.1490	6.4166	6.9050	7.4638	-
	TSBT [131]	5.1245	5.7921	6.1490	6.4166	6.9050	7.4639	10.3093
	Quasi-3D [135]	5.1533	5.8244	6.1944	6.4516	6.9518	7.5028	10.3581
2	Quasi-3D0	3.5350	4.1359	4.5331	4.7789	5.3359	5.9601	9.4872
	HSBT [5]	3.5175	4.1157	4.4927	4.7564	5.2952	5.9347	-
	TSBT [131]	3.5173	4.1156	4.4927	4.7564	5.2952	5.9348	9.4531
	Quasi-3D [135]	3.5387	4.1408	4.5376	4.7847	5.3419	5.9674	9.4974
5	Quasi-3D0	2.6435	3.0170	3.4021	3.5501	4.1053	4.7028	8.6791
	HSBT [5]	2.6301	3.0006	3.3609	3.5311	4.0621	4.6806	-
	TSBT [131]	2.6298	3.0004	3.3609	3.5310	4.0620	4.6806	8.6493
	Quasi-3D [135]	2.6458	3.0203	3.4046	3.5542	4.1095	4.7088	8.6897
10	Quasi-3D0	2.4803	2.7226	3.0928	3.1665	3.7035	4.2480	8.3359
	HSBT [5]	2.4685	2.7078	3.0528	3.1489	3.6596	4.2268	-
	TSBT [131]	2.4683	2.7077	3.0527	3.1488	3.6595	4.2267	8.3073
	Quasi-3D [135]	2.4823	2.7257	3.0946	3.1702	3.7068	4.2533	8.3463

Table 3.22 Non-dimensional critical buckling load ($\bar{N}_{cr}$) of FG sandwich beams (Type B, C-F, *L*/*h*=20).

p	Theory	1-0-1	2-1-2	2-1-1	1-1-1	2-2-1	1-2-1	1-8-1
0	Quasi-3D0	13.3993	13.3993	13.3993	13.3993	13.3993	13.3993	13.3993
	HSBT [5]	13.3730	13.3730	13.3730	13.3730	13.3730	13.3730	-
	TSBT [131]	13.3730	13.3730	13.3730	13.3730	13.3730	13.3730	13.3730
	Quasi-3D [135]	13.3981	13.3981	13.3981	13.3981	13.3981	13.3981	13.3981
0.5	Quasi-3D0	7.4649	8.0536	8.3585	8.5660	8.9631	9.3826	11.4625
	HSBT [5]	7.4490	8.0363	8.3345	8.5477	8.9372	9.3607	-
	TSBT [131]	7.4543	8.0405	8.3385	8.5512	8.9422	9.3634	11.4424
	Quasi-3D [135]	7.4689	8.0563	8.3609	8.5679	8.9647	9.3815	11.4642
1	Quasi-3D0	5.2067	5.8851	6.2654	6.5234	7.0367	7.5986	10.5393
	HSBT [5]	5.1944	5.8713	6.2378	6.5083	7.0096	7.5815	-
	TSBT [131]	5.1944	5.8713	6.2378	6.5083	7.0096	7.5815	10.5174
	Quasi-3D [135]	5.2050	5.8832	6.2633	6.5214	7.0346	7.5965	10.5375
2	Quasi-3D0	3.5662	4.1708	4.5775	4.8230	5.3927	6.0278	9.6526
	HSBT [5]	3.5574	4.1603	4.5457	4.8110	5.3615	6.0134	-
	TSBT [131]	3.5574	4.1603	4.5457	4.8110	5.3615	6.0134	9.6321
	Quasi-3D [135]	3.5648	4.1690	4.5753	4.8211	5.3906	6.0257	9.6507
5	Quasi-3D0	2.6670	3.0356	3.4291	3.5732	4.1396	4.7443	8.8217
	HSBT [5]	2.6606	3.0276	3.3948	3.5637	4.1042	4.7323	-
	TSBT [131]	2.6605	3.0275	3.3948	3.5637	4.1043	4.7323	8.8025
	Quasi-3D [135]	2.6659	3.0341	3.4266	3.5714	4.1373	4.7423	8.8196
10	Quasi-3D0	2.5090	2.7389	3.1168	3.1845	3.7318	4.2809	8.4688
	HSBT [5]	2.5033	2.7317	3.0831	3.1759	3.6952	4.2698	-
	TSBT [131]	2.5032	2.7317	3.0832	3.1759	3.6952	4.2698	8.4500
	Quasi-3D [135]	2.5082	2.7376	3.1142	3.1829	3.7293	4.2789	8.4666

Table 3.23 Non-dimensional critical buckling load ($\bar{N}_{cr}$) of FG sandwich beams (Type B, C-C, *L*/*h*=5).

p	Theory	1-0-1	2-1-2	2-1-1	1-1-1	2-2-1	1-2-1	1-8-1
0	Quasi-3D0	160.3064	160.3064	160.3064	160.3064	160.3064	160.3064	160.3064
	HSBT [5]	152.1588	152.1588	152.1588	152.1588	152.1588	152.1588	-
	TSBT [131]	152.1470	152.1470	152.1470	152.1470	152.1470	152.1470	152.1470
	Quasi-3D [135]	160.2780	160.2780	160.2780	160.2780	160.2780	160.2780	160.2780
0.5	Quasi-3D0	98.3648	105.8972	108.9555	111.8943	116.0009	120.7931	141.7160
	HSBT [5]	92.8202	99.9361	102.8605	105.6331	109.5284	114.1312	-
	TSBT [131]	92.8833	99.9860	102.9120	105.6790	109.6030	114.1710	134.2870
	Quasi-3D [135]	98.4559	105.9750	109.0360	111.9680	116.0700	120.8630	141.7880
1	Quasi-3D0	71.7633	81.0819	85.1883	89.0595	94.7381	101.5703	132.5067
	HSBT [5]	67.5184	76.2801	80.1730	83.8267	89.2223	95.7230	-
	TSBT [131]	67.4983	76.2634	80.1670	83.8177	89.2208	95.7287	125.3860
	Quasi-3D [135]	71.7654	81.0936	85.2092	89.0834	94.7675	101.6130	132.5510
2	Quasi-3D0	123.4142	50.8264	59.9292	64.5957	68.6517	75.3511	83.5671
	HSBT [5]	47.7247	56.2259	60.6127	64.4352	70.7590	78.5570	-
	TSBT [131]	47.7010	56.2057	60.6056	64.4229	70.7563	78.5608	116.6580
	Quasi-3D [135]	50.8183	59.9354	64.6133	68.6743	75.3818	83.6159	123.4770
5	Quasi-3D0	37.8590	44.8607	49.5296	52.6318	59.6057	68.0098	114.6926
	HSBT [5]	35.5811	42.0298	46.3852	49.2949	55.8338	63.7847	-
	TSBT [131]	35.5493	42.0033	46.3743	49.2763	55.8271	63.7824	108.2970
	Quasi-3D [135]	37.8295	44.8488	49.5325	52.6395	59.6248	68.0510	114.7700
10	Quasi-3D0	34.3176	40.5751	45.0701	47.3821	54.2081	62.1634	110.9318
	HSBT [5]	32.3345	38.0239	42.2062	44.3593	50.7406	58.2532	-
	TSBT [131]	104.6920	32.3019	37.9944	42.1935	44.3374	50.7315	58.2461
	Quasi-3D [135]	34.2824	40.5544	45.0660	47.3804	54.2193	62.1959	111.0120

Table 3.24 Non-dimensional critical buckling load ($\bar{N}_{cr}$) of FG sandwich beams (Type B, C-C, *L/h*=20).

p	Theory	1-0-1	2-1-2	2-1-1	1-1-1	2-2-1	1-2-1	1-8-1
0	Quasi-3D0	210.7774	210.7774	210.7774	210.7774	210.7774	210.7774	210.7774
	HSBT [5]	208.9515	208.9515	208.9515	208.9515	208.9515	208.9515	-
	TSBT [131]	208.9510	208.9510	208.9510	208.9510	208.9510	208.9510	208.9510
	Quasi-3D [135]	210.7420	210.7420	210.7420	210.7420	210.7420	210.7420	210.7420
0.5	Quasi-3D0	118.3095	127.6190	132.3616	135.6735	141.8619	148.4165	180.7913
	HSBT [5]	117.2200	126.4422	131.0594	134.4255	140.4622	147.0614	-
	TSBT [131]	117.3030	126.5080	131.1240	134.4810	140.5450	147.1040	179.2350
	Quasi-3D [135]	118.3530	127.6410	132.3830	135.6840	141.8690	148.4130	180.8010
1	Quasi-3D0	82.7901	93.5770	99.5203	103.6595	111.6956	120.5619	166.4508
	HSBT [5]	81.9944	92.6754	98.3839	102.6655	110.4792	119.4215	-
	TSBT [131]	81.9927	92.6741	98.3880	102.6650	110.4830	119.4220	164.9490
	Quasi-3D [135]	82.7434	93.5248	99.4730	103.6060	111.6480	120.5090	166.4060
2	Quasi-3D0	56.8386	66.5147	72.8955	76.8684	85.8241	95.8941	152.6477
	HSBT [5]	56.2793	65.8505	71.8837	76.1030	84.7230	94.9558	-
	TSBT [131]	56.2773	65.8489	71.8900	76.1020	84.7291	94.9563	151.2500
	Quasi-3D [135]	56.7986	66.4664	72.8506	76.8166	85.7783	95.8403	152.6000
5	Quasi-3D0	42.4914	48.5016	54.6876	57.0817	66.0121	75.6538	139.6866
	HSBT [5]	42.0814	48.0095	53.7751	56.4973	64.9930	74.8903	-
	TSBT [131]	42.0775	48.0070	53.7820	56.4958	65.0007	74.8903	138.3880
	Quasi-3D [135]	42.4596	48.4588	54.6418	57.0343	65.9671	75.6019	139.6370
10	Quasi-3D0	39.8676	43.7664	49.7084	50.9062	59.5406	68.3252	134.1743
	HSBT [5]	39.4962	43.3252	48.8443	50.3827	58.5529	67.6281	-
	TSBT [131]	39.4930	43.3233	48.8510	50.3811	58.5607	67.6270	132.9170
	Quasi-3D [135]	39.8436	43.7273	49.6622	50.8611	59.4944	68.2737	134.1220

To prove the accuracy of the research results of the thesis by calculating the percentage of errors with the research results of the thesis with the verified results [135] with the following formula:

$$Percentage\ of\ \ errors = \frac{Research\ results - Verified\ \ results}{Research\ results} \times 100\% \qquad (3.87)$$

Figure 3.9 shows that Percent error of non-dimensional fundamental frequency ($\bar{\omega}$) and non-dimensional critical buckling load ($\bar{N}_{cr}$) of FG sandwich beams (1-2-1) in tables 3.14, 3.16, 3.18, 3.20, 3.22, 3.24 with the span-to-height *L/h*=20 and t various BCs.

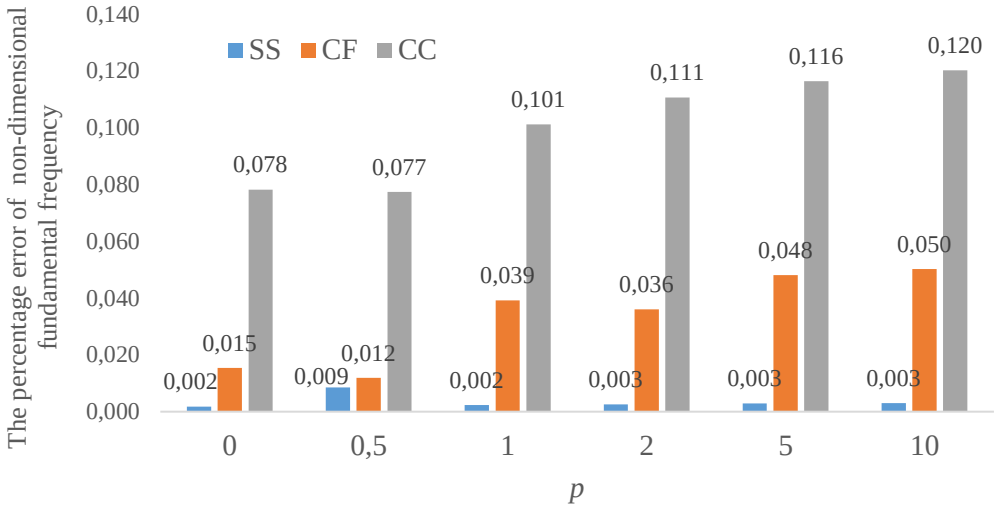

(Type B, 1-2-1, *L/h*=20).

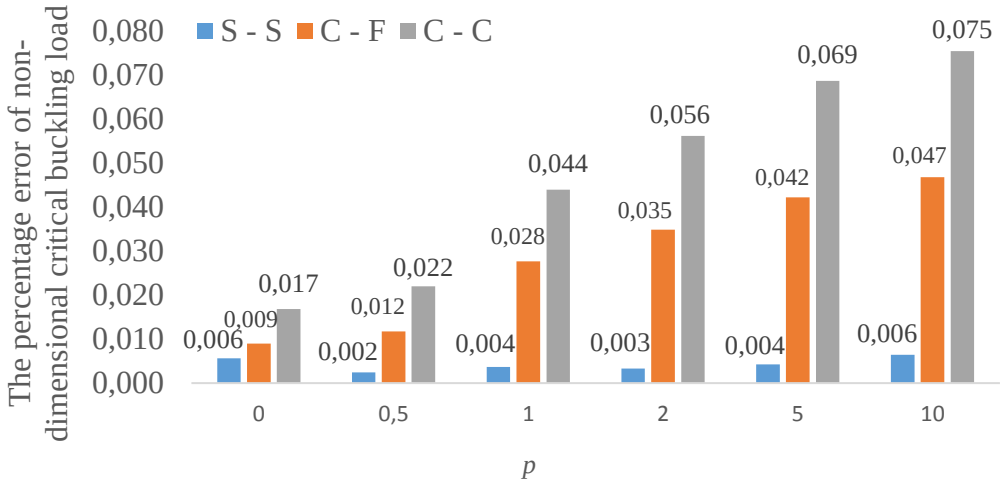

(Type B, 1-2-1, *L/h*=20)

Figure 3.9 The percentage error of non-dimensional fundamental frequency ($\bar{\omega}$) and non-dimensional critical buckling load ($\bar{N}_{cr}$) of FG sandwich beams.

Figure 3.9, it is easy to see that the percentage error of non-dimensional fundamental frequency ($\bar{\omega}$) and non-dimensional critical buckling load ($\bar{N}_{cr}$) with the S-S boundary condition, the percentage error of the thesis with Quasi-3D [135] is almost absent. The

maximum error percentage value is 0,12 for non-dimensional fundamental frequency ($\bar{\omega}$) and 0.075 for non-dimensional critical buckling load ($\bar{N}_{cr}$) of FG sandwich beams when p = 10 and the C-C boundary condition.

Moreover, the natural frequencies and critical buckling loads of FG sandwich beams of Type C are compared with those obtained from HSBT [5] in Tables 3.25-3.27. They are carried out for two values of skin-core-skin thickness ratios (1-2-1 and 2-2-1), different values of the power-law index and different boundary conditions. It can be seen again that by accounting the normal strain, the present theory provides the solution bigger than the HSBT [5].

Table 3.25 Non-dimensional fundamental frequency ($\bar{\omega}$) of FG sandwich beams with the various boundary conditions (Type C).

Scheme	*L/h*	BC	Theory	*p*					
				0	0.5	1	2	5	10
1-2-1	5	S-S	Quasi-3D0	4.0996	3.8438	3.7172	3.6119	3.5513	3.5413
			HSBT[5]	4.0691	3.7976	3.6636	3.5530	3.4914	3.4830
		C-C	Quasi-3D0	8.4529	7.8924	7.5904	7.2898	7.0032	6.8757
			HSBT[5]	8.3282	7.7553	7.4487	7.1485	6.8702	6.7543
		C-F	Quasi-3D0	1.5001	1.4076	1.3627	1.3273	1.3113	1.3118
			HSBT[5]	1.4840	1.3865	1.3393	1.3022	1.2857	1.2867
	20	S-S	Quasi-3D0	4.2711	4.0143	3.8923	3.8003	3.7708	3.7831
			HSBT[5]	4.2445	3.9695	3.8387	3.7402	3.7081	3.7214
		C-C	Quasi-3D0	9.6404	9.0524	8.7701	8.5509	8.4627	8.4755
			HSBT[5]	9.5451	8.9243	8.6264	8.3959	8.3047	8.3205
		C-F	Quasi-3D0	1.5264	1.4344	1.3907	1.3580	1.3478	1.3525
			HSBT[5]	1.5145	1.4165	1.3700	1.3350	1.3241	1.3292
2-2-1	5	S-S	Quasi-3D0	3.7142	3.6270	3.5885	3.5589	3.5411	3.5352
			HSBT[5]	3.6624	3.5692	3.5292	3.5002	3.4858	3.4830
		C-C	Quasi-3D0	7.7159	7.4082	7.2306	7.0320	6.8091	6.7045
			HSBT[5]	7.5709	7.2636	7.0901	6.9040	6.8998	6.5941
		C-F	Quasi-3D0	1.3571	1.3297	1.3191	1.3135	1.3144	1.3160
			HSBT[5]	1.3344	1.3050	1.2939	1.2884	1.2903	1.2930
	20	S-S	Quasi-3D0	3.8647	3.7990	3.7784	3.7756	3.7966	3.8110
			HSBT[5]	3.8136	3.7406	3.7177	3.7144	3.7380	3.7552
		C-C	Quasi-3D0	8.7233	8.5588	8.4999	8.4757	8.4970	8.5157
			HSBT[5]	8.5832	8.4064	8.3442	8.3205	8.3488	8.3738
		C-F	Quasi-3D0	1.3807	1.3573	1.3501	1.3495	1.3576	1.3630
			HSBT[5]	1.3607	1.3350	1.3271	1.3263	1.3353	1.3418

Table 3.26 Non-dimensional critical buckling load ($\bar{N}_{cr}$) of FG sandwich beams with the various boundary conditions (Type C).

Scheme	*L/h*	BC	Theory	*p*					
				0	0.5	1	2	5	10
1-2-1	5	S-S	Quasi-3D0	28.7884	23.8554	21.6374	19.7957	18.5212	18.1329
			HSBT[5]	27.9314	22.9869	20.7762	18.9588	17.7320	17.3775
		C-C	Quasi-3D0	100.5883	82.4783	73.9348	66.1308	59.2628	56.4049
			HSBT[5]	94.6117	77.5129	69.4877	62.2249	55.9446	53.3734
		C-F	Quasi-3D0	7.4344	6.1836	5.6304	5.1884	4.9228	4.8658
			HSBT[5]	7.3149	6.0286	5.4629	5.0154	4.7534	4.7024
	20	S-S	Quasi-3D0	30.0168	24.9914	22.7796	21.0343	20.0386	19.8622
			HSBT[5]	29.6120	24.4140	22.1386	20.3581	19.3639	19.2058
		C-C	Quasi-3D0	119.4172	99.2742	90.3696	83.2627	79.0045	78.0989
			HSBT[5]	117.0384	96.4573	87.4069	80.2465	76.0539	75.2379
		C-F	Quasi-3D0	7.5312	6.2702	5.7160	5.2800	5.0345	4.9934
			HSBT[5]	7.4254	6.1225	5.5529	5.1084	4.8634	4.8269
2-2-1	5	S-S	Quasi-3D0	22.4065	20.3457	19.4156	18.6007	17.9128	17.6221
			HSBT[5]	21.5207	19.4909	18.5897	17.8178	17.1942	16.9422
		C-C	Quasi-3D0	79.0342	69.4910	64.6563	59.7538	54.7871	52.5943
			HSBT[5]	74.0960	65.2766	60.8501	56.4008	51.9303	49.9605
		C-F	Quasi-3D0	5.7754	5.2959	5.0939	4.9372	4.8346	4.7977
			HSBT[5]	5.6078	5.1228	4.9221	4.7709	4.6809	4.6533
	20	S-S	Quasi-3D0	23.3038	21.4284	20.6576	20.0894	19.7694	19.6701
			HSBT[5]	22.6714	20.7578	19.9839	19.4292	19.1504	19.0848
		C-C	Quasi-3D0	92.7010	84.9897	81.7465	79.2375	77.6098	77.0306
			HSBT[5]	89.7255	81.9647	78.7529	76.3344	74.8949	74.4533
		C-F	Quasi-3D0	5.8444	5.3767	5.1857	5.0468	4.9722	4.9504
			HSBT[5]	5.6831	5.2064	5.0148	4.8794	4.8150	4.8016

Table 3.27 The first three non-dimensional frequencies of FG sandwich beams (Type C, C-C).

Mode	Scheme	*L/h*	Theory	*p*					
				0	0.5	1	2	5	10
1	1-2-1	5	Quasi-3D0	8.4529	7.8924	7.5904	7.2898	7.0032	6.8757
			HSBT[5]	8.3282	7.7553	7.4487	7.1485	6.8702	6.7543
		20	Quasi-3D0	9.6404	9.0524	8.7701	8.5509	8.4627	8.4755
			HSBT[5]	9.5451	8.9243	8.6264	8.3959	8.3047	8.3205
	2-2-1	5	Quasi-3D0	7.7159	7.4082	7.2306	7.0320	6.8091	6.7045
			HSBT[5]	7.5709	7.2636	7.0901	6.9040	6.8998	6.5941
		20	Quasi-3D0	8.7233	8.5588	8.4999	8.4757	8.4970	8.5157
			HSBT[5]	8.5832	8.4064	8.3442	8.3205	8.3488	8.3738
2	1-2-1	5	Quasi-3D0	20.1538	18.7348	17.9231	17.0413	16.0837	15.6231
			HSBT[5]	19.8886	18.4463	17.6290	16.7552	15.8266	15.3878
		20	Quasi-3D0	26.2039	24.5867	23.7980	23.1611	22.8406	22.8197
			HSBT[5]	25.9323	24.2300	23.4015	22.7371	22.4123	22.4014
	2-2-1	5	Quasi-3D0	18.4986	17.4894	16.8786	16.1729	15.3753	15.0105
			HSBT[5]	18.1865	17.1905	16.5950	15.9164	15.1574	14.8131
		20	Quasi-3D0	23.7284	23.2234	23.0169	22.8833	22.8435	22.8431
			HSBT[5]	23.3403	22.8045	22.5913	22.4619	22.4443	22.4623
3	1-2-1	5	Quasi-3D0	34.4230	31.9202	30.4476	28.7917	26.9294	26.0255
			HSBT[5]	34.0624	31.5260	30.0458	28.4068	26.5927	25.7241
		20	Quasi-3D0	50.4317	47.2723	45.7039	44.3844	43.5884	43.4278
			HSBT[5]	49.8846	46.5716	44.9326	43.5667	42.7705	42.6332
	2-2-1	5	Quasi-3D0	31.7174	29.7117	28.4955	27.0964	25.5375	24.8362
			HSBT[5]	31.2772	29.2997	28.1131	26.7610	25.2645	24.5968
		20	Quasi-3D0	45.7032	44.5962	44.0940	43.6868	43.4002	43.2918
			HSBT[5]	44.9445	43.7848	43.2741	42.8808	42.6431	42.5723

The first three mode shapes of FG sandwich beams with the power-law index p=2 and BCs (C-C) is illustrated in Figure 3.10. Due to small stretching deformation, the resulting mode shape is referred to as triply coupled mode, which are substantial involving axial, shear and flexure deformation.

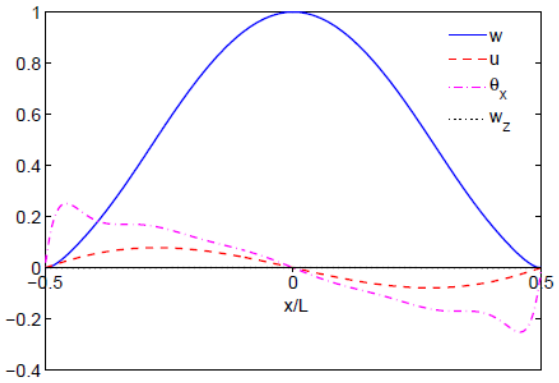

(a) Mode 1, ω_1 = 7.2898 (1-2-1)

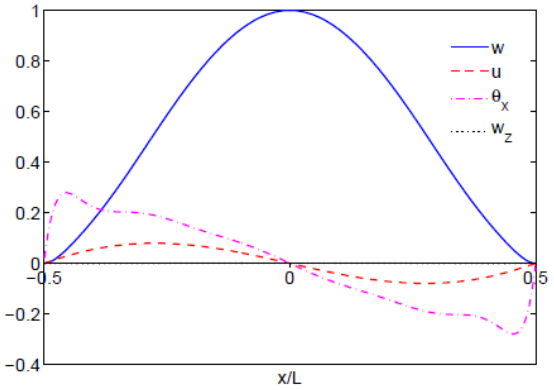

(b) Mode 1, ω_1 = 7.0320 (2-2-1)

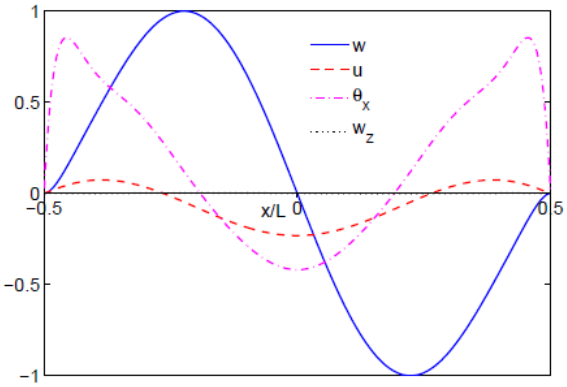

(c) Mode 2, ω_2 = 17.0413 (1-2-1)

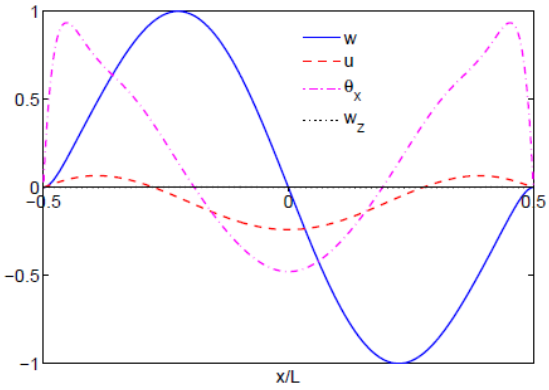

(d) Mode 2, ω_2 = 16.1729 (2-2-1)

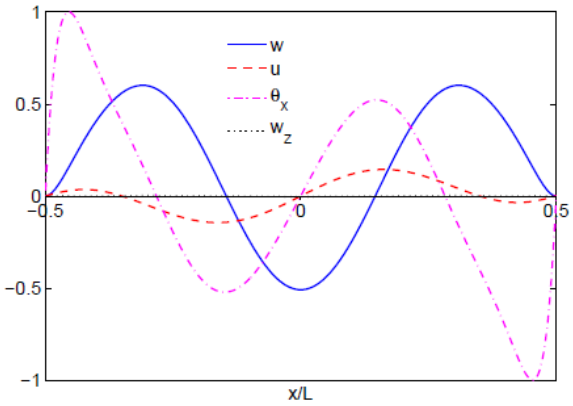

(e) Mode 3, ω_3 = 28.7917 (1-2-1)

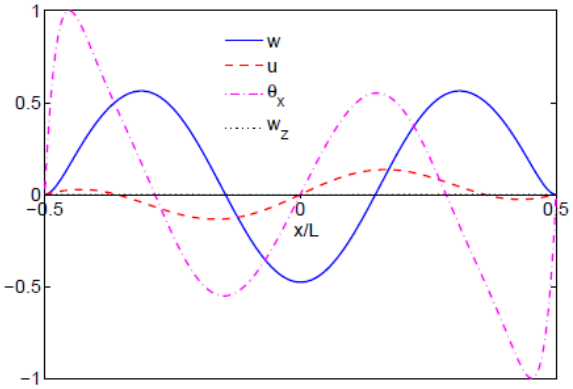

(d) Mode 3, ω_3 = 27.0964 (2-2-1)

Figure 3.10 The first three mode shapes of FG sandwich beams(Type C, *L/h* = 5, *p* = 2, C-C).

3.8 Conclusions

This chapter proposed a new higher-order shear deformation theory for static, buckling and free vibration analysis of FG beams and FG sandwich beams. The transverse shear stress accounts for a new hyperbolic distribution and satisfies the traction-free boundary conditions on the top and bottom surfaces of the beams. Governing equations of motion are derived from the Hamilton's principle and Lagrangian functional for FG beams and FG sandwich beams with homogeneous hardcore and soft core. Navier-type solution and Ritz solution are developed to solve the problem.

Numerical results are obtained to investigate effects of the power-law index, span-to height ratio and thickness ratio of layers on the deflection, stresses, critical buckling load and natural frequencies. The present model is found to be appropriate and efficient in analyzing static, buckling and vibration of FG beams and FG sandwich beams.

Chapter 4
Hygro-thermo-mechanical effects on the static, buckling and vibration behaviors of FGbeams

---

The objective of this chapter is to present hygro-thermal responses of FG beams using a higher-order shear deformation theory in which a higher-order variation of both in-plane and out of plane displacement is considered.

The structure of this chapter is as follows:

- The hygro-thermal effects on vibration and buckling analysis of functionally graded beams are presented in this chapter. The present work is based on a higher-order shear deformation theory which accounts for a hyperbolic distribution of transverse shear stress and higher-order variation of in-plane and out-of-plane displacements.
- Equations of motion are obtained from Lagrange's equations.
- This paper proposes novel Ritz functions are used to solve problems with different boundary conditions.
- Effects of power-law index, span-to-height ratio, transverse normal strain, temperature and moisture changes on the results are discussed.
- Numerical results for natural frequencies and critical buckling temperatures of functionally graded beams are compared with those obtained from previous works.

4.1 Introduction

Hygro-thermal stresses arising from a variation of temperature and moisture content can affect structural responses of engineering structures. Therefore, an accurate evaluation of environmental exposure is important to investigate hygro-thermal effects on their behaviors. Owing to the low density and high stiffness and strength, composite structures become popular in several applications of aerospace, automotive engineering, construction, etc. They became more attractive due to an introduction of functionally graded (FG) materials. The general benefit of these structures compared to conventional ones is a continuous variation of hygro-thermal elastic properties in a required direction so that interfacial issues found in laminated composite structures could be neglected.

In order to accurately predict hygro-thermo-mechanical behaviors of FG nano beams and FG plates/beams, several models and approaches have been developed in recent years. Ebrahimi and Salari [142, 143] investigated nonlocal thermo-mechanical buckling and free vibration of FG nano beams in thermal environments. Ebrahimi and Barati [144] proposed a unified formulation for dynamic analysis of nonlocal heterogeneous nano beams in hygro-thermal environment. Zidi et al. [145] analyzed static responses of FG plates under hygro-thermo-mechanical loading using a four variable refined plate theory. Zenkour et al. [146, 147] investigated hygro-thermo-mechanical effects on behaviors of FG plates on elastic foundations. Fazzolari and Carrera [66] studied thermal stability of FG sandwich plates under various through the thickness temperature distributions. Vibration and buckling analysis of FG beams under mechanical loads have been investigated by many authors based on classical beam theory (CBT) [20, 23], first-order shear deformation beam theory (FSBT) [4, 103, 120, 121, 148], higher-order shear deformation beam theory (HSBT) [5, 7, 117-119, 123, 128, 133, 139, 149-151].

For thermal environments, the thermal stability and vibration analysis of FG beams have studied by many authors with different methods. Esfahani et al. [152] studied nonlinear thermal buckling of FG beams. The nonlinear thermal dynamic buckling of FG beams is

also investigated by Ghiasian et al. [100]. Ma and Lee [153] proposed exact solutions for nonlinear bending behavior of FG beams under an in-plane thermal loading. Malekzadeh and Monajjemzadeh [154] investigated the dynamic thermal response of FG beams under a moving load. Sankar [155] studied the thermal stresses of simply supported FG beams. Wattanasakulpong et al. [99] employed the HSBT to study the buckling and vibration of FG beams under the uniform thermal loading. Sun et al. [156] investigated thermal buckling and post-buckling of FG beams on nonlinear elastic foundation. Trinh et al. [108] used Levy-type solution for studying thermo-mechanical responses of FG beams. Bhangale and Ganesan [129] analyzed thermoelastic buckling and vibration behaviors of FG sandwich beam with constrained viscoelastic core. By using the differential quadrature method, Pradhan and Murmu [85] analyzed thermo-mechanical vibration of FG sandwich beams. However, a limited number of research has been considered to investigate responses of FG beams in moisture environments. Shen [157, 158] studied nonlinear analysis of composite laminated beams in hygro-thermal environments. Moreover, it is known that Ritz method is efficient to deal with composite and FG beams with arbitrary boundary conditions. The accuracy and efficiency of this approach can be found in some representative earlier works [5, 22, 50, 150, 159-161].

The objective of this chapter is to present hygro-thermal responses of FG beams using a higher-order shear deformation theory in which a higher-order variation of both in-plane and out of plane displacement is considered. FG beams are composed of ceramic and metal mixtures, and the material properties are varied according to power-law form. New Ritz solution is developed for different boundary conditions to verify the accuracy of the present theory and to investigate the effects of the power-law index, the span-to-height ratio, the temperature and moisture content on the vibration and buckling responses of FG beams under hygro-thermal loadings.

4.2 Novel Ritz-shape functions for analysis of FG beams with various BCs

4.2.1 Material properties

An FG beam made of a mixture of ceramic and metal isotropic materials, which is embedded in a moisture and temperature environment, with length L and uniform section $b \times h$ is considered as shown in Figure 3.1a. The material properties are varied according to power-law form:

$$P(z) = (P_c - P_m)\left(\frac{2z+h}{2h}\right)^p + P_m \tag{4.1}$$

where p is the power-law index, P_c and P_m are Young's modulus E, mass density ρ, coefficient of thermal expansion α, coefficient of moisture expansion β, thermal conductivity coefficient k of ceramic and metal materials, respectively.

Moreover, the thermo-elastic material properties of FG beams are also expressed in terms of temperature T(K) [154]:

$$H = H_0\left(H_{-1}T^{-1} + 1 + H_1T + H_2T^2 + H_3T^3\right) \tag{4.2}$$

where H_{-1}, H_0, H_1, H_2, and H_3 are temperature dependent coefficients for various types of materials in Table 4.1. It should be noted that both temperature dependency (TD) and temperature independency (TID) are considered in this studied.

4.2.2 Moisture and temperature distribution

Three different moisture and temperature distributions through the beam depth are considered: Uniform moisture and temperature rise, linear moisture and temperature rise and nonlinear moisture and temperature rise.

- Uniform moisture and temperature rise: The temperature and moisture are supposed to be uniform in the beam and increased from a reference T_0 and C_0, thus their current values of temperature and moisture are:

$$\begin{aligned} T &= T_0 + \Delta T \\ C &= C_0 + \Delta C \end{aligned} \tag{4.3}$$

where T_0 and C_0 are reference temperature and moisture, respectively, which are supposed to be at the bottom surface of the beam.

Table 4.1: Temperature dependent coefficients for ceramic and metal materials.

Material	H_0	H_{-1}	H_1	H_2	H_3	H at 300 K
Al_2O_3						
E	349.55e+9	0	-3.853e-4	4.027e-7	-1.673e-10	320.24e+9
α	6.826e-6	0	1.838e-4	0	0	7.203e-6
ν	0.26	0	0	0	0	0.260
ρ	3800	0	0	0	0	3800
Si_3N_4						
E	348.43e+9	0	-3.070e-4	2.160e-7	-8.946e-11	322.27e+9
α	5.8723e-6	0	9.095e-4	0	0	7.475e-6
κ	13.723	0	-1.032e-3	5.466e-7	-7.876e-11	-
ν	0.24	0	0	0	0	0.240
ρ	2370	0	0	0	0	2370
β	0	0	0	0	0	0
ZrO_2						
E	244.27e+9	0	-1.371e-3	1.214e-6	-3.681e-10	168.06e+9
α	12.766e-6	0	-1,491e-3	1.006e-5	-6.778e-11	18.591e-6
κ	1.7	0	1.276e-4	6.648e-8	0	-
ν	0.2882	0	1.133e-4	0	0	0.298
ρ	3657	0	0	0	0	3657
SUS3O4						
E	201.04e+9	0	3.079e-4	-6.534e-7	0	207.79e+9
α	12.330e-6	0	8.086e-4	0	0	15.321e-6
κ	15.379	0	-1.264e-3	2.092e-6	-7.223e-10	-
ν	0.3262	0	-2.002e-4	3.797e-7	0	0.318
ρ	8166	0	0	0	0	8166
β	0.0005	0	0	0	0	0

- Linear moisture and temperature rise: The temperature and moisture are linearly increased as follows:

$$\begin{aligned} T(z) &= (T_t - T_b)\left(\frac{2z+h}{2h}\right) + T_b \\ C(z) &= (C_t - C_b)\left(\frac{2z+h}{2h}\right) + C_b \end{aligned} \tag{4.4}$$

where T_t and T_b are temperatures as well as C_t and C_b are moisture content at the top and bottom surfaces of the beam.

- Nonlinear moisture and temperature rise: The temperature and moisture are varied nonlinearly according to a sinusoidal law [66] as follows:

$$\begin{aligned} T(z) &= (T_t - T_b)\left[1 - \cos\frac{\pi}{2}\left(\frac{2z+h}{2h}\right)\right] + T_b \\ C(z) &= (C_t - C_b)\left[1 - \cos\frac{\pi}{2}\left(\frac{2z+h}{2h}\right)\right] + C_b \end{aligned} \tag{4.5}$$

In addition, the temperature distribution obtained from Fourier equation of steady-state one-dimensional heat conduction is also considered:

$$T(z) = T_b + \frac{T_t - T_b}{\int_{-h/2}^{h/2} \frac{1}{k(z)} dz} \int_{-h/2}^{z} \frac{1}{k(z)} dz \tag{4.6}$$

4.2.3 Kinematics

The displacement field is chosen from previous study Quasi-3D1 [149]:

$$\begin{aligned} u(x,z,t) &= u_0(x,t) - z w_{0,x} + \left[\sinh^{-1}\left(\frac{z}{h}\right) - \frac{8z^3}{3\sqrt{5}h^3}\right]\theta(x,t) \\ &= u_0(x,t) - z w_{0,x} + f_1(z)\theta(x,t) \\ w(x,z,t) &= w_0(x,t) + \left(\frac{1}{\sqrt{h^2+z^2}} - \frac{8z^2}{\sqrt{5}h^3}\right) w_z(x,t) \\ &= w_0(x,t) + f_2(z) w_z(x,t) \end{aligned} \tag{4.7}$$

where the comma indicates partial differentiation with respect to the coordinate subscript that follows; $f_2 = f_{1,z}$, u and θ are the axial displacement and rotation; and w and w_z are the transverse displacements, respectively.

The nonzero strains are given by:

$$\begin{aligned}
\varepsilon_x(x,z,t) &= u_{0,x} - zw_{0,xx} + f_1\theta_{,x} \\
\varepsilon_z(x,z,t) &= f_{2,z}w_z \\
\gamma_{xz}(x,z,t) &= f_2\left(\theta + w_{z,x}\right)
\end{aligned} \tag{4.8}$$

The elastic constitutive equations are given by:

$$\begin{Bmatrix} \sigma_{xx} \\ \sigma_{zz} \\ \sigma_{xz} \end{Bmatrix} = \begin{bmatrix} \bar{Q}_{11} & \bar{Q}_{13} & 0 \\ \bar{Q}_{13} & \bar{Q}_{11} & 0 \\ 0 & 0 & \bar{Q}_{55} \end{bmatrix} \begin{Bmatrix} \varepsilon_{xx} \\ \varepsilon_{zz} \\ \gamma_{xz} \end{Bmatrix} \tag{4.9}$$

where $\bar{Q}_{11} = \dfrac{E(z)}{1-\nu^2}$, $\bar{Q}_{13} = \dfrac{E(z)\nu}{1-\nu^2}$, $\bar{Q}_{55} = \dfrac{E(z)\nu}{2(1+\nu)}$

If the transverse normal strain effect is omitted (ε_{zz}), the components of $\bar{Q}_{ij}$ in Eq. (4.9) are reduced as: $\bar{Q}_{11} = \dfrac{E(z)}{1-\nu^2}$, $\bar{Q}_{13} = 0$, $\bar{Q}_{55} = \dfrac{E(z)\nu}{2(1+\nu)}$. It is noted that Poisson's ratio ν is supposed to be constant through the beam thickness and its value is evaluated as the average of ceramic and metal ones.

4.2.4 Lagrange's equations

The strain energy U of system is expressed by:

$$\begin{aligned}
U &= \frac{1}{2}\int_V \left(\sigma_{xx}\varepsilon_{xx} + \sigma_{zz}\varepsilon_{zz} + \sigma_{xz}\gamma_{xz}\right)dV \\
&= \frac{1}{2}\int_0^L [Au_{0,x}^2 - 2Bu_{0,x}w_{0,xx} + Dw_{0,xx}^2 + 2B^s u_{0,x}\theta_{,x} - 2D^s w_{0,xx}\theta_{,x} + H^s\theta_{,x}^2 \\
&\quad + 2\left(Xu_{0,x}w_z - Yw_{0,xx}w_z + Y^s\theta_{,x}w_z\right) + A^s\left(\theta^2 + 2\theta w_{z,x} + w_{z,x}^2\right)]\mathrm{dx}
\end{aligned} \tag{4.10}$$

where

$$(A,B,D,B^s,D^s,H^s,Z)=\int_{-h/2}^{h/2}(1,z,z^2,f_1,zf_1,f_1^2,f_{2,z}^2)\bar{Q}_{11}(z)bdz$$

$$(X,Y,Y^s)=\int_{-h/2}^{h/2}(1,z,f_1)f_{2,z}\bar{Q}_{13}(z)bdz$$

$$A^s=\int_{-h/2}^{h/2}f_2^2\bar{Q}_{55}(z)bdz$$

The work done V by axial hygro-thermal stress resultants is expressed by:

$$V=-\frac{1}{2}\int_0^L\left(N^t+N^m\right)\left(w_{,x}\right)^2dx \tag{4.11}$$

where

$$\begin{aligned}N^t&=\int_{-h/2}^{h/2}\bar{Q}_{11}(z)\alpha(z)\left[T(z)-T^0\right]bdz\\ N^m&=\int_{-h/2}^{h/2}\bar{Q}_{11}(z)\beta(z)\left[C(z)-C^0\right]bdz\end{aligned} \tag{4.12}$$

The kinetic energy K is expressed by:

$$\begin{aligned}K=\frac{1}{2}\int_V\rho(z)\left(\dot{u}^2+\dot{w}^2\right)dV=\frac{1}{2}\int_V\Big[&I_0\dot{u}_0^2-2I_1\dot{u}_0\dot{w}_{0,x}+I_2\left(\dot{w}_{0,x}\right)^2+2J_1\dot{\theta}\dot{u}_0\\&-2J_2\dot{\theta}\dot{w}_{0,x}+K_2\dot{\theta}^2+I_0\dot{w}_0^2+2L_1\dot{w}_0\dot{w}_z+L_2\dot{w}_z^2\Big]dx\end{aligned} \tag{4.13}$$

where dot-superscript denotes the differentiation with the time t; and $\mathrm{I}_0,\mathrm{I}_1,\mathrm{I}_2,\mathrm{J}_1,$ $\mathrm{J}_2,\mathrm{K}_2,\mathrm{L}_1,\mathrm{L}_2$ are the inertia coefficients defined by:

$$(I_0,I_1,I_2,J_1,J_2,K_2,L_1,L_2)=\int_{-h/2}^{h/2}\rho(z)(1,z,z^2,f_1,\mathrm{z}\,f_1,f_1^2,f_2,f_2^2)bdz \tag{4.14}$$

Lagrangian functional is used to derive the governing equations of motion:

$$\begin{aligned}\Pi=&\frac{1}{2}\int_0^L[Au_{0,x}^2-2Bu_{0,x}w_{0,xx}+Dw_{0,xx}^2+2B^su_{0,x}\theta_{,x}-2D^sw_{0,xx}\theta_{,x}+H^s\theta_{,x}^2\\&+2\left(Xu_{0,x}w_z-Yw_{0,xx}w_z+Y^s\theta_{,x}w_z\right)+A^s\left(\theta^2+2\theta w_{z,x}+w_{z,x}^2\right)]\mathrm{dx}\\&-\frac{1}{2}\int_0^L\left(N^t+N^m\right)\left(w_{0,x}\right)^2dx-\frac{1}{2}\int_V\Big[I_0\dot{u}_0^2-2I_1\dot{u}_0\dot{w}_{0,x}+I_2\left(\dot{w}_{0,x}\right)^2\\&+2J_1\dot{\theta}\dot{u}_0-2J_2\dot{\theta}\dot{w}_{0,x}+K_2\dot{\theta}^2+I_0\dot{w}_0^2+2L_1\dot{w}_0\dot{w}_z+L_2\dot{w}_z^2\Big]dx\end{aligned} \tag{4.15}$$

4.3 Ritz method

The solution field u_0, w_0, θ and w_z is approximated as in the Eq. (3.86):

$$u_0(x,t) = \sum_{j=1}^{m} \psi_j(x) u_j e^{i\omega t}$$

$$w_0(x,t) = \sum_{j=1}^{m} \varphi_j(x) w_j e^{i\omega t}$$

$$\theta(x,t) = \sum_{j=1}^{m} \psi_j(x) \theta_j e^{i\omega t}$$

$$w_z(x,t) = \sum_{j=1}^{m} \varphi_j(x) w_{zj} e^{i\omega t}$$

where ω is the natural frequency of free vibration of the beam, $\sqrt{i} = -1$ the imaginary unit, $(u_j, w_j, \theta_j \text{ and } w_{zj})$ denotes the values to be determined, $\psi_j(x)$ and $\varphi_j(x)$ are the shape functions.

4.3.1 A shape functions for Ritz method

To derive analytical solutions, the shape functions $\psi_j(x)$ and $\varphi_j(x)$ are chosen for the various boundary conditions the Hinged – Hinged (H–H), the Clamped – Hinged (C–H), and the Clamped – Clamped (C–C) beams as in Eq. (3.87): $\psi_j(x) = x^{j-1}, \varphi_j(x) = x^{j-1}$.

By substituting Eq. (3.87) into Eq. (4.16), and using Lagrange's equations:

$$\frac{\partial \Pi^*}{\partial q_j} - \frac{d}{dt}\frac{\partial \Pi^*}{\partial \dot{q}_j} = 0 \tag{4.16}$$

with q_j representing the values of $(u_j, w_j, \theta_j, w_{zj} \text{ and } \beta_j)$ that leads to:

$$\left(\begin{bmatrix} \mathbf{K}^{11} & \mathbf{K}^{12} & \mathbf{K}^{13} & \mathbf{K}^{14} & \mathbf{K}^{15} \\ {}^T\mathbf{K}^{12} & \mathbf{K}^{22} & \mathbf{K}^{23} & \mathbf{K}^{24} & \mathbf{K}^{25} \\ {}^T\mathbf{K}^{13} & {}^T\mathbf{K}^{23} & \mathbf{K}^{33} & \mathbf{K}^{34} & \mathbf{K}^{35} \\ {}^T\mathbf{K}^{14} & {}^T\mathbf{K}^{24} & {}^T\mathbf{K}^{34} & \mathbf{K}^{44} & \mathbf{K}^{45} \\ {}^T\mathbf{K}^{15} & {}^T\mathbf{K}^{25} & {}^T\mathbf{K}^{35} & {}^T\mathbf{K}^{45} & \mathbf{0} \end{bmatrix} - \omega^2 \begin{bmatrix} \mathbf{M}^{11} & \mathbf{M}^{12} & \mathbf{M}^{13} & \mathbf{0} & \mathbf{0} \\ {}^T\mathbf{M}^{12} & \mathbf{M}^{22} & \mathbf{M}^{23} & \mathbf{M}^{24} & \mathbf{0} \\ {}^T\mathbf{M}^{13} & {}^T\mathbf{M}^{23} & \mathbf{M}^{33} & \mathbf{0} & \mathbf{0} \\ \mathbf{0} & {}^T\mathbf{M}^{24} & \mathbf{0} & \mathbf{M}^{44} & \mathbf{0} \\ \mathbf{0} & \mathbf{0} & \mathbf{0} & \mathbf{0} & \mathbf{0} \end{bmatrix} \right) \begin{Bmatrix} u \\ w \\ \theta_x \\ w_z \\ \beta \end{Bmatrix} = \begin{Bmatrix} \mathbf{0} \\ \mathbf{0} \\ \mathbf{0} \\ \mathbf{0} \\ \mathbf{0} \end{Bmatrix} \tag{4.17}$$

where the components of the stiffness matrix **K** and the mass matrix **M** are given as follows:

$$
\begin{aligned}
&K_{ij}^{11} = A\int_0^L \psi_{i,x}\psi_{j,x}dx, K_{ij}^{12} = -B\int_0^L \psi_{i,x}\varphi_{j,xx}dx, K_{ij}^{13} = B^s\int_0^L \psi_{i,x}\psi_{j,x}dx,\\
&K_{ij}^{22} = D\int_0^L \varphi_{i,xx}\varphi_{j,xx}dx - N^t\int_0^L \varphi_{i,x}\varphi_{j,x}dx - N^m\int_0^L \varphi_{i,x}\varphi_{j,x}dx\\
&K_{ij}^{14} = X\int_0^L \psi_{i,x}\varphi_j dx, K_{ij}^{23} = -D^s\int_0^L \varphi_{i,xx}\psi_{j,x}dx, K_{ij}^{24} = -Y\int_0^L \varphi_{i,xx}\varphi_j dx,\\
&K_{ij}^{33} = H^s\int_0^L \psi_{i,x}\psi_{j,x}dx + A_{55}^s\int_0^L \psi_i\psi_j dx\\
&K_{ij}^{34} = Y^s\int_0^L \psi_{i,x}\varphi_j dx + A_{55}^s\int_0^L \psi_i\varphi_{j,x}dx\\
&K_{ij}^{44} = Z\int_0^L \varphi_i\varphi_j dx + A_{55}^s\int_0^L \varphi_{i,x}\varphi_{j,x}dx;\\
&M_{ij}^{11} = I_0\int_0^L \psi_i\psi_j dx, M_{ij}^{12} = -I_1\int_0^L \psi_i\varphi_{j,x}dx, M_{ij}^{13} = J_1\int_0^L \psi_i\psi_j dx,\\
&M_{ij}^{22} = I_0\int_0^L \varphi_i\varphi_j dx + I_2\int_0^L \varphi_{i,x}\varphi_{j,x}dx, M_{ij}^{23} = -J_2\int_0^L \varphi_{i,x}\psi_j dx\\
&M_{ij}^{24} = L_1\int_0^L \varphi_i\varphi_j dx, M_{ij}^{33} = K_2\int_0^L \psi_i\psi_j dx, M_{ij}^{44} = L_2\int_0^L \varphi_i\varphi_j dx
\end{aligned}
\tag{4.18}
$$

Table 4.2 Kinematic BCs of the beams.

BCs	*x=0*	*x=L*
S – S	$w=0, w_z=0$	$w=0, w_z=0$
H – H	$u=0, w=0, w_z=0$	$u=0, w=0, w_z=0$
C – H	$u=0, w=0, w_{,x}=0, \theta=0, w_z=0$	$u=0, w=0, w_z=0$
C – C	$u=0, w=0, w_{,x}=0, \theta=0, w_z=0$	$u=0, w=0, w_{,x}=0, \theta=0, w_z=0$
C – S	$u=0, w=0, w_{,x}=0, \theta=0, w_z=0$	$w=0, w_z=0$
C – F	$u=0, w=0, w_{,x}=0, \theta=0, w_z=0$	

The components of $\mathbf{K}^{15}$, $\mathbf{K}^{25}$, $\mathbf{K}^{35}$, and $\mathbf{K}^{45}$, which depend on number of boundary conditions in Table 4.2, are list below.

- For Hinged – Hinged (H – H) beams:

$$\begin{aligned}
&K_{i1}^{15}=\psi_i(0), K_{i2}^{15}=\psi_i(L), K_{ij}^{15}=0, && \text{with } j=3,4,...,6\\
&K_{i3}^{25}=\varphi_i(0), K_{i4}^{25}=\varphi_i(L), K_{ij}^{25}=0, && \text{with } j=1,2,5,6\\
&K_{ij}^{35}=0, && \text{with } j=1,2,...,6\\
&K_{i5}^{45}=\varphi_i(0), K_{i6}^{45}=\varphi_i(L), K_{ij}^{45}=0, && \text{with } j=1,2,3,4
\end{aligned} \tag{4.19}$$

- For Clamped – Hinged (C – H) beams:

$$\begin{aligned}
&K_{i1}^{15}=\psi_i(0), K_{i2}^{15}=\psi_i(L), K_{ij}^{15}=0, && \text{with } j=3,4,...,8\\
&K_{i3}^{25}=\varphi_i(0), K_{i4}^{25}=\varphi_i(L), K_{i5}^{25}=\varphi_{i,x}(0), K_{ij}^{25}=0,\\
&&& \text{with } j=1,2,6,7,8\\
&K_{i6}^{35}=\psi_i(0), K_{ij}^{35}=0, \text{with } j=1,2,...,4,7,8\\
&K_{i7}^{45}=\varphi_i(0), K_{i8}^{45}=\varphi_i(L), K_{ij}^{45}=0, && \text{with } j=1,2,...,6
\end{aligned} \tag{4.20}$$

- For Clamped – Clamped (C – C) beams:

$$\begin{aligned}
&K_{i1}^{15}=\psi_i(0), K_{i2}^{15}=\psi_i(L), K_{ij}^{15}=0, && \text{with } j=3,4,...,10\\
&K_{i3}^{25}=\varphi_i(0), K_{i4}^{25}=\varphi_i(L), K_{i5}^{25}=\varphi_{i,x}(0), K_{i6}^{25}=\varphi_{i,x}(L), K_{ij}^{25}=0,\\
&&& \text{with } j=1,2,7,...,10\\
&K_{i7}^{35}=\psi_i(0), K_{i8}^{35}=\psi_i(L), K_{ij}^{35}=0, \text{with } j=1,2,...,6,9,10\\
&K_{i9}^{45}=\varphi_i(0), K_{i10}^{45}=\varphi_i(L), K_{ij}^{45}=0, && \text{with } j=1,2,...,8
\end{aligned} \tag{4.21}$$

4.3.2 A new hybrid functions for Ritz method

In this chapter, the new hybrid functions $\psi_j(x)$ and $\varphi_j(x)$ for Ritz solution reported in Table 4.3 are proposed for six typical BCs. It is clear that they satisfy various BCs:

Table 4.3 A new hybrid functions for Ritz solution.

BCs	$\frac{\psi_j(x)}{e^{-jx/L}}$	$\frac{\varphi_j(x)}{e^{-jx/L}}$
S – S	$\cos\left(\frac{\pi}{L}x\right)$	$\sin\left(\frac{\pi}{L}x\right)$
H – H	$\sin\left(\frac{\pi}{L}x\right)$	$\sin\left(\frac{\pi}{L}x\right)$
C – S	$\sin\left(\frac{\pi}{2L}x\right)$	$\sin^2\left(\frac{\pi}{2L}x\right)\cos\left(\frac{\pi}{2L}x\right)$
C – H	$\sin\left(\frac{\pi}{L}x\right)$	$\sin^2\left(\frac{\pi}{2L}x\right)\cos\left(\frac{\pi}{2L}x\right)$
C – F	$\sin\left(\frac{\pi}{2L}x\right)$	$\sin^2\left(\frac{\pi}{2L}x\right)$
C – C	$\sin\left(\frac{\pi}{L}x\right)$	$\sin^2\left(\frac{\pi}{L}x\right)$

4.4 Numerical results and discussions

In this studied, several numerical examples are analyzed to verify the accuracy of present theory and investigate the effects of power-law index, span-to-height ratio, transverse normal strain, temperature and moisture content on buckling and vibration responses of FG beams (Type A) for various BCs in Table 4.2 and Table 4.3. FG beams are made of ceramic (Si_3N_4, Al_2O_3) and metal (SUS304) with material properties in Table 4.1.

Three types of temperature and moisture distribution through the beam depth are considered:

- Uniform moisture and temperature rise (UMR, UTR),
- Linear moisture and temperature rise (LMR, LTR),
- Nonlinear moisture and temperature rise (NLMR, NLTR).

The following non-dimensional parameters are used:

$$\bar{\omega} = \omega \frac{L^2}{h}\sqrt{\frac{I_0}{\int_{-h/2}^{h/2} E(z)\,dz}}, \hat{\omega} = \omega \frac{L^2}{h}\sqrt{\frac{12\rho_c}{E_c}}, \lambda = \Delta T_{cr}\left(\frac{L}{h}\right)^2 \alpha_m, \tag{4.22}$$

where α_m is thermal expansion coefficient of metal at $T_0(K)$. Noticing that the following relations are used in this study: $T_0 = 300(K), C_0 = 0\%, T_b - T_0 = 5(K)$.

Table 4.4 Convergence test for the non-dimensional fundamental frequency ($\bar{\omega}$) of Si_3N_4 and SUS304 beams under Fourier-law NLTR (Type A, *p*=1, *L/h*=20 and ΔT=20, ΔC=0).

BCs	Normal strain	N						
		6	8	10	12	14	16	18
H-H	$\varepsilon_{zz} = 0$	5.9735	5.9719	5.9719	5.9719	5.9719	5.9719	5.9719
H-H[b]	$\varepsilon_{zz} = 0$	6.0616	6.0612	6.0611	6.0609	6.0609	6.0609	6.0609
	$\varepsilon_{zz} \neq 0$	5.7193	5.7178	5.7178	5.7178	5.7178	5.7178	5.7178
C-H	$\varepsilon_{zz} = 0$	9.4357	9.4283	9.4271	9.4265	9.4261	9.4259	9.4257
C-H[b]	$\varepsilon_{zz} = 0$	9.4940	9.4926	9.4926	9.4920	9.4919	9.4919	9.4919
	$\varepsilon_{zz} \neq 0$	9.1075	9.0795	9.0716	9.0678	9.0656	9.0640	9.0627
C-C	$\varepsilon_{zz} = 0$	13.7367	13.7045	13.6990	13.6967	13.6953	13.6944	13.6938
C-C[b]	$\varepsilon_{zz} = 0$	13.7532	13.7457	13.7454	13.7435	13.7435	13.7435	13.7435
	$\varepsilon_{zz} \neq 0$	13.3787	13.2585	13.2321	13.2204	13.2140	13.2095	13.2057
S-S[b]	$\varepsilon_{zz} = 0$	6.0203	6.0202	6.0202	6.0202	6.0202	6.0202	6.0202
C-S[b]	$\varepsilon_{zz} = 0$	9.4814	9.4802	9.4799	9.4797	9.4797	9.4797	9.4797
C-F[b]	$\varepsilon_{zz} = 0$	2.1037	1.9894	1.9843	1.9841	1.9841	1.9841	1.9841

b: A new hybrid functions.

For convergence test, Table 4.4 reports the first natural frequency with respect to the number of series *N* of Si_3N_4/SUS304 beams with *p*=1, *L/h*=20 and Δ*T*=20, Δ*C* =0. The results are calculated with different boundary conditions and Fourier-law NLTR. In order to obtain good solution, the number of series *N* are chosen 8 for S – S, H – H, 12 for C –H, C – S, C – F and 14 for C – C beams, respectively. For this reason, these numbers are used in the following study.

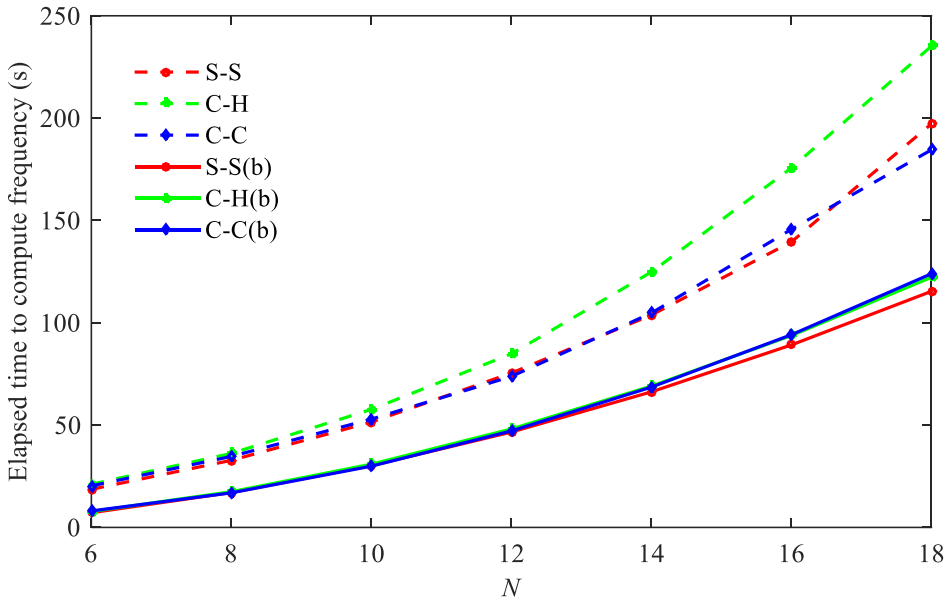

Figure 4.1 Elapsed time to compute frequency

The calculation programs in this section are implemented with Matlab software version 2015a on computers with Corei7-3632QM CPU configuration 2.20 GHz. Figure 4.1, it is easy to see that the various boundary conditions of polynomial functions in Eq. (3.87), the calculation time is longer than the corresponding boundary conditions using the hybrid function in Table 4.3. This is also proved easily because the overall matrix when using the hybrid function will be smaller than the polynomial function in Eq. (4.17). Therefore, in this case the hybrid function is more optimal than the polynomial function. "b" is used to indicate that the new hybrid functions in Figure 4.1 and this index will be used in the next examples for verification studies.

As in the first study, FG beams under uniform temperature rise (UTR) are considered. Table 4.5 presents the normalized critical temperatures of Si_3N_4/SUS304 beams for both temperature dependency (TD) and temperature independency (TID) solutions with different values of power-law index *p*. It is noted that the results reported in this research assume that the temperature resultant in Eq (4.12) is calculated with $\bar{Q}_{11} = E(z)/(1-\nu)$. The results are compared with those of Wattanasakulpong et al. [99] and Trinh et al.

[108] using HSBT. The present results without normal strain ($\varepsilon_{zz} = 0$) are in good agreement with earlier works. Figure 4.2a presents the effect of the power-law index p on the normalized critical temperatures of Si_3N_4/SUS304 beams with *L/h* = 20. It is plotted with both TD and TID solutions as well as with and without normal strain. The normalized critical temperatures decrease with the increase of *p* and the results with $\varepsilon_{zz} \neq 0$ are smaller than those with $\varepsilon_{zz} = 0$. This can be explained by the fact that the effect of transverse normal strain made beams softer. This figure also shows that the TD solutions give lower values than the TID ones, which emphasizes the importance of temperature dependency in the FG beams. Similarly, the accuracy of present theory in predicting the vibration response of Al_2O_3/SUS304 FG beams is studied in Table 4.6. The results are calculated with *p* = 0.2, 2 and ΔT = 0, 50 and 100. It is seen that good agreements between HSBTs are again found for all cases. Figure 4.2b displays the effects of UTR on the normalized fundamental frequency of Al_2O_3/SUS304 FG beams (*L/h* = 30 and *p* = 2). Obviously, the result decreases with the increase of ΔT up to critical temperatures at which the fundamental frequencies vanish. In this case, the critical temperatures of H – H, C – H and C – C in Table 4.2b beams are 52.6580 (K), 103.5923 (K) and 192.1833 (K), respectively.

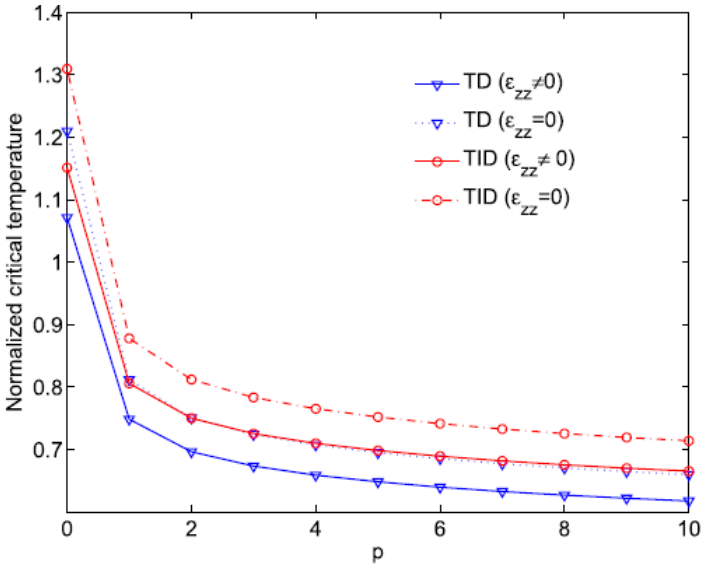

(*a*) λ *of* Si_3N_4 / *SUS304 beams with L/h=20.*

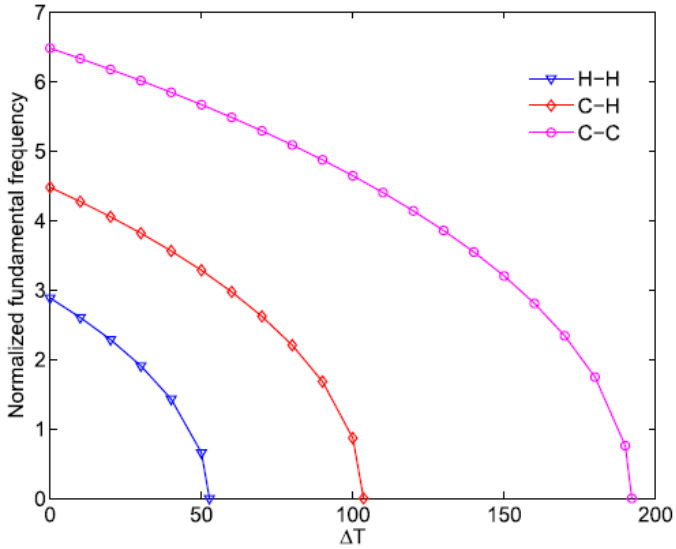

(*b*) $\bar{\omega}$ of Al_2O_3/SUS304 beams with L/h=30, p=2

Figure 4.2 Variation of normalized critical temperature and fundamental frequency of FG beams with respect to the power-law index p and the uniform temperature rise ΔT.

Table 4.5 Normalized critical temperatures (λ) of FG beams under UTR (Type A, L/h = 20, Si_3N_4/SUS304).

Temperature dependency	BCs	Theory	p					
			0	0.5	1	2	5	10
TD	H-H	HSBT ($\varepsilon_{zz}=0$)	1.309	0.970	0.878	0.812	0.752	0.714
		HSBT^b ($\varepsilon_{zz}=0$)	1.3097	0.9713	0.8781	0.8123	0.7521	0.7140
		Quasi-3D ($\varepsilon_{zz}\neq 0$)	1.210	0.897	0.811	0.751	0.695	0.660
		HSBT[108]	1.307	–	0.866	–	0.744	0.710
		HSBT [99]	1.348	–	0.876	–	0.750	0.712
	C-C	HSBT ($\varepsilon_{zz}=0$)	5.133	3.780	3.399	3.136	2.918	2.784
		HSBT^b ($\varepsilon_{zz}=0$)	5.1325	3.7816	3.3991	3.1363	2.9183	2.7837
		Quasi-3D ($\varepsilon_{zz}\neq 0$)	4.781	3.522	3.169	2.925	2.720	2.594
		HSBT[108]	5.130	–	3.398	–	2.917	2.782
	C-H	HSBT ($\varepsilon_{zz}=0$)	2.656	1.958	1.763	1.628	1.514	1.443
		HSBT^b ($\varepsilon_{zz}=0$)	2.6573	1.9598	1.7637	1.6288	1.5148	1.4435
		Quasi-3D ($\varepsilon_{zz}\neq 0$)	2.464	1.817	1.637	1.512	1.405	1.339
		HSBT[108]	2.654	–	1.758	–	1.510	1.440
	S-S	HSBT^b ($\varepsilon_{zz}=0$)	1.3093	0.9641	0.8668	0.8005	0.7456	0.7111
	C-S	HSBT^b ($\varepsilon_{zz}=0$)	2.6559	1.9562	1.7586	1.6235	1.5116	1.4417
	C-F	HSBT^b ($\varepsilon_{zz}=0$)	0.3304	0.2432	0.2187	0.2020	0.1882	0.1795
TID	H-H	HSBT ($\varepsilon_{zz}=0$)	1.151	0.882	0.806	0.750	0.698	0.665
		HSBT^b ($\varepsilon_{zz}=0$)	1.1516	0.8827	0.8059	0.7501	0.6985	0.6655
		Quasi-3D ($\varepsilon_{zz}\neq 0$)	1.071	0.820	0.748	0.696	0.648	0.617
		HSBT[108]	1.151	–	0.796	–	0.693	0.663
		HSBT [99]	1.185	–	0.805	–	0.697	0.664
	C-C	HSBT ($\varepsilon_{zz}=0$)	3.553	2.831	2.606	2.458	2.332	2.248
		HSBT^b ($\varepsilon_{zz}=0$)	3.5531	2.8337	2.6119	2.4607	2.3334	2.2413
		Quasi-3D ($\varepsilon_{zz}\neq 0$)	3.336	2.663	2.456	2.313	2.190	2.102
		HSBT[108]	3.559	–	2.609	–	2.333	2.244
	C-H	HSBT ($\varepsilon_{zz}=0$)	2.116	1.644	1.506	1.408	1.324	1.269
		HSBT^b ($\varepsilon_{zz}=0$)	2.1171	1.6457	1.5062	1.4081	1.3230	1.2682
		Quasi-3D ($\varepsilon_{zz}\neq 0$)	1.981	1.538	1.408	1.316	1.235	1.184
		HSBT[108]	2.115	–	1.503	–	1.321	1.267
	S-S	HSBT^b ($\varepsilon_{zz}=0$)	1.1512	0.8769	0.7966	0.7403	0.6930	0.6631
	C-S	HSBT^b ($\varepsilon_{zz}=0$)	2.1163	1.6430	1.5023	1.4040	1.3206	1.2668
	C-F	HSBT^b ($\varepsilon_{zz}=0$)	0.3172	0.2360	0.2128	0.1969	0.1837	0.1754

Table 4.6 Fundamental frequency ($\bar{\omega}$) of FG beams under UTR (Type A, L/h = 30, Al_2O_3/SUS304).

Temperature dependency	BCs	Theory	p=0.2			p=2		
			0	50	100	0	50	100
TD	H-H	HSBT ($\varepsilon_{zz}=0$)	2.9484	1.8416	–	3.0100	1.1810	–
		Quasi-3D ($\varepsilon_{zz}\neq 0$)	2.8232	1.6347	–	2.8826	0.8051	–
		HSBT[108]	2.9506	1.8450	–	3.0129	1.1816	–
	C-C	HSBT ($\varepsilon_{zz}=0$)	6.6373	6.1198	5.5490	6.7339	5.9821	5.1090
		Quasi-3D ($\varepsilon_{zz}\neq 0$)	6.3768	5.8352	5.2320	6.4732	5.6854	4.7553
		HSBT[108]	6.6371	6.1209	5.5489	6.7366	5.9834	5.1125
		HSBT [99]	6.6394	6.1189	5.5452	6.7355	5.9802	5.1028
	C-H	HSBT ($\varepsilon_{zz}=0$)	4.5901	3.8552	2.9281	4.6625	3.5699	1.8886
		Quasi-3D ($\varepsilon_{zz}\neq 0$)	4.4056	3.6320	2.6236	4.4772	3.3216	1.3476
		HSBT[108]	4.5898	3.8574	2.9297	4.6653	3.5731	1.8925
TID	H-H	HSBT ($\varepsilon_{zz}=0$)	2.9484	1.8191	–	3.0100	1.0859	–
		Quasi-3D ($\varepsilon_{zz}\neq 0$)	2.8232	1.6086	–	2.8826	0.6563	–
		HSBT[108]	2.9506	1.8220	–	3.0129	1.0868	–
	C-C	HSBT ($\varepsilon_{zz}=0$)	6.6373	6.1124	5.5126	6.7339	5.9605	5.0032
		Quasi-3D ($\varepsilon_{zz}\neq 0$)	6.3768	5.8266	5.1905	6.4732	5.6616	4.6378
		HSBT[108]	6.6371	6.1142	5.5141	6.7366	5.9631	5.0068
		HSBT [99]	6.6394	6.1109	5.5081	6.7335	5.9581	4.9965
	C-H	HSBT ($\varepsilon_{zz}=0$)	4.5901	3.8431	2.8594	4.6625	3.5347	1.5906
		Quasi-3D ($\varepsilon_{zz}\neq 0$)	4.4056	3.6185	2.5435	4.4772	3.2828	0.8707
		HSBT[108]	4.5898	3.8437	2.8608	4.6653	3.5391	1.5946

The next example aims to investigate the effects of linear and nonlinear temperature rise (LTR, NLTR) on the thermal buckling and vibration of FG beams. For verification purpose, the critical temperatures of Si_3N_4/SUS304 beams with L/h = 40 are reported in Table 4.7. These results are compared with those of Esfahani et al. [152], Ebrahimi and Salari [142] based on FSDT. It is observed that the present solutions are in good agreement with those of [152] for C–C beams under the Fourier-law NLTR while there are slight deviations for several values of p between the present solutions and those of [142] for H-H beams under LTR. It is noted that the superscript ‘‘a” is used to indicate that Poisson’s ratio effect is not included in the constitutive equation and thermal stress resultant ($\bar{Q}_{11}=E(z)$) and this index will be used in the next examples for verification studies.

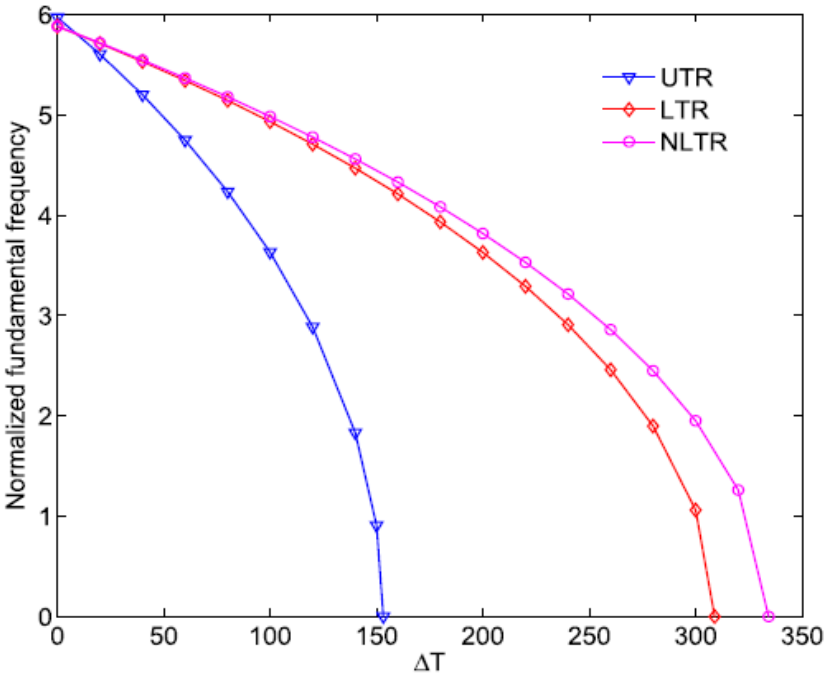

(a) p=1 and L/h=20

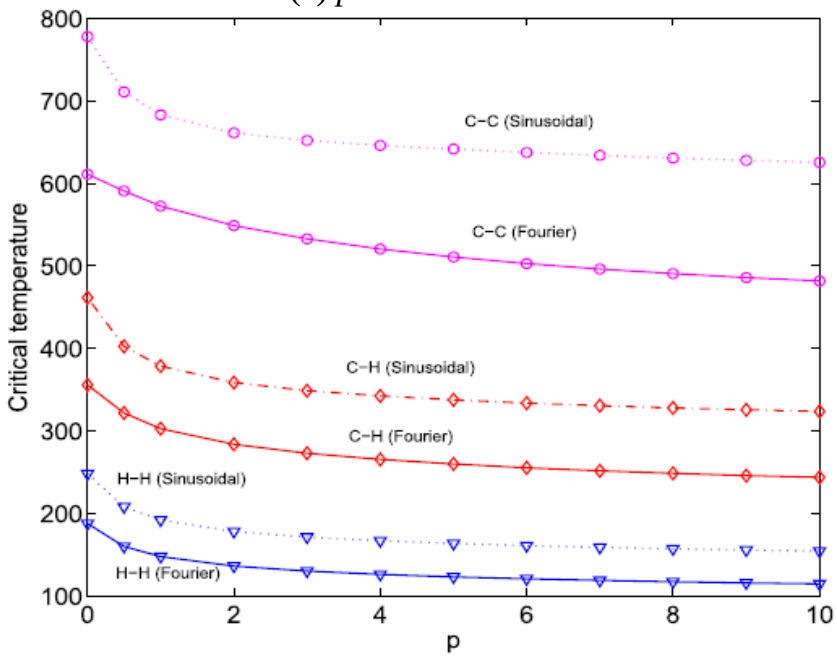

(b) L/h=30

Figure 4.3 Variation of normalized fundamental frequency of FG beams with respect to the power-law index p and temperature rise (Type A, Si_3N_4/SUS304, TD).

Table 4.7 Critical temperature (λ) of FG beams under LTR and Fourier-law NLTR (Type A, L/h = 40, Si_3N_4/SUS304, TD).

Temperature distribution	BCs	Theory	p					
			0	0.5	1	2	5	10
LTR	H-H	HSBT[a] ($\varepsilon_{zz}=0$)	116.4406	91.8046	82.9295	75.8794	69.0474	64.8133
		HSBT[b] ($\varepsilon_{zz}=0$)	116.4489	91.8593	82.9361	75.8855	69.0538	64.8135
		FSBT[142]	127.3340	95.5739	84.6229	76.4715	69.4307	–
Fourier law NLTR	C-C	HSBT[a] ($\varepsilon_{zz}=0$)	411.7059	377.7547	357.9741	337.0286	310.0925	291.3543
		HSBT[b] ($\varepsilon_{zz}=0$)	411.5244	377.7382	357.7919	336.8448	309.9130	291.1854
		FSBT[152]	412.2400	377.9600	357.9400	337.0300	310.1200	291.3500

[a] $\bar{Q}_{11}=E(z)$, *b: A new hybrid functions.*

Table 4.8 Critical temperature (λ) of FG beams under LTR for various boundary conditions (Type A, L/h = 20, Si_3N_4/SUS304, TD).

BCs	Theory	p					
		0	0.5	1	2	5	10
H-H	HSBT ($\varepsilon_{zz}=0$)	411.5245	354.710	332.653	314.449	295.2286	282.2571
	HSBT[b] ($\varepsilon_{zz}=0$)	411.6255	354.943	332.747	314.546	295.3254	282.3345
	Quasi-3D($\varepsilon_{zz}\neq 0$)	385.1274	330.2483	308.9443	291.3484	272.8943	260.5459
	HSBT[a]($\varepsilon_{zz}=0$)	411.7060	354.8756	332.8174	314.6159	295.3957	282.4179
	HSBT[108]	451.5600	360.9400	328.1300	301.5600	279.6900	265.6300
C-C	HSBT ($\varepsilon_{zz}=0$)	1156.158	1106.1719	1089.8592	1078.7302	1073.7643	1065.7153
	HSBT[b] ($\varepsilon_{zz}=0$)	1156.1584	1106.4055	1089.8592	1078.7302	1073.7642	1065.7028
	Quasi-3D($\varepsilon_{zz}\neq 0$)	1100.985	1046.4138	1027.9710	1014.8334	1006.9889	997.0252
	HSBT[a]($\varepsilon_{zz}=0$)	1157.799	1107.9445	1091.7181	1080.6962	1075.8608	1067.8635
	HSBT[108]	–	1142.1900	1062.5000	1004.6900	957.8100	921.8800
C-H	HSBT ($\varepsilon_{zz}=0$)	718.5718	652.8875	624.7796	604.3525	584.2301	568.0967
	HSBT[b] ($\varepsilon_{zz}=0$)	718.8134	653.3648	625.0102	604.5985	584.4879	568.3256
	Quasi-3D($\varepsilon_{zz}\neq 0$)	679.1061	613.3336	585.5554	564.7903	544.1176	528.0379
	HSBT[a]($\varepsilon_{zz}=0$)	719.2049	653.5143	625.4122	605.0142	584.9244	568.7844
	HSBT[108]	814.0600	667.1900	612.5000	570.3100	531.2500	507.8100
S-S	HSBT[b] ($\varepsilon_{zz}=0$)	411.5244	353.1861	329.7609	311.2492	293.4330	281.4735
C-S	HSBT[b] ($\varepsilon_{zz}=0$)	718.5673	652.6818	624.0455	603.3681	583.3933	567.8582
C-F	HSBT[b] ($\varepsilon_{zz}=0$)	116.4379	91.2109	81.8686	74.7757	68.4456	64.5543

[a] $\bar{Q}_{11}=E(z)$, *b: A new hybrid functions.*

Table 4.9 Critical temperature (λ) of FG beams under Fourier-law NLTR for various boundary conditions (Type A, L/h = 20, Si_3N_4/SUS304, TD).

BCs	Theory	p					
		0	0.5	1	2	5	10
H-H	HSBT ($\varepsilon_{zz}=0$)	411.5245	379.3918	360.9977	340.3445	311.8557	291.9825
	HSBT[b] ($\varepsilon_{zz}=0$)	411.6317	379.6568	361.1057	340.4547	311.9596	292.0785
	Quasi-3D($\varepsilon_{zz}\neq 0$)	385.1274	352.4187	334.2954	314.4406	287.6173	269.1585
	HSBT[a] ($\varepsilon_{zz}=0$)	411.7060	379.5747	361.1826	340.5314	312.0370	292.1517
	HSBT[108]	451.5600	388.7500	357.5000	327.5000	293.7500	273.7500
C-C	HSBT ($\varepsilon_{zz}=0$)	1156.1584	1204.0415	1213.1728	1202.5179	1164.6606	1124.4957
	HSBT[b] ($\varepsilon_{zz}=0$)	1156.1584	1204.2395	1213.1727	1202.5179	1164.6606	1124.4949
	Quasi-3D($\varepsilon_{zz}\neq 0$)	1100.9855	1140.8570	1146.0126	1133.6258	1093.7100	1052.6690
	HSBT[a] ($\varepsilon_{zz}=0$)	1157.7996	1205.9121	1215.1809	1204.6140	1166.8631	1126.7276
	HSBT[108]	–	–	–	1132.5000	1042.5000	972.5000
C-H	HSBT ($\varepsilon_{zz}=0$)	718.5718	709.6778	695.0922	672.6986	630.3660	596.2206
	HSBT[b] ($\varepsilon_{zz}=0$)	718.7615	710.1652	695.3885	672.9898	630.6550	596.4957
	Quasi-3D($\varepsilon_{zz}\neq 0$)	679.1061	666.0060	650.0307	627.0078	585.8770	553.3163
	HSBT[a] ($\varepsilon_{zz}=0$)	719.2049	710.3689	695.8183	673.4623	631.1354	596.9569
	HSBT[108]	814.0600	736.2500	688.7500	637.5000	572.5000	531.2500
S-S	HSBT[b] ($\varepsilon_{zz}=0$)	411.6604	377.7382	357.7919	336.8448	309.9130	291.1854
C-S	HSBT[b] ($\varepsilon_{zz}=0$)	718.5679	709.4838	694.3012	671.7779	629.8435	595.9941
C-F	HSBT[b] ($\varepsilon_{zz}=0$)	116.4405	94.7985	85.7775	78.2081	70.5864	65.8123

[a] $\bar{Q}_{11}=E(z)$, *b: A new hybrid functions.*

Tables 4.8 and 4.9 show the comparisons of the critical temperatures from the present solutions and those from [108]. It shows that there are small differences between the HSBT models. The effect of normal strain is again found in which the HSBTs over-predict critical temperatures in comparison with the Quasi-3D theory. Figure 4.3a displays the variation of fundamental frequency for UTR, LTR and Fourier-law NLTR. The results decrease with the increase of ΔT and vanish at the critical temperatures.

Table 4.10 and Figure 4.3b consider the effects of temperature distribution under Fourier – law and sinusoidal – law through the beam depth for various boundary conditions. For comparison, the critical temperature with Fourier law is smaller than that with sinusoidal one.

Table 4.10 Critical temperature (λ) of FG beams under Fourier and sinusoidal-law NLTR (Type A, L/h = 30, Si_3N_4/SUS304, TD).

Temperature distribution	BCs	Theory	p					
			0	0.5	1	2	5	10
Fourier	H-H	HSBT ($\varepsilon_{zz}=0$)	202.2578	173.5389	160.5549	148.3615	134.2035	125.0658
		HSBT^b ($\varepsilon_{zz}=0$)	202.2828	173.6457	160.5751	148.3834	134.2251	125.0851
		Quasi-3D($\varepsilon_{zz}\neq 0$)	187.7199	160.0195	147.7213	136.2821	123.1300	114.6789
	C-C	HSBT ($\varepsilon_{zz}=0$)	647.7525	630.7537	613.2717	589.7918	550.4308	519.7221
		HSBT^b ($\varepsilon_{zz}=0$)	647.7525	630.9784	613.2717	589.7918	550.4308	519.7216
		Quasi-3D($\varepsilon_{zz}\neq 0$)	611.2257	590.8552	572.5358	548.9211	510.9149	481.7654
	C-H	HSBT ($\varepsilon_{zz}=0$)	379.9401	345.7176	326.5833	306.6677	281.4281	264.1042
		HSBT^b ($\varepsilon_{zz}=0$)	380.0093	345.9351	326.6459	306.7295	281.4875	264.1611
		Quasi-3D($\varepsilon_{zz}\neq 0$)	355.7747	321.7415	302.8348	283.7695	259.9836	243.8099
	S-S	HSBT^b ($\varepsilon_{zz}=0$)	202.2578	172.5566	158.7477	146.4388	133.1738	124.6393
	C-S	HSBT^b ($\varepsilon_{zz}=0$)	379.9392	345.5418	326.0044	306.0376	281.0863	263.9608
	C-F	HSBT^b ($\varepsilon_{zz}=0$)	48.8333	36.9935	32.5143	28.9856	25.6615	23.6175
Sinusoidal	H-H	HSBT ($\varepsilon_{zz}=0$)	266.8324	224.9764	208.1080	193.4138	178.0297	168.1896
		HSBT^b ($\varepsilon_{zz}=0$)	266.8651	225.1077	208.1357	193.4415	178.0572	168.1996
		Quasi-3D($\varepsilon_{zz}\neq 0$)	248.2054	208.2022	192.1421	178.2136	163.6644	154.4077
	C-C	HSBT ($\varepsilon_{zz}=0$)	823.1910	755.8429	727.9468	706.6631	687.8553	672.7974
		HSBT^b ($\varepsilon_{zz}=0$)	823.1910	756.0849	727.9468	706.6631	687.8553	672.7655
		Quasi-3D($\varepsilon_{zz}\neq 0$)	778.0221	710.9078	683.0384	661.3097	641.8079	625.5963
	C-H	HSBT ($\varepsilon_{zz}=0$)	491.8173	430.8636	406.2229	385.4767	364.4358	349.8751
		HSBT^b ($\varepsilon_{zz}=0$)	491.8957	431.0940	406.2958	385.5505	364.5125	349.9202
		Quasi-3D($\varepsilon_{zz}\neq 0$)	461.5226	402.6337	378.6681	358.7276	337.7749	323.6678
	S-S	HSBT^b ($\varepsilon_{zz}=0$)	266.8324	223.8160	205.9487	191.0943	176.7504	167.6308
	C-S	HSBT^b ($\varepsilon_{zz}=0$)	491.8146	431.3370	405.6027	384.7870	364.0404	349.6764
	C-F	HSBT^b ($\varepsilon_{zz}=0$)	66.2418	49.9518	43.8147	39.0521	34.7447	32.1481

b: A new hybrid functions.

Moreover, Tables 4.11-4.12 present the normalized fundamental frequency of FG beams (Si_3N_4/SUS304) with L/h=20, p= 0.1, 0.5, and 1, ΔT =20 and 80, subjected to the LTR and Fourier-law NLTR. The results are compared to those of [108, 142] for different boundary conditions and good agreements between the HSBT models are again found. The final research is to analyses the effects of moisture content on the thermal vibration behavior of FG beams.

Table 4.11 Fundamental frequency ($\bar{\omega}$) of FG beams under LTR (Type A, L/h = 20, Si_3N_4/SUS304, TD).

Temperature distribution	BCs	Theory	$\Delta T(K) = 20$			$\Delta T(K) = 80$		
			p = 0.1	0.5	1	p = 0.1	0.5	1
LTR	H-H	HSBT ($\varepsilon_{zz} = 0$)	8.7846	6.8133	5.9658	8.1742	6.2547	5.4252
		HSBT[b] ($\varepsilon_{zz} = 0$)	8.8832	6.9056	6.0551	8.2857	6.3596	5.5275
		Quasi-3D($\varepsilon_{zz} \neq 0$)	8.4170	6.5248	5.7113	7.7782	5.9387	5.1433
		HSBT[a] ($\varepsilon_{zz} = 0$)	8.4391	6.5450	5.7307	7.8532	6.0088	5.2118
		HSBT[142]	8.4716	6.5742	5.7588	7.8766	6.0166	5.2128
		HSBT [108]	8.4634	6.5415	5.7114	7.8795	6.0063	5.1927
	C-C	HSBT ($\varepsilon_{zz} = 0$)	20.1188	15.6333	13.6920	19.8063	15.3661	13.4427
		HSBT[b] ($\varepsilon_{zz} = 0$)	20.1797	15.6863	13.7415	19.8706	15.4224	13.4968
		Quasi-3D($\varepsilon_{zz} \neq 0$)	19.4059	15.0816	13.2106	19.0807	14.8018	12.9487
		HSBT[a] ($\varepsilon_{zz} = 0$)	19.3522	15.0342	13.1654	19.0523	14.7779	12.9263
		HSBT[142]	19.6398	15.2580	13.3671	19.3420	15.0040	13.1304
		HSBT [108]	19.3371	15.0222	13.1554	18.9778	14.6972	12.8431
	C-H	HSBT ($\varepsilon_{zz} = 0$)	13.8663	10.7631	9.4225	13.4286	10.3728	9.0500
		HSBT[b] ($\varepsilon_{zz} = 0$)	13.9555	10.8353	9.4869	13.5244	10.4512	9.1204
		Quasi-3D($\varepsilon_{zz} \neq 0$)	13.3426	10.3565	9.0669	12.8863	9.9482	8.6764
		HSBT[a] ($\varepsilon_{zz} = 0$)	13.3283	10.3443	9.0552	12.9083	9.9697	8.6976
		HSBT[142]	13.4380	10.4238	9.1227	13.0201	10.0515	8.7674
		HSBT [108]	13.3373	10.3526	9.0635	12.8837	9.9342	8.6571
	S-S	HSBT[b] ($\varepsilon_{zz} = 0$)	8.8788	6.8788	6.0142	8.2812	6.3319	5.4848
	C-S	HSBT[b] ($\varepsilon_{zz} = 0$)	13.9370	10.8221	9.4755	13.5060	10.4380	9.1095
	C-F	HSBT[b] ($\varepsilon_{zz} = 0$)	2.9857	2.2816	1.9755	1.9407	1.2177	0.8470

[a] $\bar{Q}_{11} = E(z)$, *b: A new hybrid functions.*

Figure 4.4a presents the effect of the power-law index p on the normalized fundamental frequency of Si_3N_4/SUS304 FG beams (L/h = 20) with different values of ΔC. It shows that for a moisture rise, the fundamental frequency decreases with the increase of p and the moisture content rise makes the beams softer. These phenomena are also observed in Figure 4.4b which plots the variation of fundamental frequency with respect to the UTR. It can be seen from this figure that the frequency of the FG beams with moisture content rise ΔC =2% is smaller than that without moisture content rise, and that the critical temperatures decrease with the increase of ΔC.

Table 4.12 Fundamental frequency ($\bar{\omega}$) of FG beams under Fourier-law NLTR (Type A, L/h = 20, Si_3N_4/SUS304, TD).

Temperature distribution	BCs	Theory	$\Delta T(K) = 20$			$\Delta T(K) = 80$		
			p = 0.1	0.5	1	p = 0.1	0.5	1
Fourier-law NLTR	H-H	HSBT ($\varepsilon_{zz} = 0$)	8.7865	6.8184	5.9719	8.1855	6.2841	5.4605
		HSBT[b] ($\varepsilon_{zz} = 0$)	8.8843	6.9104	6.0611	8.2956	6.3879	5.5614
		Quasi-3D ($\varepsilon_{zz} \neq 0$)	8.4190	6.5302	5.7178	7.7900	5.9696	5.1805
		HSBT[a] ($\varepsilon_{zz} = 0$)	8.4409	6.5499	5.7366	7.8640	6.0370	5.2456
		HSBT[142]	8.4675	6.5437	5.7124	7.9265	6.0402	5.2186
		HSBT [108]	8.4730	6.5779	5.7632	7.8861	6.0431	5.2448
	C-C	HSBT ($\varepsilon_{zz} = 0$)	20.1198	15.6360	13.6953	19.8121	15.3810	13.4604
		HSBT[b] ($\varepsilon_{zz} = 0$)	20.1798	15.6885	13.7454	19.8782	15.4374	13.5129
		Quasi-3D ($\varepsilon_{zz} \neq 0$)	19.4070	15.0844	13.2140	19.0867	14.8172	12.9670
		HSBT[a] ($\varepsilon_{zz} = 0$)	19.3532	15.0369	13.1685	19.0578	14.7921	12.9432
		HSBT[142]	19.6390	15.2501	13.3558	19.3552	14.9886	13.1011
		HSBT [108]	19.3379	15.0244	13.1579	18.9832	14.7115	12.8600
	C-H	HSBT ($\varepsilon_{zz} = 0$)	13.8676	10.7669	9.4271	13.4367	10.3935	9.0747
		HSBT[b] ($\varepsilon_{zz} = 0$)	13.9409	10.8310	9.4880	13.5191	10.4672	9.1457
		Quasi-3D ($\varepsilon_{zz} \neq 0$)	13.3441	10.3605	9.0716	12.8947	9.9698	8.7022
		HSBT[a] ($\varepsilon_{zz} = 0$)	13.3297	10.3479	9.0595	12.9160	9.9896	8.7214
		HSBT[142]	13.4395	10.4211	9.1178	13.0483	10.0594	8.7648
		HSBT[108]	13.3382	10.3553	9.0669	12.8907	9.9533	8.6801
	S-S	HSBT[b] ($\varepsilon_{zz} = 0$)	8.8914	6.8873	6.0202	8.2930	6.3606	5.5191
	C-S	HSBT[b] ($\varepsilon_{zz} = 0$)	13.9551	10.8311	9.4799	13.5148	10.4584	9.1346
	C-F	HSBT[b] ($\varepsilon_{zz} = 0$)	2.9921	2.2901	1.9843	1.9651	1.2940	0.9601

[a] $\bar{Q}_{11} = E(z)$, *b: A new hybrid functions.*

Tables 4.13–4.15 present the normalized fundamental frequencies of Si_3N_4/SUS304 FG beams under the uniform, linear and nonlinear moisture (UMR, LMR, NLMR) and temperature rises. It is noted that the sinusoidal-law NLMR is used in this example. The results are calculated for the power-law indices p = 0.2, 1 and 5, ΔT = 0, 20 and 40, ΔC = 0%, 1% and 2%. The present solutions are compared with those obtained from Ebrahimi and Barati [144] based on HSBT with H-H beam. The present solutions based on HSBT without Poisson's ratio are in good agreement with those of [144] for all

moisture and temperature changes. The effect of normal strain is clearly observed in which the quasi-3D solutions are smaller the HSBT ones.

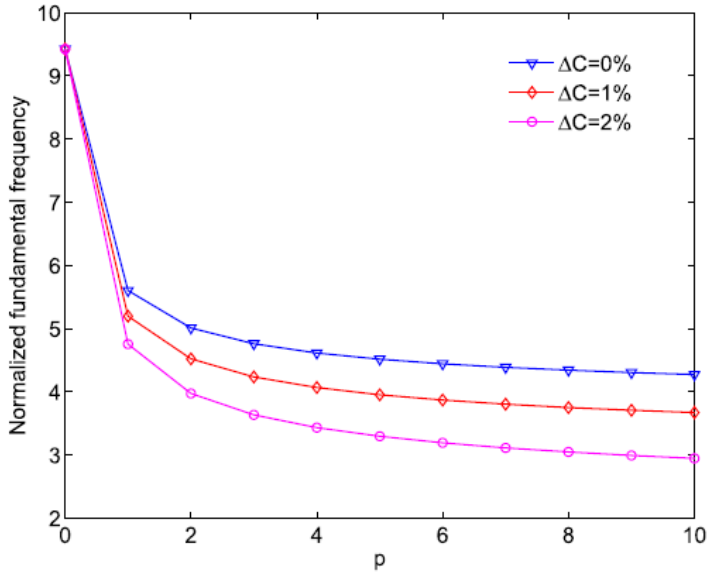

(a) ΔT=20

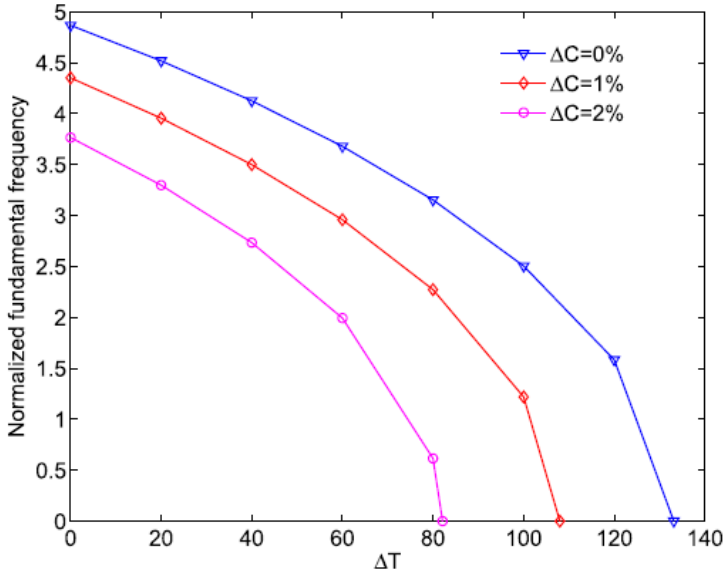

(b) p =5

Figure 4.4 Variation of normalized fundamental frequency of FG beams with respect to the power-law index, moisture and temperature rise (Type A, L/h = 20, Si_3N_4/SUS304, TD).

Table 4.13 Fundamental frequency ($\bar{\omega}$) of FG beams under uniform moisture and temperature rise for various boundary conditions (Type A, L/h = 20, Si_3N_4/SUS304, TD).

BCs	ΔC	Theory	$\Delta T(K)$ =0			$\Delta T(K)$ =20			$\Delta T(K)$ =40		
			p = 0.2	1	5	p = 0.2	1	5	p =0.2	1	5
H-H	ΔC =0%	HSBT ($\varepsilon_{zz}=0$)	8.3030	6.2144	5.0652	7.9313	5.8635	4.7304	7.5298	5.4784	4.3579
		Quasi-3D($\varepsilon_{zz}\neq 0$)	7.9769	5.9708	4.8664	7.5893	5.6046	4.5168	7.1685	5.2003	4.1250
		HSBT[a] ($\varepsilon_{zz}=0$)	7.9757	5.9694	4.8656	7.6186	5.6324	4.5441	7.2327	5.2624	4.1863
		HSBT[144]	7.9680	5.9314	4.8449	–	–	–	–	–	–
	ΔC =1%	HSBT ($\varepsilon_{zz}=0$)	8.1372	5.8496	4.5711	7.7574	5.4749	4.1958	7.3463	5.0598	3.7699
		Quasi-3D($\varepsilon_{zz}\neq 0$)	7.8043	5.5906	4.3504	7.4076	5.1971	3.9542	6.9757	4.7578	3.4988
		HSBT[a] ($\varepsilon_{zz}=0$)	7.8164	5.6192	4.3913	7.4516	5.2593	4.0309	7.0566	4.8606	3.6219
		HSBT[144]	–	–	–	7.4435	5.2167	4.0063	–	–	–
	ΔC =2%	HSBT ($\varepsilon_{zz}=0$)	7.9679	5.4606	4.0166	7.5796	5.0564	3.5824	7.1581	4.6033	3.0712
		Quasi-3D($\varepsilon_{zz}\neq 0$)	7.6278	5.1826	3.7644	7.2213	4.7549	3.2969	6.7775	4.2697	2.7327
		HSBT[a] ($\varepsilon_{zz}=0$)	7.6539	5.2457	3.8590	7.2809	4.8576	3.4421	6.8759	4.4224	2.9514
		HSBT[144]	–	–	–	–	–	–	6.8673	4.3722	2.9180
C-H	ΔC =0%	Quasi-3D ($\varepsilon_{zz}\neq 0$)	12.4092	9.2498	7.5477	12.1243	8.9822	7.2940	11.8230	8.6962	7.0206
	ΔC =1%	Quasi-3D ($\varepsilon_{zz}\neq 0$)	12.2809	8.9691	7.1716	11.9926	8.6917	6.9021	11.6876	8.3948	6.6106
	ΔC =2%	Quasi-3D[a]($\varepsilon_{zz}\neq 0$)	12.1512	8.6786	6.7731	11.8594	8.3905	6.4848	11.5505	8.0814	6.1715
C-C	ΔC =0%	Quasi-3D ($\varepsilon_{zz}\neq 0$)	17.9130	13.3399	10.8821	17.7061	13.1479	10.7012	17.4896	12.9450	10.5089
	ΔC =1%	Quasi-3D ($\varepsilon_{zz}\neq 0$)	17.8188	13.1346	10.6086	17.6106	12.9390	10.4218	17.3928	12.7321	10.2231
	ΔC =2%	Quasi-3D[a]($\varepsilon_{zz}\neq 0$)	17.7240	12.9258	10.3270	17.5146	12.7262	10.1338	17.2954	12.5153	9.9282

[a] $\bar{Q}_{11}=E(z)$

Table 4.14 Fundamental frequency ($\bar{\omega}$) of FG beams under linear moisture and temperature rise (Type A, L/h = 20, Si_3N_4/SUS304, TD).

BCs	ΔC	Theory	$\Delta T(K)$ =0			$\Delta T(K)$ =20			$\Delta T(K)$ =40		
			p=0.2	1	5	p =0.2	1	5	p =0.2	1	5
H-H	ΔC =0%	HSBT ($\varepsilon_{zz}=0$)	8.2127	6.1295	4.9846	8.0343	5.9658	4.8259	7.8474	5.7943	4.6597
		Quasi-3D($\varepsilon_{zz}\neq 0$)	7.8828	5.8824	4.7825	7.6969	5.7113	4.6164	7.5016	5.5317	4.4420
		HSBT[a] ($\varepsilon_{zz}=0$)	7.8889	5.8879	4.7882	7.7177	5.7307	4.6358	7.5382	5.5661	4.4763
		HSBT[144]	7.8817	5.8491	4.7664	–	–	–	–	–	–
	ΔC =1%	HSBT ($\varepsilon_{zz}=0$)	8.1651	5.9992	4.7669	7.9857	5.8315	4.5999	7.7976	5.6558	4.4245
		Quasi-3D($\varepsilon_{zz}\neq 0$)	7.8334	5.7466	4.5554	7.6461	5.5711	4.3800	7.4495	5.3866	4.1949
		HSBT[a] ($\varepsilon_{zz}=0$)	7.8432	5.7628	4.5793	7.6710	5.6018	4.4189	7.4904	5.4331	4.2505
		HSBT[144]	–	–	–	7.6651	5.5616	4.3962	–	–	–
	ΔC =2%	HSBT ($\varepsilon_{zz}=0$)	8.1173	5.8659	4.5388	7.9368	5.6941	4.3623	7.7475	5.5137	4.1760
		Quasi-3D($\varepsilon_{zz}\neq 0$)	7.7835	5.6076	4.3164	7.5951	5.4273	4.1300	7.3970	5.2374	3.9323
		HSBT[a] ($\varepsilon_{zz}=0$)	7.7973	5.6348	4.3603	7.6240	5.4699	4.1908	7.4423	5.2967	4.0120
		HSBT[144]	–	–	–	–	–	–	7.4365	5.2518	3.9832
C-H	ΔC =0%	Quasi-3D($\varepsilon_{zz}\neq 0$)	12.3395	9.1845	7.4860	12.2043	9.0631	7.3697	12.0640	8.9374	7.2497
	ΔC =1%	Quasi-3D($\varepsilon_{zz}\neq 0$)	12.3027	9.0839	7.3194	12.1671	8.9609	7.1996	12.0263	8.8335	7.0759
	ΔC =2%	Quasi-3D($\varepsilon_{zz}\neq 0$)	12.2659	8.9822	7.1486	12.1298	8.8574	7.0250	11.9885	8.7282	6.8974
C-C	ΔC =0%	Quasi-3D($\varepsilon_{zz}\neq 0$)	17.8621	13.2929	10.8379	17.7660	13.2106	10.7608	17.6668	13.1258	10.6817
	ΔC =1%	Quasi-3D($\varepsilon_{zz}\neq 0$)	17.8352	13.2192	10.7164	17.7389	13.1363	10.6379	17.6395	13.0509	10.5573
	ΔC =2%	Quasi-3D($\varepsilon_{zz}\neq 0$)	17.8082	13.1452	10.5933	17.7118	13.0616	10.5133	17.6122	12.9755	10.4313

[a] $\bar{Q}_{11}=E(z)$

Table 4.15 Fundamental frequency ($\bar{\omega}$) of FG beams under sinusoidal moisture and temperature rise (Type A, L/h = 20, Si_3N_4/SUS304, TD).

BCs	ΔC	Theory	$\Delta T(K)$ =0			$\Delta T(K)$ =20			$\Delta T(K)$ =40		
			p =0.2	1	5	p =0.2	1	5	p =0.2	1	5
H-H	ΔC =0%	HSBT ($\varepsilon_{zz}=0$)	8.2127	6.1295	4.9846	8.0857	6.0152	4.8730	7.9533	5.8962	4.7572
		Quasi-3D($\varepsilon_{zz}\neq 0$)	7.8828	5.8824	4.7825	7.7504	5.7629	4.6656	7.6122	5.6383	4.5440
		HSBT[a] ($\varepsilon_{zz}=0$)	7.8889	5.8879	4.7882	7.7670	5.7781	4.6811	7.6399	5.6639	4.5699
		HSBT[144]	7.8817	5.8491	4.7664	–	–	–	–	–	–
	ΔC =1%	HSBT ($\varepsilon_{zz}=0$)	8.1874	6.0529	4.8399	8.0600	5.9370	4.7244	7.9272	5.8163	4.6044
		Quasi-3D($\varepsilon_{zz}\neq 0$)	7.8565	5.8026	4.6316	7.7236	5.6813	4.5104	7.5848	5.5547	4.3841
		HSBT[a] ($\varepsilon_{zz}=0$)	7.8646	5.8143	4.6493	7.7423	5.7030	4.5385	7.6148	5.5872	4.4232
		HSBT[144]	–	–	–	7.7355	5.6625	4.5149	–	–	–
	ΔC =2%	HSBT ($\varepsilon_{zz}=0$)	8.1619	5.9753	4.6907	8.0341	5.8577	4.5710	7.9009	5.7353	4.4464
		Quasi-3D($\varepsilon_{zz}\neq 0$)	7.8300	5.7217	4.4757	7.6967	5.5985	4.3496	7.5574	5.4699	4.2180
		HSBT[a] ($\varepsilon_{zz}=0$)	7.8402	5.7398	4.5061	7.7175	5.6270	4.3912	7.5896	5.5094	4.2716
		HSBT[144]	–	–	–	–	–	–	7.5826	5.4650	4.2429
C-H	ΔC =0%	Quasi-3D($\varepsilon_{zz}\neq 0$)	12.3395	9.1845	7.4860	12.2436	9.1010	7.4057	12.1444	9.0147	7.3230
	ΔC =1%	Quasi-3D($\varepsilon_{zz}\neq 0$)	12.3199	9.1253	7.3749	12.2239	9.0411	7.2928	12.1245	8.9540	7.2085
	ΔC =2%	Quasi-3D($\varepsilon_{zz}\neq 0$)	12.3003	9.0656	7.2619	12.2041	8.9807	7.1781	12.1045	8.8930	7.0919
C-C	ΔC =0%	Quasi-3D($\varepsilon_{zz}\neq 0$)	17.8621	13.2929	10.8379	17.7948	13.2382	10.7870	17.7252	13.1818	10.7347
	ΔC =1%	Quasi-3D($\varepsilon_{zz}\neq 0$)	17.8478	13.2495	10.7567	17.7804	13.1946	10.7051	17.7107	13.1379	10.6521
	ΔC =2%	Quasi-3D($\varepsilon_{zz}\neq 0$)	17.8334	13.2059	10.6748	17.7659	13.1507	10.6225	17.6962	13.0938	10.5687

[a] $\bar{Q}_{11}=E(z)$

4.5 Conclusions

Hygro-thermal vibration and stability analysis of FG beams is presented. It is based on a higher-order shear deformation theory, which considers a higher-order distribution of transverse shear stress and both in-plane and out-of-plane displacements. These beams are subjected to hygro-thermal loadings under uniform, linear and nonlinear distributions through the beam depth. Lagrange's equations are applied to derive the characteristic dynamic equations and the New Ritz solution method is developed to solve the problems for different boundary conditions. The proposed Ritz solution converges quickly and agrees well with that from other studies. The obtained numerical results showed that:

- The critical buckling temperatures and natural frequencies derived from the quasi-3D theory, which includes normal strain, is smaller than those from the HSBT, which neglects it. This implies that the effect of normal strain is important and needs to be considered for the analysis of hygro-thermal behaviors of FG beams.
- The increase of the power-law index leads to the increase of metal volume fraction, which makes the beams softer and decreases the critical temperature and natural frequency.
- The temperature dependent solutions give lower values than the temperature independent ones, so the importance of temperature dependency in the FG beams is confirmed.
- For a temperature rise, the critical temperature and fundamental frequency derived from nonlinear temperature rise are larger than those from uniform one.
- The critical temperature and fundamental frequency calculated from Fourier-law nonlinear temperature distribution are smaller than those from sinusoidal-law one.
- The thermal buckling and vibration responses of FG beams decrease with the increase of moisture content.

In conclusion, the proposed beam model and approach is found to be simple and efficient for hygro-thermal buckling and vibration of FG beams.

Chapter 5

Size dependent effects on the thermal buckling and vibration behavior of FG beams in thermal environments

---

This chapter proposes size dependent effects on the thermal buckling and vibration behavior of FG beams in thermal environments. A general theoretical formulation is derived from the fundamental of two-dimensional elasticity theory and then novel higher-order shear deformation beam theories and Timoshenko beam theory are obtained.

The highlight of this chapter is as follows:

- The objectives of this chapter is to propose analysis of FG micro and nano beams with various boundary conditions in thermal environments.
- The nonlocal elasticity theory is based on Timoshenko's and Eringer's nonlocal elasticity ones. Hamilton's principle is used to derive equations of motion.
- The modified couple stress theory is used to perform vibration and buckling analysis on FG micro beams based on third order shear deformation beam theories. Lagrange's equations are used to obtain the governing equations of motion.
- Numerical results are carried out to verify the accuracy of the proposed theories.

5.1 Introduction

Application of functionally graded (FG) material in nano and micro structures has been an attracted topic in the engineering field. All the stated studies applied the classical continuum theory to predict the behaviour of mechanical structures. But many micros scaled beams and plates are used in different applications such as in micro electro mechanical systems (MEMS) and micro sensors or actuators and it has been observed through experimental results that their behaviour are quite size dependent in such scales [162, 163]. Classical continuum theory was not capable of capturing this size dependency; therefore, many different higher order continuum theories were introduced to improve the results obtained for micro systems. These theories predominantly, try to improve the model by introducing length scale parameters to capture the so-called size effects.

One of the first higher order continuum theories was strain gradient theory introduced by Mindlin and Eshel [164], this theory had five additional constants beside Lame' constants. Following their lead, Lam et al. [163] presented a modified theory with only three non-classical constants starting from the strain energy density function introduced by Mindlin and Eshel [164]. Use of the recent theory was more applicable; as Kong et al. [165] and Wang et al [166] used the stated theory to investigate the behaviour of micro beams considering Euler–Bernoulli and Timoshenko beam theories, respectively. In addition, stability analysis of micro beams based on strain gradient theories has been recently presented. Papargyri-Beskou et al.[167] and Lazopoulos [168] performed bending and buckling analysis of thin strain gradient elastic beams considering surface energy. The results showed that the gradient coefficient affects the buckling load significantly while the effect of surface energy is negligible. Recently, an analytical solution to bending of micro beams with various boundary conditions was presented by Akgoz and Civalek [71]

Another higher order continuum theory is couple stress theory which was presented by Toupin [13], Mindlin and Tiersten [14] and Koiter [15]. One of the good aspects of this theory was its need to only two non-classical constants (length scale parameters) in addition to two classical constants (Lame' constants). Even though, there were only two constants to obtain, application of this theory was still difficult; therefore, Yang et al.[12] modified the couple stress theory to introduce an applicable theory which can capture size dependencies considering only one additional constant other than Lame' constants. Park and Gao [17] were one of the first researchers to develop Euler–Bernoulli beam theories based on modified couple stress theory. Following from there, Kong et al. [169] obtained and analysed size dependent natural frequencies of micro beams. Use of modified couple stress theory is not limited to Euler–Bernoulli beam theory; Ma et al. [170, 171] developed new size dependent Timoshenko and Reddy–Levinson beam theories based on the stated theory and investigated static and dynamic behaviour of such micro beams. Fu and Zhang [172] modelled microtubules based on Timoshenko beam theory considering modified couple stress theory and analysed micro scale effects on buckling of such systems. Akgoz and Civalek [73] studied buckling behaviour of protein microtubules based on strain gradient and modified couple stress theories using Euler–Bernoulli beam model. In another study, they presented buckling analysis of axially loaded micro-scaled beams based on the stated theories [69]. Akgöz et al. [173] studied vibration response of non-homogenous and non-uniform micro beams and investigated in conjunction with Bernoulli–Euler beam and modified couple stress theory. Şimşek and Reddy [174] analysed the modified couple stress theory (MCST), a unified higher order beam theory which contains various beam theories as special cases is proposed for buckling of a functionally graded (FG) micro beam embedded in elastic Pasternak medium. In light of the modified couple stress theory, Thai et al. [175] investigated Size-dependent behaviour of functionally graded sandwich micro beams.

The understanding of mechanical behaviours of FG nanostructures in a such context is essential in the development of structures to meet performance requirements. Potential application of FG nano beams in recent years led to the development of the field of computational nano mechanics. In practice, the classical continuum theories fail to accurately predict the mechanical behaviour of nanostructures due to small dimensions of a such structure. To overcome this adverse, Eringen [10, 78] proposed size-dependent continuum theory known as the nonlocal elasticity theory. According to this approach, the stress at a reference point in an elastic continuum not only depends on the strain at the point but also on strains at every point of the body.

Based on the nonlocal elasticity of Eringen, many researches on static, buckling and vibration of isotropic nano beams have been investigated, only some representative references are cited. Reddy [176] reformulated local beam theory by using the nonlocal differential constitutive relations of Eringen to study bending, vibration, and buckling behaviours of nano beams in which an analytical solution has been obtained to bring out the effect of the nonlocal behaviour of nano beams. Aydogdu [177] proposed a generalized nonlocal beam theory to study bending, buckling, and free vibration of nano beams by using the nonlocal constitutive equations of Eringen. Xia et al. [178] used the differential quadrature method to study bending, post buckling, and free vibration for nonlinear micro beams in which a nonlinear model has been conducted within the context of non-classical continuum mechanics by introducing a material length-scale parameter. Pradhan and Murmu [179] developed a single nonlocal beam model to investigate the bending and vibration characteristics of a nano cantilever beam. Phadikar and Pradhan [180] presented finite element formulations for nonlocal elastic Euler–Bernoulli beam and Kirchhoff plate. Finite element results for bending, vibration, and buckling for nonlocal beam with four classical boundary conditions have been computed. Thai [181] proposed a nonlocal beam theory for bending, buckling and vibration of simply-supported isotropic nano beams using Navier solution. Thai and Vo [182]

developed a nonlocal sinusoidal shear deformation beam theory for bending, buckling and free vibration of simply-supported nano beams. For FG nano-beams, the studies on static, buckling and vibration behaviours of FG nano-beams have been considered by many authors. Eltaher et al. [183] presented free vibration analysis of functionally graded (FG) size-dependent nano beams using finite element method in which the size-dependent FG nano-beam has been investigated on the basis of the nonlocal continuum model. Results from this work showed the significance of the material distribution profile, nonlocal effect, and boundary conditions on the dynamic characteristics of nano-beams. Ebrahimi and Salari [184] analysed thermo-mechanical effects on vibration of nonlocal temperature dependent FG nano-beams with various boundary conditions in which nonlocal Euler-Bernoulli beam theory has been used. Eltaher et al. [185] presented static and buckling responses of FG nano-beams with different boundary conditions using finite element method. Ebrahimi and Salari [143] used nonlocal Timoshenko beam theory for analysis of thermal buckling and free vibration of FG nano-beams in which Navier solution has been applied for analysis of simply-supported FG nano beams.

In light of Timoshenko's theory, Simsek and Yurtcu [186] analysed bending and buckling of simply supported FG nano-beams using Navier solution. Ebrahimi and Barati [144] investigated effects of moisture and temperature on free vibration characteristics of simply supported FG nano-beams resting on elastic foundation by developing various refined beam theories.

This chapter has also expanded to FG nano-beams with various boundary conditions by Ebrahimi and Barati [187] using differential transform method. A literature review shows that the studies on behaviours of FG nano-beams considered effects of transverse shear deformation by using nonlocal first-order shear deformation beam theory (FOBT) and nonlocal higher-order shear deformation beam theory (HOBT), and most of them studied FG simply-supported nano beams using Navier-type solution. Some of researches tried to solve FG nano-beams with different boundary condition using finite

element method and trigonometric series solution. Moreover, it also reveals that the number of researches considered effects of normal strain on behaviours of FG nano-beams are limited. Tounsi et al. [188] proposed a nonlocal beam theory for analysis of stretching effect of isotropic nano beams. Ebrahimi and Barati [189] applied a nonlocal strain gradient elasticity theory to wave dispersion behaviour of a size-dependent FG nano-beam in thermal environment in which the theory contains two scale parameters corresponding to both nonlocal and strain gradient effects and a quasi-3D sinusoidal beam theory considering shear and normal deformations is employed. A literature review on the behaviour analysis of FG nano-beams shows that most of previous works study FG nano beams with the simply-supported boundary conditions, a number of researches investigated various boundary conditions are still limited.

The modified couple stress theory is used to perform a buckling analysis on FG micro beams based on third order shear deformation (Reddy) beam theories in thermal environment. In addition, the nonlocal elasticity theory is based on Timoshenko's and Eringer's nonlocal elasticity ones. The beam is assumed to be functionally graded in the thickness direction; while Poisson ratio is assumed to be constant, but it is not neglected. The principal of minimum potential energy is applied to obtain the governing equations and boundary conditions of the FG beam. To analyse different boundary conditions, Ritz method is used to solve the governing equations numerically.

The objectives of this chapter is to propose analysis of FG micro and nano beams with various boundary conditions in thermal environments. Numerical results are compared to the earlier works and to investigate the effects of material distribution through the beam thickness, the span-to-height ratio, the scale length parameter and the boundary conditions on the natural frequencies and the thermal buckling of FG micro and nano beams.

5.2 Geometry of FG beams

Geometry of beams as in Figure 5.1 with rectangular section $b \times h$ and length L. In this study, it is made of a mixture of isotropic ceramic and metal whose properties continuously in the beam, as follows:

$$P(z) = (P_c - P_m)\left(\frac{2z+h}{2h}\right)^p + P_m \tag{5.1}$$

where *P*(z) is material elastic moduli as Young modulus *E(z)*, Poisson's ratio ν*(z)*, mass density $\rho(z)$, at location *z*; P_c, P_m are material elastic properties of ceramic and metal, p is power-law material parameter, respectively.

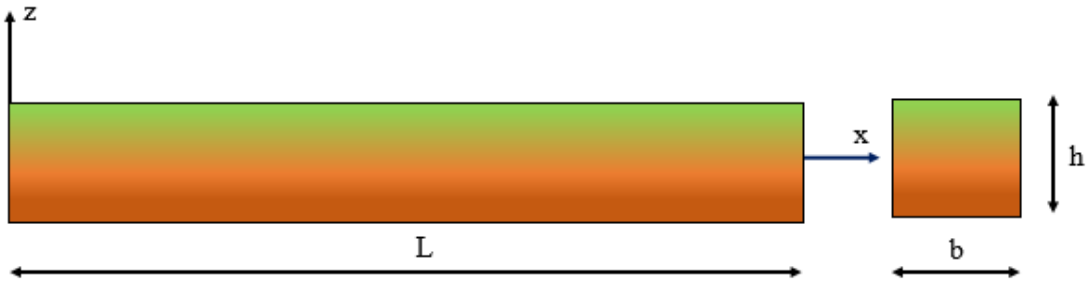

Figure 5.1 Geometry of FG beams (Type A).

5.3 Theory of FG micro and nano beams

5.3.1. Kinetic and strain

The displacement field of Timoshenko beams is given by:

$$\begin{aligned} u(x,z,t) &= u_0(x,t) + z\theta(x,t) \\ w(x,z,t) &= w_0(x,t) \end{aligned} \tag{5.2}$$

where the comma indicates the partial differentiation with respect to the coordinate subscript that follows; $u_0(x,t)$, $\theta(x,t)$, $w_0(x,t)$ are axial displacement, rotation and transverse displacement at the mid-plan of the nano beams, respectively.

$$\begin{aligned} \varepsilon_x &= u_{0,x} + z\theta_{,x} = \varepsilon_x^{(0)} + z\varepsilon_x^{(1)} \\ \gamma_{xz} &= \gamma_{xz}^{(0)} = \theta + w_{0,x} \end{aligned} \tag{5.3}$$

5.3.2. Equations of motion

Lagrangian functional is used to derive the equations of motion:

$$\Pi = U + V - K \tag{5.4}$$

where *U, V* and *K* denote the strain energy, potential and kinetic energy, respectively.

The variation of strain energy *U* of system is given by:

$$U = \int_V \left(\sigma_x \varepsilon_x + \sigma_{xz}\gamma_{xz}\right) dV = \int_0^L \left(N_x \varepsilon_x^{(0)} + M_x \varepsilon_x^{(1)} + Q\gamma_{xz}^{(0)}\right) dx \tag{5.5}$$

where the stress resultants are defined as:

$$\begin{aligned} \left(N_x, M_x\right) &= \int_{-h/2}^{h/2} \left(1, z\right)\sigma_x b dz \\ Q &= \int_{-h/2}^{h/2} k^s \sigma_{xz} b dz \end{aligned} \tag{5.6}$$

where k^s is shear correction factor which is supposed to be 5/6.

The variation of kinetic energy *K* of system is written by:

$$\begin{aligned} K &= \int_V \rho(z)\left(\dot{u}^2 + \dot{w}^2\right) dV \\ &= \int_0^L \left[I_0 \dot{u}_0^2 + I_2 \dot{\theta}^2 + 2I_1 \dot{u}_0 \dot{\theta} + I_0 \dot{w}_0^2 \right] dx \end{aligned} \tag{5.7}$$

where dot-superscript denotes the differentiation with respect to the time t; ρ is the mass density of each layer, and I_0, I_1, I_2 are the inertia coefficients defined by:

$$\left(I_0, I_1, I_2\right) = \int_{-h/2}^{h/2} \left(1, z, z^2\right)\rho(z) b dz \tag{5.8}$$

Substituting Eqs. (5.5) and (5.7) into Eq. (5.4)

$$\begin{aligned} \Pi = \int_0^L \Big[& N_x \varepsilon_x^{(0)} + M_x \varepsilon_x^{(1)} + Q\gamma_{xz}^{(0)} \\ & - \left(I_0 \dot{u}_0^2 + I_2 \dot{\theta}^2 + 2I_1 \dot{u}_0 \dot{\theta} + I_0 \dot{w}_0^2 \right) \Big] dx \end{aligned} \tag{5.9}$$

Leads to the following equations of motion:

$$
\begin{aligned}
&N_{x,x} = I_0\ddot{u} + I_1\ddot{\theta} \\
&M_{x,x} - Q = I_1\ddot{u} + I_2\ddot{\theta} \\
&Q_{,x} = I_0\ddot{w}
\end{aligned}
\tag{5.10}
$$

5.3.3. Nonlocal elasticity theory for FG nano beams

Based on the Eringen's nonlocal elasticity theory [78], nonlocal constitutive equations are expressed by:

$$
\left(1-\mu\nabla^2\right)\sigma_{ij} = t_{ij} \tag{5.11}
$$

where ∇ denotes Laplacian operator; $\mu = \left(e_0 a\right)^2$ is parameter of scale length that considers the influences of small size on the response of nanostructures with e_0 is a constant appropriate to each material, a is an internal characteristics length (e.g., latticeparameter, granular distance) and t_{ij} are global stresses. The constitutive equations of FG nano beams are hence written under the following expressions:

$$
\begin{aligned}
&\sigma_x - \mu\sigma_{x,xx} = Q_{11}\left(z\right)\varepsilon_x \\
&\sigma_{xz} - \mu\sigma_{xz,xx} = Q_{55}\left(z\right)\gamma_{xz}
\end{aligned}
\tag{5.12}
$$

where $Q_{11}\left(z\right) = \dfrac{E\left(z\right)}{1-\nu^2}$, $Q_{55}\left(z\right) = \dfrac{E\left(z\right)\nu}{2\left(1+\nu\right)}$

Substituting Eqs. (5.3) into Eqs. (5.12) and then subsequent results into the stress resultants in Eqs. (5.6), the following nonlocal constitutive equations of stress resultants are defined as:

$$
\begin{aligned}
&N_x - \mu N_{x,xx} = Au_{,x} + B\theta_{,x} \\
&M_x - \mu M_{x,xx} = Bu_{,x} + D\theta_{,x} \\
&Q - \mu Q_{,xx} = A^s\left(\theta + w_{,x}\right)
\end{aligned}
\tag{5.13}
$$

where A, B, D, A^s are the stiffness's of FG nano beams which are defined by:

$$\left(A,B,D\right)=\int_{-h/2}^{h/2}\left(1,z,z^2\right)Q_{11}\left(z\right)bdz$$
$$A^s=\int_{-h/2}^{h/2}k^sQ_{55}\left(z\right)bdz \tag{5.14}$$

Substituting Eqs (5.10) into Eqs (5.13) leads to the expressions of stress resultants as follows:

$$\begin{aligned}N_x&=\mu\left(I_0\ddot{u}_{,x}+I_1\ddot{\theta}_{,x}\right)+Au_{,x}+B\theta_{,x}\\M_x&=\mu\left(I_0\ddot{w}+I_1\ddot{u}_{,x}+I_2\ddot{\theta}_{,x}\right)+Bu_{,x}+D\theta_{,x}\\Q&=\mu I_0\ddot{w}_{,x}+A^s\left(\theta+w_{,x}\right)\end{aligned} \tag{5.15}$$

Substituting Eqs. (5.15) into Eq. (5.4) yields:

$$\begin{aligned}\prod=\frac{1}{2}\int_0^L\Big[&Au_{0,x}^2+2B\theta_{,x}u_{0,x}+D\theta_{,x}^2+A^s\theta^2+2\theta w_{0,x}+A^sw_{0,x}^2\\&+\mu\left(I_0\ddot{u}_{0,x}+I_1\ddot{\theta}_{,x}\right)u_{0,x}+\mu\left(I_0\ddot{w}_0+I_1\ddot{u}_{0,x}+I_2\ddot{\theta}_{,x}\right)\theta_{,x}\\&+\mu I_0\ddot{w}_{0,x}\left(\theta+w_{0,x}\right)-\left(I_0\dot{u}_{0,x}^2+I_2\dot{\theta}^2+2I_1\dot{u}_0\dot{\theta}+I_0\dot{w}_0^2\right)\Big]dx\end{aligned} \tag{5.16}$$

In Eq 5.16, the parameter of scale length (μ) is only included in the components of the mass matrix, so studying FG nano beam only for free vibration is appropriate.

5.3.4. Modified couple stress theory (MCST)

The displacement field is chosen from previous study HSBT1:

$$u(x,z,t)=u_0(x,t)-zw_{0,x}+f(z)\theta\left(x,t\right)$$
$$w\left(x,z,t\right)=w_0\left(x,t\right)$$

where u_0,θ are the mid-plane axial displacement and rotation, w_0 denotes the mid-plane transverse displacement of the beam, the comma indicates partial differentiation with respect to the coordinate subscript that follows.

Based on the MCST [12], the rotation about the x-, y-, z- axes are determined by:

$$\theta_x(x,z,t)=\frac{1}{2}\left(w_{,y}+v_{,z}\right)=0$$
$$\theta_y(x,z,t)=\frac{1}{2}\left(u_{,z}+w_{,x}\right)=\frac{1}{2}\left[\, f_{,z}(z)\theta-2w_{,x}\,\right] \tag{5.17}$$
$$\theta_z(x,z,t)=\frac{1}{2}\left(v_{,x}-u_{,y}\right)=0$$

The strain and curvature fields of beams is obtained as:

$$\varepsilon_{xx}(x,z,t)=u_{0,x}-zw_{0,xx}+f\theta_{,x}$$
$$\gamma_{xz}(x,z,t)=f_{,x}\theta$$
$$\chi_{xy}(x,z,t)=\frac{\partial\theta_y}{\partial x}=\frac{1}{2}\left[\, f_{,z}(z)\theta_{,x}-2w_{0,xx}\,\right] \tag{5.18}$$
$$\chi_{zy}(x,z,t)=\frac{\partial\theta_y}{\partial z}=\frac{1}{2}\,f_{,zz}(z)\theta$$

The elastic constitutive equations are given by:

$$\begin{Bmatrix}\sigma_{xx}\\ \sigma_{zz}\\ \sigma_{xz}\end{Bmatrix}=\begin{bmatrix}\bar{Q}_{11} & \bar{Q}_{13} & 0\\ \bar{Q}_{13} & \bar{Q}_{11} & 0\\ 0 & 0 & \bar{Q}_{55}\end{bmatrix}\begin{Bmatrix}\varepsilon_{xx}\\ \varepsilon_{zz}\\ \gamma_{xz}\end{Bmatrix} \tag{5.19}$$

where

$$\bar{Q}_{11}(x,z)=\frac{E(x,z)}{1-\nu^2},\ \bar{Q}_{13}(x,z)=\frac{E(x,z)\nu}{1-\nu^2},\ \bar{Q}_{55}(x,z)=\frac{E(x,z)}{2(1-\nu)} \tag{5.20a}$$

If the transverse normal strain effect is omitted$\left(\varepsilon_{zz}=0\right)$, the components of Q_{ij} in Eq. (5.19) are reduced as:

$$Q_{11}(x,z)=\frac{E(x,z)}{1-\nu^2},\ Q_{13}(z)=0,\ Q_{55}(x,z)=\frac{E(x,z)}{2(1-\nu)} \tag{5.20b}$$

The couple stress-curvature relation can be introduced as [12]:

$$\begin{Bmatrix}m_{xy}\\ m_{zy}\end{Bmatrix}=\begin{bmatrix}Q_{44} & 0\\ 0 & Q_{66}\end{bmatrix}\begin{Bmatrix}\chi_{xy}\\ \chi_{zy}\end{Bmatrix} \tag{5.21}$$

where

$$Q_{44}(x,z)=Q_{66}(x,z)=Q_{55}(x,z)\varsigma^2=\frac{E(x,z)}{2(1-\nu)}\varsigma^2 \tag{5.22}$$

with ς are respectively the MLSPs in x-directions.

5.3.5. Variation formulation for MCST

The strain energy of the FG beams can be stated as:

$$\begin{aligned} U &= \frac{1}{2}\int_V \left(\sigma_{xx}\varepsilon_{xx}+\sigma_{xz}\gamma_{xz}+m_{xy}\chi_{xy}+m_{zy}\chi_{zy}\right)dV \\ &= \frac{1}{2}\int_0^L \Big[Au_{0,x}^2-2Bu_{0,x}w_{0,xx}+\left(A^m+D\right)w_{0,xx}^2+2B^s u_{0,x}\theta_{,x} \\ &\quad -2\left(\frac{B^m}{2}+D^s\right)w_{0,xx}\theta_{,x}+\left(H^s+\frac{D^m}{4}\right)\theta_{,x}^2+\left(A^s+\frac{H^m}{4}\right)\theta^2\Big]dx \end{aligned} \tag{5.23}$$

where $A, B, D, B^s, D^s, H^s, A^s, A^m, B^m, D^m, H^m$ are the stiffness of FG beams given by:

$$\begin{aligned} \left(A,\, B,\, D,\, B^s,\, D^s,\, H^s\right) &= \int_{-h/2}^{h/2}\left(1, z, z^2, f, zf, f^2\right)Q_{11}(x,z)bdz \\ A^s &= \int_{-h/2}^{h/2} g^2 Q_{55}(x,z)bdz \\ \left(A^m,\, B^m,\, D^m\right) &= \int_{-h/2}^{h/2}\left(1, f_{,z}, f_{,z}^2\right)Q_{44}(x,z)bdz \\ H^m &= \int_{-h/2}^{h/2} f_{,zz}^2 Q_{66}(x,z)bdz \end{aligned} \tag{5.24}$$

The work done V by axial thermal stress is expressed by:

$$V=-\frac{1}{2}\int_0^L N^t\left(w_{0,x}\right)^2 dx \tag{5.25}$$

where

$$N^t=\int_{-h/2}^{h/2} Q_{11}(z)\alpha(z)\left[T(z)-T^0\right]bdz \tag{5.26}$$

The kinetic energy K is obtained as:

$$K=\frac{1}{2}\int_V \rho(z)\left(\dot{u}^2+\dot{w}^2\right)dV$$
$$=\frac{1}{2}\int_0^L\Big[I_0\dot{u}_0^2-2I_1\dot{u}_0\dot{w}_{0,x}+I_2\dot{w}_{0,x}^2+2J_1\dot{\theta}\dot{u}_0 \qquad (5.27)$$
$$-2J_2\dot{\theta}\dot{w}_{0,x}+K_2\dot{\theta}^2+I_0\dot{w}_0^2\Big]dx$$

where the differentiation with respect to the time t is denoted by dot-superscript convention; $\rho(z)$ is the mass density of the each layer and $I_0, I_1, I_2, J_1, J_2, K_2, L_1, L_2$ are the inertia coefficients, defined by:

$$(I_0, I_1, I_2, J_1, J_2, K_2)=\int_{-h/2}^{h/2}\rho(z)(1, z, z^2, f, fz, f^2)bdz \qquad (5.28)$$

By substituting Eqs (5.23), (5.25) and (5.27) into Eq (5.4), Lagrangian functional is explicitly expressed as:

$$\Pi=\frac{1}{2}\int_0^L\Bigg[Au_{0,x}^2-2Bu_{0,x}w_{0,xx}+\left(A^m+D\right)w_{0,xx}^2+2B^s u_{0,x}\theta_{,x}-2\left(\frac{B^m}{2}+D^s\right)w_{0,xx}\theta_{,x}$$
$$+\left(H^s+\frac{D^m}{4}\right)\theta_{,x}^2+\left(A^s+\frac{H^m}{4}\right)\theta^2\Bigg]dx+\frac{1}{2}\int_0^L N^t\left(w_{0,x}\right)^2dx \qquad (5.29)$$
$$-\frac{1}{2}\int_0^L\Big[I_0\dot{u}_0^2-2I_1\dot{u}_0\dot{w}_{0,x}+I_2\dot{w}_{0,x}^2+2J_1\dot{\theta}\dot{u}_0-2J_2\dot{\theta}\dot{w}_{0,x}+K_2\dot{\theta}^2+I_0\dot{w}_0^2\Big]dx$$

In Eq 5.29, the parameter of MLSPs (ς) is only included in the components of the stiffness matrix, so it is necessary to study the FG micro beam for the various problems such as vibration, buckling, static. . .

5.4 Ritz method (RM)

5.4.1. Ritz method for nonlocal theory

Based on the RM, the displacements *(u_0, w_0, θ)* are approximated in the following forms:

$$u_0(x,t)=\sum_{j=1}^{m}\psi_j(x)u_j e^{i\omega t},\ w_0(x,t)=\sum_{j=1}^{m}\varphi_j(x)w_j e^{i\omega t}$$
$$\theta(x,t)=\sum_{j=1}^{m}\psi_j(x)\theta_j e^{i\omega t} \qquad (5.30)$$

where u_j, w_j, θ_j are unknown values to be determined; $i^2 = -1$; ω is natural frequency; $\psi_j(x)$ and $\varphi_j(x)$ are the shape functions which are proposed in Table 5.1 for the Simply-supported (S – S), the Clamped – Clamped (C – C) and the Clamped – Free (C-F) boundary conditions (BCs). The shape functions satisfy the BCs given in Table 5.2.

Table 5.1 Kinematic BCs of nano beams.

BCs	Position	Value
S-S	x=0	$w = 0$
	x=L	$w = 0$
C-F	x=0	$u = 0, w = 0, w_{,x} = 0, \theta = 0$
	x=L	-
C-C	x=0, x=L	$u = 0, w = 0, w_{,x} = 0, \theta = 0$

Substituting Eqs. (5.30) into Eq. (5.16), the following characteristic equation is obtained:

$$\left(\begin{bmatrix} \mathbf{K}^{11} & \mathbf{0} & \mathbf{K}^{13} \\ \mathbf{0} & \mathbf{K}^{22} & \mathbf{K}^{23} \\ {}^{T}\mathbf{K}^{13} & {}^{T}\mathbf{K}^{23} & \mathbf{K}^{33} \end{bmatrix} - \omega^2 \left(\begin{bmatrix} \mathbf{M}^{11} & \mathbf{0} & \mathbf{M}^{13} \\ \mathbf{0} & \mathbf{M}^{22} & \mathbf{0} \\ {}^{T}\mathbf{M}^{13} & \mathbf{0} & \mathbf{M}^{33} \end{bmatrix} + \mu \begin{bmatrix} \mathbf{M}_n^{11} & \mathbf{0} & \mathbf{M}_n^{13} \\ \mathbf{0} & \mathbf{M}_n^{22} & \mathbf{M}_n^{23} \\ {}^{T}\mathbf{M}_n^{13} & {}^{T}\mathbf{M}_n^{23} & \mathbf{M}_n^{33} \end{bmatrix} \right) \right) \begin{Bmatrix} \mathbf{u} \\ \mathbf{w} \\ \boldsymbol{\theta} \end{Bmatrix} = \begin{Bmatrix} \mathbf{0} \\ \mathbf{0} \\ \mathbf{0} \end{Bmatrix} \quad (5.31)$$

Table 5.2 The shape functions.

BCs	$\psi_j(x)$	$\varphi_j(x)$
S-S	$\cos\frac{j\pi x}{L}$	$\sin\frac{j\pi x}{L}$
C-F	$\sin\frac{(2j-1)\pi x}{2L}$	$1-\cos\frac{(2j-1)\pi x}{2L}$
C-C	$\sin\frac{2j\pi x}{L}$	$1-\cos\frac{2j\pi x}{L}$

where the components of stiffness matrix **K** and mass matrix **M** are given by:

$$K_{ij}^{11} = A\int_0^L \psi_{i,x}\psi_{j,x}dx, K_{ij}^{13} = B\int_0^L \psi_{i,x}\psi_{j,x}dx, K_{ij}^{22} = A^s\int_0^L \varphi_{i,x}\varphi_{j,x}dx$$

$$K_{ij}^{23} = A^s\int_0^L \varphi_{i,x}\psi_j dx, K_{ij}^{33} = D\int_0^L \psi_{i,x}\psi_{j,x}dx + A^s\int_0^L \psi_i\psi_j dx$$

$$M_{ij}^{11} = I_0\int_0^L \psi_i\psi_j dx, M_{ij}^{13} = I_1\int_0^L \psi_i\psi_j dx, M_{ij}^{22} = I_0\int_0^L \varphi_i\varphi_j dx, M_{ij}^{33} = I_2\int_0^L \psi_i\psi_j dx \tag{5.32}$$

$$M_{nij}^{11} = I_0\int_0^L \psi_{i,x}\psi_{j,x}dx, M_{nij}^{13} = I_1\int_0^L \psi_{i,x}\psi_{j,x}dx$$

$$M_{nij}^{22} = I_0\int_0^L \varphi_{i,x}\varphi_{j,x}dx, M_{nij}^{23} = I_0\int_0^L \psi_i\varphi_{j,x}dx, M_{nij}^{33} = I_2\int_0^L \psi_{i,x}\psi_{j,x}dx$$

5.4.2. Ritz method for MCST

By using Ritz method, the displacement field in Eq. (5.29) is approximated by:

$$u(x,t) = \sum_{j=1}^{m} \psi_j(x) u_j e^{i\omega t}$$

$$w(x,t) = \sum_{j=1}^{m} \varphi_j(x) w_j e^{i\omega t} \tag{5.33}$$

$$\theta(x,t) = \sum_{j=1}^{m} \psi_j(x) \theta_j e^{i\omega t}$$

where u_j, w_j, θ_j are unknown values to be determined; $i^2 = -1$; ω is natural frequency; $\psi_j(x)$ and $\varphi_j(x)$ are the hybrid functions for Ritz solution reported in Table 4.3 are proposed for six typical BCs. They satisfy various BCs: The Simply-Supported (S – S), the Clamped – Free (C – F), the Clamped – Clamped (C – C), the Clamped – Simply supported (C – S), the Hinged – Hinged (H – H), the Clamped – Hinged (C – H). A characteristic problem for vibration and thermal buckling response is obtained through the stiffness matrix **K** and mass matrix **M**:

$$\left(\begin{bmatrix} \mathbf{K}^{11} & \mathbf{K}^{12} & \mathbf{K}^{13} \\ {}^T\mathbf{K}^{12} & \mathbf{K}^{22} & \mathbf{K}^{23} \\ {}^T\mathbf{K}^{13} & {}^T\mathbf{K}^{23} & \mathbf{K}^{33} \end{bmatrix} - \omega^2 \begin{bmatrix} \mathbf{M}^{11} & \mathbf{M}^{12} & \mathbf{M}^{13} \\ {}^T\mathbf{M}^{12} & \mathbf{M}^{22} & \mathbf{M}^{23} \\ {}^T\mathbf{M}^{13} & {}^T\mathbf{M}^{23} & \mathbf{M}^{33} \end{bmatrix} \right) \begin{Bmatrix} \mathbf{u} \\ \mathbf{w} \\ \boldsymbol{\theta} \end{Bmatrix} = \begin{Bmatrix} \mathbf{0} \\ \mathbf{0} \\ \mathbf{0} \end{Bmatrix} \tag{5.34}$$

where

$$K_{\mathrm{ij}}^{11} = A\int_0^L \psi_{i,\mathrm{x}}\psi_{\mathrm{j,x}}dx, K_{\mathrm{ij}}^{12} = -B\int_0^L \psi_{i,\mathrm{x}}\varphi_{\mathrm{j,xx}}dx$$

$$K_{\mathrm{ij}}^{13} = B^s\int_0^L \psi_{i,\mathrm{x}}\psi_{\mathrm{j,x}}dx,$$

$$K_{\mathrm{ij}}^{22} = \left(A^m + D\right)\int_0^L \varphi_{i,\mathrm{xx}}\varphi_{\mathrm{j,xx}}dx - N^t\int_0^L \varphi_{i,\mathrm{x}}\varphi_{\mathrm{j,x}}dx \tag{5.35}$$

$$K_{\mathrm{ij}}^{23} = -\left(D^s + \frac{B^m}{2}\right)\int_0^L \varphi_{i,\mathrm{xx}}\psi_{\mathrm{j,x}}dx$$

$$K_{\mathrm{ij}}^{33} = \left(H^s + \frac{D^m}{4}\right)\int_0^L \psi_{i,\mathrm{x}}\psi_{\mathrm{j,x}}dx + \left(A^s + \frac{H^m}{4}\right)\int_0^L \psi_i\psi_{\mathrm{j}}dx$$

$$M_{\mathrm{ij}}^{11} = I_0\int_0^L \psi_i\psi_{\mathrm{j}}dx, M_{\mathrm{ij}}^{12} = -I_1\int_0^L \psi_i\varphi_{\mathrm{j,x}}dx, M_{\mathrm{ij}}^{13} = J_1\int_0^L \psi_i\psi_{\mathrm{j}}dx$$

$$M_{\mathrm{ij}}^{22} = I_0\int_0^L \varphi_i\varphi_{\mathrm{j}}dx + I_2\int_0^L \varphi_{i,\mathrm{x}}\varphi_{\mathrm{j,x}}dx, M_{\mathrm{ij}}^{23} = -J_2\int_0^L \varphi_{i,\mathrm{x}}\psi_{\mathrm{j}}dx$$

$$M_{\mathrm{ij}}^{33} = K_2\int_0^L \psi_i\psi_{\mathrm{j}}dx$$

5.5 Temperature distribution for MCST

Two different temperature distributions through the beam depth are considered: Linear temperature rise and nonlinear temperature rise.

- Linear temperature rise: The temperature is linearly increased as follows:

$$T(z) = (T_t - T_b)\left(\frac{2z+h}{2h}\right) + T_b \tag{5.36}$$

where T_t and T_b are temperatures at the top and bottom surfaces of the beam.

- Nonlinear temperature rise: The temperature is varied nonlinearly according to a sinusoidal law [66] as follows:

$$T(z) = (T_t - T_b)\left[1 - \cos\frac{\pi}{2}\left(\frac{2z+h}{2h}\right)\right] + T_b \tag{5.37}$$

5.6 Numerical results and discussions

Example 1: Vibration responses of FSBT and the Eringen's nonlocal elasticity theory for FG nano beam (Type A, the various BCs)

A number of FG nano beams are considered in this section to verify the accuracy and efficiency of the present theory, and to investigate effects of the material parameter *p*, the span-to-height ratio *L/h* , the scale parameter μ and BCs on the natural frequencies of FG nano beams. The FG nano beams are supposed to be made of steel and Alumina (Al_2O_3) whose properties are followed: $E_m = 210GPa$, $\rho_m = 7800\,kg/m^3$, $E_c = 390GPa$, $\rho_c = 3960\,kg/m^3$, $\nu_m = \nu_c = 0.3$. The FG nano beam geometry is given as follows: *L*=10000 nm, *b*=1000 nm, *h*=100 nm. For simplicity, the following nondimensional frequency is introduced:

$$\hat{\omega} = \frac{\omega L^2}{h}\sqrt{\frac{12\rho_c}{E_c}} \tag{5.38}$$

The fundamental natural frequencies with respect to the series number *N* for different boundary conditions are given in Table 5.3. It is observed that the responses converge quickly for three boundary conditions: *p* = 1 with *L/h*=10 and 20 for vibration. Thus, these numbers of series terms will be used for vibration analysis, respectively throughout the numerical research.

Table 5.3: Convergence studies for fundamental frequencies of FG nano beams (Type A, *p*=1, $\mu = 1(nm)^2$).

L/h	BC	Numbers of series *N*							
		2	4	6	8	10	12	14	16
10	S – S	6.5836	6.5836	6.5836	6.5836	6.5836	6.5836	6.5836	6.5836
	C – F	2.4250	2.4204	2.4196	2.4193	2.4191	2.4190	2.4190	2.4190
	C – C	14.3765	14.2975	14.2763	14.2664	14.2607	14.2569	14.2542	14.2522
20	S – S	6.6515	6.6515	6.6515	6.6515	6.6515	6.6515	6.6515	6.6515
	C – F	2.4368	2.4329	2.4323	2.4321	2.4320	2.4320	2.4320	2.4320
	C – C	14.8479	14.7948	14.7845	14.7805	14.7785	14.7772	14.7764	14.7757

Tables 5.4 – 5.6 figure out the effects of nonlocal parameter and material graduation on the frequencies of the simply– supported (S-S), the clamped – free (C-F) and the clamped – clamped (C-C) beams, respectively. It is concluded that, as the material graduation

increases the frequencies decreased. Also, as the nonlocal parameter increases the frequencies decreased, for the both cases.

Table 5.4 The non-dimensional first natural frequencies with respect to the material distribution and the span-to-height ratio of FG nano beams (Type A, S-S).

μ	L/h	Theory	Material parameter p					
			0	0.5	1	2	5	10
$\mu=0(nm)^2$	20	FSDT	9.8281	7.7141	6.9670	6.3960	5.9169	5.6520
		Eltaher et al[183]	9.8797	7.8061	7.0904	6.5244	6.0025	5.7058
	50	FSDT	9.8629	7.7412	6.9916	6.4191	5.9389	5.6730
		Eltaher et al[183]	9.8724	7.7998	7.0852	6.5189	5.9990	5.7001
	100	FSDT	9.8679	7.7451	6.9952	6.4224	5.9421	5.6760
		Eltaher et al[183]	9.8700	7.7981	7.0833	6.5182	5.9970	5.7005
$\mu=1(nm)^2$	20	FSDT	9.3831	7.3647	6.6515	6.1065	5.6492	5.3963
		Eltaher et al[183]	9.4238	7.4458	6.7631	6.2233	5.7256	5.4425
	50	FSDT	9.4106	7.3862	6.6710	6.1248	5.6666	5.4128
		Eltaher et al[183]	9.4172	7.4403	6.7583	6.2191	5.7218	5.4389
	100	FSDT	9.4146	7.3892	6.6738	6.1274	5.6691	5.4152
		Eltaher et al[183]	9.4162	7.4396	6.7577	6.2185	5.7212	5.4384
$\mu=2(nm)^2$	20	FSDT	8.9932	7.0587	6.3751	5.8528	5.4146	5.1722
		Eltaher et al[183]	9.0257	7.1312	6.4774	5.9604	5.4837	5.2126
	50	FSDT	9.0153	7.0759	6.3907	5.8675	5.4285	5.1854
		Eltaher et al[183]	9.0205	7.1269	6.4737	5.9571	5.4808	5.2098
	100	FSDT	9.0184	7.0783	6.3930	5.8696	5.4305	5.1874
		Eltaher et al[183]	9.0197	7.1263	6.4731	5.9567	5.4803	5.2094

Table 5.5 The non-dimensional first natural frequencies with the nonlocal parameter of FG nano beams (Type A, C-F, L/h=100, N=10).

μ (nm)^2	Theory	Material parameter p					
		0	0.5	1	2	5	10
0	FSDT	3.5161	2.7597	2.4925	2.2885	2.1173	2.0225
	Eltaher et al [183]	3.5167	2.7600	2.4932	2.2884	2.1168	2.0221
1	FSDT	3.5153	2.7591	2.4919	2.2879	2.1168	2.0220
	Eltaher et al [183]	3.5292	2.7693	2.5134	2.2982	2.1268	2.0310
2	FSDT	3.5145	2.7584	2.4914	2.2874	2.1163	2.0215
	Eltaher et al [183]	3.5461	2.7841	2.5149	2.3084	2.1360	2.0405
3	FSDT	3.5137	2.7578	2.4908	2.2869	2.1158	2.0211
	Eltaher et al [183]	3.5632	2.8019	2.5259	2.3186	2.1458	2.0498

Figure 5.2 illustrates the fundamental frequencies with changing of the non-locality parameter, material distribution at L/h=100 and the variation of boundary conditions. It can be concluded that, the frequency decreases with high rate where the power exponent in range from 0 to 4 than that the power exponent in interval between 4 and 10. The

frequency decreases as the non-locality parameter increased from 0 to $5.0*10^{-12}$ with the same rate.

Table 5.6 The non-dimensional first natural frequencies with the nonlocal parameter of FG nano beams (Type A, C-C, L/h=100, N=10).

μ (nm)^2	Theory	Material parameter p					
		0	0.5	1	2	5	10
0	FSDT	22.3597	17.5498	15.8506	14.5525	13.4636	12.8607
	Eltaher et al[183]	22.3744	17.5613	15.8612	14.5626	13.4733	12.8698
1	FSDT	21.0991	16.5604	14.9570	13.7321	12.7047	12.1358
	Eltaher et al[183]	21.1096	16.5686	14.9645	13.7394	12.7116	12.1423
2	FSDT	20.0255	15.7177	14.1958	13.0334	12.0583	11.5183
	Eltaher et al[183]	20.0330	15.7235	14.2013	13.0386	12.0633	11.5230
3	FSDT	19.0974	14.9892	13.5379	12.4294	11.4995	10.9845
	Eltaher et al[183]	19.1028	14.9934	13.5419	12.4332	11.5032	10.9880

Figure 5.3 illustrates the frequency within the different span-to-height ratio (L/h=10, 20, 50, 100). When the ratio of length and height is 10 then there is a difference than the other ratios. The ratio of length and height of 100 is almost identical to that of length and height of 50. In this study, we use the ratio L/h = 100 to study for another problem.

Figure 5.4 illustrates the non-dimensional frequency within the different boundary conditions at material at graduation p=1, the non-locality parameter μ=1 (nm)^2 and the constant span-to-height ratio (L/h=100). In this figure, it indicates that the dimensionless frequency will be gradually decreasing from C-C, S-S and C-F. The largest non-dimensional frequency decreases when the material constant is between 0 and 2. Then, the non-dimensional frequency tends to move vertically as the material constant increases.

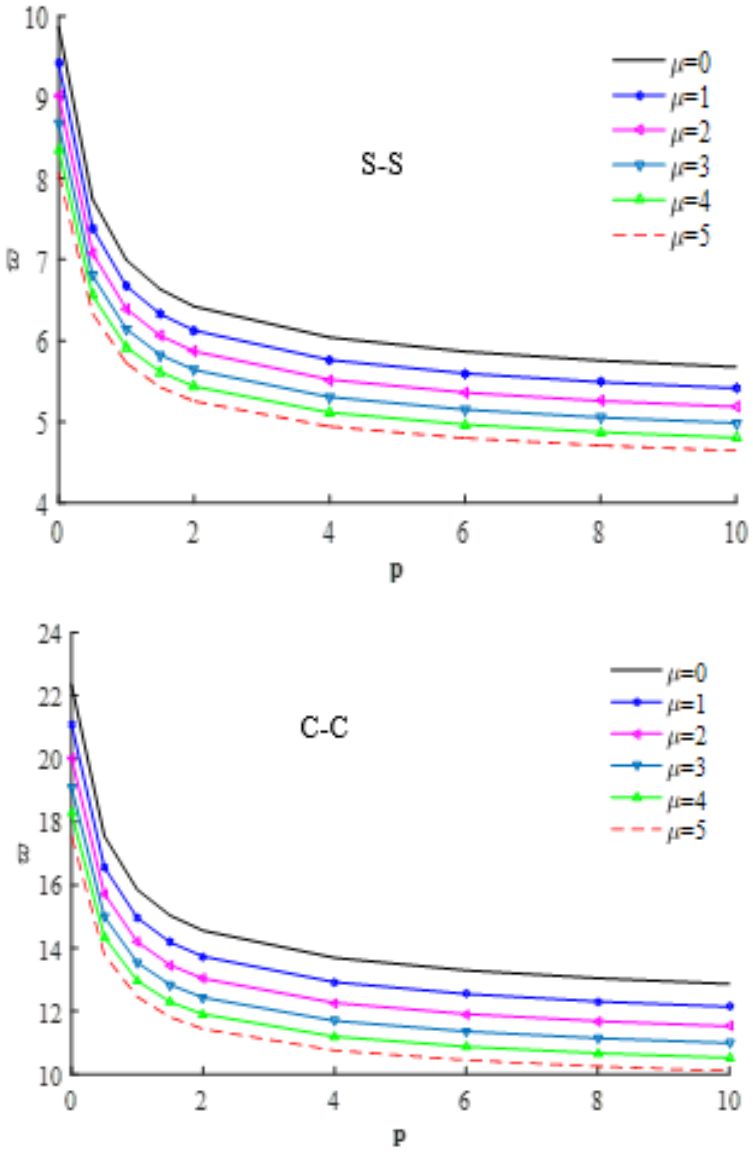

Figure 5.2 The non-dimensional frequency with material graduation for different non-locality parameter with the various BCs

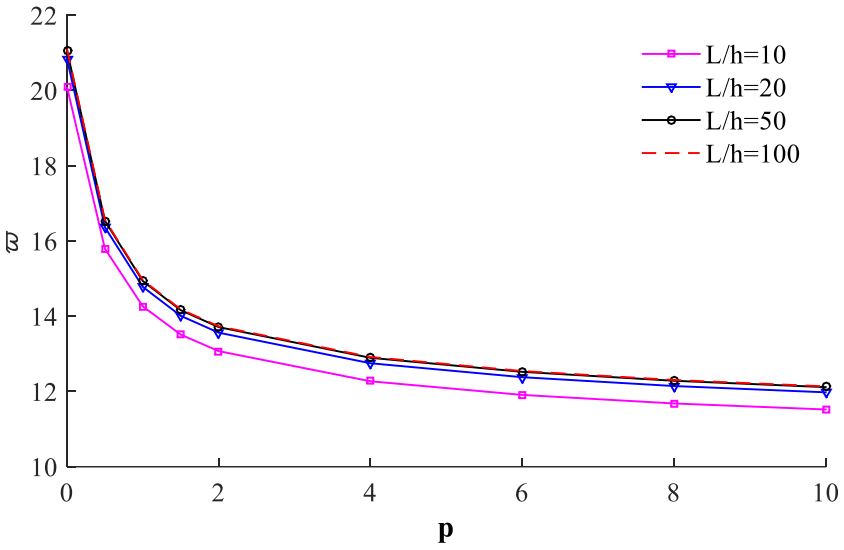

Figure 5.3 The non-dimensional frequency with material graduation for the various slenderness ratio (Type A, C-C, $\mu = 1(nm)^2$)

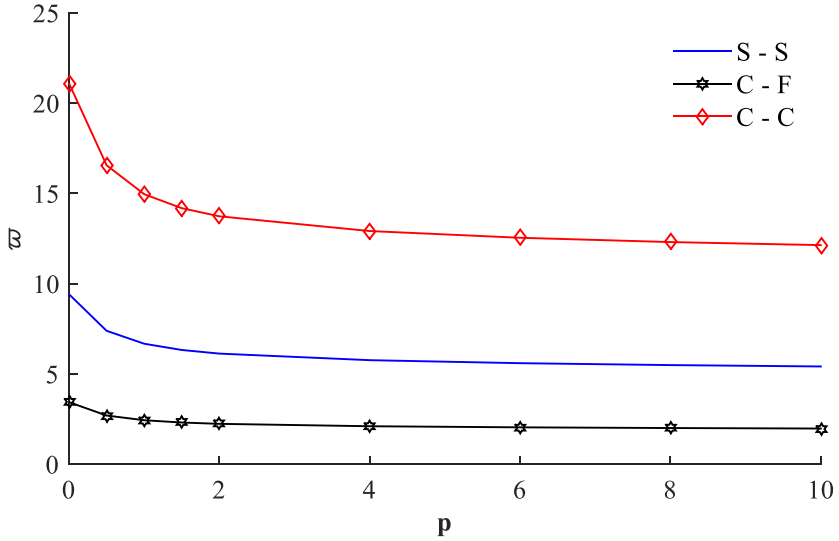

Figure 5.4 The non-dimensional frequency with material graduation for the various BCs (Type A, $\mu = 1(nm)^2$)

Example 2: Vibration and the thermal bucking responses of HSBT1 and the MCST for FG micro beam (Type A, the various BCs)

With FG micro beam, several numerical examples are analysed to verify the accuracy of present theory and investigate the effects of the power-law index, the span-to-height ratio, transverse normal strain, temperature content on the thermal buckling and vibration responses of FG micro beams for the various boundary conditions. FG micro beams are made of ceramic (Si_3N_4) and metal (SUS304) with material properties in Table 4.1.

$$\widehat{\omega} = \frac{\omega L^2}{h}\sqrt{\frac{12\rho_c}{E_c}},\ \lambda = \Delta T_{cr}\frac{L^2}{h^2}\alpha_m \tag{5.39}$$

where α_m is thermal expansion coefficient of metal at T_0 (K). Noticing that the following relations are used in this paper: T_0 = 300(K), T_b - T_0 = 5(K). FG micro beams with various BCs are considered to evaluate the convergence.

Table 5.7 Convergence studies for The non-dimensional fundamental frequencies of FG micro beams with various BCs and ς / h (Type A, p=1, L/h=5, Si_3N_4/ SUS304)

BC	ς / h	Numbers of series N					
		4	6	8	10	12	14
S – S	0	5.7999	5.7903	5.7901	5.7901	5.7901	5.7901
	1	13.7349	13.7116	13.7110	13.7106	13.7106	13.7106
C – H	0	5.8948	5.8819	5.8706	5.8634	5.8658	5.8658
	1	13.9757	13.9694	13.9688	13.9686	13.9686	13.9686
C – C	0	11.4679	11.3501	11.3150	11.3113	11.3020	11.3020
	1	29.6718	29.5644	29.5579	29.5575	29.5575	29.5575
C – S	1	17.1822	17.1749	17.1749	17.1749	17.1749	17.1749
H – H	1	13.9757	13.9694	13.9688	13.9686	13.9686	13.9686
C – F	1	7.0661	5.2521	5.0352	5.0255	5.0250	5.0250

The non-dimensional fundamental frequencies with respect to the series number N are given in Table 5.7. The results indicate that N = 10 is the convergence point for natural frequency and critical buckling thermal load, respectively.

Table 5.8 Fundamental frequency ($\bar{\omega}$) of FG micro beams under LTR (Type A, *L/h* =5, 20, Si_3N_4/ SUS304, TD).

BCs	*L/h*	ς	Theory	ΔT(K)=20			ΔT(K)=80		
				p=0.1	0.5	1	*p*=0.1	0.5	1
H-H	5	$\varsigma = 0$	$HSBT^M$	8.5461	6.6715	5.8604	8.5127	6.6480	5.8422
		$\varsigma = h/4$	$HSBT^M$	9.7618	7.6202	6.6863	9.7340	7.6036	6.6735
		$\varsigma = h/2$	$HSBT^M$	12.6565	9.8918	8.6639	12.6370	9.8850	8.6632
		$\varsigma = h$	$HSBT^M$	20.0936	15.7030	13.7186	20.0860	15.6952	13.7027
	20	$\varsigma = 0$	HSBT[190]	8.7846	6.8133	5.9658	8.1742	6.2547	5.4252
		$\varsigma = 0$	$HSBT^M$	8.8938	6.9090	6.0551	8.2961	6.3630	5.5274
		$\varsigma = h/4$	$HSBT^M$	10.0829	7.8466	6.8706	9.5607	7.3732	6.4144
		$\varsigma = h/2$	$HSBT^M$	13.0127	10.1517	8.8776	12.6144	9.7969	8.5385
		$\varsigma = h$	$HSBT^M$	20.9696	16.3963	14.3217	20.7296	16.1946	14.1358
C-C	5	$\varsigma = 0$	$HSBT^M$	16.6163	12.9435	11.3294	16.5953	12.9417	11.3241
		$\varsigma = h/4$	$HSBT^M$	19.5454	15.2455	13.3278	19.5343	15.2544	13.3459
		$\varsigma = h/2$	$HSBT^M$	26.1986	20.4659	17.8814	26.1932	20.4860	17.9144
		$\varsigma = h$	$HSBT^M$	43.4752	34.0009	29.6949	43.3131	33.9156	29.6466
	20	$\varsigma = 0$	HSBT[190]	20.1188	15.6333	13.6920	19.8063	15.3661	13.4427
		$\varsigma = 0$	$HSBT^M$	20.2018	15.6929	13.7410	19.8906	15.4281	13.4944
		$\varsigma = h/4$	$HSBT^M$	22.8674	17.7948	15.5702	22.5962	17.5680	15.3616
		$\varsigma = h/2$	$HSBT^M$	29.4390	22.9653	20.0741	29.2328	22.8038	19.9321
		$\varsigma = h$	$HSBT^M$	47.2739	36.9628	32.2796	47.1565	36.8971	32.2399

M: Micro Beam

The non-dimensional fundamental frequencies of the FG micro beams with the various BCs and the span-to-height are given in Tables 5.8–5.9. For macro FG beams (ς = 0), the present results again agree well with those of HSBT[190]. Some new results for FG beams are shown to serve as benchmarks for future studies. The results are increased as ς increases but the results are decreased as ΔT increases. This response can be expected because an increase in the material length scale parameters (MLSPs) leads to an increase in the beams' stiffness.

Table 5.9 Fundamental frequency ($\bar{\omega}$) of FG micro beams under NLTR (Type A, *L/h* =5 and 20, Si_3N_4/ SUS304, TD).

BCs	*L/h*	ς	Theory	ΔT(K)=20			ΔT(K)=80		
				p=0.1	0.5	1	*p*=0.1	0.5	1
H-H	5	$\varsigma = 0$	HSBT^M	8.5538	6.6746	5.8633	8.5398	6.6606	5.8548
		$\varsigma = h/4$	HSBT^M	9.7647	7.6229	6.6889	9.7458	7.6148	6.6850
		$\varsigma = h/2$	HSBT^M	12.6587	9.8939	8.6659	12.6461	9.8936	8.6716
		$\varsigma = h$	HSBT^M	20.4317	15.9858	13.9774	20.4286	16.0007	14.0019
	20	$\varsigma = 0$	HSBT[190]	8.7865	6.8184	5.9719	8.1855	6.2841	5.4605
		$\varsigma = 0$	HSBT^M	8.9452	6.9585	6.1036	8.5219	6.5803	5.7409
		$\varsigma = h/4$	HSBT^M	10.1282	7.8902	6.9134	9.7573	7.5616	6.5992
		$\varsigma = h/2$	HSBT^M	13.0478	10.1854	8.9108	12.7640	9.9394	8.6782
		$\varsigma = h$	HSBT^M	20.9914	16.4173	14.3423	20.8210	16.2812	14.2207
C-C	5	$\varsigma = 0$	HSBT^M	16.6153	12.9452	11.3212	16.6068	12.9338	11.3187
		$\varsigma = h/4$	HSBT^M	19.5494	15.2484	13.3307	19.5437	15.2420	13.3241
		$\varsigma = h/2$	HSBT^M	26.2007	20.4677	17.8832	26.006	20.4516	17.8200
		$\varsigma = h$	HSBT^M	43.3062	33.8716	29.5816	43.2164	33.7187	29.4497
	20	$\varsigma = 0$	HSBT[190]	20.1198	15.6360	13.6953	19.8121	15.3810	13.4604
		$\varsigma = 0$	HSBT^M	20.2298	15.7199	13.7675	20.0104	15.5412	13.6047
		$\varsigma = h/4$	HSBT^M	22.8922	17.8186	15.5937	22.7001	17.6669	15.4583
		$\varsigma = h/2$	HSBT^M	29.4583	22.9838	20.0923	29.3133	22.8802	20.0069
		$\varsigma = h$	HSBT^M	47.2859	36.9743	32.2909	47.2065	36.9444	32.2862

M: Micro Beam

Figures. 5.5 and 5.6 show variation of the natural frequencies and the normalized critical temperature **(** λ **)** with respect to ς ratio of *L/h*=5 and 20 beams. As ς increases, their variation depends on BCs. The C – C beam has the biggest variation and the C – F beam has the smallest variation.

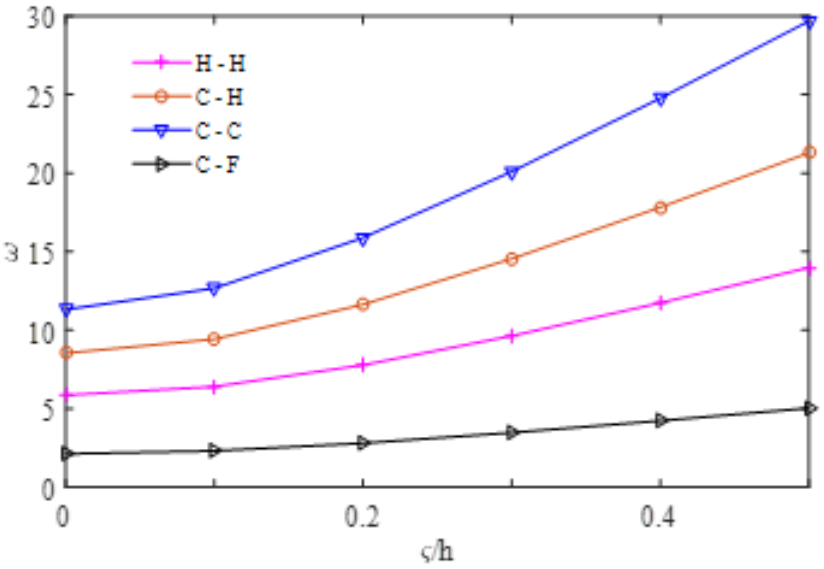

(a) *L/h*=5

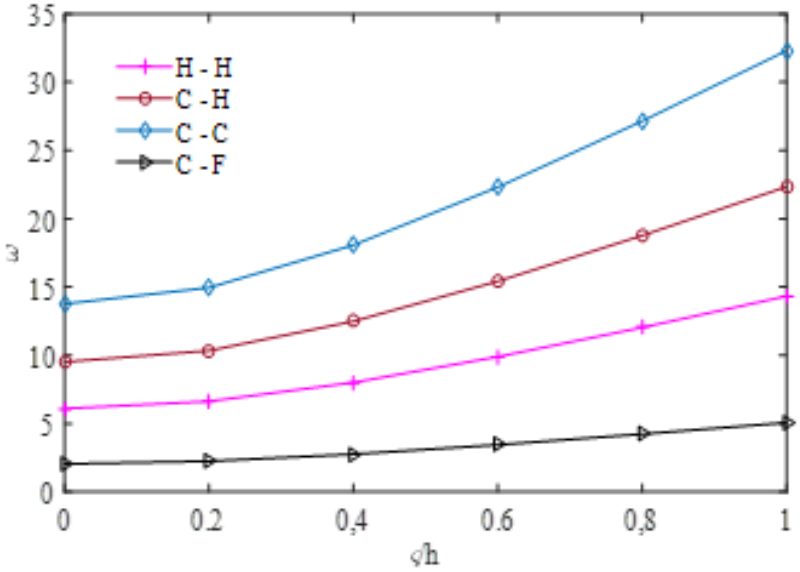

(b) *L/h*=20

Figure 5.5 Effect of the MLSP on the natural frequencies (ω) of FG micro beams with NLT, various BCs (Type A, *p*=1, Si_3N_4/SUS304, *L/h*=5 and 20).

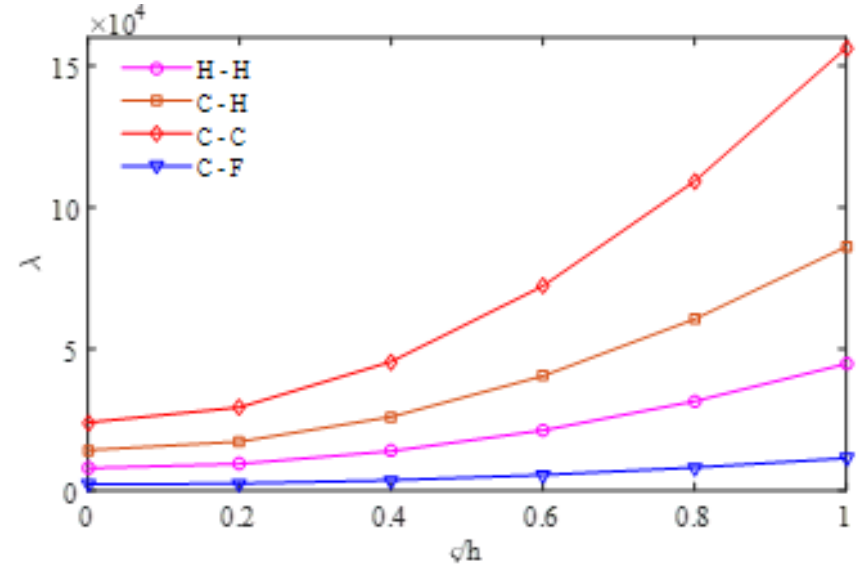

(a) *L*/*h*=5

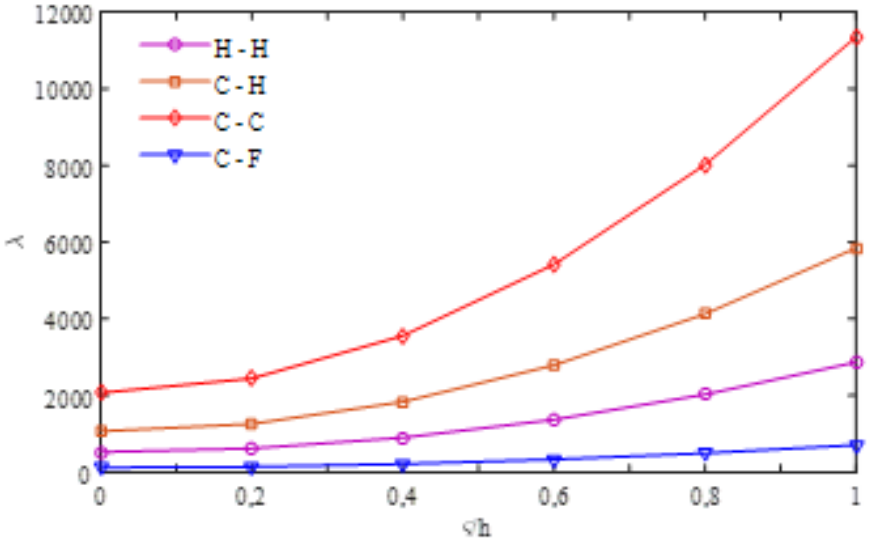

(b) *L*/*h*=20

Figure 5.6 Effect of the MLSP on the normalized critical temperature (λ) of FG micro beams with NLT, various BCs (Type A, *p*=1, Si_3N_4/SUS304, *L*/*h*=5 and 20).

5.7 Conclusions

The free vibration analysis of FG nano beams modeled according to Timoshenko beam theory is studied. The size-dependent (nonlocal) effect is introduced according to Eringen's nonlocal elasticity model. The vibrational problem governing the axial and lateral deformations is derived using the virtual-work principle. Ritz method is used to approximate the axial and lateral displacements, respectively. The fundamental frequencies of a FG nano beams are investigated versus the nonlocal and material-distribution parameters for different BCs of FG nano beams. The obtained results show that, the material-distribution profile may be manipulated to select a specific design frequency. It is also shown that, the nonlocal parameter has a notable effect on the fundamental frequencies of FG nano beams.

The size effect, which is included by the modified couple stress theory, on vibration and thermal buckling behaviors of FG micro beams is investigated in this chapter 5. The governing equations of motion are derived from Lagrange's equations. The frequencies, critical buckling loads, displacements and stresses of FG micro beams with various BCs are obtained. The results indicate that the present study is efficiency for predicting behaviors of FG micro beams.

Chapter 6
A finite element model for analysis of FG beams

Finite element method (FEM) for vibration and buckling of functionally graded beams based on a refined shear deformation theory is present.

The highlight of this chapter is follows:

- Governing equations of motion and various boundary conditions are derived from the Hamilton's principle.
- Effects of power-law index, span-to-height ratio and various boundary conditions on the natural frequencies, critical buckling loads of FG beams will be discussant.
- Numerical results show that the above-mentioned effects play very important role on the vibration and buckling analysis of FG beams

---

6.1 Introduction

In order to avoid the limitations of the analytical approaches, various studies have been focused on the development of efficient finite elements.

Alshorbagy et al.[102] investigated free vibration characteristics of FG beams by using a finite element method. The equations of motion are derived using Euler–Bernoulli beam theory and the virtual work principle. The material constituents of beams assumed to be varying through the thickness or longitudinal directions according to a simple power law. The effects of various boundary conditions, power law index, and slenderness ratio are investigated. Mohanty et al. [191] carried out a finite element analysis to investigate the effect of various parameters on static and dynamic behavior of FG beam. It is concluded that the critical buckling load increases with the increase of the power law index for FG beam with steel rich bottom whereas this trend reverses for aluminum rich bottom. Also, beams having properties according to a power law are more stable as compared with beams having properties according to exponential law for the case of steel rich bottom. Jing et al. [192] applied a finite volume method for the static and free vibration analysis of FG beams using Timoshenko beam theory. It is assumed that material properties vary in the thickness direction by power law. Kahya and Turan [193] proposed a new five-nodded beam element for the vibration and buckling analysis of FG beams based on the FSDT. Frikha et al. [194] developed a new mixed finite element for FG beams based on HSDT of Reddy. The performance of the element is checked through static analysis of cantilevered and simply supported beams. Chakraborty et al. [103] developed a new beam element to study the thermos elastic behavior of FG cantilever beam based on the FSDT. Both exponential and power law variations of material property distribution are used to examine different stress variations. It has been found that the presence of FGM layer in structures results in a significant difference in its response from its parent material beams due to the presence of coupled stiffness and inertial parameters.

In this chapter, which is extended from the previous work [5], finite element model for vibration and buckling of FG beams is studied. The developed theory accounts for parabolic variation of the transverse shear strain and stress through the beam depth, and satisfy the stress-free boundary conditions on the top and bottom surfaces of the beam. Governing equations of motion and boundary conditions are derived from the Hamilton's principle. Effects of power-law index, span-to-height ratio and various boundary conditions on the natural frequencies, critical buckling loads and load-frequency curves of sandwich beams are discussed. Numerical results show that the above-mentioned effects play very important role on the vibration and buckling analysis of FG beams.

6.2 Finite element formulation

6.2.1 FG beams

Geometry of FG beams as in Figure 6.1 with rectangular section $b \times h$ and length L. In this study, it is made of a mixture of isotropic ceramic and metal whose properties vary continuously in the beam, i.e., Young modulus E, Poisson's ratio ν, mass density ρ vary exponentially in both axial (x – axis) and the thickness directions (z – axis) as follows:

$$P(z) = (P_c - P_m)\left(\frac{2z+h}{2h}\right)^p + P_m \tag{6.1}$$

where *P(z)* is material elastic moduli as Young modulus $E(z)$, Poisson's ratio $\nu(z)$, mass density $\rho(z)$, at location *z*; P_c, P_m are material elastic properties of ceramic and metal, respectively; p is power-law material parameter.

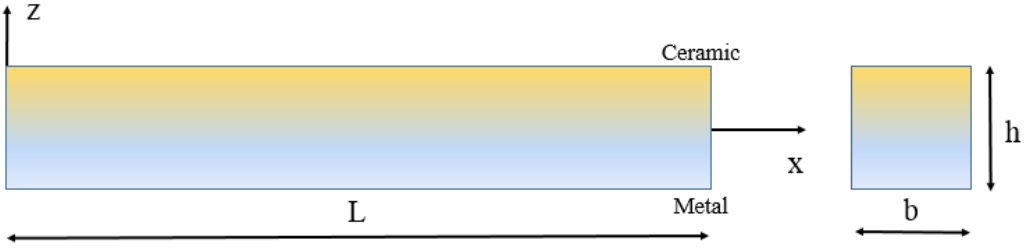

Figure 6.1 Geometry of FG beam

6.2.2 Higher-order shear deformation beam theory

The displacement field of the present theory can be obtained as (HSBT1):

$$u(x,z,t) = u_0(x,t) - zw_{0,x}(x,t) + \left[\sinh^{-1}\left(\frac{rz}{h}\right) - \frac{8rz^3}{3h^3\sqrt{r^2+4}}\right]\theta(x,t) \qquad (r=1)$$

$$= u_0(x,t) - zw_{0,x}(x,t) + f(z)\theta(x,t) \qquad (6.2)$$

$$w(x,z,t) = w_0(x,t)$$

where u_0, θ are the mid-plane axial displacement and rotation, w_0 denotes the mid-plane transverse displacement of the beam, the comma indicates partial differentiation with respect to the coordinate subscript that follows.

The nonzero strains associated with the displacement field are:

$$\varepsilon_x(x,z,t) = \frac{\partial u}{\partial x} = u_{0,x} - zw_{0,xx} + f\theta_{,x}$$

$$= \varepsilon^0 - z\varepsilon^1 + f\varepsilon^2 \qquad (6.3)$$

$$\gamma_{xz}(x,z,t) = \frac{\partial u}{\partial z} + \frac{\partial w}{\partial x} = f_{,z}(z)\theta$$

where $\varepsilon^0, \varepsilon^1,$ and ε^2 are the axial strain and curvatures of the beam, respectively.

6.2.3 Constitutive Equations

The strains and stresses are related by:

$$\begin{Bmatrix}\sigma_x\\ \sigma_z\\ \sigma_{xz}\end{Bmatrix} = \begin{bmatrix}\bar{Q}_{11} & \bar{Q}_{13} & 0\\ \bar{Q}_{13} & \bar{Q}_{11} & 0\\ 0 & 0 & \bar{Q}_{55}\end{bmatrix}\begin{Bmatrix}\varepsilon_x\\ \varepsilon_z\\ \gamma_{xz}\end{Bmatrix} \qquad (6.4)$$

where $Q_{11} = \frac{E(z)}{1-\nu^2}$, $Q_{13} = \frac{E(z)\nu}{1-\nu^2}$, $Q_{55} = \frac{E(z)\nu}{2(1+\nu)}$

6.2.4 Variational Formulation

In order to derive the equations of motion, Hamilton's principle is used:

$$0 = \int_0^T \left(\delta U + \delta V - \delta K \right) \mathrm{d}t \tag{6.5}$$

where $\delta U, \delta V$ and δK denote the virtual variation of the strain energy, kinetic energy and potential energy, respectively. The variation of the strain energy can be stated as:

$$\begin{aligned} \delta U &= \int_A \left[\int_{-h/2}^{h/2} \left(\sigma_{xx} \delta \varepsilon_{xx} + \sigma_{xz} \delta \gamma_{xz} \right) dz \right] \mathrm{d}A \\ &= \int_0^L \left[N_x \frac{\partial \delta u_0}{\partial x} - M_x^b \frac{\partial^2 \delta w_0}{\partial x^2} - M_x^s \frac{\partial \delta \theta}{\partial x} + Q_x \delta \gamma_{xz} \right] b dx \end{aligned} \tag{6.6}$$

where $dA = dxdy$ và $\mathrm{N}_x, \mathrm{M}_x^b, \mathrm{M}_x^s, \mathrm{Q}_{xz}$ are the stress resultants, defined as:

$$\begin{aligned} N_x &= \int_{-h/2}^{h/2} \sigma_{xx}(z) \mathrm{b} \mathrm{d}z \\ M_x^b &= \int_{-h/2}^{h/2} z \sigma_{xx}(z) \mathrm{b} \mathrm{d}z \\ M_x^s &= \int_{h/2}^{h/2} f \sigma_{xx}(z) \mathrm{b} \mathrm{d}z \\ Q_{xz} &= \int_{h/2}^{h/2} f_{,z} \sigma_{xz}(z) \mathrm{b} \mathrm{d}z \end{aligned} \tag{6.7}$$

By using Eqs. (6.3), (6.4) and (6.7), the constitutive equations for stress resultants and strains are obtained:

$$\begin{Bmatrix} \mathbf{N}_x \\ \mathbf{M}_x^b \\ \mathbf{M}_x^s \\ \mathbf{Q}_x \end{Bmatrix} = \begin{bmatrix} \mathbf{A} & \mathbf{B} & \mathbf{B}^s & 0 \\ \mathbf{B} & \mathbf{D} & \mathbf{D}^s & 0 \\ \mathbf{B}^s & \mathbf{D}^s & \mathbf{H}^s & 0 \\ 0 & 0 & 0 & \mathbf{A}^s \end{bmatrix} \begin{Bmatrix} u_{0,x} \\ w_{0,xx} \\ \theta_{,x} \\ \theta \end{Bmatrix} \tag{6.8}$$

where $\mathrm{A}, \mathrm{B}, \mathrm{D}, \mathrm{B}^s, \mathrm{D}^s, \mathrm{H}^s$ and A^s are the stiffness's of FG beams and given by:

$$A, B, D, B^s, D^s, H^s = \int_{h_{n-1}}^{h_n} \left(1, z, z^2, f, zf, f^2 \right) Q_{11}(z) \mathrm{d}z \tag{6.9a}$$

$$A^s = \int_{h_{n-1}}^{h_n} g^2 Q_{55}(z)\mathrm{d}z \tag{6.9b}$$

The variation of the potential energy by the axial force N_{xx}^0 can be written as:

$$\delta V = -\int_0^L N_{xx}^0 w_{0,x} \delta w_{0,x} b\, dx \tag{6.10}$$

The variation of the kinetic energy can be expressed as:

$$\begin{aligned}\delta K &= \int_V \rho(z)\left(\dot{u}\delta\dot{u} + \dot{w}\delta\dot{w}\right)\mathrm{d}z\mathrm{d}A \\ &= \int_0^L \Big[\delta\dot{u}_0 \left(I_0\dot{u}_0 - I_1\dot{w}_{0,x} + J_1\dot{\theta}\right) + \delta\dot{\theta}\left(I_0\dot{\theta}\right) + \delta\dot{w}_{0,x}\left(-I_1\dot{u}_0 + I_2\dot{w}_{0,x} - J_2\dot{\theta}\right) \\ &\quad + \delta\dot{\theta}\left(J_1\dot{u}_0 - J_2\dot{w}_{0,x} + K_2\dot{\theta}\right)\Big] dx\end{aligned} \tag{6.11}$$

where dot-superscript prime indicates the differentiation with respect to the time *t*; and $I_0, I_1, I_2, J_1, J_2, K_2$ are the mass inertias, defined by:

$$\left(I_0, I_1, I_2, J_1, J_2, K_2\right) = \int_{-h/2}^{h/2} \rho(z)\left(1, z, z^2, f, fz, f^2\right)\mathrm{d}z \tag{6.12}$$

By substituting Eqs. (6.6), (6.10) and (6.11) into Eq. (6.5), the following weak statement is obtained:

$$\begin{aligned}0 = \int_{t_1}^{t_2}\int_0^l \Big[& N_x \frac{\partial \delta u_0}{\partial x} - M_x^b \frac{\partial^2 \delta w_0}{\partial x^2} - M_x^s \frac{\partial \delta\theta}{\partial x} + Q_x \delta\gamma_{xz} - N_{xx}^0 w_{0,x}\delta w_{0,x} - \Big(\delta\dot{u}_0\left(I_0\dot{u}_0 - I_1\dot{w}_{0,x}\right. \\ & \left. + J_1\dot{\theta}\right) + \delta\dot{\theta}\left(I_0\dot{\theta}\right) + \delta\dot{w}_{0,x}\left(-I_1\dot{u}_0 + I_2\dot{w}_{0,x} - J_2\dot{\theta}\right) + \delta\dot{\theta}\left(J_1\dot{u}_0 - J_2\dot{w}_{0,x} + K_2\dot{\theta}\right)\Big)\Big] dx dt\end{aligned} \tag{6.13}$$

6.2.5 Governing Equations of Motion

The equilibrium equations of the present study can be obtained by integrating the derivatives of the varied quantities by parts and collecting the coefficients of δu, δw and $\delta\theta$:

$$\delta u_0 : \frac{\partial N_x}{\partial x} = I_0\ddot{u}_0 - I_1\ddot{w}_{0,x} + J_1\ddot{\theta}$$
$$\delta w_0 : \frac{\partial^2 M_x^s}{\partial x^2} + N_{xx}^0 w_{0,xx} + q = -I_1\ddot{u}_{0,x} + I_2\ddot{w}_{0,xx} - J_2\ddot{\theta}_{,x} \tag{6.14}$$
$$\delta\theta : \frac{\partial^2 M_x^b}{\partial x^2} + Q_{x,x} = J_1\ddot{u}_{0,x} - J_2\ddot{w}_{0,xx} + K_2\ddot{\theta}_{,x} + I_0\ddot{\theta}$$

By substituting Eq. (6.8) into Eq. (6.14), the explicit form of the governing equations of motion can be expressed with respect to the stiffness's

$$\begin{aligned} &Au_{0,xx} - Bw_{0,xxx} + B^s\theta_{,xx} = I_0\ddot{u}_0 - I_1\ddot{w}_{0,x} + J_1\ddot{\theta} \\ &Bu_{0,xxx} - Dw_{0,xxxx} - D^s\theta_{,xxx} + N_{xx}^0 w_{0,xx} \\ &\qquad = -I_1\ddot{u}_{0,x} + I_2\ddot{w}_{0,xx} - J_2\ddot{\theta}_{,x} \\ &B^s u_{0,xxx} - D^s w_{0,xxxx} - H^s\theta_{,xxx} + A^s\theta_{,xx} \\ &\qquad = J_1\ddot{u}_{0,x} - J_2\ddot{w}_{0,xx} + K_2\ddot{\theta}_{,x} + I_0\ddot{\theta} \end{aligned} \tag{6.15}$$

6.2.6 Finite Element Formulation

The present theory for FG beams described in the previous chapter was implemented via a displacement based finite element method. The variational statement in Eq. (6.13) requires that the axial displacement u and rotation θ are only once differentiable and C^0- continuous, whereas the transverse displacement w must be twice differentiable and C^1-continuous. The field variables are therefore approximated as follows:

$$\begin{aligned} u(x) &= \sum_{j=1}^{2} u_j \psi_j^e(x) \\ w(x) &= \sum_{j=1}^{4} \Delta w_j \varphi_j^e(x) \\ \theta(x) &= \sum_{j=1}^{2} \theta_j \psi_j^e(x) \end{aligned} \tag{6.16}$$

In order to satisfy the continuity of C^0 of the axial displacement and rotation, Lagrange's shape functions are hence chosen, which are given as in Eq. (6.17) and plotted in Figure 6.2.

$$\psi_1(x)=1-\frac{x}{l_e},\psi_2(x)=\frac{x}{l_e} \tag{6.17}$$

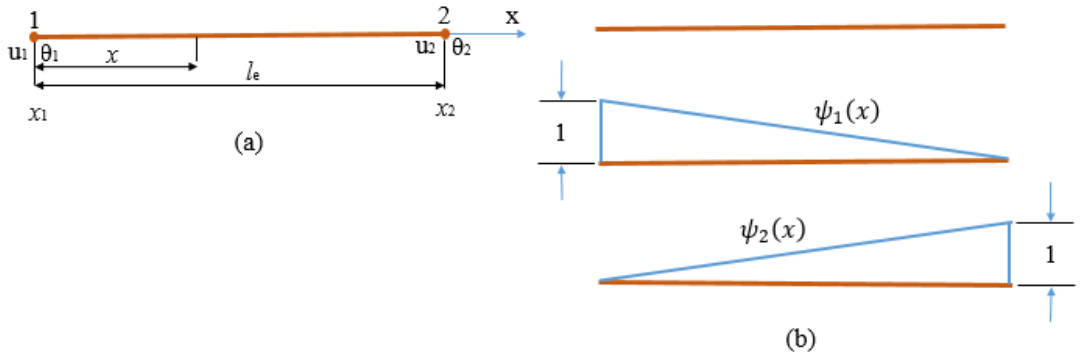

Figure 6.2 Two-nodes beam element

Moreover, in order to satisfy the C^1-continuity condition of the transverse displacement, a second-order polynomial can be selected for the shape function, however it requires a three-node finite element with 3 values of associated node displacement. In practice, this approach is complicated to implement and programming. Moreover, it is observed that the essential variables of the beams [28] are $u, w, w_{,x}, \theta$, that enables to use a two-node finite element and a Hermite-cubic interpolation function.

The transverse displacement of the beams is therefore approximated as follows:

$$w(x)=w_1\varphi_1^e+\beta_1\varphi_2^e+w_2\varphi_3^e+\beta_2\varphi_4^e=\sum_{j=1}^{4}\Delta w_j\varphi_j^e(x) \tag{6.18}$$

where the shape functions $\varphi_j^e(x)$ are given by:

$$\begin{aligned}\varphi_1(x)&=1-3\left(\frac{x}{l_e}\right)^2+2\left(\frac{x}{l_e}\right)^3;\quad \varphi_2(x)=x-\frac{2x^2}{l_e}+\frac{x^3}{l_e^2}\\ \varphi_3(x)&=3\left(\frac{x}{l_e}\right)^2-2\left(\frac{x}{l_e}\right)^3;\quad \varphi_4(x)=-\frac{x^2}{l_e}+\frac{x^3}{l_e^2}\end{aligned} \tag{6.19}$$

The variations of these shape functions are also displayed in Figure 6.3 in which it is observed that the shape functions satisfy the delta knoneckor condition.

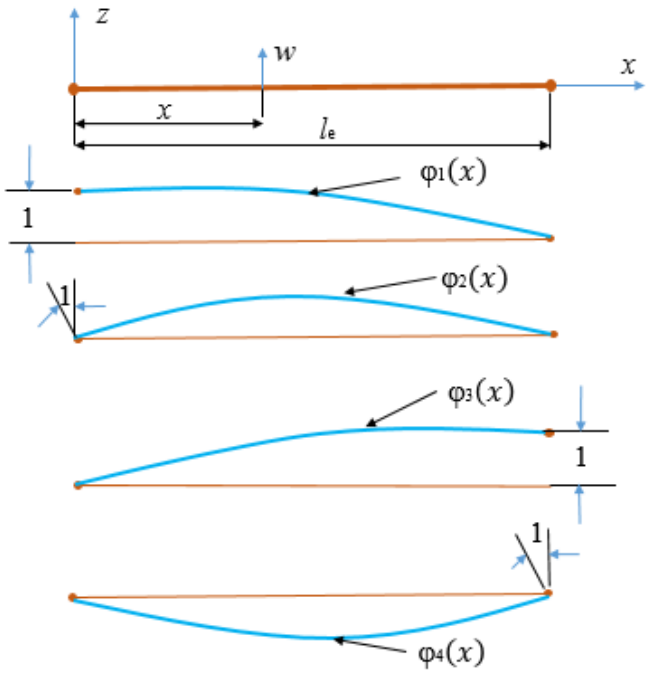

Figure 6.3 Hermite shape functions in a beam element

Substituting these expressions in Eq. (6.17) and Eq. (6.19) into the corresponding weak statement in Eq. (6.13), the finite element model of a typical element can be expressed as the standard eigenvalue problem:

$$\left(\mathbf{K} - N_{xx}^{0}\,\mathbf{G} - \omega^{2}\,\mathbf{M}\right)\boldsymbol{\chi} = \mathbf{0} \tag{6.20}$$

Eqs. (6.20) are equations of motion of the beam from which the bending, buckling and vibration responses of the beam can be obtained. The solution of Eq. (6.20) will allow to calculate the critical thermal buckling loads of FG beam.

$$\left(\mathbf{K} - N_{xx}^{0}\,\mathbf{G}\right)\boldsymbol{\chi} = \mathbf{0}$$

or the natural frequencies of FG beam.

$$\left(\mathbf{K} - \omega^{2}\,\mathbf{M}\right)\boldsymbol{\chi} = \mathbf{0}$$

where **K**, **G** and **M** are the element stiffness matrix, element geometric stiffness matrix and element mass matrix, respectively. The explicit forms of them are given by:

$$K_{\mathrm{ij}}^{11}=\int_0^L A\psi_{i,\mathrm{x}}\psi_{\mathrm{j,x}}dx, K_{\mathrm{ij}}^{12}=-\int_0^L B\psi_{i,\mathrm{x}}\varphi_{\mathrm{j,xx}}dx, K_{\mathrm{ij}}^{13}=\int_0^L B^s\psi_{i,\mathrm{x}}\psi_{\mathrm{j,x}}dx$$

$$K_{\mathrm{ij}}^{22}=\int_0^L D\varphi_{i,\mathrm{xx}}\varphi_{\mathrm{j,xx}}dx, K_{\mathrm{ij}}^{23}=-\int_0^L D^s\varphi_{i,\mathrm{xx}}\psi_{\mathrm{j,x}}dx, \tag{6.21a}$$

$$K_{\mathrm{ij}}^{33}=\int_0^L\left(H^s\psi_{i,\mathrm{x}}\psi_{\mathrm{j,x}}+A^s\psi_i\psi_{\mathrm{j}}\right)dx, G_{\mathrm{ij}}^{22}=\int_0^L\varphi_{i,\mathrm{x}}\varphi_{\mathrm{j,x}}dx$$

$$M_{\mathrm{ij}}^{11}=\int_0^L I_0\psi_i\psi_{\mathrm{j}}dx, M_{\mathrm{ij}}^{12}=-\int_0^L I_1\psi_i\varphi_{\mathrm{j,x}}dx, M_{\mathrm{ij}}^{13}=\int_0^L J_1\psi_i\psi_{\mathrm{j}}dx$$

$$M_{\mathrm{ij}}^{22}=\int_0^L I_0\varphi_i\varphi_{\mathrm{j}}dx+\int_0^L I_2\varphi_{i,x}\varphi_{\mathrm{j,x}}dx, M_{\mathrm{ij}}^{23}=-\int_0^L J_2\varphi_{i,x}\psi_{\mathrm{j}}dx \tag{6.21b}$$

$$M_{\mathrm{ij}}^{33}=\int_0^L K_2\psi_i\psi_{\mathrm{j}}dx,$$

In Eq. (6.20), N_{xx}^0 is the axial force or the thermal force, ω is the natural frequency, χ is the eigenvector of nodal displacements corresponding to an eigenvalue:

$$\chi=\left\{u\ w\ \theta\right\}^T \tag{6.22}$$

6.3 Numerical results and discussions

<u>Example:</u> Vibration and the thermal bucking responses of HSBT1 using FEM for analysis FG beam (Type A, various BCs)

For verification purpose, the fundamental natural frequencies and critical buckling loads of FG beams with different values of the span-to-height ratio for the three boundary conditions, which are the Clamped – Clamped (C – C), the Clamped – Free (C – F) and the Simply – supported (S – S) are given in Tables 1-4 FG material properties are assumed to be:

For simplicity, the non-dimensional natural frequencies and the critical buckling loads are defined as:

$$\bar{N}_{cr} = N^0_{xxcr}\frac{12L^2}{E_m h^3}, \bar{\omega} = \frac{\omega L^2}{h}\sqrt{\frac{\rho_m}{E_m}} \tag{6.23}$$

Table 6.1 Ceramic and metal materials.

Materials	E (GPa)	ρ (kg/m^3)	ν
Ceramic			
Alumina (Al_2O_3)	380	3960	0.3
Metal			
Aluminum (Al)	70	2702	0.3

Therefore, this number of elements is used throughout the numerical examples. The results obtained from the present theory are compared with those of HSBT [5] and [117]. In order to verify the convergence of the present polynomial series solution, Table 6.2 presents the fundamental frequency and critical buckling loads for three boundary conditions of FG beams. The solutions are calculated for the power-law index (p=1) and span-to-height ratio (L/h=5). The solutions of S-S and C-F boundary conditions converge more quickly than C-C one. The results indicate that N_e = 8 is the convergence point for natural frequency, and critical buckling load, respectively. Thus, this number is used hereafter. It can be stated that the convergence of present solution appears to be faster than that of the solution from [5] (m = 12).

Tables 6.3-6.4 present the comparison of the natural frequencies and critical buckling loads of FG beams (Type A) with three boundary conditions. They are calculated for various values of the power-law index and compared to the solutions obtained from the third-order shear deformation beam theory (TSBT) ([5], [117]). It is seen that the solutions obtained derived from the proposed theory are in excellent agreement with those obtained from previous results for both deep and thin beams.

Figures 6.4-6.5 display the variation of the fundamental frequency and critical buckling load with respect to the power-law index and the span-to-height ratio of FG beams. Three curves are observed for three boundary conditions, the highest curve corresponds to the

C-C case and the lowest one is the C-F case. The results decrease with an increase of the power-law index.

Table 6.2: Convergence of the non-dimensional fundamental frequency($\bar{\omega}$) and the critical buckling load $\left(N_{cr}\right)$ of FG beams (Type A, p = 1 and L/h = 5)

BCs	Theory	Number of elements N_e						
		6	8	10	12	14	16	18
Fundamental frequency $(\bar{\omega})$								
S-S	HSBT[F]	3.9711	3.9711	3.9711	3.9711	3.9711	3.9711	3.9711
	HSBT [5]	3.9907	3.9904	3.9904	3.9904	3.9904	3.9904	3.9904
C-F	HSBT[F]	1.4633	1.4633	1.4633	1.4633	1.4633	1.4633	1.4633
	HSBT [5]	1.4645	1.4638	1.4635	1.4633	1.4633	1.4633	1.4633
C-C	HSBT[F]	7.9501	7.9501	7.9501	7.9501	7.9501	7.9501	7.9501
	HSBT [5]	8.0309	8.0031	7.9704	7.9572	7.9518	7.9500	7.9493
Critical buckling load $\left(N_{cr}\right)$								
S-S	HSBT[F]	24.5841	24.5841	24.5841	24.5841	24.5841	24.5841	24.5841
	HSBT [5]	24.5873	24.5840	24.5840	24.5840	24.5840	24.5840	24.5840
C-F	HSBT[F]	6.5352	6.5352	6.5352	6.5352	6.5352	6.5352	6.5352
	HSBT [5]	6.5352	6.5352	6.5352	6.5352	6.5352	6.5352	6.5352
C-C	HSBT[F]	79.4884	79.4884	79.4884	79.4884	79.4884	79.4884	79.4884
	HSBT [5]	81.3950	79.4992	79.4888	79.4888	79.4888	79.4888	79.4888

F: Finite element method

Table 6.3 Comparison of the non-dimensional critical buckling load of FG beams with various boundary conditions (Type A, L/h=5 and 10).

L/h	BCs	Reference	p					
			0	0.5	1	2	5	10
5	S-S	HSBT [5]	48.8406	32.0013	24.6894	19.1577	15.7355	14.1448
		HSBT[F]	48.5960	31.8593	24.5841	19.0710	15.6425	14.0509
	C-C	HSBT [5]	154.5610	103.7167	80.5940	61.7666	47.7174	41.7885
		HSBT[F]	152.1513	102.2467	79.4884	60.8802	46.8791	40.9865
	C-F	HSBT [5]	13.0771	8.5000	6.5427	5.0977	4.2772	3.8820
		HSBT[F]	13.0595	8.4900	6.5352	5.0916	4.2703	3.8748
10	S-S	HSBT [5]	52.3083	34.0002	26.1707	20.3909	17.1091	15.5278
		HSBT[F]	52.2378	33.9600	26.1412	20.3665	17.0816	15.4995
	C-C	HSBT [5]	195.3623	128.0053	98.7885	76.6538	62.9580	56.5926
		HSBT[F]	194.3840	127.4390	98.3400	76.2881	62.5728	56.2052
	C-F	HSBT [5]	13.3741	8.6694	6.6678	5.2025	4.3974	4.0045
		HSBT[F]	13.3091	8.6324	6.6405	5.1796	4.3711	3.9775

F: Finite element method

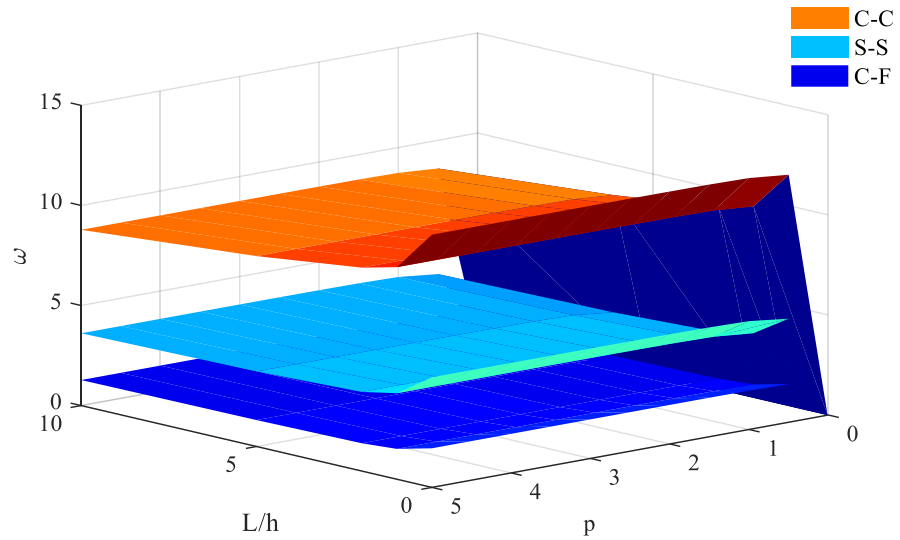

Figure 6.4 Effects of p and L/h on the nondimensional fundamental frequency $(\bar{\omega})$ of FG beams (Type A)

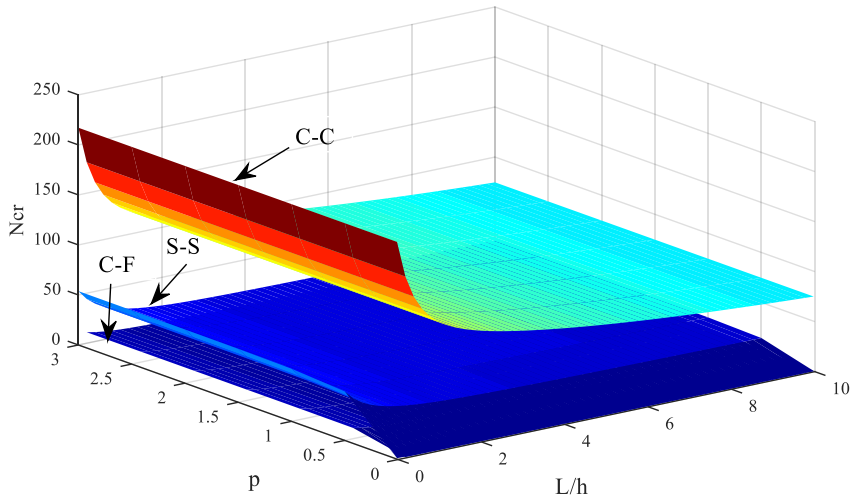

Figure 6.5 Effects of p and L/h on the critical buckling load (N_{cr}) of FG beams (Type A)

Table 6.4 Comparison of the non-dimensional fundamental natural frequency of FG beams with the various boundary conditions (Type A, *L/h*=5 and 20).

L/h	BCs	Reference	*p*					
			0	0.5	1	2	5	10
5	S-S	HSBT [117]	5.1527	4.4107	3.9904	3.6264	3.4012	3.2816
		HSBT [5]	5.1528	4.4102	3.9904	3.6264	3.4009	3.2815
		HSBT^{F}	5.1528	4.4011	3.9711	3.5972	3.3736	3.2650
	C-C	HSBT [117]	10.0699	8.7463	7.9499	7.1766	6.4940	6.1652
		HSBT [5]	10.0726	8.7463	7.9518	7.1776	6.4929	6.1658
		HSBT^{F}	10.0698	8.7439	7.9501	7.1768	6.4932	6.1654
	C-F	HSBT [117]	1.8952	1.6182	1.4633	1.3325	1.2592	1.2183
		HSBT [5]	1.8957	1.6182	1.4636	1.3328	1.2594	1.2187
		HSBT^{F}	1.8952	1.6178	1.4633	1.3326	1.2592	1.2184
20	S-S	HSBT [117]	5.4603	4.6516	4.2050	3.8361	3.6485	3.5390
		HSBT [5]	5.4603	4.6506	4.2051	3.8361	3.6485	3.5390
		HSBT^{F}	5.4603	4.6500	4.2037	3.8341	3.6465	3.5378
	C-C	HSBT [117]	12.2238	10.4287	9.4316	8.5975	8.1448	7.8859
		HSBT [5]	12.2243	10.4269	9.4319	8.5977	8.1446	7.8860
		HSBT^{F}	12.2228	10.4260	9.4313	8.5973	8.1441	7.8851
	C-F	HSBT [117]	1.9495	1.6605	1.5011	1.3696	1.3033	1.2645
		HSBT [5]	1.9496	1.6602	1.5011	1.3696	1.3034	1.2646
		HSBT^{F}	1.9496	1.6601	1.5010	1.3696	1.3033	1.2645

F: Finite element method

6.4 Conclusions

Based on refined shear deformation theory, the nondimensional fundamental frequency $(\bar{\omega})$ and the critical buckling load (N_{cr}) of FG beams (Type A) is presented. Governing equations of motion and various boundary conditions are derived from the Hamilton's principle. Finite element model is developed to determine the natural frequencies, critical buckling loads. Effects of the power-law index (*p)*, the span-to-height ratio (*L/h*), and various boundary conditions are discussed. The present model can provide accurate and reliable results in analyzing the nondimensional fundamental frequency $(\bar{\omega})$ and the critical buckling load (N_{cr}) problem of FG beams.

Chapter 7
Conclusions and Recommendations

7.1 Conclusions

In this dissertation, the author has proposed some beam models for static, buckling and vibration analysis of functionally graded isotropic and sandwich beams embedded in hygro-thermo-mechanical environments.

The main conclusions of the thesis can be summarized as follows

- The dissertation has introduced a brief literature review on computational theories and methods of composite beams, from which several novel findings were found and proposed.
- It presented more details of the composite materials, its microstructure and method of estimating the effective elastic properties. A literature reviews also focused on the topics that are relevant to this research, such as beam theories, analytical and numerical approaches for bending, buckling and vibration analysis of beams in Hygro-thermo-mechanical environment.
- The thesis proposed a novel general higher-order shear deformation beam theory for analysis of functionally graded beams. A general theoretical formulation of higher-order shear deformation beam theory is derived from the fundamental of two-dimensional elasticity theory and then novel different higher-order shear deformation beam theories are obtained. Moreover, two other beam models are also proposed. A HSBT model with a new inverse hyperbolic-sine higher-order shear function and a novel three-variable quasi-3D shear deformation beam theory for analysis of functionally graded beams are proposed.
- It investigated effects of moisture and temperature rises on vibration and buckling responses of functionally graded beams. The present work was based on a higher-order shear deformation theory which accounts for a hyperbolic distribution of both in-plane and out-of-plane displacements. The temperature and moisture are supposed to be varied uniformly, linearly and non-linearly.
- The effects of scale-size on the buckling and vibration behaviors of functionally graded beams is proposed in thermal environments. A general theoretical

formulation is derived from the fundamental of two-dimensional elasticity theory. The effects of boundary conditions on the behaviors of functionally graded beam are considered.

- A finite element model for vibration and buckling of functionally graded beams based on a refined shear deformation theory is presented. Governing equations of motion and boundary conditions are derived from the Hamilton's principle. Effects of the power-law index, the span-to-height ratio and various boundary conditions on the natural frequencies, critical buckling loads of functionally graded beams are discussed.

Some remaining limitations of the thesis are as follows:

- Behavior analysis of nano FG beams can not use the higher-order shear deformation theory.
- Using the ritz method, the accuracy depends on the approximation function.
- Research results for the problem A novel three-variable quasi-3D shear deformation theory has not been as expected.

7.2 Recommendations

During the research process, the thesis also encountered certain difficulties and limitations as above. Therefore, some problems exist in the thesis which will be developed in the near future:

- Analysis of FGM beam behavior with different numerical methods should also be considered soon.
- Develop two-dimensional elasticity solution for vibration analysis of composite beams with various boundary conditions.
- Develop FGM beam models with more complex geometry.
- Develop and analyze behavior behaviours of thin-walled FG beam and FG sandwich beams.

References

[1] Y. Ghugal and R. Shimpi, "A review of refined shear deformation theories for isotropic and anisotropic laminated beams," Journal of reinforced plastics and composites, vol. 20, pp. 255-272, 2001.
[2] A. S. Sayyad and Y. M. Ghugal, "Modeling and analysis of functionally graded sandwich beams: A review," Mechanics of Advanced Materials and Structures, pp. 1-20, 2018.
[3] T.-K. Nguyen, K. Sab, and G. Bonnet, "First-order shear deformation plate models for functionally graded materials," Composite Structures, vol. 83, pp. 25-36, 2008.
[4] T.-K. Nguyen, T. P. Vo, and H.-T. Thai, "Static and free vibration of axially loaded functionally graded beams based on the first-order shear deformation theory," Composites Part B: Engineering, vol. 55, pp. 147-157, 2013.
[5] T.-K. Nguyen, T. T.-P. Nguyen, T. P. Vo, and H.-T. Thai, "Vibration and buckling analysis of functionally graded sandwich beams by a new higher-order shear deformation theory," Composites Part B: Engineering, vol. 76, pp. 273-285, 2015.
[6] J. Mantari, A. Oktem, and C. G. Soares, "A new higher order shear deformation theory for sandwich and composite laminated plates," Composites Part B: Engineering, vol. 43, pp. 1489-1499, 2012.
[7] T. P. Vo, H.-T. Thai, T.-K. Nguyen, and F. Inam, "Static and vibration analysis of functionally graded beams using refined shear deformation theory," Meccanica, vol. 49, pp. 155-168, 2014.
[8] T.-K. Nguyen, "A higher-order hyperbolic shear deformation plate model for analysis of functionally graded materials," International Journal of Mechanics and Materials in Design, vol. 11, pp. 203-219, 2015.
[9] H.-T. Thai, T. P. Vo, T. Q. Bui, and T.-K. Nguyen, "A quasi-3D hyperbolic shear deformation theory for functionally graded plates," Acta Mechanica, vol. 225, pp. 951-964, 2014.
[10] A. C. Eringen, "On differential equations of nonlocal elasticity and solutions of screw dislocation and surface waves," Journal of applied physics, vol. 54, pp. 4703-4710, 1983.
[11] J. Peddieson, G. R. Buchanan, and R. P. McNitt, "Application of nonlocal continuum models to nanotechnology," International Journal of Engineering Science, vol. 41, pp. 305-312, 2003.
[12] F. Yang, A. Chong, D. C. C. Lam, and P. Tong, "Couple stress based strain gradient theory for elasticity," International Journal of Solids and Structures, vol. 39, pp. 2731-2743, 2002.
[13] R. A. Toupin, "Elastic materials with couple-stresses," Archive for Rational Mechanics and Analysis, vol. 11, pp. 385-414, 1962.

[14] R. Mindlin and H. Tiersten, "Effects of couple-stresses in linear elasticity," Archive for Rational Mechanics and analysis, vol. 11, pp. 415-448, 1962.
[15] W. Koiter, "Couple-stress in the theory of elasticity," in Proc. K. Ned. Akad. Wet, 1964, pp. 17-44.
[16] R. D. Mindlin, "Micro-structure in linear elasticity," Archive for Rational Mechanics and Analysis, vol. 16, pp. 51-78, 1964.
[17] S. Park and X. Gao, "Bernoulli–Euler beam model based on a modified couple stress theory," Journal of Micromechanics and Microengineering, vol. 16, p. 2355, 2006.
[18] J. Reddy, "Microstructure-dependent couple stress theories of functionally graded beams," Journal of the Mechanics and Physics of Solids, vol. 59, pp. 2382-2399, 2011.
[19] M. Şimşek, "Nonlocal effects in the forced vibration of an elastically connected double-carbon nanotube system under a moving nanoparticle," Computational Materials Science, vol. 50, pp. 2112-2123, 2011.
[20] M. Aydogdu and V. Taskin, "Free vibration analysis of functionally graded beams with simply supported edges," Materials & design, vol. 28, pp. 1651-1656, 2007.
[21] T. Kant and K. Swaminathan, "Analytical solutions for the static analysis of laminated composite and sandwich plates based on a higher order refined theory," Composite structures, vol. 56, pp. 329-344, 2002.
[22] M. Aydogdu, "Vibration analysis of cross-ply laminated beams with general boundary conditions by Ritz method," International Journal of Mechanical Sciences, vol. 47, pp. 1740-1755, 2005.
[23] K. Pradhan and S. Chakraverty, "Free vibration of Euler and Timoshenko functionally graded beams by Rayleigh–Ritz method," Composites Part B: Engineering, vol. 51, pp. 175-184, 2013.
[24] M. Şimşek, "Static analysis of a functionally graded beam under a uniformly distributed load by Ritz method," International Journal of Engineering & Applied Sciences, vol. 1, pp. 1-11, 2009.
[25] R. Bellman and J. Casti, "Differential quadrature and long-term integration," Journal of Mathematical Analysis and Applications, vol. 34, pp. 235-238, 1971.
[26] P. Sharma, "Efficacy of Harmonic Differential Quadrature method to vibration analysis of FGPM beam," Composite Structures, vol. 189, pp. 107-116, 2018.
[27] M. F. Shojaei and R. Ansari, "Variational differential quadrature: a technique to simplify numerical analysis of structures," Applied Mathematical Modelling, vol. 49, pp. 705-738, 2017.
[28] J. N. Reddy, "A simple higher-order theory for laminated composite plates," Journal of applied mechanics, vol. 51, pp. 745-752, 1984.
[29] V. Kahya and M. Turan, "Vibration and stability analysis of functionally graded sandwich beams by a multi-layer finite element," Composites Part B: Engineering, vol. 146, pp. 198-212, 2018.

[30] J. Lin, J. Li, Y. Guan, G. Zhao, H. Naceur, and D. Coutellier, "Geometrically Nonlinear bending analysis of functionally graded beam with variable thickness by a meshless method," Composite Structures, vol. 189, pp. 239-246, 2018.
[31] T. Bui, A. Khosravifard, C. Zhang, M. Hematiyan, and M. Golub, "Dynamic analysis of sandwich beams with functionally graded core using a truly meshfree radial point interpolation method," Engineering structures, vol. 47, pp. 90-104, 2013.
[32] T. Yu, H. Hu, J. Zhang, and T. Q. Bui, "Isogeometric analysis of size-dependent effects for functionally graded microbeams by a non-classical quasi-3D theory," Thin-Walled Structures, vol. 138, pp. 1-14, 2019.
[33] T. Yu, J. Zhang, H. Hu, and T. Q. Bui, "A novel size-dependent quasi-3D isogeometric beam model for two-directional FG microbeams analysis," Composite Structures, vol. 211, pp. 76-88, 2019.
[34] T. N. Nguyen, C. H. Thai, and H. Nguyen-Xuan, "On the general framework of high order shear deformation theories for laminated composite plate structures: a novel unified approach," International Journal of Mechanical Sciences, vol. 110, pp. 242-255, 2016.
[35] T. N. Nguyen, T. D. Ngo, and H. Nguyen-Xuan, "A novel three-variable shear deformation plate formulation: Theory and Isogeometric implementation," Computer Methods in Applied Mechanics and Engineering, vol. 326, pp. 376-401, 2017.
[36] C. H. Thai, A. Ferreira, and H. Nguyen-Xuan, "Isogeometric analysis of size-dependent isotropic and sandwich functionally graded microplates based on modified strain gradient elasticity theory," Composite Structures, vol. 192, pp. 274-288, 2018.
[37] G. Liu, K. Dai, and T. T. Nguyen, "A smoothed finite element method for mechanics problems," Computational Mechanics, vol. 39, pp. 859-877, 2007.
[38] T. Nguyen-Thoi, T. Bui-Xuan, P. Phung-Van, H. Nguyen-Xuan, and P. Ngo-Thanh, "Static, free vibration and buckling analyses of stiffened plates by CS-FEM-DSG3 using triangular elements," Computers & structures, vol. 125, pp. 100-113, 2013.
[39] T. Nguyen-Thoi, P. Phung-Van, S. Nguyen-Hoang, and Q. Lieu-Xuan, "A coupled alpha-FEM for dynamic analyses of 2D fluid–solid interaction problems," Journal of Computational and Applied Mathematics, vol. 271, pp. 130-149, 2014.
[40] N. D. Duc, K. Seung-Eock, and D. Q. Chan, "Thermal buckling analysis of FGM sandwich truncated conical shells reinforced by FGM stiffeners resting on elastic foundations using FSDT," Journal of Thermal Stresses, vol. 41, pp. 331-365, 2018.
[41] N. D. Duc, K. Seung-Eock, T. Q. Quan, D. D. Long, and V. M. Anh, "Nonlinear dynamic response and vibration of nanocomposite multilayer organic solar cell," Composite Structures, vol. 184, pp. 1137-1144, 2018.
[42] N. D. Duc, K. Seung-Eock, N. D. Tuan, P. Tran, and N. D. Khoa, "New approach to study nonlinear dynamic response and vibration of sandwich composite cylindrical panels with auxetic honeycomb core layer," Aerospace Science and Technology, vol. 70, pp. 396-404, 2017.

[43] N. D. Duc and H. Van Tung, "Mechanical and thermal postbuckling of higher order shear deformable functionally graded plates on elastic foundations," Composite Structures, vol. 93, pp. 2874-2881, 2011.
[44] T. I. Thinh, "Static behavior and vibration control of piezoelectric cantilever composite plates and comparison with experiments," Computational Materials Science, vol. 49, pp. S276-S280, 2010.
[45] T. I. Thinh and T. H. Quoc, "Finite element modeling and experimental study on bending and vibration of laminated stiffened glass fiber/polyester composite plates," Computational Materials Science, vol. 49, pp. S383-S389, 2010.
[46] H. Van Tung, "Thermal and thermomechanical postbuckling of FGM sandwich plates resting on elastic foundations with tangential edge constraints and temperature dependent properties," Composite Structures, vol. 131, pp. 1028-1039, 2015.
[47] H. Van Tung, "Nonlinear axisymmetric response of FGM shallow spherical shells with tangential edge constraints and resting on elastic foundations," Composite Structures, vol. 149, pp. 231-238, 2016.
[48] D. K. Nguyen, "Large displacement behaviour of tapered cantilever Euler–Bernoulli beams made of functionally graded material," Applied Mathematics and Computation, vol. 237, pp. 340-355, 2014.
[49] D. K. Nguyen, "Large displacement response of tapered cantilever beams made of axially functionally graded material," Composites Part B: Engineering, vol. 55, pp. 298-305, 2013.
[50] T.-K. Nguyen, N.-D. Nguyen, T. P. Vo, and H.-T. Thai, "Trigonometric-series solution for analysis of laminated composite beams," Composite Structures, vol. 160, pp. 142-151, 2017.
[51] T.-K. Nguyen, V.-H. Nguyen, T. Chau-Dinh, T. P. Vo, and H. Nguyen-Xuan, "Static and vibration analysis of isotropic and functionally graded sandwich plates using an edge-based MITC3 finite elements," Composites Part B: Engineering, vol. 107, pp. 162-173, 2016.
[52] N. Quan, N. H. Son, and N. Q. Tuan, "Minimum Volume of the Longitudinal Fin with Rectangular and Triangular Profiles by a Modified Newton–Raphson Method," International Journal of Computational Methods, vol. 15, p. 1850034, 2018.
[53] M. Koizumi, "FGM activities in Japan," Composites Part B: Engineering, vol. 28, pp. 1-4, 1997.
[54] S. Suresh and A. Mortensen, Fundamentals of functionally graded materials: The Institut of Materials, 1998.
[55] Y. Miyamoto, W. Kaysser, B. Rabin, A. Kawasaki, and R. G. Ford, Functionally graded materials: design, processing and applications vol. 5: Springer Science & Business Media, 2013.
[56] N. Wattanasakulpong, "Thermal buckling and elastic vibration analysis of functionally graded beams and plates using improved third-order shear deformation

theory," School of Mechanical and Manufacturing Engineering, The University of New South Wales, 2012.
[57] M. Dao, P. Gu, A. Maewal, and R. Asaro, "A micromechanical study of residual stresses in functionally graded materials," Acta materialia, vol. 45, pp. 3265-3276, 1997.
[58] T.-K. Nguyen, K. Sab, and G. Bonnet, "Green's operator for a periodic medium with traction-free boundary conditions and computation of the effective properties of thin plates," International Journal of Solids and Structures, vol. 45, pp. 6518-6534, 2008.
[59] K. Wakashima, T. Hirano, and M. Niino, "Functionally Gradient Materials(Fgm) Architecture: A New Type of Ceramic-Metal Assemblage Designed for Hot Structural Components," 1990.
[60] A. Akbarzadeh, A. Abedini, and Z. Chen, "Effect of micromechanical models on structural responses of functionally graded plates," Composite Structures, vol. 119, pp. 598-609, 2015.
[61] F. Delale and F. Erdogan, "The crack problem for a nonhomogeneous plane," Journal of Applied Mechanics, vol. 50, pp. 609-614, 1983.
[62] J. Mantari and C. G. Soares, "Bending analysis of thick exponentially graded plates using a new trigonometric higher order shear deformation theory," Composite Structures, vol. 94, pp. 1991-2000, 2012.
[63] S.-H. Chi and Y.-L. Chung, "Mechanical behavior of functionally graded material plates under transverse load—Part I: Analysis," International Journal of Solids and Structures, vol. 43, pp. 3657-3674, 2006.
[64] F. Ebrahimi and A. Jafari, "A higher-order thermomechanical vibration analysis of temperature-dependent FGM beams with porosities," Journal of Engineering, vol. 2016, 2016.
[65] Y. Kiani and M. Eslami, "An exact solution for thermal buckling of annular FGM plates on an elastic medium," Composites Part B: Engineering, vol. 45, pp. 101-110, 2013.
[66] F. Fazzolari and E. Carrera, "Thermal stability of FGM sandwich plates under various through-the-thickness temperature distributions," Journal of Thermal Stresses, vol. 37, pp. 1449-1481, 2014.
[67] Q. Yang, B. Zheng, K. Zhang, and J. Zhu, "Analytical solution of a bilayer functionally graded cantilever beam with concentrated loads," Archive of Applied Mechanics, vol. 83, pp. 455-466, 2013.
[68] H. Nguyen-Xuan, C. H. Thai, and T. Nguyen-Thoi, "Isogeometric finite element analysis of composite sandwich plates using a higher order shear deformation theory," Composites Part B: Engineering, vol. 55, pp. 558-574, 2013.
[69] B. Akgöz and Ö. Civalek, "Strain gradient elasticity and modified couple stress models for buckling analysis of axially loaded micro-scaled beams," International Journal of Engineering Science, vol. 49, pp. 1268-1280, 2011.

[70] M. Aydogdu, "Semi-inverse method for vibration and buckling of axially functionally graded beams," Journal of Reinforced Plastics and Composites, vol. 27, pp. 683-691, 2008.
[71] B. Akgöz and Ö. Civalek, "Analysis of micro-sized beams for various boundary conditions based on the strain gradient elasticity theory," Archive of Applied Mechanics, vol. 82, pp. 423-443, 2012.
[72] A. H. Akbarzadeh, A. Abedini, and Z. T. Chen, "Effect of micromechanical models on structural responses of functionally graded plates," Composite Structures, vol. 119, pp. 598-609, 2015/01/01/ 2015.
[73] B. Akgöz and Ö. Civalek, "Application of strain gradient elasticity theory for buckling analysis of protein microtubules," Current Applied Physics, vol. 11, pp. 1133-1138, 2011.
[74] S. Akavci and A. Tanrikulu, "Buckling and free vibration analyses of laminated composite plates by using two new hyperbolic shear-deformation theories," Mechanics of Composite Materials, vol. 44, p. 145, 2008.
[75] M. Benatta, I. Mechab, A. Tounsi, and E. A. Bedia, "Static analysis of functionally graded short beams including warping and shear deformation effects," Computational Materials Science, vol. 44, pp. 765-773, 2008.
[76] C. W. Bert, S. Jang, and A. Striz, "Nonlinear bending analysis of orthotropic rectangular plates by the method of differential quadrature," Computational Mechanics, vol. 5, pp. 217-226, 1989.
[77] Y. S. Al Rjoub and A. G. Hamad, "Free vibration of functionally Euler-Bernoulli and Timoshenko graded porous beams using the transfer matrix method," KSCE Journal of Civil Engineering, vol. 21, pp. 792-806, 2017.
[78] A. C. Eringen, "Nonlocal polar elastic continua," International journal of engineering science, vol. 10, pp. 1-16, 1972.
[79] S. K. Jang, C. W. Bert, and A. G. Striz, "Application of differential quadrature to static analysis of structural components," International Journal for Numerical Methods in Engineering, vol. 28, pp. 561-577, 1989.
[80] A. G. Striz, S. K. Jang, and C. W. Bert, "Nonlinear bending analysis of thin circular plates by differential quadrature," Thin-Walled Structures, vol. 6, pp. 51-62, 1988.
[81] P. Laura and R. Gutierrez, "Analysis of vibrating Timoshenko beams using the method of differential quadrature," Shock and Vibration, vol. 1, pp. 89-93, 1993.
[82] K. Liew, J.-B. Han, Z. Xiao, and H. Du, "Differential quadrature method for Mindlin plates on Winkler foundations," International Journal of Mechanical Sciences, vol. 38, pp. 405-421, 1996.
[83] J.-B. Han and K. Liew, "An eight-node curvilinear differential quadrature formulation for Reissner/Mindlin plates," Computer Methods in Applied Mechanics and Engineering, vol. 141, pp. 265-280, 1997.

[84] S. Lam, "Application of the differential quadrature method to two-dimensional problems with arbitrary geometry," Computers & structures, vol. 47, pp. 459-464, 1993.
[85] S. Pradhan and T. Murmu, "Thermo-mechanical vibration of FGM sandwich beam under variable elastic foundations using differential quadrature method," Journal of Sound and Vibration, vol. 321, pp. 342-362, 2009.
[86] C. W. Bert and M. Malik, "Differential quadrature method in computational mechanics: a review," Applied mechanics reviews, vol. 49, pp. 1-28, 1996.
[87] M. Matbuly, O. Ragb, and M. Nassar, "Natural frequencies of a functionally graded cracked beam using the differential quadrature method," Applied mathematics and computation, vol. 215, pp. 2307-2316, 2009.
[88] A. Fereidoon and A. Mohyeddin, "Bending analysis of thin functionally graded plates using generalized differential quadrature method," Archive of Applied Mechanics, vol. 81, pp. 1523-1539, 2011.
[89] S. Sahraee and A. Saidi, "Free vibration and buckling analysis of functionally graded deep beam-columns on two-parameter elastic foundations using the differential quadrature method," Proceedings of the Institution of Mechanical Engineers, Part C: Journal of Mechanical Engineering Science, vol. 223, pp. 1273-1284, 2009.
[90] M. Yas and N. Samadi, "Free vibrations and buckling analysis of carbon nanotube-reinforced composite Timoshenko beams on elastic foundation," International Journal of Pressure Vessels and Piping, vol. 98, pp. 119-128, 2012.
[91] M. Şimşek, "Buckling of Timoshenko beams composed of two-dimensional functionally graded material (2D-FGM) having different boundary conditions," Composite Structures, vol. 149, pp. 304-314, 2016.
[92] K. Pradhan and S. Chakraverty, "Effects of different shear deformation theories on free vibration of functionally graded beams," International Journal of Mechanical Sciences, vol. 82, pp. 149-160, 2014.
[93] K. K. Pradhan and S. Chakraverty, "Generalized power-law exponent based shear deformation theory for free vibration of functionally graded beams," Applied Mathematics and Computation, vol. 268, pp. 1240-1258, 2015.
[94] F. A. Fazzolari, "Quasi-3D beam models for the computation of eigenfrequencies of functionally graded beams with arbitrary boundary conditions," Composite Structures, vol. 154, pp. 239-255, 2016.
[95] D. Chen, J. Yang, and S. Kitipornchai, "Elastic buckling and static bending of shear deformable functionally graded porous beam," Composite Structures, vol. 133, pp. 54-61, 2015.
[96] D. Chen, J. Yang, and S. Kitipornchai, "Free and forced vibrations of shear deformable functionally graded porous beams," International Journal of Mechanical Sciences, vol. 108, pp. 14-22, 2016.
[97] D.-G. Zhang, "Nonlinear bending analysis of FGM beams based on physical neutral surface and high order shear deformation theory," Composite Structures, vol. 100, pp. 121-126, 2013.

[98] D.-G. Zhang, "Thermal post-buckling and nonlinear vibration analysis of FGM beams based on physical neutral surface and high order shear deformation theory," Meccanica, vol. 49, pp. 283-293, 2014.
[99] N. Wattanasakulpong, B. G. Prusty, and D. W. Kelly, "Thermal buckling and elastic vibration of third-order shear deformable functionally graded beams," International Journal of Mechanical Sciences, vol. 53, pp. 734-743, 2011.
[100] S. Ghiasian, Y. Kiani, and M. Eslami, "Nonlinear thermal dynamic buckling of FGM beams," European Journal of Mechanics-A/Solids, vol. 54, pp. 232-242, 2015.
[101] J. N. Reddy, Mechanics of laminated composite plates and shells: theory and analysis: CRC press, 2004.
[102] A. E. Alshorbagy, M. Eltaher, and F. Mahmoud, "Free vibration characteristics of a functionally graded beam by finite element method," Applied Mathematical Modelling, vol. 35, pp. 412-425, 2011.
[103] A. Chakraborty, S. Gopalakrishnan, and J. Reddy, "A new beam finite element for the analysis of functionally graded materials," International Journal of Mechanical Sciences, vol. 45, pp. 519-539, 2003.
[104] A. El-Ashmawy, M. Kamel, and M. A. Elshafei, "Thermo-mechanical analysis of axially and transversally Function Graded Beam," Composites Part B: Engineering, vol. 102, pp. 134-149, 2016.
[105] M. Lezgy-Nazargah, "Fully coupled thermo-mechanical analysis of bi-directional FGM beams using NURBS isogeometric finite element approach," Aerospace Science and Technology, vol. 45, pp. 154-164, 2015.
[106] K. S. Anandrao, R. Gupta, P. Ramchandran, and G. V. Rao, "Non-linear free vibrations and post-buckling analysis of shear flexible functionally graded beams," Structural Engineering and Mechanics, vol. 44, pp. 339-361, 2012.
[107] K. S. Anandrao, R. Gupta, P. Ramchandran, and G. V. Rao, "Thermal post-buckling analysis of uniform slender functionally graded material beams," Structural Engineering and Mechanics, vol. 36, pp. 545-560, 2010.
[108] L. C. Trinh, T. P. Vo, H.-T. Thai, and T.-K. Nguyen, "An analytical method for the vibration and buckling of functionally graded beams under mechanical and thermal loads," Composites Part B: Engineering, vol. 100, pp. 152-163, 2016.
[109] B. Shvartsman and J. Majak, "Numerical method for stability analysis of functionally graded beams on elastic foundation," Applied Mathematical Modelling, vol. 40, pp. 3713-3719, 2016.
[110] T. A. Huynh, X. Q. Lieu, and J. Lee, "NURBS-based modeling of bidirectional functionally graded Timoshenko beams for free vibration problem," Composite Structures, vol. 160, pp. 1178-1190, 2017.
[111] G. Giunta, S. Belouettar, and A. Ferreira, "A static analysis of three-dimensional functionally graded beams by hierarchical modelling and a collocation meshless solution method," Acta Mechanica, vol. 227, pp. 969-991, 2016.

[112] Y. Yang, C. Lam, and K. Kou, "Forced vibration analysis of functionally graded beams by the meshfree boundary-domain integral equation method," Engineering Analysis with Boundary Elements, vol. 72, pp. 100-110, 2016.
[113] L. F. Qian and H. K. Ching, "Static and dynamic analysis of 2-D functionally graded elasticity by using meshless local petrov-galerkin method," Journal of the Chinese Institute of Engineers, vol. 27, pp. 491-503, 2004.
[114] B. V. Sankar, "An elasticity solution for functionally graded beams," Composites Science and Technology, vol. 61, pp. 689-696, 2001.
[115] Z. Zhong and T. Yu, "Analytical solution of a cantilever functionally graded beam," Composites Science and Technology, vol. 67, pp. 481-488, 2007.
[116] S. Ben-Oumrane, T. Abedlouahed, M. Ismail, B. B. Mohamed, M. Mustapha, and A. B. El Abbas, "A theoretical analysis of flexional bending of Al/Al2O3 S-FGM thick beams," Computational Materials Science, vol. 44, pp. 1344-1350, 2009.
[117] H.-T. Thai and T. P. Vo, "Bending and free vibration of functionally graded beams using various higher-order shear deformation beam theories," International Journal of Mechanical Sciences, vol. 62, pp. 57-66, 2012.
[118] S. Kapuria, M. Bhattacharyya, and A. Kumar, "Bending and free vibration response of layered functionally graded beams: a theoretical model and its experimental validation," Composite Structures, vol. 82, pp. 390-402, 2008.
[119] G. Giunta, S. Belouettar, and E. Carrera, "Analysis of FGM beams by means of classical and advanced theories," Mechanics of Advanced Materials and Structures, vol. 17, pp. 622-635, 2010.
[120] X.-F. Li, "A unified approach for analyzing static and dynamic behaviors of functionally graded Timoshenko and Euler–Bernoulli beams," Journal of Sound and vibration, vol. 318, pp. 1210-1229, 2008.
[121] S.-R. Li and R. C. Batra, "Relations between buckling loads of functionally graded Timoshenko and homogeneous Euler–Bernoulli beams," Composite Structures, vol. 95, pp. 5-9, 2013.
[122] R. Kadoli, K. Akhtar, and N. Ganesan, "Static analysis of functionally graded beams using higher order shear deformation theory," Applied Mathematical Modelling, vol. 32, pp. 2509-2525, 2008.
[123] X.-F. Li, B.-L. Wang, and J.-C. Han, "A higher-order theory for static and dynamic analyses of functionally graded beams," Archive of Applied Mechanics, vol. 80, pp. 1197-1212, 2010.
[124] M. Touratier, "An efficient standard plate theory," International journal of engineering science, vol. 29, pp. 901-916, 1991.
[125] K. Soldatos, "A transverse shear deformation theory for homogeneous monoclinic plates," Acta Mechanica, vol. 94, pp. 195-220, 1992.
[126] M. Karama, K. Afaq, and S. Mistou, "Mechanical behaviour of laminated composite beam by the new multi-layered laminated composite structures model with

transverse shear stress continuity," International Journal of solids and structures, vol. 40, pp. 1525-1546, 2003.
[127] E. Carrera, "Theories and finite elements for multilayered plates and shells: a unified compact formulation with numerical assessment and benchmarking," Archives of Computational Methods in Engineering, vol. 10, pp. 215-296, 2003.
[128] M. Şimşek, "Fundamental frequency analysis of functionally graded beams by using different higher-order beam theories," Nuclear Engineering and Design, vol. 240, pp. 697-705, 2010.
[129] R. K. Bhangale and N. Ganesan, "Thermoelastic buckling and vibration behavior of a functionally graded sandwich beam with constrained viscoelastic core," Journal of Sound and Vibration, vol. 295, pp. 294-316, 2006.
[130] M. C. Amirani, S. Khalili, and N. Nemati, "Free vibration analysis of sandwich beam with FG core using the element free Galerkin method," Composite Structures, vol. 90, pp. 373-379, 2009.
[131] T. P. Vo, H.-T. Thai, T.-K. Nguyen, A. Maheri, and J. Lee, "Finite element model for vibration and buckling of functionally graded sandwich beams based on a refined shear deformation theory," Engineering Structures, vol. 64, pp. 12-22, 2014.
[132] E. Carrera, G. Giunta, and M. Petrolo, Beam structures: classical and advanced theories: John Wiley & Sons, 2011.
[133] D. S. Mashat, E. Carrera, A. M. Zenkour, S. A. Al Khateeb, and M. Filippi, "Free vibration of FGM layered beams by various theories and finite elements," Composites Part B: Engineering, vol. 59, pp. 269-278, 2014.
[134] M. Filippi, E. Carrera, and A. Zenkour, "Static analyses of FGM beams by various theories and finite elements," Composites Part B: Engineering, vol. 72, pp. 1-9, 2015.
[135] T. P. Vo, H.-T. Thai, T.-K. Nguyen, F. Inam, and J. Lee, "A quasi-3D theory for vibration and buckling of functionally graded sandwich beams," Composite Structures, vol. 119, pp. 1-12, 2015.
[136] T. P. Vo, H.-T. Thai, T.-K. Nguyen, F. Inam, and J. Lee, "Static behaviour of functionally graded sandwich beams using a quasi-3D theory," Composites Part B: Engineering, vol. 68, pp. 59-74, 2015.
[137] J. Mantari and J. Yarasca, "A simple and accurate generalized shear deformation theory for beams," Composite Structures, vol. 134, pp. 593-601, 2015.
[138] J. Mantari, "A refined theory with stretching effect for the dynamics analysis of advanced composites on elastic foundation," Mechanics of Materials, vol. 86, pp. 31-43, 2015.
[139] A. I. Osofero, T. P. Vo, T.-K. Nguyen, and J. Lee, "Analytical solution for vibration and buckling of functionally graded sandwich beams using various quasi-3D theories," Journal of Sandwich Structures & Materials, vol. 18, pp. 3-29, 2016.
[140] E. Reissner, "ON TRANVERSE BENDING OF PLATES, INCLUDING THE EFFECT OF TRANSVERSE SHEAR DEFORMATION," 1974.

[141] G. Shi, "A new simple third-order shear deformation theory of plates," International Journal of Solids and Structures, vol. 44, pp. 4399-4417, 2007.
[142] F. Ebrahimi and E. Salari, "Nonlocal thermo-mechanical vibration analysis of functionally graded nanobeams in thermal environment," Acta Astronautica, vol. 113, pp. 29-50, 2015.
[143] F. Ebrahimi and E. Salari, "Thermal buckling and free vibration analysis of size dependent Timoshenko FG nanobeams in thermal environments," Composite Structures, vol. 128, pp. 363-380, 2015.
[144] F. Ebrahimi and M. R. Barati, "A unified formulation for dynamic analysis of nonlocal heterogeneous nanobeams in hygro-thermal environment," Applied Physics A, vol. 122, p. 792, 2016.
[145] M. Zidi, A. Tounsi, M. S. A. Houari, and O. A. Bég, "Bending analysis of FGM plates under hygro-thermo-mechanical loading using a four variable refined plate theory," Aerospace Science and Technology, vol. 34, pp. 24-34, 2014.
[146] A. Zenkour, "Hygro-thermo-mechanical effects on FGM plates resting on elastic foundations," Composite Structures, vol. 93, pp. 234-238, 2010.
[147] A. Zenkour, M. Allam, and A. Radwan, "Effects of transverse shear and normal strains on FG plates resting on elastic foundations under hygro-thermo-mechanical loading," International Journal of Applied Mechanics, vol. 6, p. 1450063, 2014.
[148] S. Sina, H. Navazi, and H. Haddadpour, "An analytical method for free vibration analysis of functionally graded beams," Materials & Design, vol. 30, pp. 741-747, 2009.
[149] T.-K. Nguyen and B.-D. Nguyen, "A new higher-order shear deformation theory for static, buckling and free vibration analysis of functionally graded sandwich beams," Journal of Sandwich Structures & Materials, vol. 17, pp. 613-631, 2015.
[150] T.-K. Nguyen, T. P. Vo, B.-D. Nguyen, and J. Lee, "An analytical solution for buckling and vibration analysis of functionally graded sandwich beams using a quasi-3D shear deformation theory," Composite Structures, vol. 156, pp. 238-252, 2016.
[151] J. Yarasca, J. Mantari, and R. Arciniega, "Hermite–Lagrangian finite element formulation to study functionally graded sandwich beams," Composite Structures, vol. 140, pp. 567-581, 2016.
[152] S. Esfahani, Y. Kiani, and M. Eslami, "Non-linear thermal stability analysis of temperature dependent FGM beams supported on non-linear hardening elastic foundations," International Journal of Mechanical Sciences, vol. 69, pp. 10-20, 2013.
[153] L. Ma and D. Lee, "Exact solutions for nonlinear static responses of a shear deformable FGM beam under an in-plane thermal loading," European Journal of Mechanics-A/Solids, vol. 31, pp. 13-20, 2012.
[154] P. Malekzadeh and S. Monajjemzadeh, "Dynamic response of functionally graded beams in a thermal environment under a moving load," Mechanics of Advanced Materials and Structures, vol. 23, pp. 248-258, 2016.
[155] B. V. Sankar and J. T. Tzeng, "Thermal stresses in functionally graded beams," AIAA journal, vol. 40, pp. 1228-1232, 2002.

[156] Y. Sun, S.-R. Li, and R. C. Batra, "Thermal buckling and post-buckling of FGM Timoshenko beams on nonlinear elastic foundation," Journal of Thermal Stresses, vol. 39, pp. 11-26, 2016.
[157] H.-S. Shen, "Nonlinear analysis of functionally graded fiber reinforced composite laminated beams in hygrothermal environments, Part I: Theory and solutions," Composite Structures, vol. 125, pp. 698-705, 2015/07/01/ 2015.
[158] H.-S. Shen, "Nonlinear analysis of functionally graded fiber reinforced composite laminated beams in hygrothermal environments, Part II: Numerical results," Composite Structures, vol. 125, pp. 706-712, 2015/07/01/ 2015.
[159] M. Aydogdu, "Buckling analysis of cross-ply laminated beams with general boundary conditions by Ritz method," Composites Science and Technology, vol. 66, pp. 1248-1255, 2006.
[160] M. Aydogdu, "Free vibration analysis of angle-ply laminated beams with general boundary conditions," Journal of reinforced plastics and composites, vol. 25, pp. 1571-1583, 2006.
[161] J. Mantari and F. Canales, "Free vibration and buckling of laminated beams via hybrid Ritz solution for various penalized boundary conditions," Composite Structures, vol. 152, pp. 306-315, 2016.
[162] N. Fleck, G. Muller, M. Ashby, and J. Hutchinson, "Strain gradient plasticity: theory and experiment," Acta Metallurgica et Materialia, vol. 42, pp. 475-487, 1994.
[163] D. C. Lam, F. Yang, A. Chong, J. Wang, and P. Tong, "Experiments and theory in strain gradient elasticity," Journal of the Mechanics and Physics of Solids, vol. 51, pp. 1477-1508, 2003.
[164] R. D. Mindlin and N. Eshel, "On first strain-gradient theories in linear elasticity," International Journal of Solids and Structures, vol. 4, pp. 109-124, 1968.
[165] S. Kong, S. Zhou, Z. Nie, and K. Wang, "Static and dynamic analysis of micro beams based on strain gradient elasticity theory," International Journal of Engineering Science, vol. 47, pp. 487-498, 2009.
[166] B. Wang, J. Zhao, and S. Zhou, "A micro scale Timoshenko beam model based on strain gradient elasticity theory," European Journal of Mechanics-A/Solids, vol. 29, pp. 591-599, 2010.
[167] S. Papargyri-Beskou, K. Tsepoura, D. Polyzos, and D. Beskos, "Bending and stability analysis of gradient elastic beams," International Journal of Solids and Structures, vol. 40, pp. 385-400, 2003.
[168] K. Lazopoulos and A. Lazopoulos, "Bending and buckling of thin strain gradient elastic beams," European Journal of Mechanics-A/Solids, vol. 29, pp. 837-843, 2010.
[169] S. Kong, S. Zhou, Z. Nie, and K. Wang, "The size-dependent natural frequency of Bernoulli–Euler micro-beams," International Journal of Engineering Science, vol. 46, pp. 427-437, 2008.

[170] H. Ma, X.-L. Gao, and J. Reddy, "A microstructure-dependent Timoshenko beam model based on a modified couple stress theory," Journal of the Mechanics and Physics of Solids, vol. 56, pp. 3379-3391, 2008.
[171] H. Ma, X.-L. Gao, and J. Reddy, "A nonclassical Reddy-Levinson beam model based on a modified couple stress theory," International Journal for Multiscale Computational Engineering, vol. 8, 2010.
[172] Y. Fu and J. Zhang, "Modeling and analysis of microtubules based on a modified couple stress theory," Physica E: Low-dimensional Systems and Nanostructures, vol. 42, pp. 1741-1745, 2010.
[173] B. Akgöz and Ö. Civalek, "Free vibration analysis of axially functionally graded tapered Bernoulli–Euler microbeams based on the modified couple stress theory," Composite Structures, vol. 98, pp. 314-322, 2013.
[174] M. Şimşek and J. Reddy, "A unified higher order beam theory for buckling of a functionally graded microbeam embedded in elastic medium using modified couple stress theory," Composite Structures, vol. 101, pp. 47-58, 2013.
[175] H.-T. Thai, T. P. Vo, T.-K. Nguyen, and J. Lee, "Size-dependent behavior of functionally graded sandwich microbeams based on the modified couple stress theory," Composite Structures, vol. 123, pp. 337-349, 2015.
[176] J. Reddy, "Nonlocal theories for bending, buckling and vibration of beams," International Journal of Engineering Science, vol. 45, pp. 288-307, 2007.
[177] M. Aydogdu, "A general nonlocal beam theory: its application to nanobeam bending, buckling and vibration," Physica E: Low-dimensional Systems and Nanostructures, vol. 41, pp. 1651-1655, 2009.
[178] W. Xia, L. Wang, and L. Yin, "Nonlinear non-classical microscale beams: Static bending, postbuckling and free vibration," International Journal of Engineering Science, vol. 48, pp. 2044-2053, 2010.
[179] S. Pradhan and T. Murmu, "Application of nonlocal elasticity and DQM in the flapwise bending vibration of a rotating nanocantilever," Physica E: Low-dimensional Systems and Nanostructures, vol. 42, pp. 1944-1949, 2010.
[180] J. Phadikar and S. Pradhan, "Variational formulation and finite element analysis for nonlocal elastic nanobeams and nanoplates," Computational materials science, vol. 49, pp. 492-499, 2010.
[181] H.-T. Thai, "A nonlocal beam theory for bending, buckling, and vibration of nanobeams," International Journal of Engineering Science, vol. 52, pp. 56-64, 2012.
[182] H.-T. Thai and T. P. Vo, "A nonlocal sinusoidal shear deformation beam theory with application to bending, buckling, and vibration of nanobeams," International Journal of Engineering Science, vol. 54, pp. 58-66, 2012/05/01/ 2012.
[183] M. Eltaher, S. A. Emam, and F. Mahmoud, "Free vibration analysis of functionally graded size-dependent nanobeams," Applied Mathematics and Computation, vol. 218, pp. 7406-7420, 2012.

[184] F. Ebrahimi and E. Salari, "Thermo-mechanical vibration analysis of nonlocal temperature-dependent FG nanobeams with various boundary conditions," Composites Part B: Engineering, vol. 78, pp. 272-290, 2015.
[185] M. Eltaher, S. A. Emam, and F. Mahmoud, "Static and stability analysis of nonlocal functionally graded nanobeams," Composite Structures, vol. 96, pp. 82-88, 2013.
[186] M. Şimşek and H. Yurtcu, "Analytical solutions for bending and buckling of functionally graded nanobeams based on the nonlocal Timoshenko beam theory," Composite Structures, vol. 97, pp. 378-386, 2013.
[187] F. Ebrahimi and M. R. Barati, "Small-scale effects on hygro-thermo-mechanical vibration of temperature-dependent nonhomogeneous nanoscale beams," Mechanics of Advanced Materials and Structures, vol. 24, pp. 924-936, 2017.
[188] A. Tounsi, S. Benguediab, M. S. A. Houari, and A. Semmah, "A new nonlocal beam theory with thickness stretching effect for nanobeams," International Journal of Nanoscience, vol. 12, p. 1350025, 2013.
[189] F. Ebrahimi and M. R. Barati, "Wave propagation analysis of quasi-3D FG nanobeams in thermal environment based on nonlocal strain gradient theory," Applied Physics A, vol. 122, p. 843, 2016.
[190] T.-K. Nguyen, B.-D. Nguyen, T. P. Vo, and H.-T. Thai, "Hygro-thermal effects on vibration and thermal buckling behaviours of functionally graded beams," Composite Structures, vol. 176, pp. 1050-1060, 2017.
[191] S. Mohanty, R. Dash, and T. Rout, "Static and dynamic stability analysis of a functionally graded Timoshenko beam," International Journal of Structural Stability and Dynamics, vol. 12, p. 1250025, 2012.
[192] L.-l. Jing, P.-j. Ming, W.-p. Zhang, L.-r. Fu, and Y.-p. Cao, "Static and free vibration analysis of functionally graded beams by combination Timoshenko theory and finite volume method," Composite Structures, vol. 138, pp. 192-213, 2016.
[193] V. Kahya and M. Turan, "Finite element model for vibration and buckling of functionally graded beams based on the first-order shear deformation theory," Composites Part B: Engineering, vol. 109, pp. 108-115, 2017.
[194] A. Frikha, A. Hajlaoui, M. Wali, and F. Dammak, "A new higher order C0 mixed beam element for FGM beams analysis," Composites Part B: Engineering, vol. 106, pp. 181-189, 2016.